Unravelling the Interaction of a Re(I)dppz Metallo-Intercalator with an RNA Internal Loop

---

Dissertation

zur
Erlangung der naturwissenschaftlichen Doktorwürde
(Dr. sc. nat.)

vorgelegt der
Mathematisch-naturwissenschaftlichen Fakultät
der
Universität Zürich

von
Elena Alberti
aus
Italien

Promotionskommission

Prof. Dr. Roland K. O. Sigel (Vorsitz)
Dr. Daniela Donghi (Leitung der Dissertation)
Prof. Dr. Oliver Zerbe
Dr. Michael P. Coogan

Zürich, 2017

Acknowledgements

First and foremost, I would like to thank Dr. Daniela Donghi for giving me this challenging PhD project and for helping me along the way, and Prof. Dr. Roland K.O. Sigel for the opportunity to work in his laboratories and for his advices.

A special thank goes to Dr. Michael P. Coogan, whose contribution was essential not only because he provided us with the metal complex used in this study, but also because he was always ready to discuss and to give me hints.

I would like also to thank Prof. Dr. Oliver Zerbe for his precious help during our PhD committee meetings and also in many more circumstances.

I am also grateful to Prof. Dr. Janez Plavec for agreeing to be the external referee of this thesis.

Another particular thank is for Prof. Dr. Giampaolo Barone and Dr. Angelo Spinello for the nice collaboration, for the exchange of ideas and for their help with one of the chapter of this thesis, to which they actively contributed.

Thanks also to Joana Palou-Mir and Dr. Miquel Barceló-Oliver for the collaboration on the ITC experiments and for the nice time at the conferences and here in Zurich.

I also would like to thank Dr. Silke Johanssen for her help with writing, she started reading and correcting my first Forschungskredit project few months after my PhD began and she concluded nowadays going through some parts of my thesis.

Another person I would thank is Severin Koch, who did his FGP project on the synthesis of the novel Re(I)dppz complex presented in this thesis. It was a pleasure to work with such a curious and hardworking student.

A heartfelt thank is for Matthias Frei that selflessly translated the summary of this thesis, I really appreciated this immeasurable kindness.

Moreover, I would like to thank Ramona Erni, Dr. Sabine Stockhause and Beatrice Spichtig that made my life easier in many cases over the course of my PhD.

I also acknowledge the CMSZH graduate school for the financial support for conferences, language courses, for organizing useful soft skills classes and for the

amazing annual retreat. I had the great chance to organize two of them together with colleagues and friends which I thank for making this experience fruitful and enjoyable.

Many more people made this journey feasible and more pleasant being colleagues and friends.

With tears in my eyes I would like to thank Dr. Marianthi Zampakou that supported me in thousand ways along this path. Our lives came across only four years ago in Zurich but I feel like our friendship began much earlier in another time and another world.

Another special thank goes to Dr. Alicia Dominguez-Martin, Dr. Magdalena Rowinska-Zyrek and Dr. Bhaumik Sunil Dave. Alicia for supporting me and showing me always a different and better perspective (Buddha-style). Magda for listening to me, organizing nice dinners and barbeques and to open for me and Jack the doors of her place in Poland, I will never forget anything. Bhaumik for the nice discussion on our projects and for all the help in the lab with computers and more.

I am grateful to Simona Bartova for the work done together in a nice atmosphere and for being a good friend in the lab and outside.

I would like also to thank Fabio Amadei. It was love at first sight, but that kind of love that stands without hugs and kisses.

Thanks to Kenneth Adea and Meng Zhao for all those lunch, dinners and trips together that were simply amazing and necessary to break the dullness of daily life.

Thanks to Irina Markova and Ilaria Przytula-Mally, even if it was short, I enjoyed a lot the time spent together.

In general, I would like to thank all the members of the Freisinger-Sigel lab for the pleasant working atmosphere.

Another essential part of this experience is represented by the “italian family in Zurich”: Anastasia, Nicola, Natalia, Fabio, Gloria, Cristina, Simona, Samuelino and Matteo. This last one was here next to me from the beginning till the end of this path, sharing difficulties and nice moments, and tolerating me with my bad character without giving up in being a friend.

Finally, I would like to thank my family, Mami, Papi, Zabbi, Ema and Pi, and my lifelong italian friends, Leli, Manu, Simo, Puc, Sara and Tommi, for their support across the countries.

My last thank goes to Jack, who is the bedrock of my life.

Table of contents

1. Introduction

1.1. Thesis outline

The potential of metal complexes as therapeutic and diagnostic agents is well acknowledged and a wide number of studies have been reported on their ability to bind DNA. [1,2] However also RNA is a very fascinating target thanks to its involvement in several biological processes and to its complex structural diversity. [3–6] Indeed, DNA and RNA show significant structural differences, that can lead to diverse interaction modes, making RNA an attractive molecule for the development of specific therapeutic and diagnostic agents. [4,7] In this thesis we investigated the binding of metal complexes and metal ions with RNA with the final goal of obtaining insights on their interaction to be used for a rational design of structure-selective probes.

We chose to work with the 27 nucleotides long RNA construct in Figure 1.1, herein named RNA-l. This model system derives from the mitochondrial group II intron ribozyme *Sc*.ai5γ, [8–10] and its NMR structure in solution (Figure 1.2) was solved in the group of Prof. Dr. Roland K.O. Sigel. [11] It is a crucial part of domain 1 of the group II intron ai5γ from *Saccharomyces cerevisiae*. This area, ζ element, along with the κ element forms the κ-ζ region that correctly structured, allows the catalytic activity of the whole RNA, upon interaction with domain 5. [12,13] This construct was chosen for its great potential as probe for different secondary structural feature that are common in RNA, because it contains a GU wobble, a terminal and an internal loop. This latter one is particularly interesting since internal loops are known to offer potential binding sites for small molecules. [4,14] We studied the non-covalent binding of RNA-l with a potential bio-imaging agent provided by the group of Dr. Michael P. Coogan (University of Lancaster, United Kingdom), namely [Re(CO)$_3$(dppz)(3-CH$_2$OH-Py)]$^+$ (complex 1 in Figure 1.3). The DNA binding properties of this class of metallo-intercalators which have the general formula [Re(CO)$_3$(dppz)(X)]$^+$, where

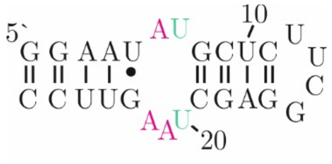

Figure 1.1 Secondary structure of RNA-l. Colours highlight the internal loop structure, in magenta A6, A21 and A22, while in green U7 and U20.

X can be a wide variety of ligands, have been already reported. [15] These complexes were proved to interact with DNA and to accumulate not only in DNA but also in RNA-rich regions of the cell. [15] In particular, complex 1 was shown to localize in the nucleus, in the mitochondria, and in some other perinuclear regions of the cytoplasm, and to have one of the highest binding constant with calf thymus DNA (CT-DNA) amongst the pool of similar complexes. [15] Most likely this is due to the presence of the hydroxymethyl moiety, that can favour hydrogen bonding with DNA. [15] Despite its cellular localisation and the presence of the hydroxyl group that could also favour RNA interaction, the RNA binding properties of complex 1 were not investigated so far. For all of these reasons, we decided to study the binding of complex 1 and RNA using RNA-l as model system. Data on the interaction of Cd(II), Mg(II) and Co(III)hexammine and RNA-l were used to identify metal ion binding sites [9] and to support the findings on the metal complex interaction.

Figure 1.2 NMR solution structure of RNA-l. [11] The colours highlight the internal loop structure, in magenta A6, A21 and A22, while in green U7 and U20. The same colour code is also used in Figure 1.1.

Moreover, in this study we used RNA-h and DNA-h (Figure 1.3a/b). The first one is an RNA construct, in which the internal loop is substituted by regular Watson-Crick base pairs, and it was designed as such to probe its interaction with complex 1. The second one is an analogous DNA sequence exploited to understand the differences in

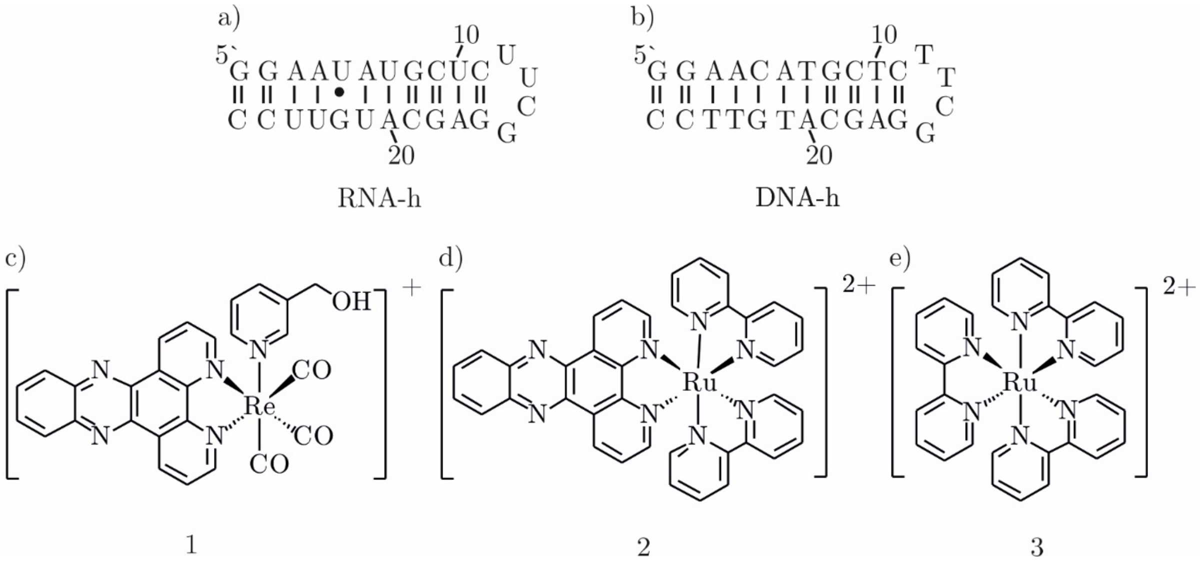

Figure 1.3 Secondary structure of a) RNA-h, b) DNA-h and chemical structures of c) $[Re(CO)_3(dppz)(3\text{-}CH_2OH\text{-}Py)]^+$ (1), d) $[Ru(bpy)_2(dppz)]^{2+}$ (2) and e) $[Ru(bpy)_3]^{2+}$ (3).

RNA and DNA binding. Furthermore, to investigate the role of the dppz moiety in the binding to RNA-l, we used $[Ru(bpy)_2(dppz)]^{2+}$ (complex 2), and $[Ru(bpy)_3]^{2+}$ (complex 3) represented in Figure 1.3d/e.

This thesis exploits as main technique NMR spectroscopy, that allowed us to localise the interaction occurring between the internal loop of RNA-l and complex 1. Furthermore, to complete our investigation optical methods, such as UV-Vis and fluorescence titrations, including displacement assays were also performed. Besides these methods, ITC experiments were performed in collaboration with Dr. Miquel Barceló-Oliver (University of Balearic Islands, Spain). Finally, a computational approach, applied by Prof. Dr. Giampaolo Barone and Dr. Angelo Spinello (University of Palermo, Italy), was used to further characterize the position of complex 1 in the RNA internal loop.

1.2. Metal complexes interacting with nucleic acids

Metal complexes can interact with nucleic acids either in a covalent or non-covalent way. [2,7,16,17] As for the first kind of interaction, for example cisplatin and its derivatives are known to bind DNA via direct coordination of the platinum centre to the N7 of adjacent guanines. [18] The second kind, the non-covalent one, can occur in different ways, such as hydrophobic groove binding, electrostatic binding, intercalation or insertion. [16,19] All of these different modes of interaction have been characterized in solution and in solid state for DNA, [17,19] whereas less information are available on the RNA binding to date. An overview of the latest results on the interaction of RNA and metal complexes is reported in our recently published review and some examples are listed in the next section (Section 1.2.1). [7]

1.2.1. Examples of metal complexes-RNA interaction

There are several examples of metal complexes studied for their ability to behave as probes for RNA tertiary structures. [20] For instance, $[Rh(DIP)_3]^{3+}$ (DIP = 4,7-diphenyl-1,10-phenanthroline) was reported to be able to selectively target GU mismatches and exposed guanines in small and large RNAs, [21] confirming the potential of metal complexes as shape-selective probes for RNA.

Metal complexes were also studied as antiviral agents. [4] An example is represented by the Δ- and Λ-$[Ru(bpy)_2(eilatin)]^{2+}$ (bpy = 2,2′-bipyridine; eilatin is an heptacyclic aromatic marine alkaloid) complexes found to inhibit HIV-1 Rev-RRE interaction *in vitro*. This behaviour is likely due to their interaction with the bulged regions of RRE. [22] Furthermore, it was reported that while free eilatin shows selectivity for electron-poor polymeric purines, Ru-eilatin complexes have a preference for the polypyrimidine r(U), proving that, upon incorporation into octahedral metal complexes, the binding preferences of an intercalating ligand can change. [23]

The strategy of synthesizing new metal complexes by conjugating a metal centre and organic ligands already known for their ability to bind DNA is also well established and documented. [19] Following a similar approach, it was published a study on platinum conjugates of neomycin B and guanidinoneomycin B reacted with the construct RRE JW, a minimized Rev-binding RRE construct. [24] Indeed, aminoglycoside antibiotics showed selectivity for RNA binding over DNA. Their conjugation to a metal centre might lead to the development of RNA binding agents able to permanently damage the RRE RNA. This study showed that, although the two diverse Pt-derivatives with neomycinc B and guanidinoneomycin B bind different sites, both of them selectively prefer the interaction with RRE RNA over the one with calf thymus DNA (CT-DNA), even in the presence of an excess of this last one. This result proves that the combination of a metal centre and organic ligands, already known for their ability of binding selectively RNA, can lead to the design of very promising molecules able to preferentially target RNA. [24]

1.3. Metal complexes in bio-imaging

A particular category of metal complexes interacting with nucleic acids is represented by all of those compounds that show potential as bio-imaging agents. [1,16,25,26] Among these luminescent metal complexes, the d^6 metal complexes, such as Re(I), Ru(II) and Ir(III) derivatives, have been extensively studied in the past years. [17,19,26,27] In general, metal complexes show photophysical, spectroscopic and electrochemical properties that can be tuned to develop chemical probes able to target RNA and DNA. [16] The presence of a metal core can have a twofold importance. Indeed, it influences the photophysical properties of the complex, and it serves as an anchor for the organic ligands in the coordination sphere. [25,27] Different functionalisation of these ligands can lead to metal complexes able to aim at different targets. [28] Moreover, to be exploited as bio-imaging agents, metal complexes must fulfil some criteria, such as having a good radiation tissue penetration and at the same time show an emission that differs from the auto-fluorescence of the cell. This is normally satisfied by molecules with red shifted emission profiles. [25,27] In addition, they must show a large Stokes shift in order to avoid self-quenching. Besides all of these favourable photophysical characteristics, metal complexes must satisfy some other criteria. [25,27] Indeed, they must be stable, i.e. chemically inert, and soluble in aqueous media, they must be non-toxic and non-cytotoxic. They must show an easy cellular uptake that preferably does not need co-agents to assist the permeability. This is generally achieved by high lipophilic compounds. In addition to all of these features, it is also very important that these complexes preferentially interact with a specific target in the cell and do not spread throughout the cellular compartments without any selectivity. [25,27] All of these chemical and photophysical features are desirable in a metal complex in order to be a suitable fluorophore for biological applications.

1.3.1. Ruthenium(I)dppz complexes

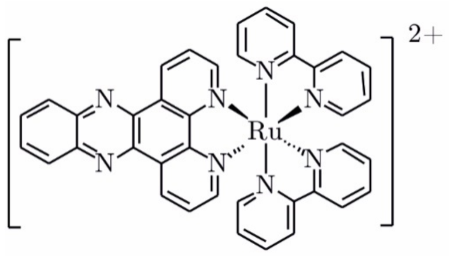

Figure 1.4 Chemical structure of $[Ru(bpy)_2(dppz)]^{2+}$ (2).

In this field, one of the best studied class of luminescent metal complexes is represented by octahedral ruthenium(II) compounds. [19,29] Among these, the ones that contain the dppz moiety showed the highest affinity with DNA. [30–32] The progenitor of this family of complexes based on a $[Ru(bpy)_n]^{2+}$ core is the pivotal complex $[Ru(bpy)_2(dppz)]^{2+}$ (bipy = 2,2’ bipyridine, dppz = dipyrido[3,2-a:2′,3′-c] phenazine), represented in Figure 1.4, whose DNA binding was studied by Barton and co-workers in the ’90. [32] This complex is known as “DNA light switch” because in water its emission is quenched and is restored only upon interaction with DNA. Indeed, water totally deactivates its excited state by hydrogen bonding to the endocyclic N atoms of the dppz ligand. Then, in the presence of B-DNA, the dppz moiety intercalates into its major groove and water is displaced, creating a less polar environment that results in the restoring of the emission of the complex. Indeed, intercalative binding reduces non-radiative deactivation of the excited state, resulting in a higher emission efficiency. [19,28,29] Interestingly, the interaction of this complex with A-DNA leads to barely measurable emission. [32] This different behaviour is a crucial feature that makes this complex appealing as an optical probe able to discriminate among the various DNA conformations. Only recently, Barton and co-workers studied the behaviour of *rac*-$[Ru(bpy)_2(dppz)]^{2+}$ in the presence of different RNA constructs. [33] Comparing the metal complex behaviour in the presence of RNA and DNA mismatches, they showed that this complex is sensitive to CA mismatches in short RNAs, although the overall emission intensity is much lower than with DNA. This study suggests that this complex is able to interact with RNA regions that are thermodynamically unstable, and it is a better probe for RNA than for DNA mismatches. Moreover, comparing the behaviour of *rac*-$[Ru(bpy)_2(dppz)]^{2+}$ and the one of ethidium bromide with mismatched RNA, the authors speculated that the ruthenium interaction occurs via minor groove metallo-insertion of the dppz moiety.

1.3.2. Rhenium(I)dppz complexes

Mononuclear Re(I)dppz complexes have received less attention, compared to the above-mentioned ruthenium complexes. However, the DNA binding of some rhenium complexes have been already studied by Coogan and co-workers. [15] Although it is well known that they bind nucleic acids, [15] there are no information on their RNA interaction and in general the field is still rather unexplored. [7]

Complexes with the general formula [Re(CO)$_3$(dppz)(X)] (dppz = dipyrido[3,2-a:2’,3’-c]phenazine, Figure 1.5), where Re-dppz is the emissive core and X is the axial ligand that can be easily functionalized with a wide variety of groups (some examples are represented by the following moieties -MeCN, -Py, -PyCH$_2$OH, -PyCH$_2$Cl) show weak or no emission in water. However, it is possible to observe an enhancement of their emission upon DNA binding. [15,34,35] Coogan and co-workers have been working on this class of rhenium(I) tricarbonyl derivatives for a long time, aiming at obtaining an in depth understanding of their cellular uptake and localization within the cell. [15] Published data on the CT-DNA binding of these Re(I)dppz complexes showed that an interaction with DNA occurs and it is most likely due to the intercalation of the dppz moiety in the major groove. [15] Moreover, it was shown that the pyridine in axial position can be functionalized to obtain complexes that maintain similar photophysical properties but are able to localize in various compartments in the cell. [15] Indeed, cellular uptake assays demonstrate that the differently functionalized complexes accumulate in diverse areas in the cell, involving both DNA and RNA rich-regions. [15] In particular, [Re(CO)$_3$(dppz)(3-CH$_2$OH-Py)]$^+$ (complex 1, Figure 1.3) was shown to localise in the nucleus, in mitochondria and in some other perinuclear regions of the cytoplasm and it displayed high

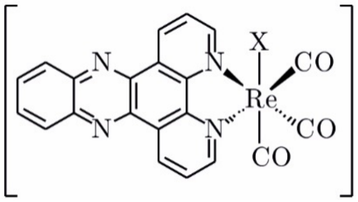

Figure 1.5 Chemical structure of [Re(CO)$_3$(dppz)(X)].

binding constant (K_b) to CT-DNA ($K_b = 5.59 \times 10^5 M^{-1}$). [15]

Fuelled by these findings and by the lack of data on RNA binding preferences of rhenium complexes we decided to investigate the interaction of complex 1 with RNA.

1.4. Metal complexes and nucleic acids: a dynamic interaction

The interaction occurring between metal complexes and nucleic acids can be studied exploiting many different biophysical, photophysical and spectroscopic techniques. [16,19,26] Among all of these techniques, NMR and X-ray crystallography are the most powerful tools used to experimentally determine the three-dimensional structure of biological macromolecules at near atomic resolution. However, these two methods have some differences and very often their information are complementary. [36] Indeed, X-ray can provide with very precise atomic details but the insights on long range dynamics are limited in view of the solid nature of the sample used in this kind of studies. [36] On the contrary, NMR spectroscopy gives data that reflect the conformational freedom in solution of a molecule in its free form or in the interaction with other species. [19,37]

The interaction of nucleic acids and metal complexes, metal ions, small organic molecules and proteins has been widely studied via NMR spectroscopy. [19,30,38–41] However, in some cases, the intrinsic dynamics of an interaction is in a time scale not suitable to be observed via NMR spectroscopy making the data analysis not trivial and nearly hampering the usage of this technique for interaction studies or structural determination. Hence, an in depth structural study can be performed only when the dynamics of the system is in slow exchange. [42] For instance, literature data reported that the addition of bulky Ru(II)-dimer to an RNA double helix with an A bulge motif is responsible for a large degree of line broadening, indicating intermediate exchange kinetics. [43]

In our case, for the interaction between RNA-1 and complex 1, we also observe a dynamic situation. Indeed, general broadening along with a shift of all of the signals of complex 1 is visible. On the contrary, only a few resonances of RNA-1 undergo broadening, shift or complete disappearance indicating the presence of a localised interaction (Chapter 2).

1.5. Basic structural features of nucleic acids

Nucleic acids, RNA and DNA, are among the macromolecular targets for metal complexes in the cell. [16,17] They are polymers consisting of four different monomers called nucleotides. Each of these building blocks consists of a phosphate group, a sugar ring and a nucleobase. As shown in Figure 1.6, the

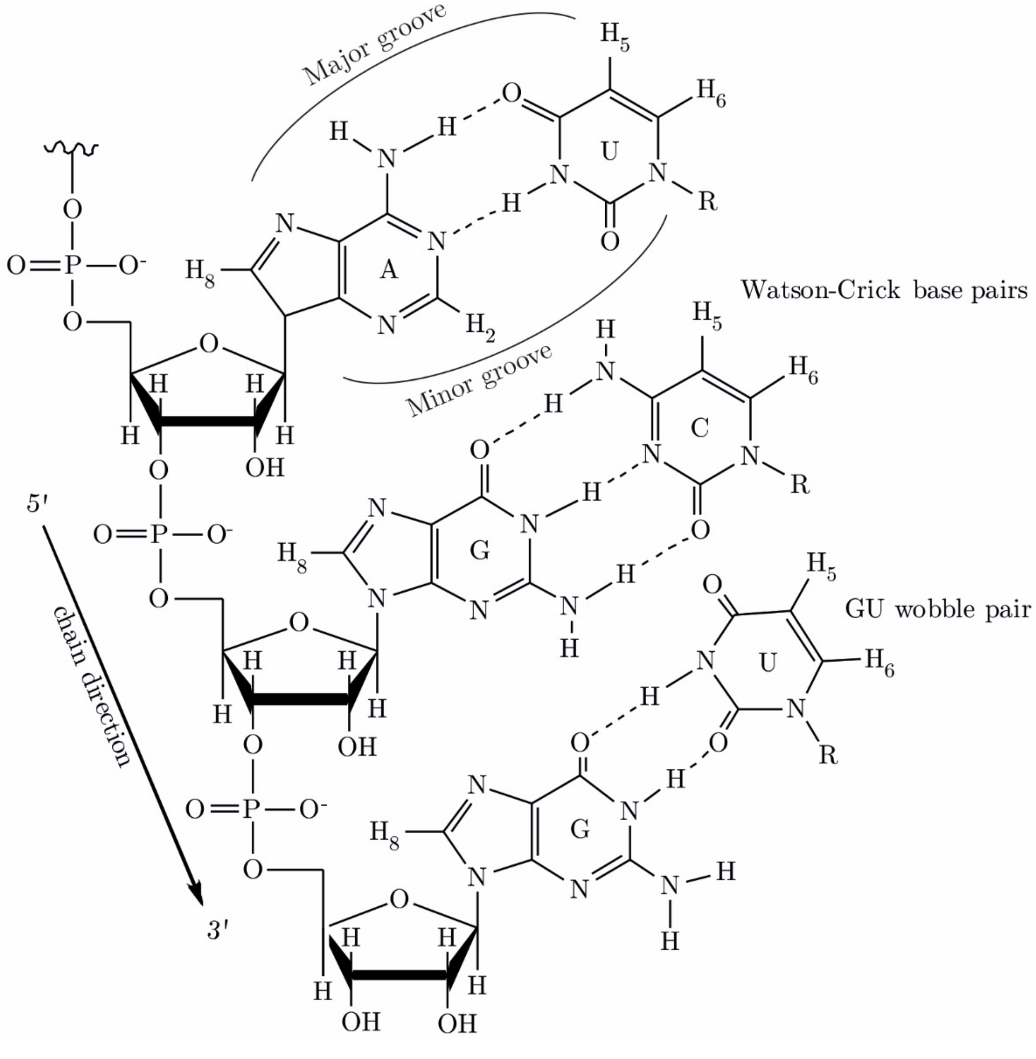

Figure 1.6 Schematic representation of an RNA strand with two canonical base pairs and a GU wobble. The location of the major and minor groove is also indicated for the AU base pair.

typical nucleobases for DNA are guanine (G), adenine (A), cytosine (C) and thymine (T). This last one is substituted by uracil (U) in RNA. The bases are divided in two subcategories according to their structure, purine and pyrimidine. A and G are part of the first one, while T/U and C belong to the second one. [44–46]

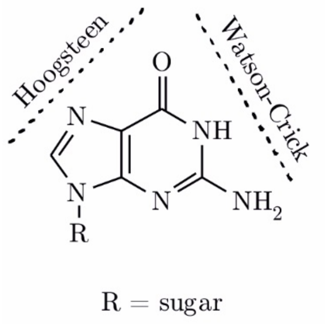

Figure 1.7 Representation showing the Hoogsteen and Watson-Crick sites.

The nucleobases are covalently linked to the sugar ring that differs from DNA to RNA for a 2'-hydroxyl group. This difference from 2'-deoxyribose for DNA to ribose in the case of RNA makes the latter one prone to self-cleavage via in-line nucleophilic attack on the neighbouring 3′-phosphate group, enabling RNA to exploit its catalytic activity. Moreover, this diversity is also responsible for their structural differences. [44,45]

Neighbouring nucleotides are bound through the phosphate groups that link the 5'-end of one sugar to the 3'-end of the next, creating the negatively charged backbone with its typical directionality (5′- to 3′-direction), as shown in Figure 1.6. The strand, that constitutes the primary structure of nucleic acids, ends with a hydroxyl group on the sugar moiety at the 3'-end and a terminal phosphate group at the 5'-end for both DNA and RNA. [44,45]

In general, nucleic acids are arranged in a double-stranded secondary structure, duplex, which results from the hybridization of complementary strands in an antiparallel way, forming the base pairs. In the canonical Watson-Crick base pairs G pairs with C and T/U pairs with A and they represent the most abundant ones. [47] Besides these, there are many other examples of non-regular base pairs. [44,47] For example, there are the Hoogsteen base pairs, in which a different edge of the nucleobase is involved in the hydrogen bond with respect to the Watson-Crick ones (Figure 1.7), and they are naturally occurring in both DNA and RNA or the G-U wobbles (Figure 1.6), present only in RNA. [44,47,48] Apart from the formation of hydrogen bonds between nucleotides, the π-π interactions between the stacked aromatic rings of neighbouring nucleobases play the most important role in the stabilization of the duplex. [44]

The formed duplexes can adopt various conformations, like A-, B- and Z-form, whose parameters are summarized in Table 1.1. [45]

Table 1.1 Some parameters for the A-form, B-form and Z-form helices of nucleic acids. [45]

	A-helical form	**B-helical form**	**Z-helical form**
Helix Sense	Right-handed	Right-handed	Left-handed
Average base pairs per turn	11	10.4	12
Helical pitch (Å)	32	34	45
Rise per base pair (Å)	2.9	3.4	3.7
Glycosidic angle	Anti	Anti	Anti/Syn
Sugar pucker	C3' endo	C2' endo	C2'/C3' endo
Helix diameter (Å)	25.5	23.7	45

In nature, DNA is typically found in B-form, while RNA in A-form (Figure 1.8) and this is strongly dependent on their sugar pucker conformation. Indeed, the presence of the 2'-OH group of ribose is forcing the RNA sugar into

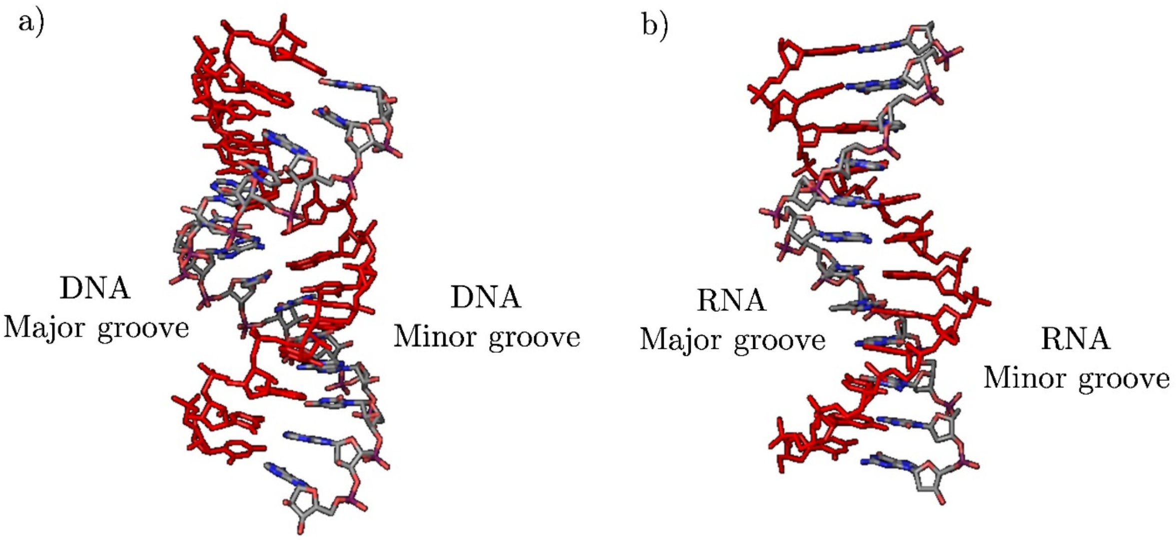

Figure 1.8 3D representation of a) B-DNA and b) A-RNA conformations obtained from pdb file 1BNA and 1RNA respectively. In both cases, one of the chains is represented in red and the other one is represented following the conventional colour code by atom.

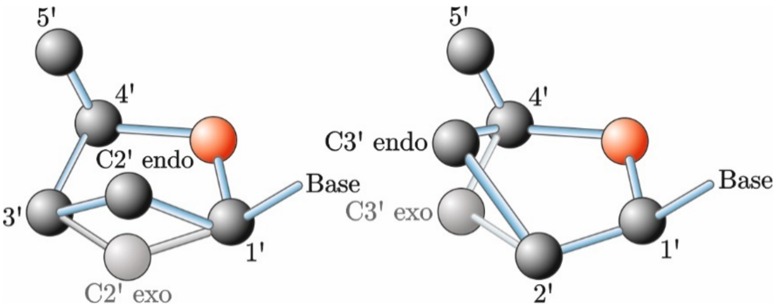

Figure 1.9 Representation of the sugar pucker conformations C2′ endo/exo and C3′ endo/exo.

a C3' endo conformation (Figure 1.9, right) giving rise to an A-form helix, while in DNA the sugar is in a C2' endo arrangement (Figure 1.9, left), that results in a B-form duplex. [17,46]

As shown in Figure 1.8, these two conformations differ in a way that DNA double helix has a wide major groove and a narrow minor groove, whereas RNA double helix has a deeper and narrower major groove and a wider shallow minor groove. Moreover, DNA is normally found in nature as double-stranded, while RNA is transcribed as a single strand and then it folds in a complex structure that includes double helical regions as well as bulges, loops, hairpins and junctions, as depicted in Figure 1.10. These non-helical regions are stabilized by stacking interactions and hydrogen bonds and can serve as binding sites for other molecules. [49]

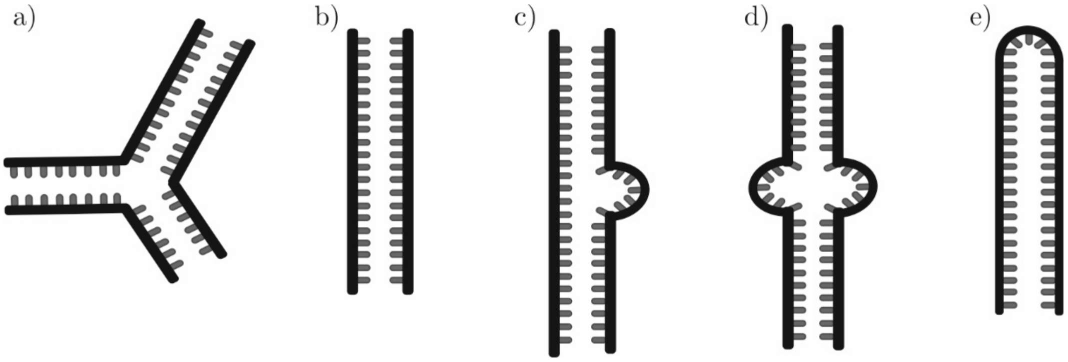

Figure 1.10 Schematic representation of some RNA secondary structural features like a) three way junction, b) double-stranded helix, c) bulge, d) internal loop and e) hairpin.

This wide variety of secondary structural features gives to RNA the possibility of creating tertiary interactions which are crucial for the RNA folding and consequently for the fulfilment of its functions. [4,49,50]

1.6. Our RNA and DNA model systems

In the current study, we used two RNA constructs and a DNA one. The first RNA sequence is called RNA-l and its secondary structure is shown in Figure 1.11 (right). It is 27 nucleotides long and derives from the domain 1 of the mitochondrial group II intron *Sc.*ai5γ from *Saccharomyces cerevisiae.* In its structure, it contains two artificially inserted regions. One is represented by the UUCG tetraloop, marked with stars, that serves to stabilize the whole construct. [10] The other one corresponds to the two consecutive GC base pairs at the beginning of the construct (in grey) added to increase the transcription yield. [51] Moreover, it contains an 11 nucleotides long asymmetric internal loop highlighted with italic letters. The loop starts with a GU wobble base pair, its core is made of three stacked adenines (in magenta) in a zipper like conformation and a UU mismatch (in green). [10,11] This loop is biologically relevant as it is

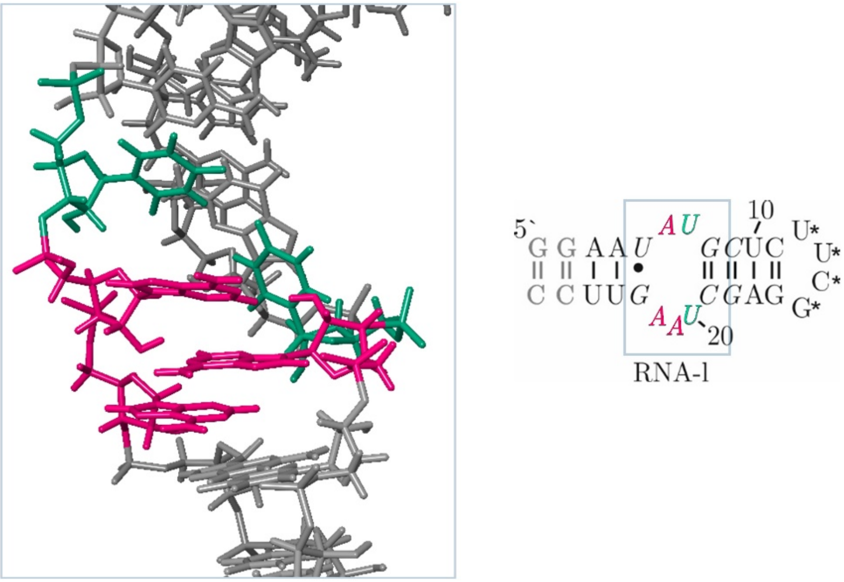

Figure 1.11 On the right, the secondary structure of RNA-l is represented. In grey are highlighted the first two base-pairs added to increase the transcription yield. The UUCG loop added for stabilization reasons is marked with stars, and the internal loop with italic letters. On the left there is the NMR solution structure of the internal loop of RNA-l. In both structures, A6, A21 and A22 are highlighted in magenta and U7 and U20 in green.

part, along with the κ element, of the κ-ζ region of the *Sc*.ai5γ group II intron that represents a relevant tertiary folding contact, [8,9,14] as it will be discussed more in depth in the next section. Moreover, the structure of the internal loop (Figure 1.11, left) is much different from the one of canonical Watson-Crick base pairs. Thanks to their particular structural conformation, internal loops are reported in the literature for providing potential binding pockets for selective recognition by small molecules. [4,14,50,52,53] The presence of the internal loop, as well as the other widespread RNA secondary structural features, such as GU wobble and terminal loop, makes this construct a very interesting model system for our studies. In addition, its NMR structure in solution is available, [11] making easier the evaluation of possible structural changes upon binding of metal ions and metal complexes.

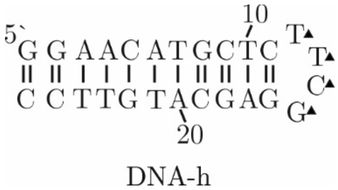

Figure 1.12 Secondary structure of DNA-h. The TTCG tetraloop is highlighted with blank triangles.

The second RNA construct is named RNA-h, it is 26 nucleotides long and it was designed as modification of RNA-l. As shown in Figure 1.13, in this construct two consecutive Watson-Crick base pairs substitute the five nucleotides of the internal loop to probe the role of this feature in the interaction. The rest of the sequence was kept unchanged. Indeed, the UUCG terminal loop, the GU wobble base pair and the two GC base pairs at the 5'-end are still part of the construct.

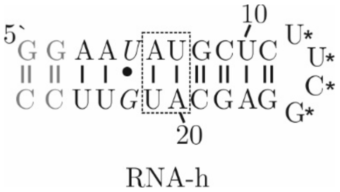

Figure 1.13 Secondary structure of RNA-h. In grey are highlighted the first two base-pairs added to increase the transcription yields. The UUCG loop added for stabilization reasons is marked with stars, the GU wobble base-pairs with italics letters. Finally, the box is used to highlight the base pairs which substitute the internal loop.

Finally, DNA-h in Figure 1.12, is also part of our studies and it was used to evaluate the binding behaviour of complex 1 with a short DNA sequence. This construct is the DNA analogous of RNA-h, it is 26 nucleotides long and contains a TTCG terminal loop.

1.7. RNA-l as part of the group II Intron *Sc.*ai5γ

RNA-l is not only important as an RNA model system containing widespread RNA structural features, but also for its role in the group II intron ai5γ from *Saccharomyces cerevisiae*, whose secondary structure contains six domains (D1-6, Figure 1.14). [54] D1 along with D5 represents the minimal catalytic core of this intron. [55] Indeed, D5 is a highly conserved hairpin that contains functional groups that are essential for catalysis and for its binding to other domains. [55] D1 is an independent folding unit, that forms a platform for other domains to dock. [56] RNA-l includes the ζ region highlighted with bold letters in Figure 1.14 and naturally occurring in D1. Within this domain, the ζ element, along with the κ element in grey letters, forms the κ-ζ region that is crucial for the initial compaction of D1 then followed by the folding of the whole group II intron. [12,13] The ζ region, consists in an internal loop that can act as a receptor for the

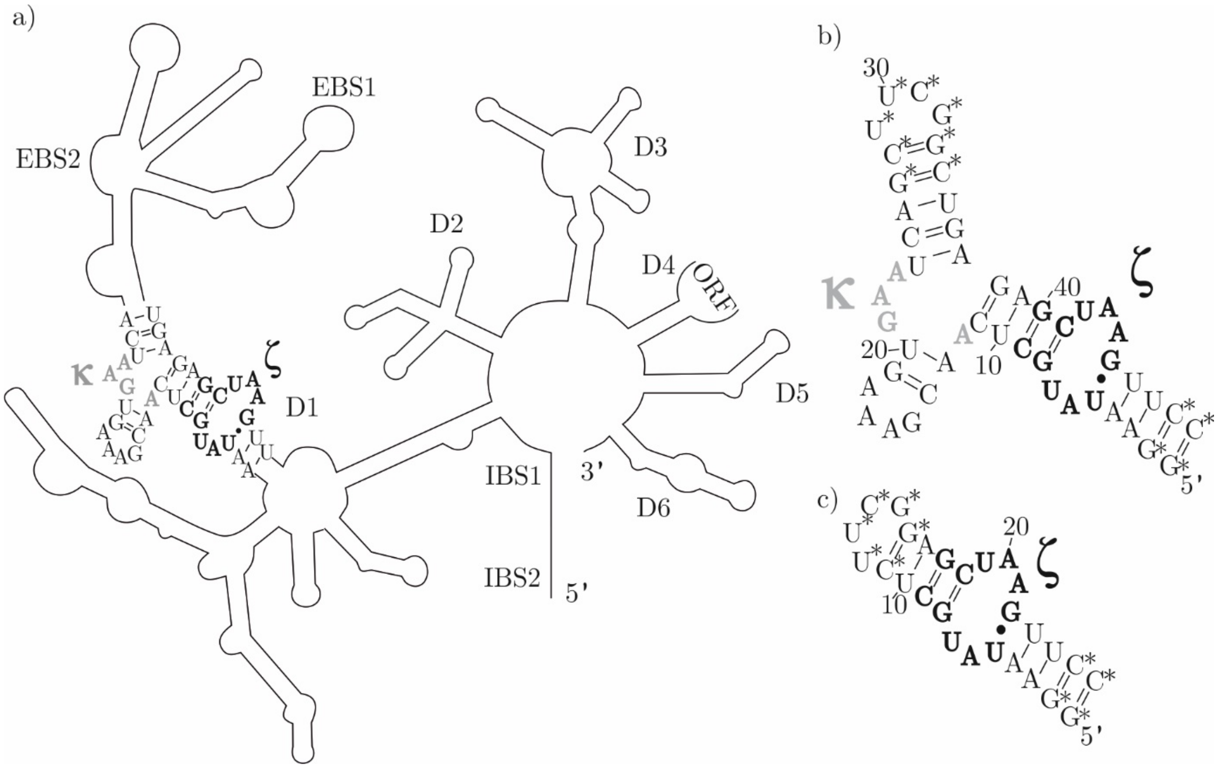

Figure 1.14 a) Secondary structure of the group II intron *Sc.*ai5γ with the κ-ζ region highlighted. The structure contains six domains (D1-D6) that originate from a central wheel. D4 may contain an open reading frame (ORF); b) secondary structure of D1κζ; c) secondary structure of RNA-l. κ and ζ are highlighted in grey and bold respectively. All the base pairs added to stabilize the constructs and to help the transcription are marked with stars.

GAAA tetraloop in the context of the whole intron. [54] Generally, GNRA (where N is any nucleotide and R is a purine) tetraloop-receptor interactions represent crucial tertiary folding motifs that are well studied in the literature. [10,14,57–59]

The structure of D1κζ (panel b in Figure 1.14) that includes RNA-l was solved via NMR in solution.[10] Moreover, its need for metal ions was investigated in depth, showing that Mg(II) ions allow this region to adopt the correct structure, [8,10] ensuring a precondition to have tertiary interaction with D5 and hence catalytic activity. [12,13] This result gives a great example of the importance of metal ions for the RNA structure and consequently function, that will be discussed more in depth in Section 1.8. Moreover, more studies using Mg(II) mimics such as Cd(II) and Co(III)hexammine were exploited to identify the Mg(II) binding sites in D1κζ. Interestingly, besides the strong binding at the 5'-end triphosphate due to the formation of macrochelates in the presence of Cd(II), all of the many remaining interaction sites, mostly located in non-canonical RNA regions, were equally accessible. [8] Hence, to evaluate more in detail the metal ion binding properties of the internal loop, NMR experiments were recorded on the isolated ζ region, [9] as it is presented in Section 2.7.

1.8. The crucial role of metal ions in RNA structure and function

RNA can adopt a very wide and complex variety of structures that cannot be achieved in the absence of metal ions. [60] Metal ions play many important roles, spanning from helping to obtain a correct secondary structure and to assist the folding, to the involvement in RNA functions. [60] Indeed, they are needed to counterbalance the negative charge of the phosphate backbone. The monovalent ions are usually responsible for this charge neutralization, enabling the formation of the secondary structures, [61] whereas the divalent ions stabilize the tertiary structure. [61,62] Upon RNA folding, the phosphate groups of the backbone become closer in space and intensify the negative charge density, creating preferential binding pockets for metal ions. [63,64] The stability of an RNA structure depends on both aspects, the neutralization of the phosphate charges and the site specifically bound metal ions.

Among the most important metal ions in the cellular environment, we find K(I) and Mg(II). [63] The first one is the most abundant intracellular monovalent ion and it is essential to neutralize the RNA charges allowing the pre-organization of the structure. [37] However, its role it is not limited only to charge screening, [65] since, for instance, it has been reported that ribosomal RNA unfolds upon reduction of K(I). The latter metal ion, Mg(II), is considered a crucial divalent metal ion in the cell as RNA co-factor since it takes part in RNA folding and catalysis. [54,66] An example of its involvement in catalysis is represented by the two-metal ion mechanism for the phosphoryl transfer reactions catalysed by the group I and group II introns. In this case, Mg(II) ions have a two-fold role, on the one hand they activate the attacking nucleophile and on the other hand they stabilize the leaving group. [67]

Due to the importance of metal ions, there are many studies in the literature on their RNA binding properties. [8,37,39,51] These are performed by means of a wide variety of methods, including NMR, that represents the main technique used in this thesis and it will be briefly discussed in the following section.

1.8.1. NMR Spectroscopy to study metal ion binding sites

As described in the previous section, K(I) and Mg(II) are the most relevant physiological metal ions interacting with RNA. Since both of them lack of easily exploitable spectroscopic properties, their RNA interactions have often been studied via NMR evaluating indirectly their effect on the RNA structure. [51,68] Indeed, it is common to map the chemical shift perturbations or the line broadening effects induced by the presence of metal ions on RNA resonances. [8,68] In some cases, from such indirect detection methods it is possible to obtain more than the simple localisation of metal ions binding sites. For instance, it is possible to determine the affinity of a metal ion for a site via the analysis of the chemical shift changes of the proton resonances affected by an interaction during a titration. [37] Besides ^{1}H NMR, also ^{15}N chemical shift mapping has been applied to study metal ion binding to RNA and large chemical shift changes of N7 upon metal ion addition can in some cases indicate inner sphere interaction (Figure 1.15). [8,9,37,69,70]

Sometimes, Mn(II), Cd(II) and cobalt(III)hexammine are used in order to mimic Mg(II) binding, whereas Tl(I) and NH_4^+ to mimic K(I) binding. [9,71] In particular, Mn(II) and Cd(II), due to their stronger polarizability, are favoured

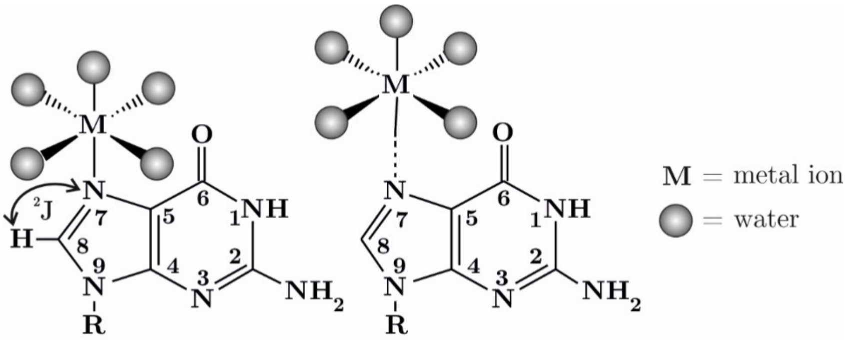

Figure 1.15 Inner sphere (left) and outer sphere coordination (right) of metal ions to a guanine–N7 are here depicted. The ^{2}J coupling observed between, e.g., N7 and H8 with [^{1}H,^{15}N]-HSQC experiments is indicated for the inner sphere binding example.

to interact via inner sphere coordination, or direct binding to the nucleobases, which normally occurs with the purine N7 (Figure 1.15, left). On the contrary, cobalt(III)hexammine with its kinetically inert ligands interacts via outer sphere interaction (Figure 1.15, right). [51,68]

1.9. NMR spectroscopy of RNA interaction with small molecules

NMR is a very powerful technique that can provide with many different kind of information, such as distances between nuclei, scalar couplings, chemical shifts, relaxation times, and diffusion coefficients. In the literature NMR spectroscopy has been used not only to obtain structural data but also information about dynamics. [36,72–75]

In this thesis we used the following experiments to obtain data on the interaction of our nucleic acid constructs and metal complexes.

1D ^{1}H NMR experiments on the exchangeable protons, recorded in H_2O/D_2O, were used as a fast check to obtain indications on the secondary structure of the nucleic acids and to gain a first qualitative insight into the binding, as it will be further discussed in Section 1.9.2. These data were also supported by 1D ^{1}H NMR experiments in D_2O.

Then, for a deeper investigation, 2D experiments were used. [^{1}H,^{1}H]-NOESY spectra recorded in D_2O gave information on the distances of non-exchangeable protons. In this experiment, the magnetization is transferred via space thanks to the Nuclear Overhauser Effect among nuclei that are close enough (up to 5-6 Å). This transfer of magnetization results in cross peaks in the 2D spectrum. Their intensity is proportional to the interatomic distance and gives important structural data, as described at greater length in the next section. [76]

Besides [^{1}H,^{1}H]-NOESY spectra, other 2D NMR experiments are crucial to confirm the assignment of the resonances of a nucleic acid and are useful to evaluate the interaction with other molecules. For instance, [^{1}H,^{1}H]-TOCSY experiments were used to complement and confirm what observed in the [^{1}H,^{1}H]-NOESY experiments because they are easier to interpret being the resonances in the spectrum generally less overlapped. Indeed, only the connections between H6 and H5 protons, along with some other intramolecular connections among the sugar protons, like for instance H1'-H2'/H3', are observed. [72–75]

^{2}J-[^{1}H,^{15}N]-HSQC spectra (^{2}J coupling observed between, e.g. N7 and H8 is indicated in Figure 1.15) were used to assign the purine nitrogen, such as N1, N3, N7 and N9. These experiments normally show well dispersed cross peaks and they are interesting since N7 atoms often can act as direct coordination sites for metal ions. [8,9,69,70] For these reasons, in this thesis they were used to obtain a clear evaluation of the chemical shift changes upon interaction to identify metal ion and metal complex binding sites.

Other NMR experiments are interesting tools to characterize the binding between small molecules with macromolecules, such as DOSY (Diffusion Ordered SpectroscopY) NMR and STD (Saturation Transfer Difference) NMR. For instance, DOSY NMR experiments [77] are widely exploited in interaction studies. This method is based on the application of a gradient field, which allows to monitor the translational diffusion motion of the components of a sample. This technique was herein used to qualitatively evaluate the intermolecular interactions of our metal complexes with RNA (Section 2.11.2), [78] but it can also be used to calculate the diffusion coefficients of the single species in a mixture. [79] STD experiments are also generally used to study the interaction of macromolecular receptors with small ligands. [80,81] In the early stages, this technique was exploited to fast-screen compound libraries, [81] whereas nowadays it is also used to calculate dissociation constants and, as done in this thesis (Section 4.1), to obtain information on the proximity of the protons of a ligand to the ones of a receptor. [82,83]

1.9.1. [^{1}H,^{1}H]-NOESY spectra in D_2O

[^{1}H,^{1}H]-NOESY experiments are essential to characterize and to obtain the 3D structure of nucleic acids. In RNA helical regions it is possible to find a characteristic pattern of cross peaks arising from the fact that the aromatic protons H6 and H8 are spatially close to their own H1' proton, and also to the H1' of the upstream 5' nucleotide.

Hence, following this connectivity along a nucleic acid strand, as indicated by means of red arrows in Figure 1.16, it is possible to assign the sugar protons H1' and the aromatic protons H6/H8 of the whole construct. This path is named "sequential walk" because it allows to assign a polynucleotide chain by "walking" from nucleotide to nucleotide. [76]

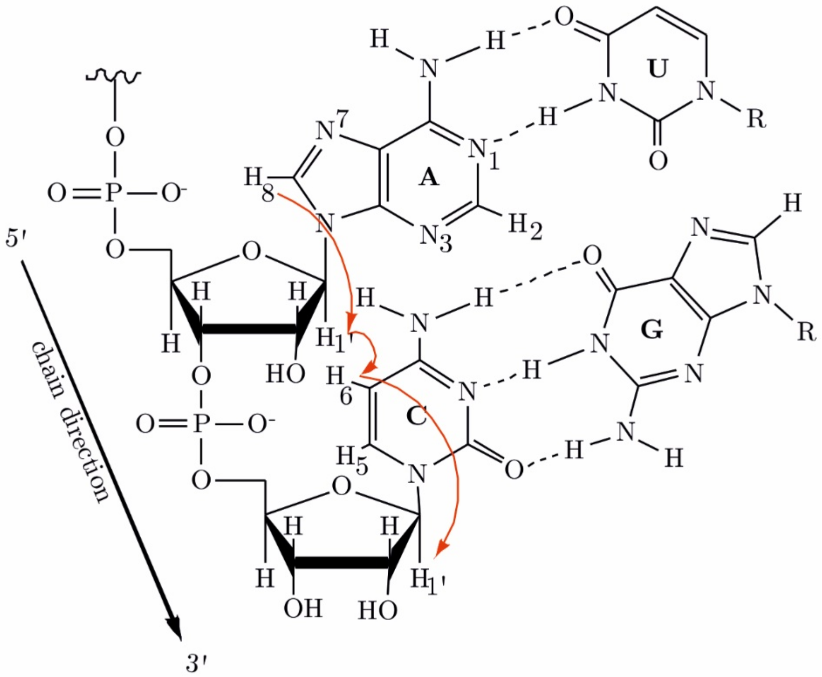

Figure 1.16 Example of sequential walk path. Through-space connections are indicated with red arrows. The base pairs AU and GC are examples of stable hydrogen bonds in canonical Watson-Crick base pairs.

In a [^{1}H,^{1}H]-NOESY spectrum there are other interesting NOE correlations that not only assist and confirm the assignment, but also give information on the stacking, on the inter-helical proximity, and on the conformation of the non-canonical regions. Indeed, for instance, it is possible to observe cross peaks for H2' and H3' to H6/H8 adding data on the position of a nucleobase and its own sugar. We can also observe NOE connections between aromatic protons, e.g. H2 to H6/H8, of different nucleotides that can give information on their stacking. Another example is represented by the cross peaks that involve H2 protons of adenines. These are the only non-exchangeable protons in regular Watson-Crick base pairs that point away from the own sugar-phosphate backbone and thus, they are potentially able to provide with valuable inter-strand connections. [36,72–75]

1.9.2. ^{1}H NMR spectra in water: a strategy to confirm the secondary structure and gain insights into the binding

1D ^{1}H NMR and [^{1}H,^{1}H]-NOESY experiments in water are usually used to confirm the secondary structure of a nucleic acid. Indeed, imino protons exchange very fast with the solvent and can be observed only if they are engaged in stable hydrogen bonds, as represented in Figure 1.16. [84] 1D ^{1}H NMR experiments in water represent one of the most exploited tool in this thesis, since, although they are very simple, they can give very precious information. As it will be discussed in the next chapter, first and foremost, 1D ^{1}H NMR spectra were used to provide information on the quality of the RNA and DNA samples because only a well-structured non-degraded sample could show the correct number of imino signals. Then they were exploited as preliminary evidence of binding. This was possible because the imino proton resonances of our nucleic acid constructs were well resolved and quite intense under the conditions chosen for the interaction studies, allowing a good evaluation of their changes. Titrations with several additions of metal complex into RNA solutions were performed, which enabled to identify the presence of a localised interaction site to be then further investigated using 2D NMR experiments. Hence, 1D ^{1}H NMR spectra in water were an essential tool that opened a cascade of more in depth studies on the systems that were at first sight more promising and interesting.

1.10. Thesis structure

This thesis intends to study in depth the interaction between a Re(I)dppz complex, namely [Re(CO)$_3$(dppz)(3-CH$_2$OH-Py)]$^+$ (complex 1), and RNA-l and RNA-h, using also ruthenium complexes and a DNA construct for the sake of comparison (structures in Figure 1.1 and Figure 1.3). The main technique used is NMR spectroscopy, whose findings are presented in the next chapter (Chapter 2). The NMR data on the metal ion binding sites come from a recent publication [9] from Bartova *et al.* in which I took part. Moreover, optical studies and ITC experiments were exploited to complement this investigation and the results obtained are collected in Chapter 3. The latter ones were performed by Dr. Miquel Barceló-Oliver (University of Balearic Islands). The study of the binding site of complex 1 and RNA-l was also investigated via molecular dynamics (MD), supported by NMR experiments, as described in Chapter 4. The MD simulations were performed by Prof. Dr. Giampaolo Barone and Dr. Angelo Spinello (University of Palermo). Finally, in the last chapter (Chapter 5), the preliminary results on the synthesis of a novel Re(I)dppz complex, designed to overcome the water solubility issues encountered using complex 1, are described. This work was carried out during a research project with the master student Severin Koch.

2. RNA binding sites for metal ions and metal complexes: an NMR study

This chapter mainly deals with the study of the interaction of metal ions and complex 1 [15] with RNA-l (Figure 2.1a). RNA-h, DNA-h, (Figure 2.1b/c) as well as complex 2 and 3 (Figure 2.1e/f) were exploited as comparison to confirm some crucial findings.

Prior to any interaction study, it was necessary to characterize all the constructs involved in this study and assign their NMR resonances.

2.1. Assignment of the non-exchangeable proton resonances of RNA-l in PBS

[^{1}H,^{1}H]-NOESY experiments were used to assign the resonances of RNA-l in the sequential walk area, where the connections between the sugar proton H1' of a nucleotide and the H8/H6 proton of the next nucleobase are observed. As described in Section 1.9.1, following this pattern allows to "walk" through the RNA structure linking the residues that compose the nucleic acid strand. RNA-l, whose importance is discussed in Section 1.7, is 27 nucleotides long, a suitable length for 2D NMR characterization that results in [^{1}H,^{1}H]-NOESY spectra with a good signal dispersion. This construct comprises two stable helical regions, whose NOE peaks are well resolved and intense, connected by an internal loop that is more dynamic and gives broader and less strong connections. This latter

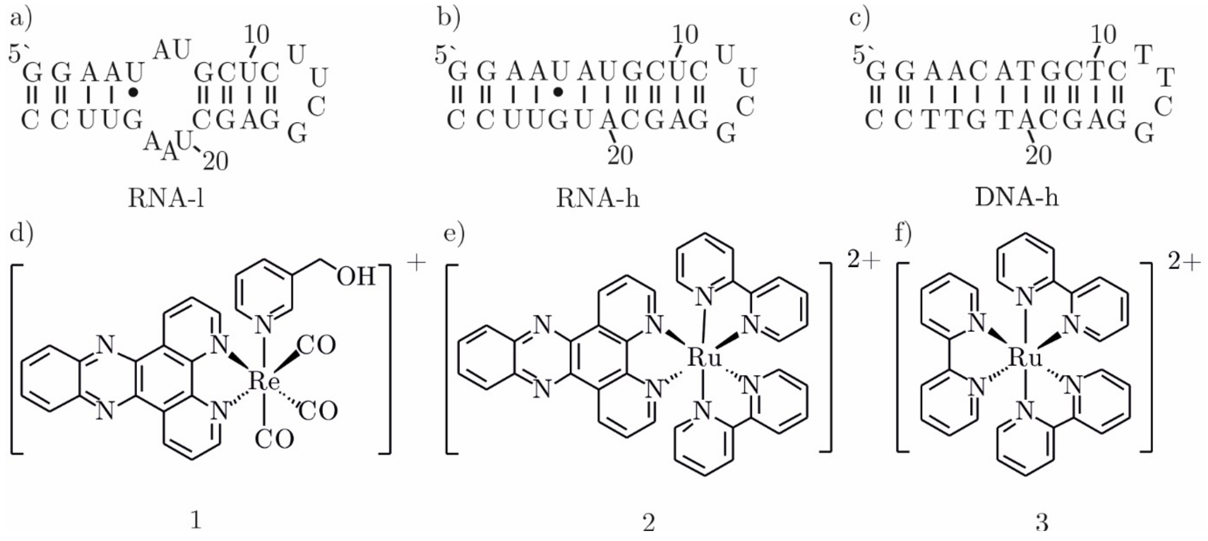

Figure 2.1 Secondary structures of a) RNA-l, b) RNA-h and c) DNA-h and chemical structures of d) [Re(CO)$_3$(dppz)(3-CH$_2$OH-py)]$^+$ (1), e) [Ru(bpy)$_2$(dppz)]$^{2+}$ (2) and f) [Ru(bpy)$_3$]$^{2+}$ (3).

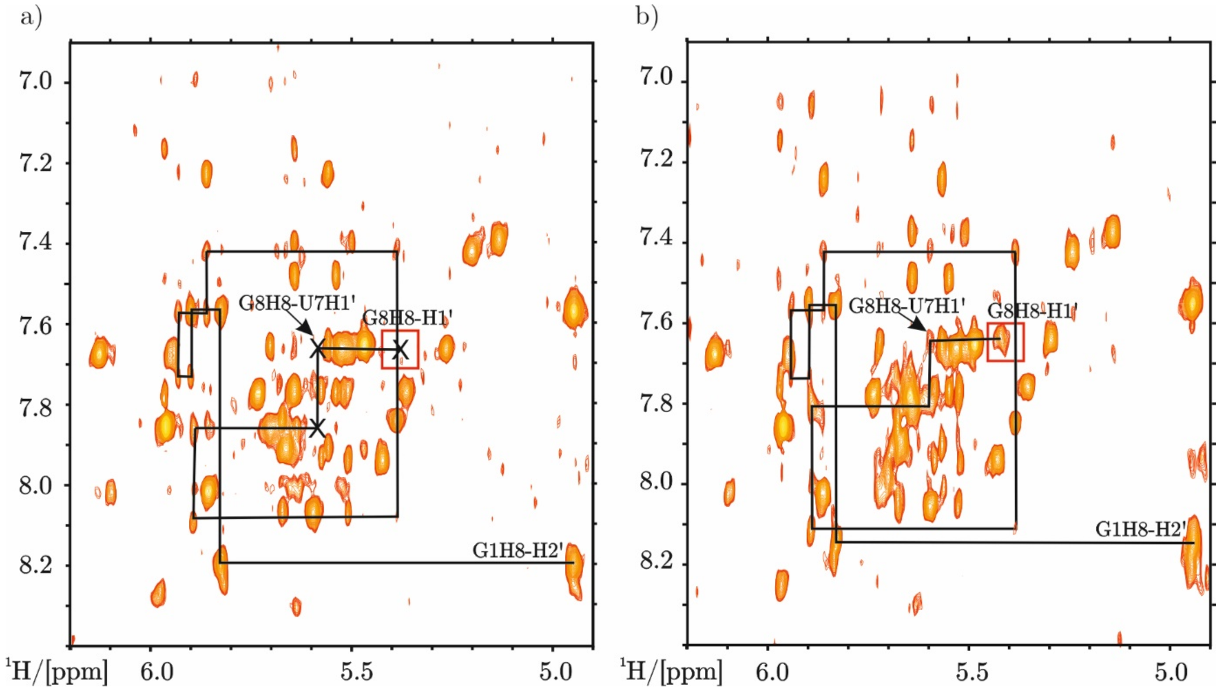

Figure 2.2 $[^1H,^1H]$-NOESY (sequential walk region) of a) RNA-l 0.22 mM, PBS, pD 7.4, 298 K, 700 MHz and b) RNA-l 0.35 mM, PBS, pD 6.7, 303 K, 700 MHz.

region consists of three stacked adenines and a UU mismatch. Moreover, RNA-l has a UUCG tetraloop, known to be a particularly stable RNA motif [85] that gives rise to peculiar cross peaks already reported in literature. [74,86,87] The NMR structure in solution of RNA-l was previously solved in the group of Prof. Dr. Roland K.O. Sigel in 60 mM KCl, pH 6.2-6.3, at 303 K. [11] However, in this thesis, as the interaction of complex 1 and CT-DNA was studied previously in PBS, [15] we decided to adopt this buffer as solvent for our studies for the sake of comparison. Being the internal loop region of RNA-l very dynamic and sensitive to pH and temperature, we performed experiments to find the best conditions in PBS to observe all of the RNA NOE signals. Figure 2.2a shows the sequential walk region of a $[^1H,^1H]$-NOESY of RNA-l recorded in PBS with pH 7 at 298 K. The sequential walk path is interrupted at U7H6-H1' and some of the NOE contacts of the internal loop are not visible. On the contrary, in the $[^1H,^1H]$-NOESY spectrum recorded on RNA-l in PBS with pH 6.2-6.4 at 303 K it is possible to follow the sequential walk connections through the whole RNA sequence and fully assign this region of the spectrum (Figure 2.1b, assignment

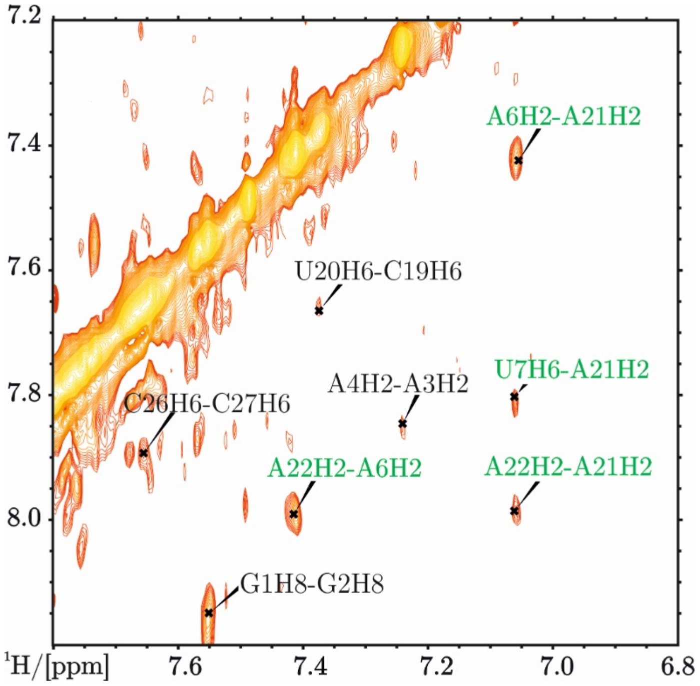

Figure 2.3 Section of [^{1}H,^{1}H]-NOESY of RNA-l (0.35 mM, PBS, pD 6.7, 303 K, 700 MHz).

in Appendix 1). Moreover, these latter conditions enabled us to observe and assign some NOE correlations, such as A6H2-A21H2, U7H6-A21H2, A22H2-A21H2 and A22H2-A6H2, labelled in green in Figure 2.3 that confirmed the formation of the stacked internal loop structure. These [^{1}H,^{1}H]-NOESY spectra look overall similar to the ones in the presence of KCl used to calculate the structure. [11]

2.2. Assignment of the exchangeable proton resonances of RNA-l in PBS

Imino proton resonances reflect the stability of the base pairs, hence a signal is observed only if the hydrogen bond between two nucleotides is stable. Eleven signals are visible in the imino proton region of the spectrum of RNA-l in water at 293 K (Figure 2.4). Seven of these peaks, one of which is due to the overlap of two resonances (U10H3 and U24H3), are ascribed to the eight regular Watson-Crick base pairs present in the construct. Among these signals, lower intensity and wider linewidth is observed for G1H1, that corresponds to the first base pair in the sequence, a rather flexible area, and for G8H1 that is right after the core of the dynamic internal loop region. This latter motif does not give

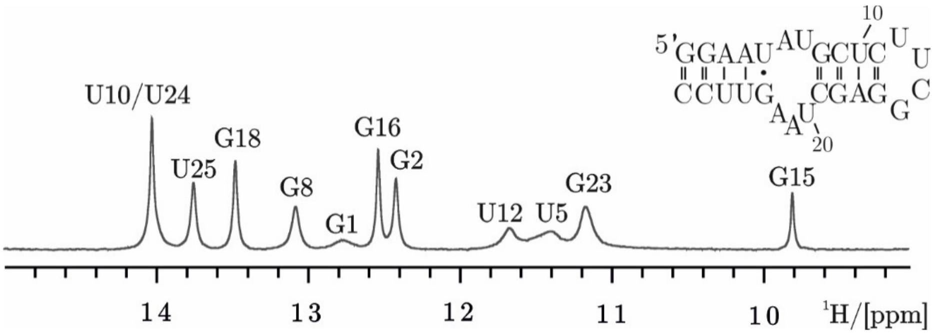

Figure 2.4 Imino proton region of ^{1}H spectra of RNA-l (0.2 mM, PBS, pD 6.7, 293 K, 600 MHz) with assignment.

signals in this region, whereas the terminal UUCG loop shows two upshifted peaks, one very broad at 11.6 ppm (U12H3) and a sharper one at 9.8 ppm (G15H1). This last resonance can be considered a diagnostic signal for the formation of the hairpin. Finally, the two remaining resonances (U5H3 and

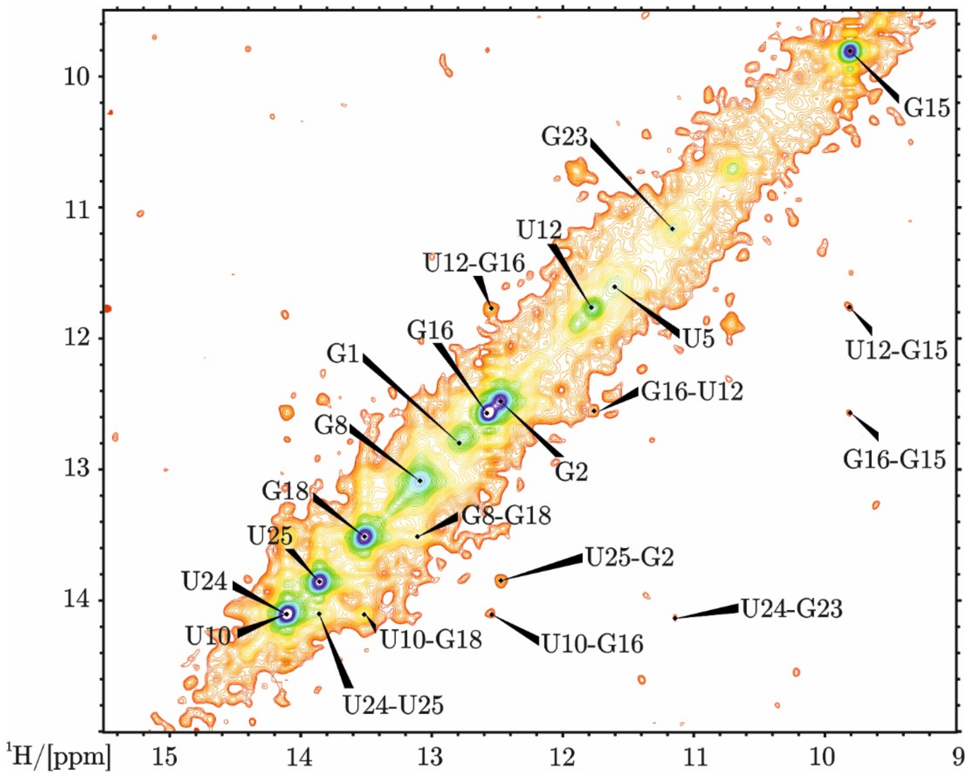

Figure 2.5 Section of [^{1}H,^{1}H]-NOESY (imino proton region) of RNA-l (0.2 mM, PBS, pH 7.2, 278 K, 600 MHz) with assignment. Overall, the intensity of the signals is weak and the assignment was confirmed with experiments in 60 mM KCl that showed a better signal to noise ratio.

G23H1) between 11 and 12 ppm are due to the non-canonical base pair of the sequence, the GU wobble. [88] In general, at lower temperature all of the signals appear sharper and especially the upfield shifted peaks, U12H3, U5H3 and G23H1, as well as the one corresponding to G1, show significantly higher intensity and smaller linewidth. For this reason, the assignment was obtained using [^{1}H,^{1}H]-NOESY experiments in water recorded at 278 K (Figure 2.5) where the signals were stronger. The assignment was then extended to 293 K by comparison (Appendix 2). Taking into account that the higher the temperature, the less intense the imino signals, 293 K was chosen as a compromise temperature that allows to perform interaction studies and show rather intense signals.

2.3. RNA-l stability in PBS with DMSO

RNA-l resonances in the imino proton region were monitored at different DMSO concentrations to check the possible influence of the organic solvent on the RNA structure. DMSO is used when complex 1 is added to the RNA solution, owing to its poor water solubility.

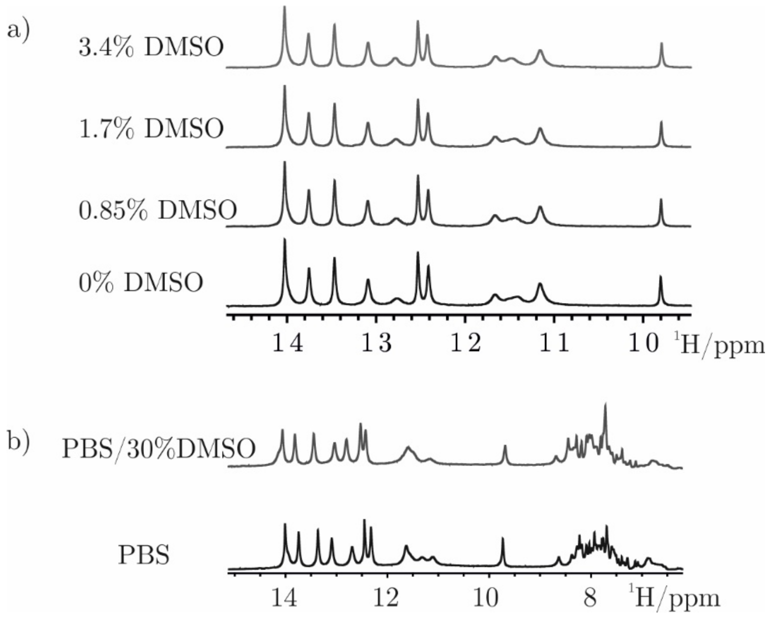

Figure 2.6 a) ^{1}H NMR spectra (imino proton region) of RNA-l in the presence of increasing amounts of DMSO up to 3.4 % (0.23 mM, PBS D_2O/H_2O, pH 7.1, 293 K, 600 MHz); b) ^{1}H NMR spectrum (imino and aromatic proton region) of RNA-l in the presence of 30% DMSO (0.1 mM, PBS, pH 7.1, 293 K, 500 MHz).

At little DMSO concentrations (up to 3.4% in Figure 2.6a), the RNA imino signals do not undergo any changes, suggesting that the RNA overall structure is maintained. Contrarily, in the presence of 30% of DMSO in PBS, all of the resonances are generally lower in intensity and some of them are slightly shifted. However, overall the RNA structure seems to be preserved and DMSO seems not to have a strong influence on the RNA structure.

2.4. Assignment of the non-exchangeable proton resonances of RNA-h in PBS

RNA-h is a 26 nucleotides long hairpin with a GU wobble motif and a UUCG tetraloop (Section 1.6, Figure 2.1b). Its short length and the absence of very dynamic regions, allowed to obtain a well resolved [^{1}H,^{1}H]-NOESY spectrum, whose sequential walk area was fully assigned, and the assignment confirmed by means of [^{1}H,^{1}H]-TOCSY experiments. Both 2D experiments were recorded at

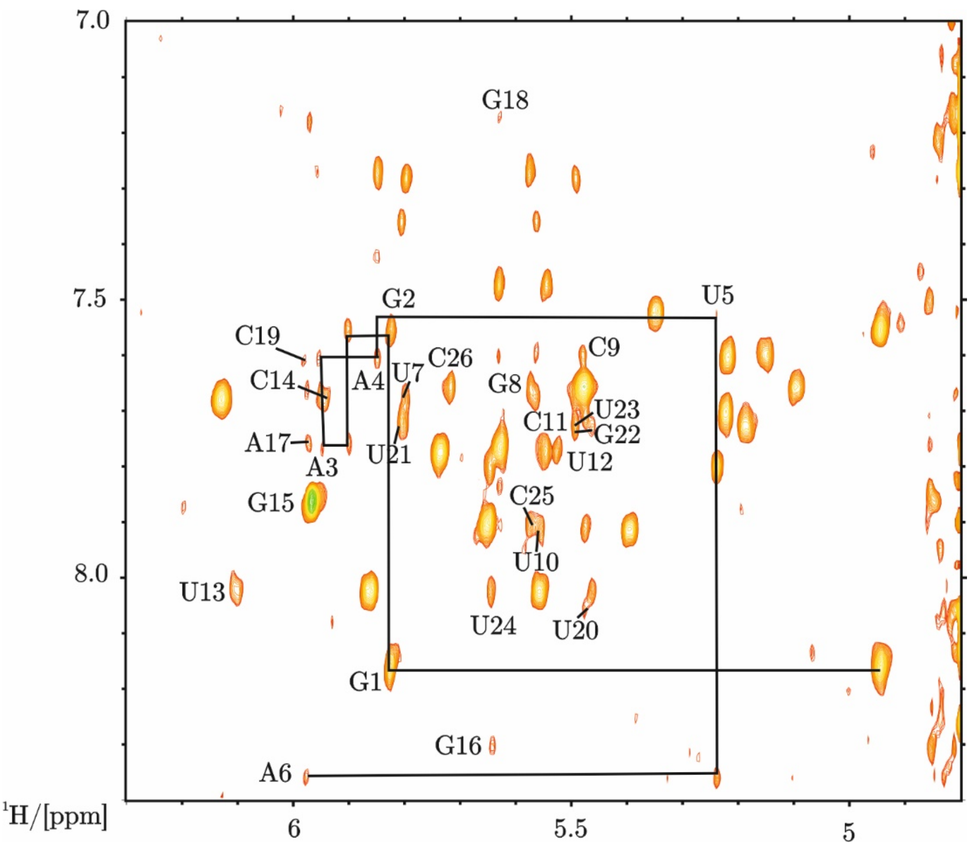

Figure 2.7 [^{1}H,^{1}H]-NOESY (sequential walk region) of RNA-h (0.14 mM, PBS, pD 6.9, 298 K, 700 MHz) with assignment and sequential walk path from G1 to A6 as an example.

298 K (Figure 2.7 and assignment in Appendix 3) and at 303 K without showing any significant difference.

2.5. Assignment of the exchangeable proton resonances of RNA-h in PBS

The ^{1}H NMR spectrum of RNA-h in water shows fourteen signals in the imino region (Figure 2.8), as expected from the RNA sequence. Ten peaks count for the ten regular Watson-Crick base pairs RNA-h is made up of. Nine of these peaks are sharp and intense due to their involvement in stable hydrogen bonds, whereas one, that corresponds to G1H1, shows little intensity and larger linewidth because it is located at the beginning of the sequence, as in the case of RNA-l. The remaining four signals are more upfield shifted in the spectrum and they belong to nucleotides placed in the UUCG loop, U12H3 at 11.6 ppm and G15H1 at 9.7 ppm, and to the GU wobble base pair, U5H3 at 11.4 ppm and G22H1 at 10.8 ppm. These last two signals are sharper than in the case of RNA-l, because RNA-h structure is more rigid. Indeed, the internal loop in the centre of RNA-l is a very dynamic motif that partially loosens the hydrogen bonding of the closest base pairs.

As in the case of RNA-l, we exploited the fact that at lower temperature the hydrogen bonds are more stable and the resulting peaks are more intense. Hence, the assignment was obtained using [^{1}H,^{1}H]-NOESY spectra in water recorded at 278 K (Figure 2.9) and, by comparison, extended to 293 K (Appendix 2).

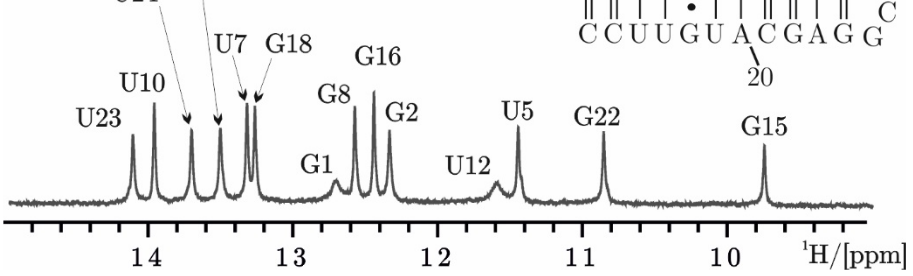

Figure 2.8 ^{1}H spectra (imino proton region) of RNA-h (0.2 mM, PBS, pD 6.7, 293 K, 600 MHz) with assignment.

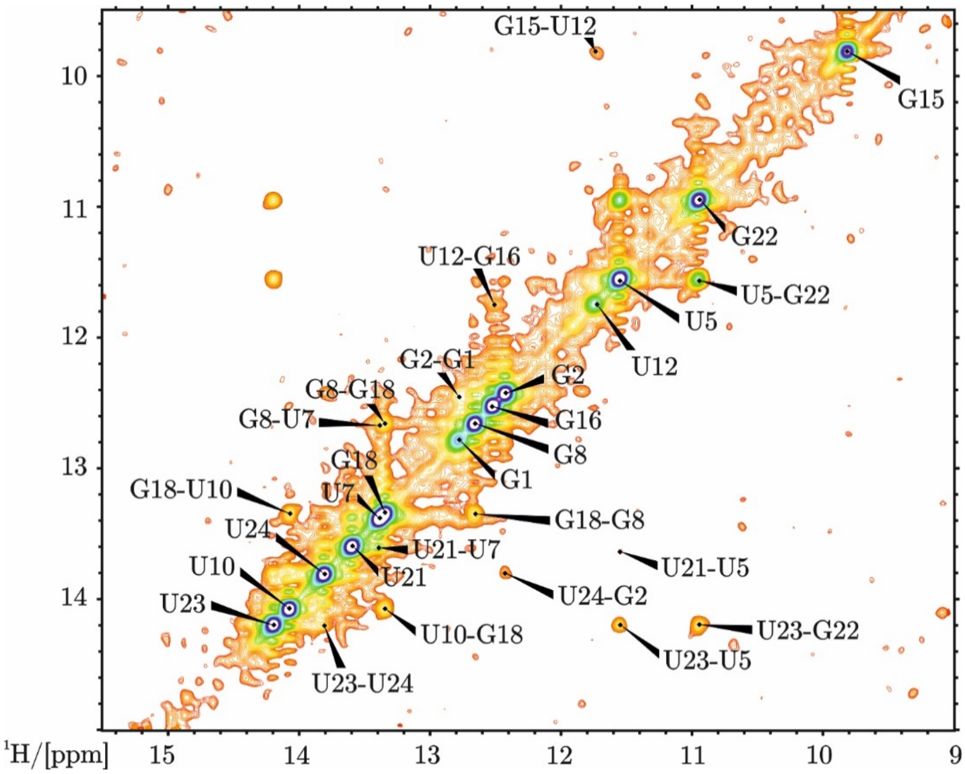

Figure 2.9 Section of [^{1}H,^{1}H]-NOESY (imino proton region) of RNA-h (0.2 mM, PBS, pH 7, 278 K, 700 MHz) with assignment. The overall intensity of the spectrum is weak and the assignment was confirmed via comparison to the one of RNA-l.

2.6. Assignment of the exchangeable proton resonances of DNA-h in PBS

DNA-h is a short DNA hairpin consisting of eleven base pairs and a TTCG closing loop (Section 1.6, Figure 2.1c). Although eleven signals should be visible in its ^{1}H NMR spectrum, only nine signals are observed (Figure 2.10). This is

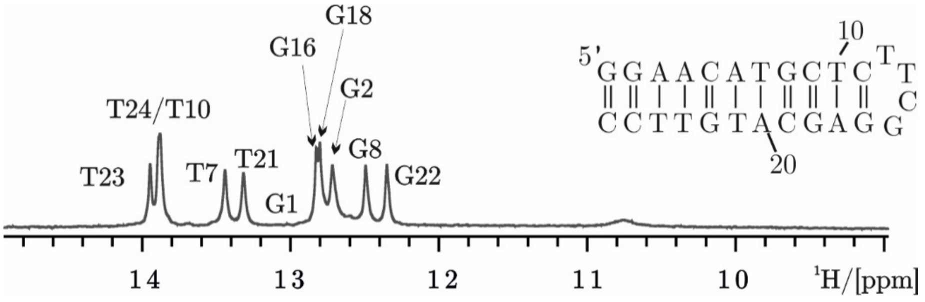

Figure 2.10 ^{1}H spectrum (imino proton region) of DNA-h (0.2 mM, PBS, pD 6.7, 293 K, 600 MHz) with assignment.

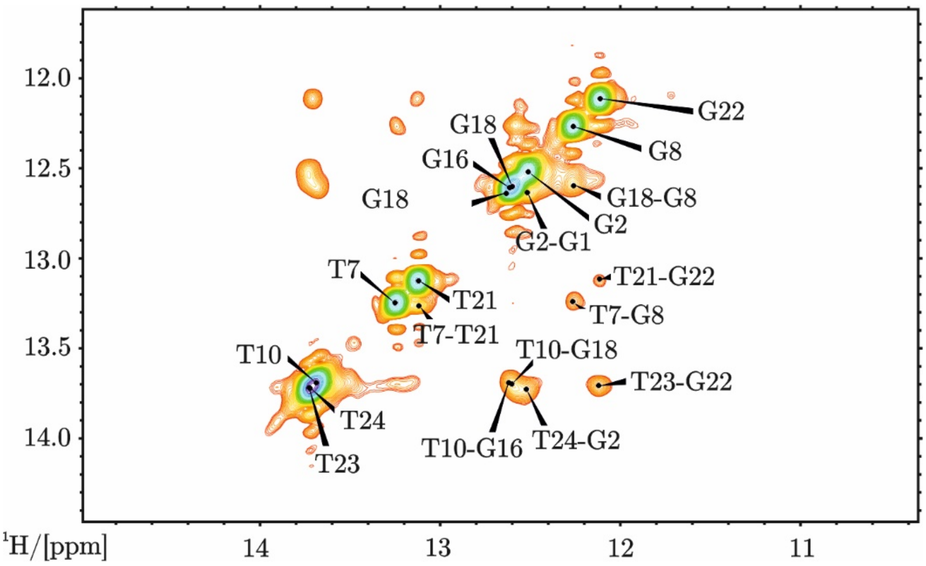

Figure 2.11 Section of [^{1}H,^{1}H]-NOESY (imino proton region) of DNA-h (0.1 mM, PBS, pH 7.2, 283 K, 700 MHz) with assignment.

due to the fact that one peak counts for two resonances, T24H3 and T10H3, and moreover G1H1 is very broad and almost not visible. No resonances are observable for the terminal tetraloop in this region. This behaviour is not unusual, indeed TTCG DNA loops are less stable than UUCG RNA loops and their structure is more flexible, and no imino signals are observable. [89]

Although the peaks are already quite intense at 293 K, we decreased the temperature to 283 K to obtain a better resolved spectrum, but no significant differences were observed. The assignment was anyway achieved using [^{1}H,^{1}H]-NOESY experiment at 283 K (Figure 2.11) and then extended to 293 K (Appendix 2).

2.7. Metal ion binding sites in RNA-l

As already described at greater length in Section 1.8, metal ions play a key role not only in RNA structure, but also in its function. Indeed, first of all they are needed to counterbalance the overall negative charge of the polyphosphate backbone, then they can also be allocated in specific binding pockets, and, moreover, they can be involved in catalysis. [39,90] It is very interesting to evaluate the metal ions binding behaviour in the presence of RNA-l because this construct possesses a twofold significance. Indeed, as already described in Section 1.7, it is part of the group II intron *Sc.*ai5γ and moreover, it offers many common RNA secondary structural features, such as a GU wobble, a UUCG tetraloop and an internal loop. This latter one is especially appealing since it might act as preferential interaction site or binding pocket.

NMR experiments, such as 1D ^{1}H NMR, ^{31}P NMR, ^{113}Cd NMR, ^{2}J-[^{1}H,^{15}N]-HSQC, [^{1}H,^{31}P]-HSQC-NOESY and [^{1}H,^{1}H]-NOESY were used to study the interaction of Mg(II), Cd(II), cobalt(III)hexammine and Mn(II) with RNA-l. [9] Mg(II) can bind to RNA in two ways, inner sphere or outer sphere binding (Section 1.8.1) Co(III)hexammine is used to mimic Mg(II) outer sphere binding, whereas Cd(II) the inner sphere one. Generally, the interpretation of RNA chemical shift changes upon metal ion addition is very challenging, because their variations can be due to a combination of factors such as direct binding, close by binding, or also metal induced conformational changes. Therefore, only a qualitative evaluation was done.

These metal ion binding studies were recently reported in a joint publication [9] with Simona Bartova, a visiting PhD student in the group of Prof. Dr. Roland K.O. Sigel. Below are reported some results that were used to predict potential binding sites of metal complexes in RNA-l. The figures of the following sections are adapted from the publication. [9]

2.7.1. ^{2}J-[^{1}H,^{15}N]-HSQC experiments to study the binding of Mg(II), Cd(II) and cobalt(III)hexammine to RNA-l

^{2}J-[^{1}H,^{15}N]-HSQC titration experiments were used to simultaneously follow chemical shift changes in N7/N9/H8 and N3/N1/H2 resonances. This kind of experiment shows a very good spectral dispersion making easier the evaluation of chemical shift changes. The inner sphere interaction at purine N7 represents the most reported direct binding site for metal ions and it results in strong upfield shifts of ^{15}N resonances. [69,70,91] Prior to any interaction assay (Figure 2.12), the purine ^{15}N resonances of RNA-l were fully assigned (Appendix 4).

In general, as shown in the bar plot in Figure 2.13, Cd(II) additions (spectrum in Figure 2.12) induce more significant chemical shift variations compared to

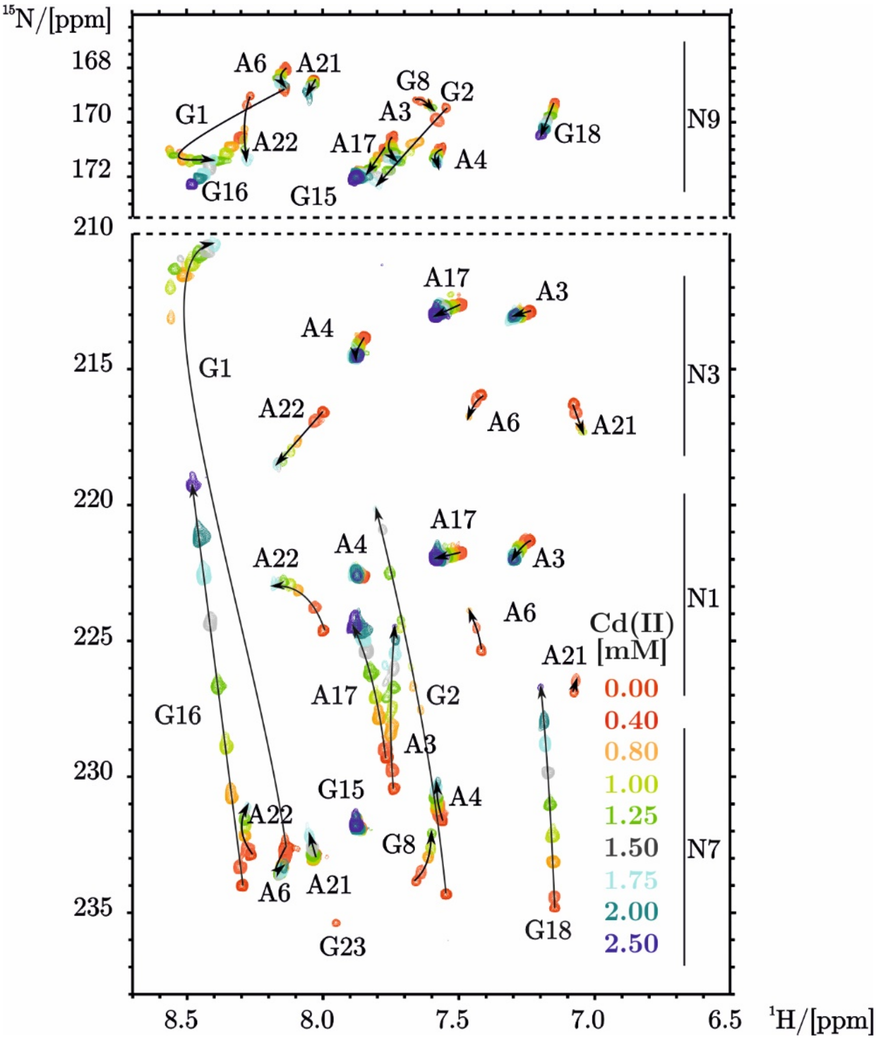

Figure 2.12 ^{2}J-[^{1}H,^{15}N]-HSQC spectrum of ^{15}N labelled RNA-1 titrated with increasing amounts of Cd(II) (0.9 mM, 60 mM $KClO_4$, pD 6.8, 300 K, 700 MHz). Arrows indicate a significant induced shift upon addition of Cd(II).

Mg(II) (spectrum in Appendix 5) and cobalt(III)hexammine (spectrum in Appendix 6). All investigated metal ions cause changes of the resonances of G8 and G18, which are part of the GAAA receptor, an important feature which allows tertiary contacts when the construct is part of a large ribozyme (Section 1.7). [14,49] The strong upfield shift of G18N7 ($\Delta\delta$ of about 8 ppm) upon Cd(II) binding suggests inner sphere coordination, whereas Co(III)hexammine causes a significant shift of H8 with no shift of N7 ascribable to outer sphere coordination or to close by coordination. [91] G18N7 resonance variations upon Mg(II) addition show a trend similar to Cd(II), but significantly weaker. This result can be due to either partial direct Mg(II) coordination at G18N7 or to coordination close by. Concerning the resonance G8N7, all metal ions influenced its chemical shift in a comparable way causing line broadening likely due to

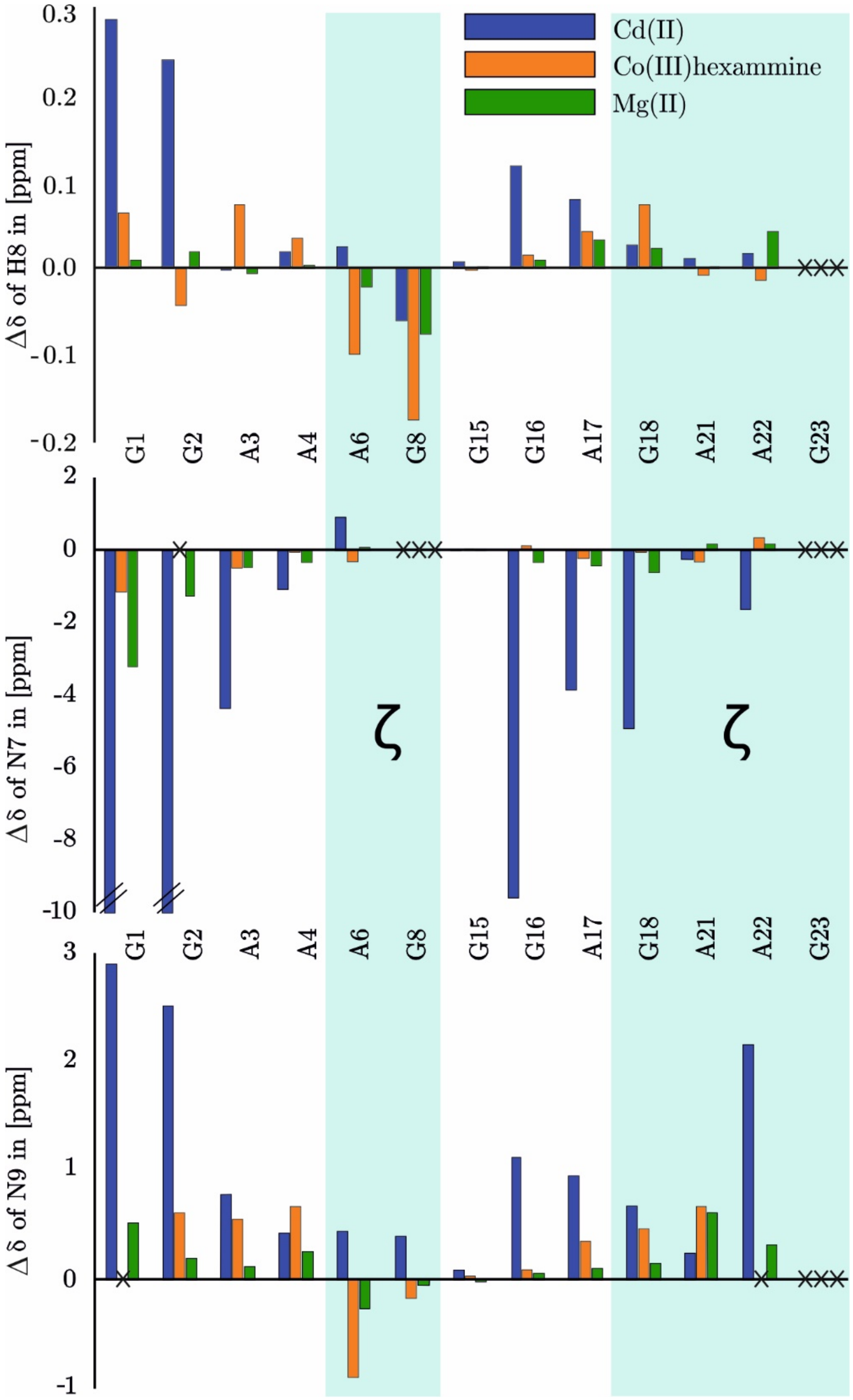

Figure 2.13 Comparison of H8, N7 and N9 chemical shift variations of RNA-l in the presence of Cd(II), cobalt(III)hexammine and Mg(II) at the molar ratio $M^{n+}/RNA = 2.9$. The crosses indicate signals that disappeared during metal ion titration and the green areas underline the ζ region of RNA-l.

dynamics, although at different metal ion concentrations (2.4 equiv. for Cd(II), 1.1 equiv. for cobalt(III)hexammine and 2.3 equiv for Mg(II)).

In the case of Cd(II), in addition to the one of G8 and G18, a strong N7 chemical shift change is also observed for G1 (Figure 2.12) with a Δδ of about 22 ppm, suggesting a macrochelate formation at the 5'-end, also in accordance with previous experiments performed on a more extended construct named D1κζ (see Section 1.7). [8]

Moreover, strong changes in N7 chemical shift are also observed for G2 with a Δδ of about 14 ppm and G16 of about 15 ppm. Besides this significant shift, in the case of guanine residues the N7 shift is also associated to a strong shift in the N9 resonance, indicative of direct binding, that is not observed for the adenines. These N7 chemical shift changes confirm the well-known ability of Cd(II) to bind guanines. However, it is interesting to note that N7 chemical shift changes of about 5/6 ppm are also observed for the N7 resonance of A3 and A17, but no shift of the N9 resonance is observed, suggesting that there is no direct binding.

In the case of Mg(II) titrations, for the N7 resonance of G1 we observe a similar behaviour as in the case of Cd(II), but smaller shift that can be followed until a Δδ of about 4 ppm, then at 4.6 equivalents of Mg(II) the signal broadens up and cannot be anymore monitored. Only little shifts were observed for the other guanines with Mg(II). Negligible changes were observed for cobalt(III)hexammine.

It is not trivial to evaluate the chemical shift changes in the internal loop region. For A6 with Cd(II) we observe only a small downfield shift of N9, N7, and H8 resonances, while in the case of Co(III)hexammine there is an upfield shift. In the case of Mg(II) the shift of N9 and H8 resonances is less pronounced than with Co(III)hexammine, while the N7 resonance is almost not influenced. This result suggests that there is no direct binding but only an electrostatic interaction at A6, with Co(III)hexammine having the strongest effect owing to its higher positive charge. Concerning A22, Cd(II) seems to have a stronger effect than Mg(II) and Co(III)hexammine on its N9 resonance, showing a consistent trend for the N1 and N3 signals. As for A21, in the presence of the three metal ions used, only little chemical shift changes are observed for its N7 and H8 resonances and the most pronounced shift is the one of N9 signal. In general, all of the signals of A21 and also A6 are affected by strong line broadening that supports the hypothesis of predominant electrostatic interaction in the internal loop. However, the chemical shift changes were slightly different for the three metal ions, and it is not possible to exclude outer or inner sphere contribution to the binding. Interestingly, in the case of A22N1, the chemical shift variations are similar for Cd(II) and Mg(II), while cobalt(II)hexammine induces a different effect, and this might indicate a direct Cd(II) and Mg(II) binding site. This hypothesis is strengthened by the fact that purine N1 in non-canonical regions, such as it can be the internal loop, are accessible for metal ion coordination. [8]

All of these findings suggest that Cd(II) has the strongest effect on the G residues of the helical regions, whereas only a generalised electrostatic interaction takes place at the RNA internal loop.

2.7.2. [^{1}H,^{31}P]-HSQC-NOESY experiments to study the binding of Mg(II), Cd(II) and cobalt(III)hexammine to RNA-l

^{31}P NMR and [^{1}H,^{31}P]-HSQC-NOESY experiments of RNA-l were recorded in the absence and the presence of increasing amounts of the three metal ions to confirm the results obtained by ^{2}J-[^{1}H,^{15}N]-HSQC spectra and to assess the metal ions binding sites.

RNA has a negatively charged phosphate backbone that offers suitable metal ion binding sites, therefore the changes of ^{31}P resonances were followed by means of ^{31}P NMR and [^{1}H,^{31}P]-HSQC-NOESY. 1D ^{31}P NMR shows a well distinguishable set of signals for the G1 triphosphate, G1TP (Figure 2.14, upper left), and the rest of the resonances are clustered at about 0 ppm (Figure 2.14, lower panel) and therefore, only some of them were confidently assigned. Hence, 2D [^{1}H,^{31}P]-HSQC-NOESY spectra were recorded to help the assignment (not shown). This 2D experiment is based on the correlation between the phosphates of the backbone and the aromatic and sugar protons of neighbouring residues. Then 1D and 2D experiments were used to monitor the changes in the presence of Mg(II), Cd(II) and cobalt(III)hexammine. In general, all of the three metal ions caused very strong line broadening and the disappearance of ^{31}P resonances

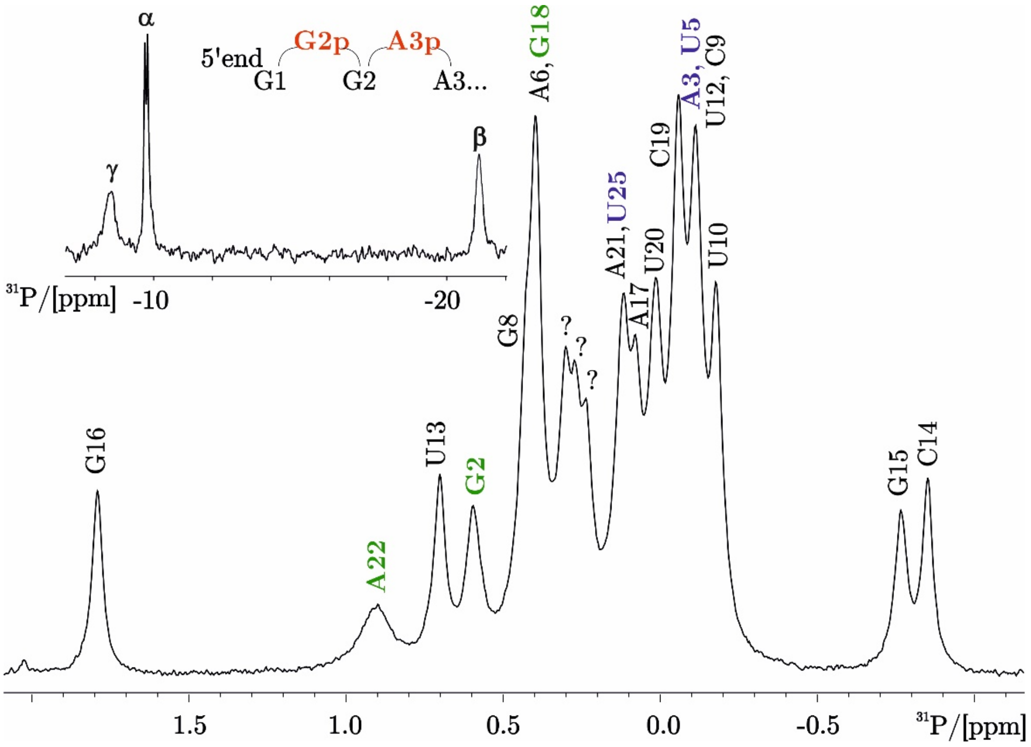

Figure 2.14 1D ^{31}P NMR spectrum of RNA-l with the assignment obtained from [^{1}H,^{31}P]- HSQC-NOESY, (0.64 mM, 60 mM KCl, pD 6.7, 300 K, 500 MHz). Overlapped resonances are indicated in blue, while weak resonances in green. The spectra assignment was confirmed by [^{1}H,^{1}H]-NOESY and for the triphosphate and the UUCG tetraloop resonances by literature data. [86,87]

in 2D spectra, so 1D ^{31}P NMR were mainly used to evaluate the changes upon metal ion addition (Appendix 7 and Figure 2.14). U13p, C14p and G15p, named according to scheme in Figure 2.14 (upper left), can be easily followed in the spectrum and they are only slightly shifted and broadened in the presence of the three metal ions, confirming that there is no interaction at the UUCG tetraloop. G2p and A22p resonances show significant changes, a result that is in agreement with what observed in the ^{2}J-[^{1}H,^{15}N]-HSQC spectra. [8] The behaviour of the ^{31}P resonances at the 5'-end is also in accordance with ^{15}N resonances behaviour in the same region. Indeed, the presence of Cd(II) causes broadening and shifting of the β-phosphate and γ-phosphate resonances at the beginning of the construct, and only little line broadening of the α-phosphate signal. This can be the result of direct coordination of Cd(II) to the β and γ-phosphates (α, β, γ-phosphates are represented in Appendix 8) and N7 of G1TP. [92,93] In the case of Mg(II) the resonances undergo a broadening and a shift that is similar to the one visible for Cd(II), while only slight shifting was observed for cobalt(III)hexammine additions (data not shown). This behaviour confirms the findings obtained via the analysis of the ^{15}N chemical shift changes, which point to the formation of Cd(II) induced macrochelate.

2.7.3. [^{1}H,^{1}H]-NOESY experiments to study Mn(II) binding to RNA-l

^{1}H chemical shift changes and line broadening after Mn(II) additions are generally monitored to identify possible metal ion inner sphere binding sites. [51,68] In this case, [^{1}H,^{1}H]-NOESY experiments were recorded on a 0.9 mM RNA-l sample prepared with natural abundance nucleotides, in the presence of increasing amounts of Mn(II) (data not shown). At 30 μM of Mn(II) G1H8-H1' clearly disappears, confirming inner sphere coordination at the 5'-end. At 60 μM concentration of Mn(II), cross peaks belonging to residues at the internal loop, such as A22H2-A6H2, A22H2-A6H1' and G23H8-A22H1', are also not visible, thus suggesting further interaction at this site.

2.8. 1D experiments on RNA-l and complex 1

1D NMR experiments represent the easiest and fastest way that can be exploited to obtain a first insight into the binding of a metal complex to RNA. In this case, the binding of complex 1 to RNA-l was investigated by 1D ^{1}H NMR experiments in water and D_2O, evaluating the changes in the regions of both the imino and the aromatic proton resonances. Complex 2, also known as “DNA light switch” complex, [32] was used as mimic of complex 1 because they share the same dppz scaffold, although their axial ligands are different.

2.8.1. 1D NMR spectra of RNA-l and complex 1 in water

1D NMR experiments in water on RNA-l in the presence of increasing amounts of complex 1 gave a first evidence of binding. Since the imino proton signals reflect the stability of the base-paired regions of RNA-l, [8,9] variations at these resonances, e.g., intensity, linewidth, chemical shift, give hints on the structural changes induced in the RNA by the interaction with complex 1. [49]

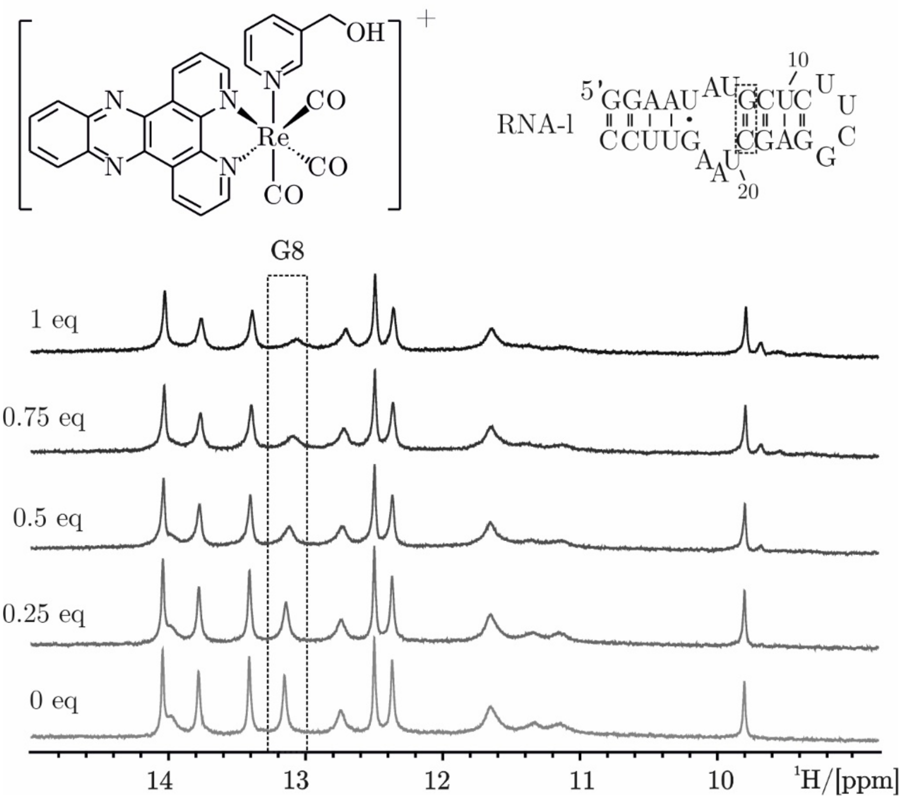

Figure 2.15 Overlay of ^{1}H spectra (imino region) of RNA-l with increasing amount of complex 1 (0.2 mM, PBS with 2% DMSO, pH 7, 293 K, 700 MHz). The dashed square highlights the imino proton signal of the base pair G8-C19, whose intensity is significantly reduced over the titration with complex 1.

At 1 equivalents of rhenium complex, only one resonance is strongly affected, namely G8H1, belonging to the first base pair after the UU mismatch in the internal loop. The intensity of this signal is decreased by 75% and an upfield shift of 0.08 ppm is visible (Figure 2.15).

This strong intensity loss observed for the resonance corresponding to G8-C19 is the result of the loosening of the hydrogen bond of this base pair which is likely due to the interaction of complex 1 and RNA-l in this area, that is the one of the internal loop. Besides this significant change, the rest of the RNA resonances are affected by only a slight general broadening, suggesting that after a first specific interaction in the region of the loop, then the binding of complex 1 is more generalized to the whole construct.

In our experimental conditions due to the low water solubility of complex 1, it was not possible to reach an excess of ligand in solution. Hence, to mimic the

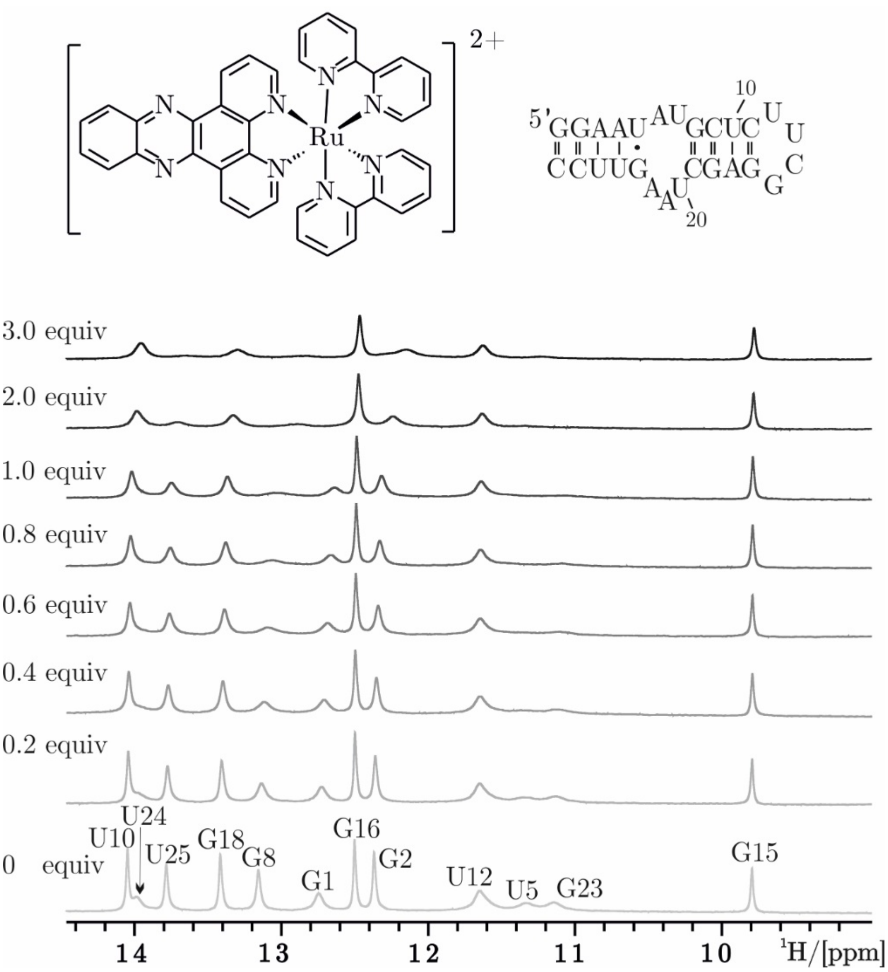

Figure 2.16 ^{1}H spectra (imino proton region) of RNA-l with increasing amounts of complex 2 (0.19 mM, PBS, pH 6.9, 293 K, 700 MHz).

rhenium complex, we used complex 2, the ruthenium complex whose scaffold is based on the same dppz moiety but that has higher water solubility. Employing complex 2 enabled us to monitor the RNA behaviour in the presence of a three-fold excess of dppz bearing complex. Between 0.2 and 1 equivalent of complex 2, the intensity of G8H1 is selectively reduced with a slight effect on the rest of the resonances (Figure 2.16). In excess of metal complex most of the signals are strongly broadened, except for G15H1, G16H1 and U12H3. The result of this experiment has a twofold importance. On the one hand, we proved that the driving force of the binding is associated with the dppz moiety that interacts with the RNA internal loop. This can be concluded since complex 1 and complex 2 behave in an analogous manner with RNA-l, showing firstly a selective interaction at G8 in the internal loop region, and then an overall unspecific

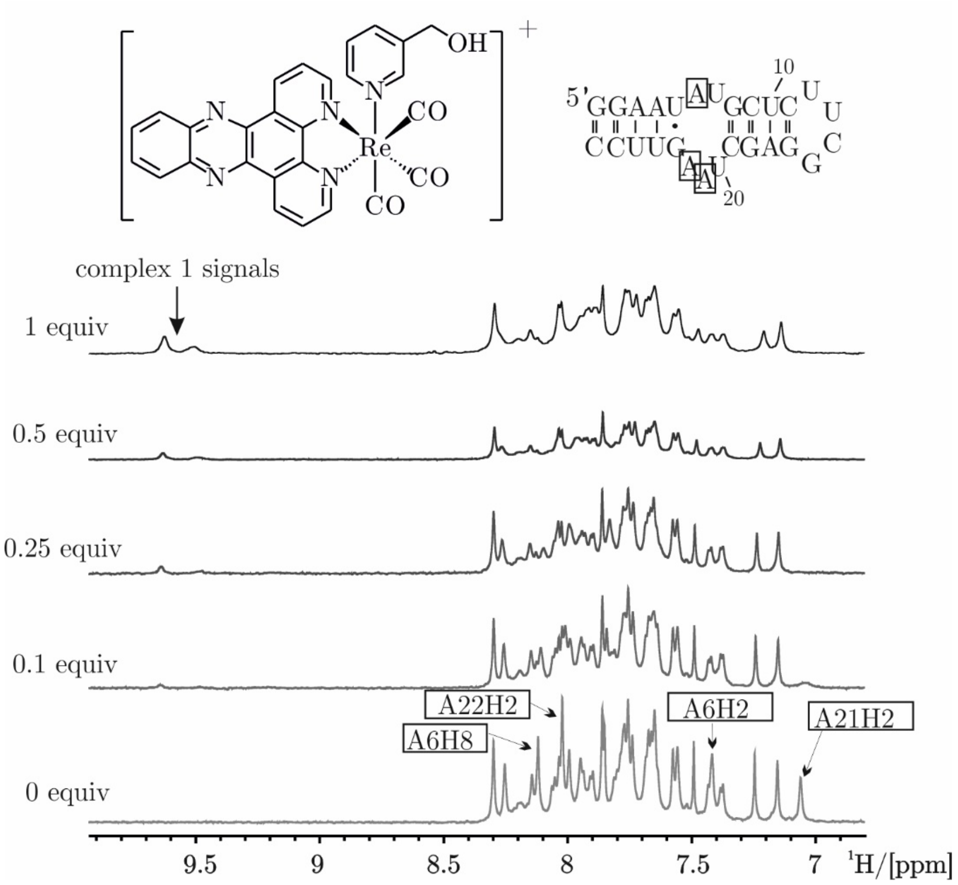

Figure 2.17 ^{1}H spectra (aromatic region) of RNA-l in the presence of increasing amounts of complex 1 (0.35 mM, pD 6.8, 303 K, 700 MHz). The peaks that are first affected by complex addition are labelled.

binding. On the other hand, we could conclude that at such excess of metal complex, the signals belonging to terminal loop appear only moderately affected, suggesting that this area and its neighbouring nucleotides are not influenced by the metal complex interaction.

2.8.2. 1D NMR spectra of RNA-l and complex 1 in D_2O

To obtain a more complete evaluation of the RNA changes in the presence of complex 1, we performed experiments in D_2O to evaluate the behaviour of the RNA aromatic protons. At first, a one-step addition of 0.25 equivalents of complex 1 to a solution of RNA-l was done and changes in the RNA resonances were observed, confirming the presence of an interaction. The situation was monitored over 20 hours resulting stable (Appendix 9). Hence, extended titrations were performed. An equimolar amount of complex 1 was added to

RNA-l in four steps, 0.1, 0.25, 0.5 and 1 equiv. (Figure 2.17). At 0.25 equiv. of complex 1 the signals belonging to the internal loop nucleotides, such as A21H2, A6H2/H8, A22H2 disappear or strongly broaden up in the spectrum. Interestingly, the resonances belonging to complex 1 are not visible in the first steps of the titration, but they only appear, with strong changes in chemical shifts, upon increase of metal complex concentration. Experiments at variable temperature on equimolar mixtures of complex 1 and complex 2 with RNA-l in D_2O were exploited to understand the behaviour of the metal complex signals. These resonances, not visible at 303 K in the presence of RNA-l, only appear at higher temperature or in excess of metal complex, as it can be seen in Figure 2.18 where the resonances of complex 1 (left) and complex 2 (right) are marked with stars. Similar disappearance is already reported in the literature for complex 2 upon DNA interaction. [43] In our case, this result suggests that there is an interaction, that this binding is highly dynamic and that the system is at coalescence at the conditions used for the experiment.

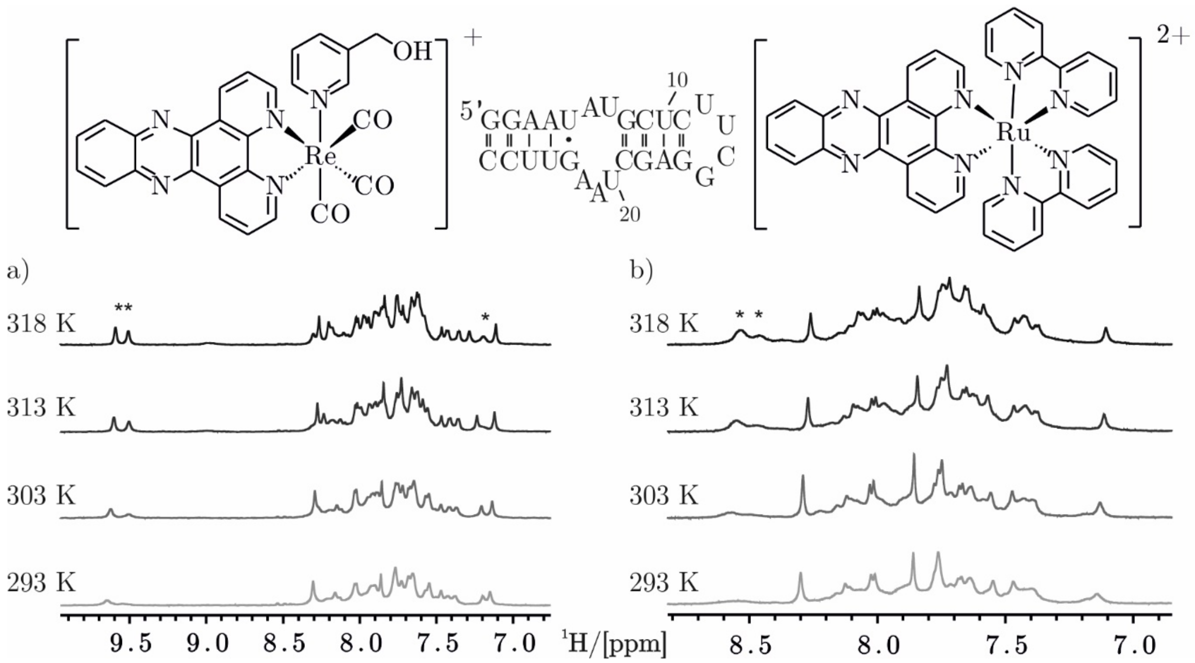

Figure 2.18 Variable temperature ^{1}H spectra (aromatic region) of RNA-l in the presence of 1 equivalent of complex 1 (0.35 mM, PBS, pD 6.8, 700 MHz); b) ^{1}H variable temperature spectra of RNA-l in the presence of 1 equivalent of complex 2 (0.49 mM, PBS, pD 6.8, 600 MHz). The peaks of complex 1 and complex 2 become more intense by increasing the temperature (the asterisks mark some of them, that are better visible in the spectra at higher temperatures).

To obtain information on the behaviour of the RNA aromatic resonances in the presence of an excess of dppz bearing complex, we used complex 2. Prior to extended titrations, a one-step addition of 0.25 equivalents of complex 2 to a sample of RNA-l was done, confirming the presence of an interaction, and the resonances were monitored over 20 hours ensuring a stable situation (Appendix 10). Then, RNA-l was titrated with complex 2 up to 2 equivalents in five steps (0.1, 0.25, 0.5, 1 and 2 equivalents). Similar changes are observed for complex 1 and complex 2, except for some little differences (Figure 2.19). At 0.25 equiv. of metal complex, the resonances belonging to the loop region, that disappeared in the presence of complex 1, are in this case still visible although affected by strong broadening (comparison between Figure 2.17 and Figure 2.19).

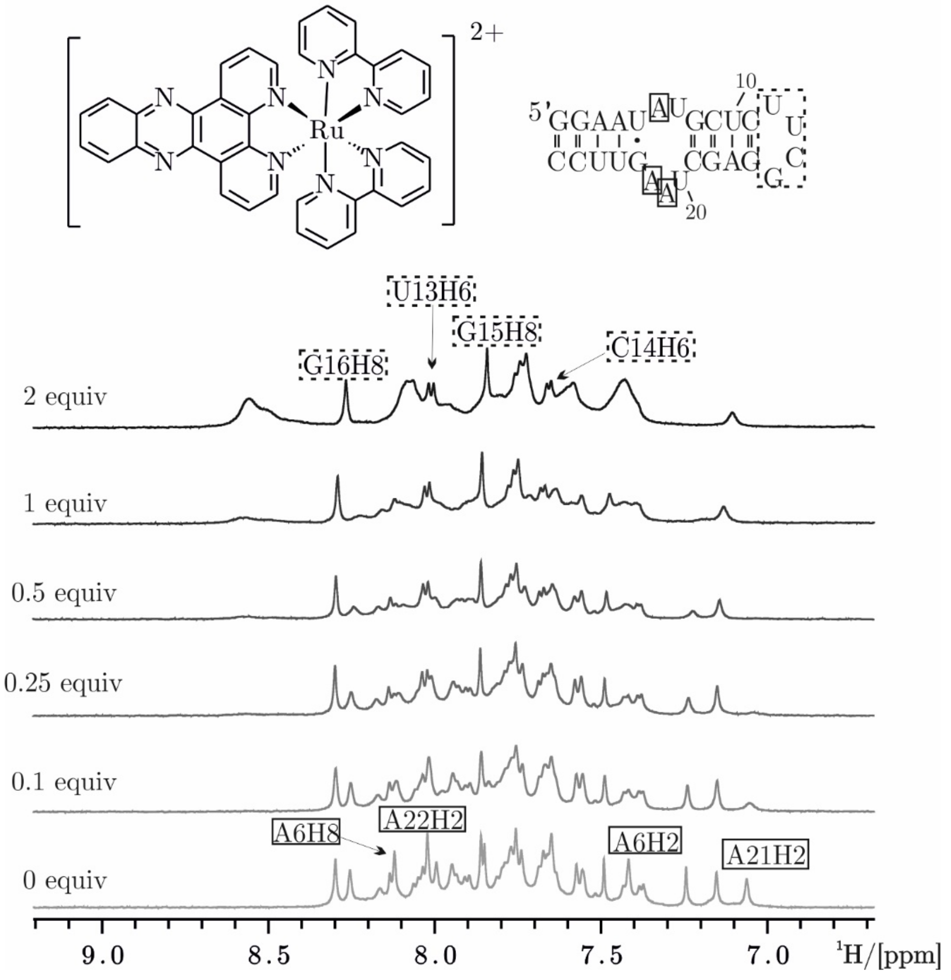

Figure 2.19 ^1H spectra (aromatic region) of RNA-l with increasing amounts of complex 2 (0.49 mM, PBS, pD 6.8, 303 K, 600 MHz). The peaks that are first affected by complex addition are labelled with squares in the first spectrum, while peaks that remain sharp for the whole titration are labelled with dashed squares in the last spectrum.

Along the same line, at 1 equiv. of complex 2 all of the resonances suffer from a general broadening and a very broad signal at 8.55 ppm is visible (Figure 2.19), most likely belonging to the metal complex. At 2 equivalents of ruthenium complex, its resonances start to be clearly detectable and the RNA signals to be strongly broadened, except for U13H6, C14H6, G15H8, G16H8. These resonances maintained their intensity and linewidth over the whole titration, a result in accordance with what observed for the RNA-l imino resonances in excess of complex 2 (compare Figure 2.16 and Figure 2.19), allowing us to confidently conclude that the terminal loop is not affected by the interaction.

2.9. 2D NMR experiments to assess the binding of complex 1 to RNA-l

As seen in the 1D ^{1}H NMR experiments in D_2O (Section 2.8.2), it is very difficult to precisely follow the chemical shift changes due to a strong overlap of signals in the aromatic region. Therefore, [^{1}H,^{1}H]-NOESY spectra were recorded to follow the variations in chemical shifts and intensity and the possible line broadening of the resonances of the sequential walk region in the presence of increasing amounts of complex 1. Moreover, ^{2}J-[^{1}H,^{15}N]-HSQC experiments were recorded to obtain information also on the shifts of the ^{15}N resonances of RNA-l in the presence of complex 1.

2.9.1. [^{1}H,^{1}H]-NOESY spectra on RNA-l and complex 1

[^{1}H,^{1}H]-NOESY experiments were recorded in the absence and in the presence of increasing amount of complex 1 (0.1, 0.25, 0.5 and 1 equivalents) to assess the metal complex binding sites. Variations of the cross peaks intensity, linewidth and chemical shift in the sequential walk region were evaluated. [73–75] At 0.1 equivalent of complex 1, most of the changes, such as signal broadening, disappearance as well as shifts of the resonances, were already detected. Afterwards, in spite of the increasing amount of metal complex in solution, the situation remained rather stable and only slight variations could be observed. The bar plot in Figure 2.20 represents the chemical shifts of H1' and H6/H8 protons in the presence of 1 equivalent of complex 1. The graph shows that the majority of the resonances of RNA-l in the sequential walk area are only little affected by the presence of complex 1, except for the internal loop signals, highlighted in pink and green boxes. Indeed, the H1' and H6/H8 signals of A6, U7, G8, U20 and A21 are not visible anymore in the spectrum, as displayed by the crosses in Figure 2.20. An example is presented in the upper panel of Figure 2.22 where it is shown that the cross peak A6H8-H1' disappears when complex 1 is in solution. As a consequence of the disappearance of these signals, the sequential walk path in the [^{1}H,^{1}H]-NOESY spectrum could be followed only from G1 to U5, from C9 to C19 and from A22 to C27, even though nucleotides close to the internal loop show a significant change in intensity, linewidth and shift. In accordance with the findings obtained via 1D ^{1}H NMR, the resonances of the nucleotides in the terminal loop, in the dashed box (Figure 2.20), show the smallest changes, suggesting that there is no interaction in this region.

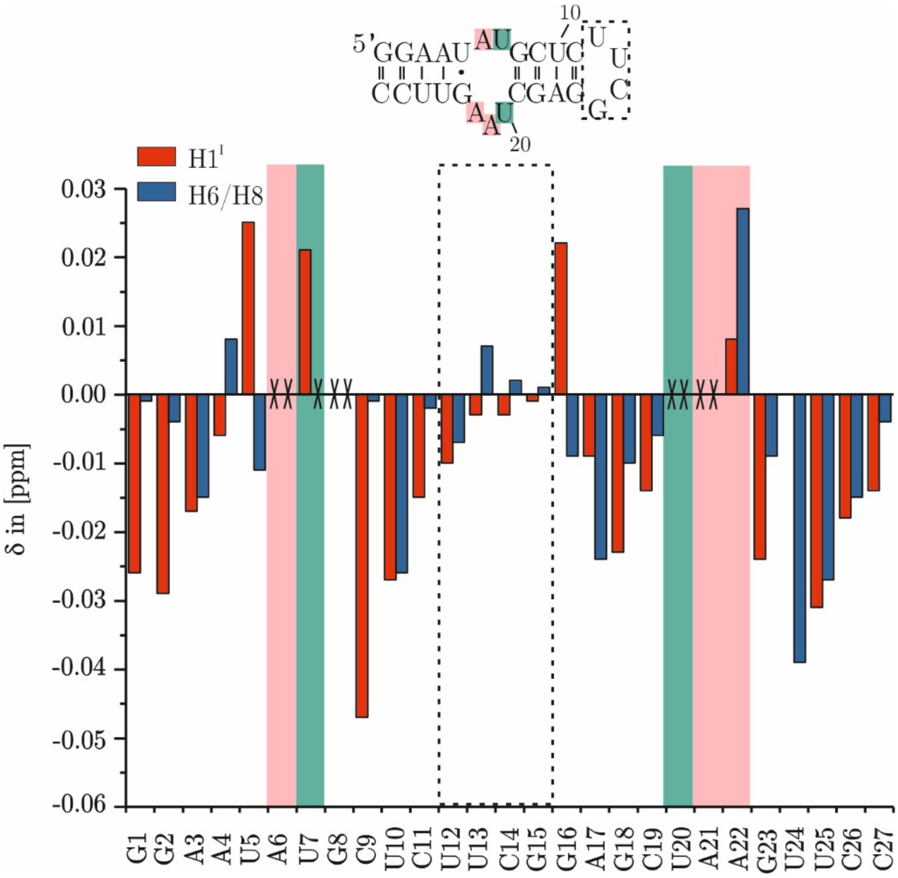

Figure 2.20 Comparison of H8/H6 and H1' chemical shift changes of RNA-1 in the presence of 1 equivalent of complex 1. (0.35 mM, PBS with 2% DMSO, pD 6.8, 303 K, 700 MHz). Crosses show resonances not found in the spectrum at 1 equivalent of complex 1.

Besides the resonances connecting the sequential walk path, some more NOE contacts are also interesting. Indeed, the three stacked adenines, A6, A21 and A22, that form the internal loop, give intense cross peaks, such as A21H2-A6H1', A21H2-U7H1' (upper panel of Figure 2.22) and A6H2-A21H2, U7H6-A21H2, A22H2-A21H2 (lower panel of Figure 2.22), as a result of their stacking interactions. [10] These signals are no longer visible upon addition of complex 1, thus indicating an interaction at this site, but also system dynamics.

These results are confirmed by [^{1}H,^{1}H]-TOCSY titrations (Figure 2.21). Indeed at 1 equivalent of complex 1, the cross peaks corresponding to U20H6-H5, U7H6-H5 (also visible in the [^{1}H,^{1}H]-NOESY in Figure 2.22) and A21H1'-H2' in the internal loop are not observable. On the contrary, the cross peaks of nucleotides in the terminal loop or close by, like e.g. C11H6-H5, do not show any variation of their chemical shift.

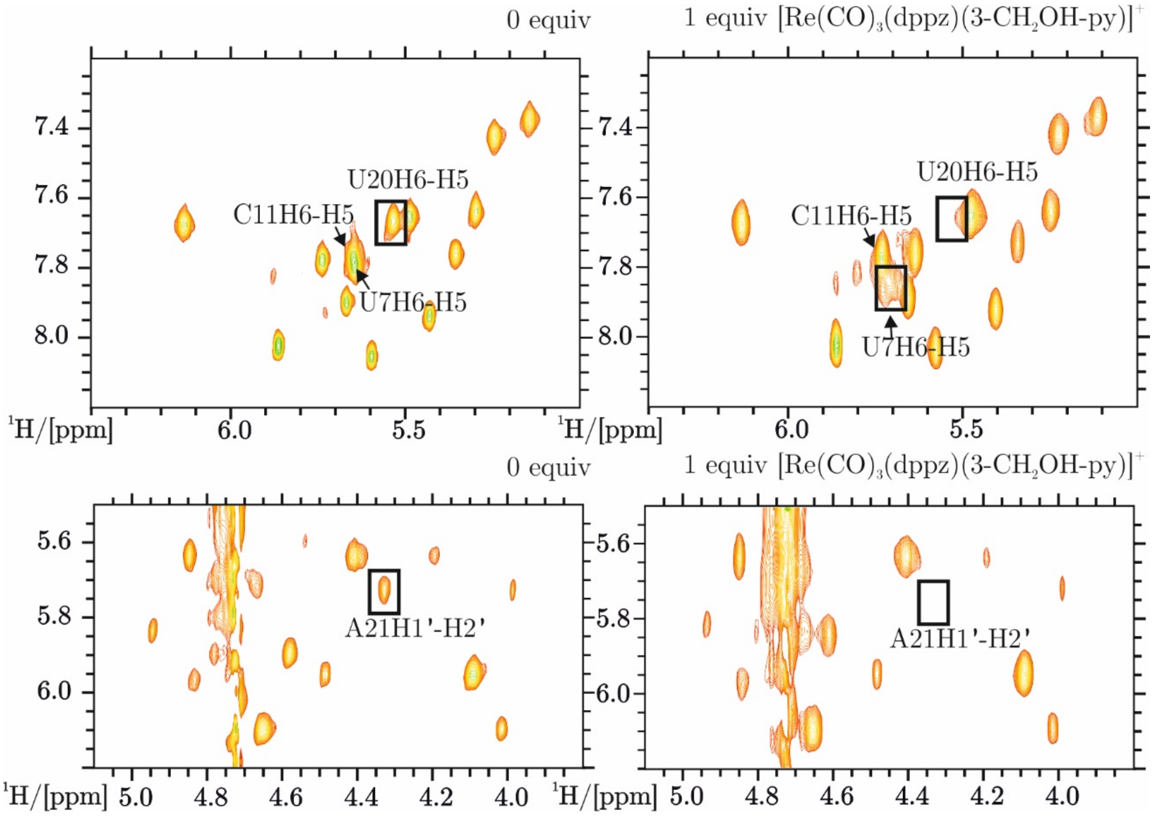

Figure 2.21 Portions of [^{1}H,^{1}H]-TOCSY spectra recorded on RNA-1 in the absence (left) and in the presence (right) of 1 equivalent of complex 1 (0.35 mM, PBS, pD 6.8, 303 K, 700 MHz).

For the sake of comparison, $[^1H,^1H]$-NOESY and $[^1H,^1H]$-TOCSY were performed in the same way using complex 2, and similar results were obtained as in the case of complex 1 (Appendix 11 and Appendix 12). Indeed, at 1 equivalent of ruthenium complex, chemical shift changes, line broadening and disappearance of signals of nucleotides at the internal loop were also observed.

All of these findings, in agreement with the results from the 1D NMR experiments, confirmed that complex 1 and complex 2 behave similarly in the presence of RNA-l suggesting the involvement of the dppz moiety in the localised binding at the RNA internal loop. In addition to this, fast dynamics was

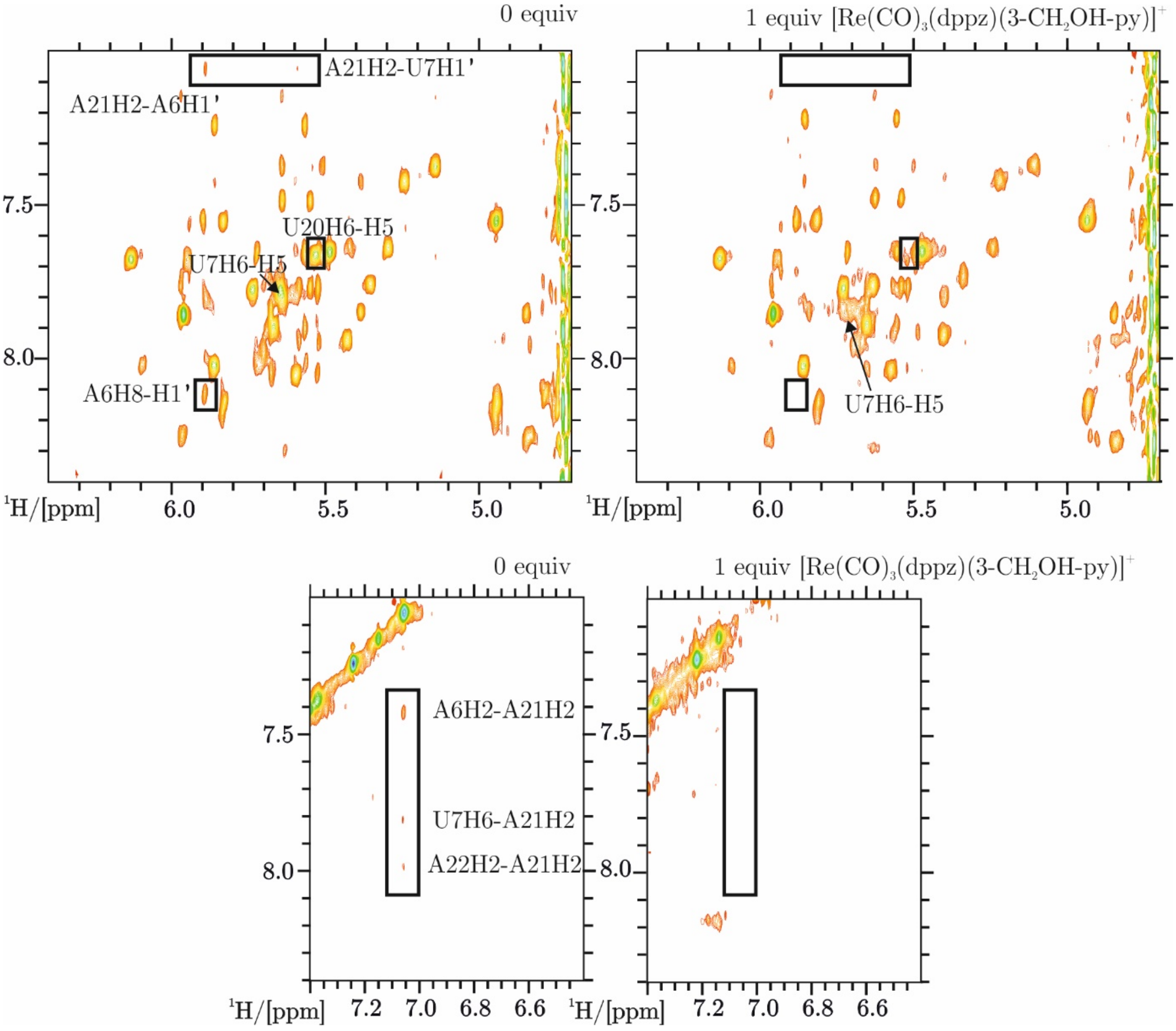

Figure 2.22 Sections of $[^1H,^1H]$-NOESY spectra recorded on RNA-l in the absence (left) and in the presence (right) of 1 equiv. of complex 1 (0.35 mM, PBS, pD 6.8, 303 K, 700 MHz). The boxes indicate some of the cross peaks belonging to nucleotides in the internal loop that either disappear or broaden upon metal complex addition.

confirmed hampering further NMR structural studies that would allow a more in depth understanding of the interaction.

2.9.2. ^{2}J-[^{1}H,^{15}N]-HSQC spectra on RNA-l and complex 1

^{2}J-[^{1}H,^{15}N]-HSQC NMR experiments, also previously applied to study metal ion binding to RNA-l (Section 2.7.1) [9] were used to monitor the chemical shift changes of N7/N9/H8 and N3/N1/H2 resonances of RNA-l upon addition of complex 1.

^{2}J-[^{1}H,^{15}N]-HSQC spectra generally show very well dispersed signals (assignment available in Appendix 4), and they can be exploited to confidently evaluate the chemical shift changes and the possible disappearance of some signals, as observed in [^{1}H,^{1}H]-NOESY spectra that however show more overlapped signals. ^{2}J-[^{1}H,^{15}N]-HSQC experiments were conducted on ^{15}N labelled RNA-l samples in the absence and in the presence of increasing amounts of complex 1. Upon addition of 0.25 equivalents of complex 1, as observable in Figure 2.23, the intensity of the resonances of nucleotides close to the internal loop such as G8N7-H8 significantly decreases, whereas signals belonging to residues in the loop, like A6N3/N1-H2 and A21N3/N1-H2 completely disappear.

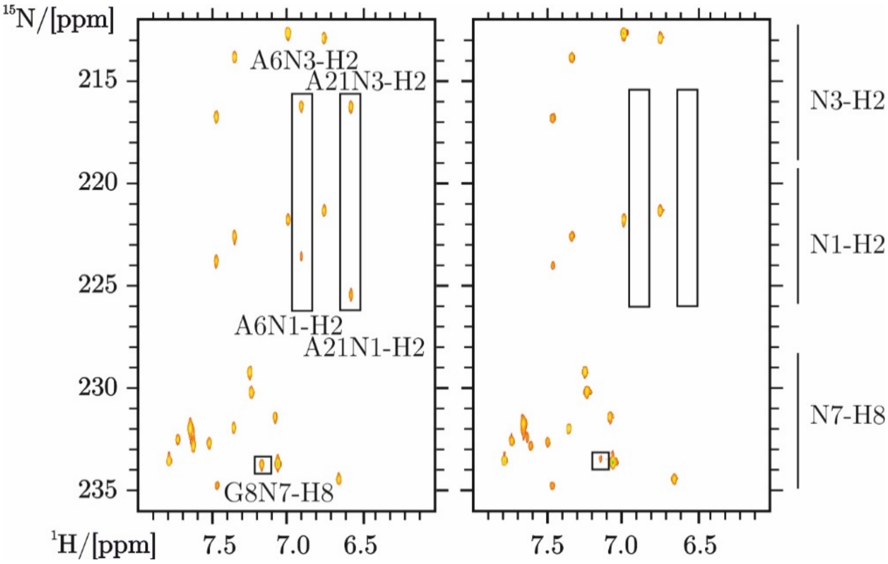

Figure 2.23 [^{1}H,^{15}N]-HSQC spectra recorded on a ^{15}N labelled RNA-l sample in the absence (left) and in the presence (right) of 0.25 equivalents of complex 1 (0.18 mM, PBS with 2% DMSO, pD 6.8, 303K, 600 MHz).

1D ^{1}H NMR experiments were also performed on these samples showing disappearance of the RNA signals and lower intensity for the resonances of complex 1, that increases at higher temperature. This confirms dynamics and coalescence at room temperature as described in Section 2.8.2. Moreover, the fact that the signals of H2 protons are rapidly and strongly affected, but H8 protons signals do not show significant variations, suggests that the complex interacts via the minor groove (minor groove indicated in Figure 1.6). The results obtained by the ^{2}J-[^{1}H,^{15}N]-HSQC NMR spectra are in accordance with the findings of 1D ^{1}H NMR, [^{1}H,^{1}H]-NOESY and [^{1}H,^{1}H]-TOCSY spectra, proving the presence of a specific interaction at the internal loop. All of these experiments could also confirm that the system is in fast exchange regime, thus preventing further NMR structural characterization.

2.10. Interaction of RNA-h and DNA-h with complex 1

In RNA-h, the internal loop is substituted by regular Watson-Crick base pairs. 1D ^{1}H NMR titration experiments in water (Figure 2.24) interestingly do not show any changes at G8H1, that in the case of RNA-l was the most affected resonance. They show an overall broadening and a loss of intensity of about 30% for the majority of the resonances, but no significant chemical shift changes. Interestingly, G1H1 at the 5'-end shows an upfield shift of 0.15 ppm and G15H1, G16H1 and U12H3 in the terminal loop, whose resonances are marked with stars, display an intensity variation only of about 5%.

This behaviour can be explained in two ways. On the one hand, all of the RNA constructs are prepared via *in vitro* transcription, and as such, they contain a triphosphate group at the 5'-end, which might be responsible for an electrostatic interaction at G1. On the other hand, it is known that the last nucleotides of a construct have higher mobility due to a less tight base pairing that results in a flexible region that can more easily accommodate the metal complex.[94] In order to test these two hypotheses, we prepared a dephosphorylated sample of RNA-h (Appendix 8 and Section 6.7) and performed the titration under the same conditions (Appendix 13). No significant differences were observed between spectra obtained upon addition of complex 1 to the RNA bearing the triphosphate group and to the dephosphorylated one. This very

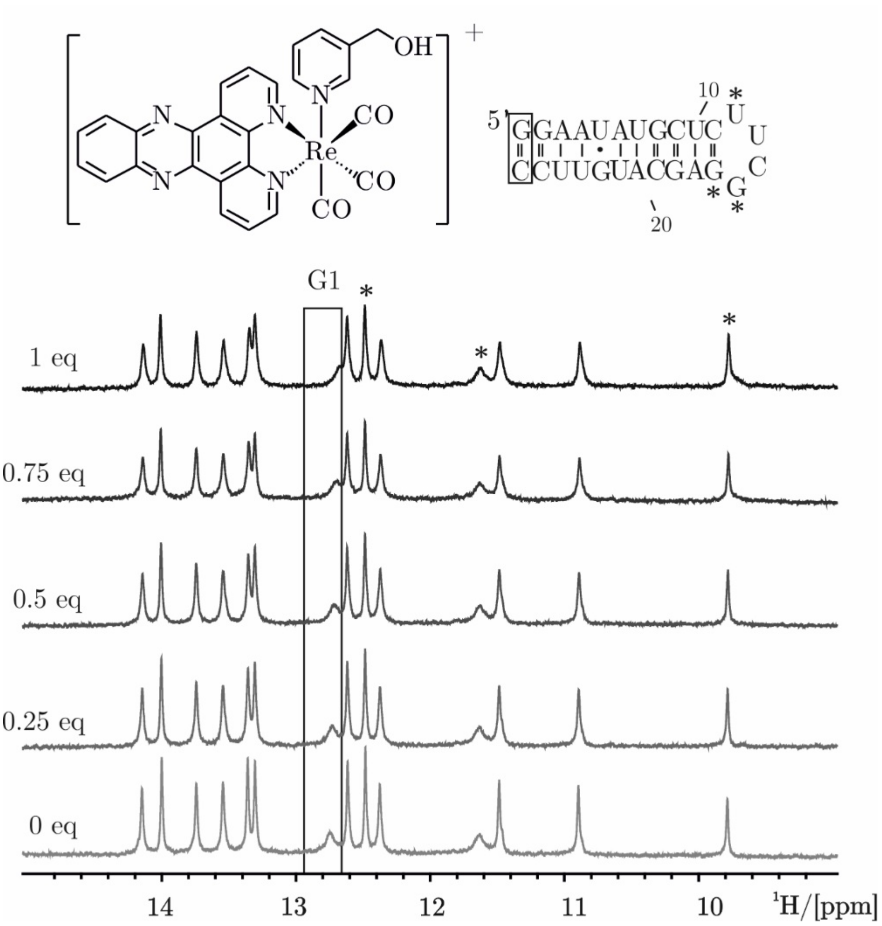

Figure 2.24 Overlay of ^{1}H spectra (imino region) of RNA-h recorded in the presence of increasing amount of complex 1 (0.2 mM, PBS with 2% DMSO, pH 7, 293 K, 700 MHz). The square indicates the base pair G1-C26, whose intensity is significantly reduced over the titration with complex 1. The stars highlight the resonances of the terminal loop that undergo the smallest variation in intensity.

similar behaviour confirms that electrostatic interaction plays a minor role in the RNA binding, supporting the second hypothesis. Moreover, a dephosphorylated sample of RNA-l was also prepared and titrated with increasing amount of complex 1 to evaluate the possibility of binding at the 5'-end. No significant differences were observed with respect to the sample with the triphosphate group, confirming that the internal loop behaves as a preferential binding site whose affinity is higher than the one for the flexible 5'-end region.

Finally, a short DNA hairpin with a TTCG terminal loop was used to probe possible preferential interactions in the binding with short DNAs. In this case, all the imino resonances of DNA-h suffer from general broadening with a loss of

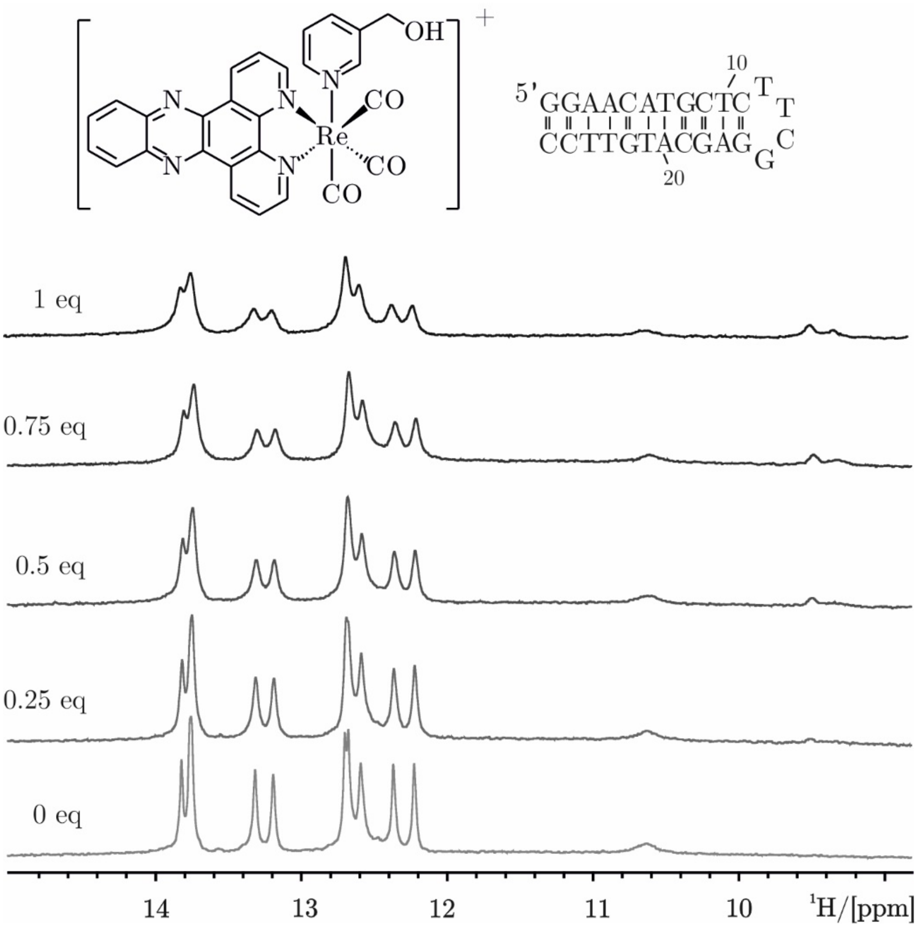

Figure 2.25 Overlay of ^{1}H spectra (imino region) of DNA-h recorded in the presence of increasing amount of complex 1 (0.2 mM, PBS with 2% DMSO, pH 7, 293K, 700 MHz).

20-25% of intensity upon addition of complex 1, suggesting an overall interaction to the DNA double helix and no specific binding (Figure 2.25).

Hence, we can conclude that the presence of the RNA internal loop in RNA-l is crucial to have a preferential interaction, because only a slight electrostatic attraction at the 5'-end was detected for RNA-h that does not contain this feature. Moreover, an overall binding is observed for the short DNA hairpin used in these studies.

2.11. Role of the dppz moiety in the binding at the RNA internal loop

To clarify the role of the dppz unit, known in the literature as DNA intercalating moiety, [15] in the interaction with the RNA internal loop of RNA-l, we compared the behaviour of complex 1 and complex 2, that bears the dppz group, to the one of complex 3 that does not have this unit in its ligand system.

2.11.1. Interaction of complex 1, complex 2 and complex 3 with RNA-l

1D ^{1}H NMR spectra of RNA-l were recorded in D_2O in the presence of 0.25 equivalents of complex 1, complex 2 and complex 3. A stack plot of the spectra is shown in Figure 2.26.

A similar behaviour was observed for complex 1 and complex 2, while no changes in the aromatic resonances could be detected upon addition of complex 3, which is missing the dppz moiety. When RNA-l is in the presence of complex 1 and complex 2, some of its signals readily disappear, some others undergo a general broadening and the metal complex resonances are not visible, most likely due to a dynamic situation. Besides an overall similar interaction pattern in the case of the two metal complexes with RNA-l, some differences can be found. Indeed, the behaviour of the resonance belonging to A21H2 is remarkable. This signal disappears upon addition of 0.25 equivalents of complex 1, whereas it is still visible even though significantly broadened in the presence of complex 2. The observed behaviour might be due to a slightly difference in interaction owing to the different charge of the two complexes, to

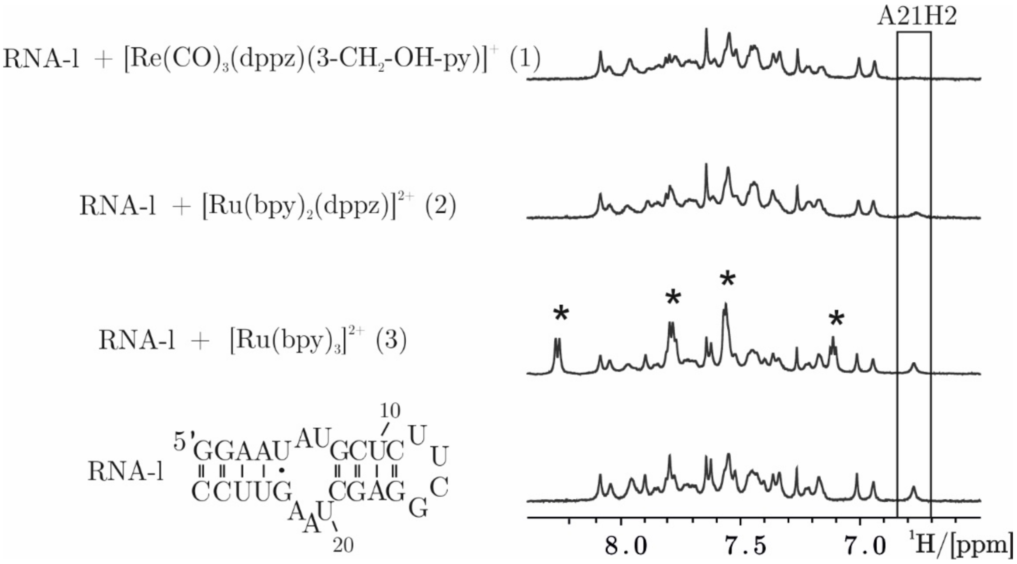

Figure 2.26 Overlay of ^{1}H spectra (aromatic region) of RNA-l recorded in the presence of 0.25 equiv. of complex 1, 2 and 3 (0.1 mM, PBS with 2% DMSO, pD 6.8, 293K, 600 MHz). The stars indicate the signals of complex 3 in the spectrum.

dynamics and/or to the ancillary ligands. In the case of complex 3, the metal complex resonances are still visible and sharp, only downfield shifted by 0.03 ppm, most likely due to the diverse environment owing to the presence of RNA in solution, whose signals are instead unchanged.

2.11.2. DOSY NMR experiments on complex 1, complex 2 and complex 3 with RNA-l

DOSY spectra were performed to confirm the involvement of the dppz moiety in the binding at the RNA internal loop. DOSY NMR is a well-known method whose application spans from the screening of multi-components mixtures, relying on its ability of resolving the interaction partners by their difference in

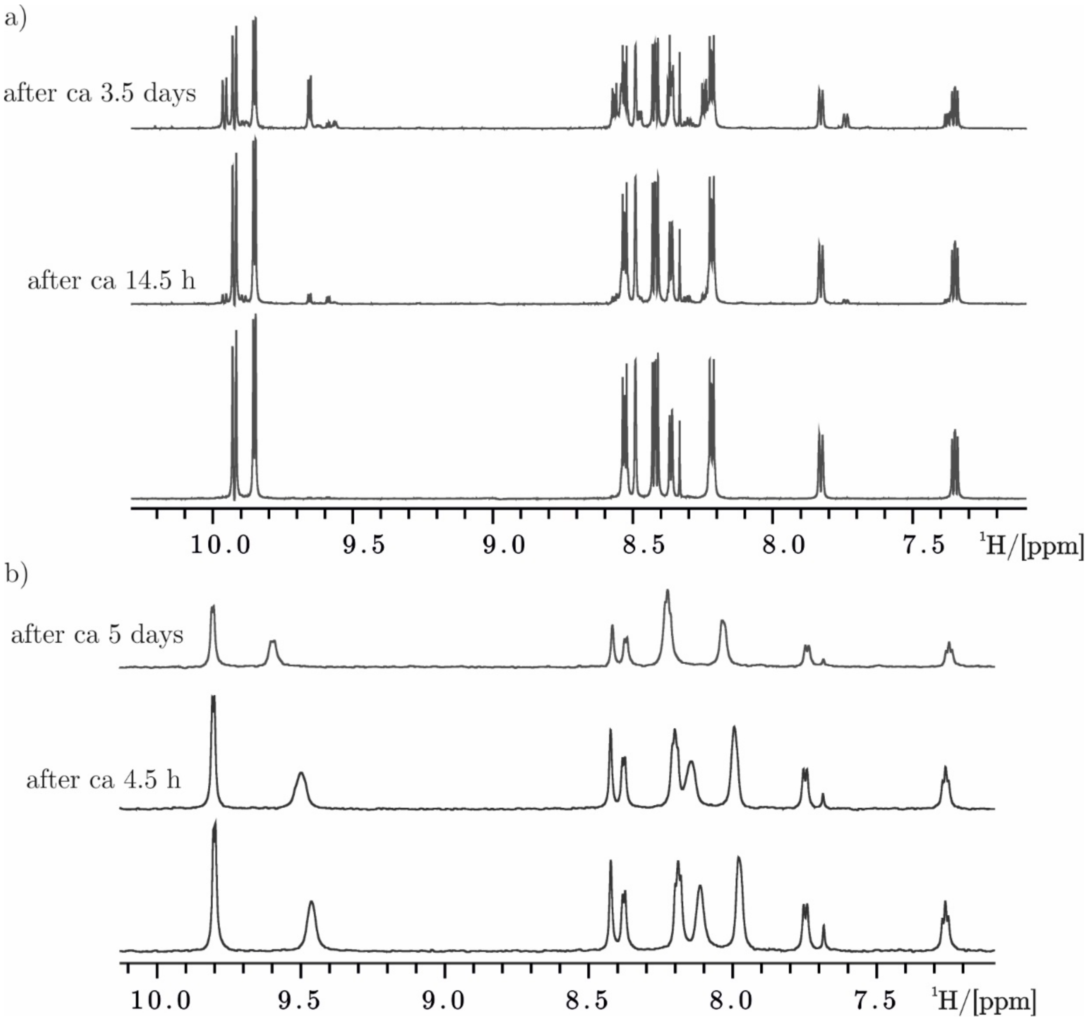

Figure 2.27 Time evolution of ^{1}H NMR spectra of complex 1 in DMSO (0.35 mM, DMSO, 303 K, 700 MHz); b) Time evolution of ^{1}H NMR spectra of complex 1 in PBS with 2 % DMSO (0.35 mM, PBS with 2% DMSO, 303 K, 700 MHz).

diffusion rate, to the study of the interaction between small molecules and macromolecules. [78,95,96] DOSY spectra were recorded on 1:1 mixtures of the three metal complexes and RNA-l and compared to reference experiments of the free RNA-l, complex 2 and complex 3 in the same conditions.

A DOSY spectrum of complex 1 was not recorded owing to its poor water solubility in aqueous medium. Indeed, a 0.35 mM solution of complex 1 in PBS with 2% of DMSO showed precipitation within two hours. ^{1}H NMR stability assays over *ca.* 5 days were performed on complex 1 in pure DMSO and in PBS with 2% of DMSO (Figure 2.27) in the absence of RNA-l. In the first case (panel a), we observe the formation of degradation products, while in the latter one (panel b) it is visible an overall decrease of the intensity of all the resonances and a yellow precipitate in the NMR tube. On the contrary, when complex 1 is in solution with RNA-l, the resonances of the metal complex are stable over 4.5 days, suggesting the presence of an interaction that increases the stability of complex 1 in aqueous solution (compare Figure 2.28 and Figure 2.27b). This

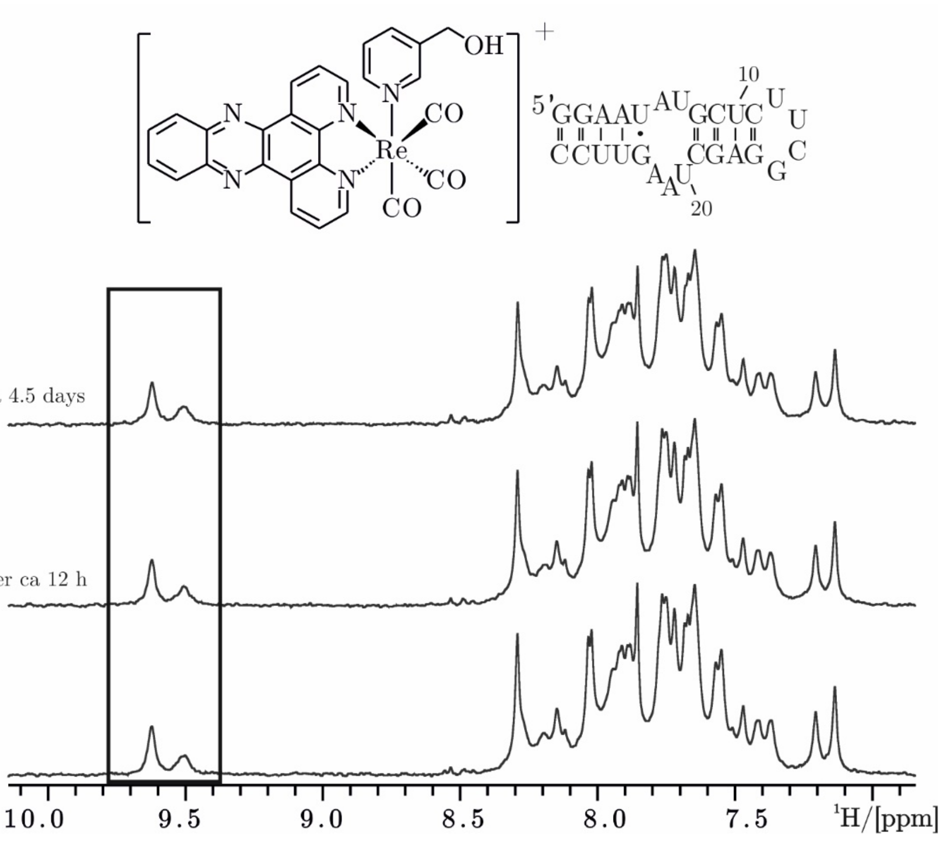

Figure 2.28 Time evolution of ^{1}H NMR spectra of a 1:1 mixture of RNA-l and complex 1 (0.35 mM, PBS with 2% DMSO, 303 K, 700 MHz).

avoids early precipitation and allows to record a DOSY experiment. The DOSY spectrum of the equimolar solution of complex 1 and RNA-l (panel b of

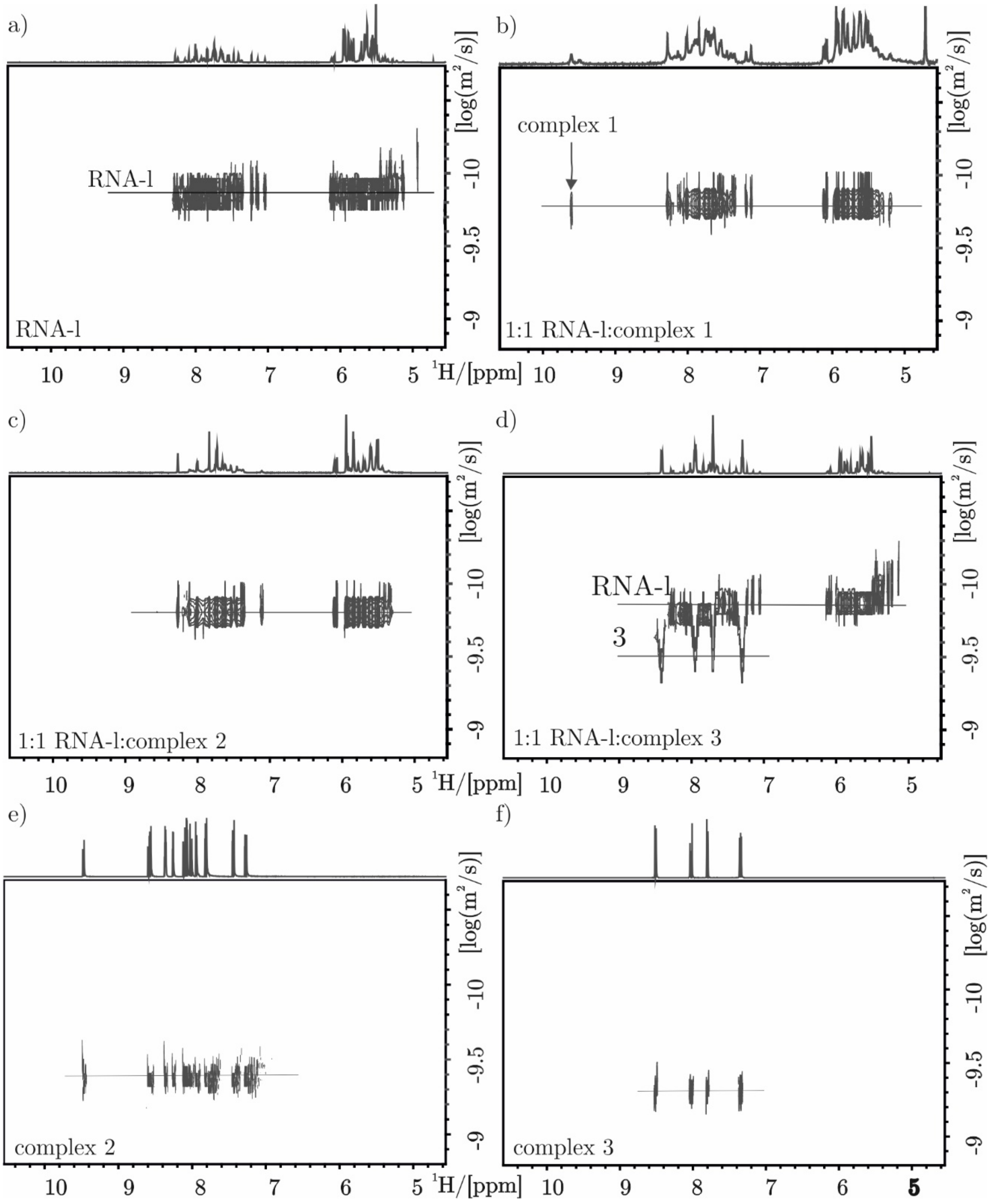

Figure 2.29 DOSY NMR spectra of 0.34 mM of a) free RNA-l and b) equimolar mixture of RNA-l and complex 1, c) RNA-l and complex 2 and d) RNA-l and complex 3, e) free complex 2 and f) free complex 3 (in the case of complex 1 the sample was prepared in PBS with 2% DMSO, whereas in the case of complex 2 and complex 3, PBS was used as solvent, pD 7.0, 303 K, 700 MHz).

Figure 2.29) shows only one set of signals, suggesting that the two components interact and diffuse together.

Similarly to what observed for complex 1 and RNA-l, the DOSY experiment recorded on the equimolar mixture of complex 2 and RNA-l (panel c of Figure 2.29) shows a single signal for the two species, confirming the binding. Interestingly, the resonances of complex 2 are not visible in the mixture with RNA-l, thus confirming a dynamic situation. On the contrary in the case of complex 3 and RNA-l, the DOSY spectrum (panel d of Figure 2.29) displays two distinct set of signals, with two different diffusion coefficients ascribable to the free metal complex and the free RNA-l respectively. All of these findings support the involvement of the dppz moiety in the interaction with the RNA internal loop.

2.12. Conclusion

The NMR data collected on the metal ion binding of Cd(II), Mg(II) and cobalt(III)hexamine to RNA-l confirmed the tendency of Cd(II) to coordinate to G-helical residues and showed the formation of Cd(II) induced macrochelate at the 5'-end triphosphate. Moreover, small chemical shift changes in the internal loop region in the presence of the three metal ions, suggest the presence of a general electrostatic interaction in this area and the possibility of this RNA secondary feature to act as a binding site for small molecules. However, the chemical shift changes of the resonances at the internal loop are slightly different for the diverse ions, showing a more prominent influence of cobalt(III)hexammine on A6, whereas Cd(II) and Mg(II) induce more variations on A22, perhaps with also a direct binding contribution. All of these findings were confirmed by the Mn(II) line broadening experiments that showed that the 5’-end and the internal loop are the most influenced regions. [9]

Our NMR studies on complex 1 and RNA-l showed a marked tendency of the RNA internal loop to act as preferential binding pocket, although the interaction evolves into a more generalised binding in the presence of an excess of metal complex. Similar results were obtained using complex 2, that bears the same dppz moiety although different ancillary ligands, suggesting the involvement of this group in the binding. This finding was confirmed by the results obtained with complex 3, which does not have a dppz moiety. Indeed, spectra of solutions containing complex 3 and RNA-l did not show any interaction. Concerning the interaction with RNA-h, where the internal loop is substituted by regular Watson-Crick base pairs, we only observe an electrostatic interaction at the 5'-end. This result suggests that the presence of the internal loop is essential to observe an RNA selective binding. Finally, with a short DNA sequence, such as DNA-h, complex 1 shows an overall unspecific binding.

To conclude, the findings discussed in this chapter show that the internal loop of RNA-l can act as a preferential binding pocket for metal ions and metal complexes. Therefore, these data provide useful information to evaluate how the presence of non-canonical features in RNA can offer binding sites for small molecules, fuelling further studies on the design of structure-selective RNA binding probes.

3. Optical studies and ITC experiments

Besides NMR spectroscopy, the interaction of nucleic acids and small molecules can be studied with a wide variety of other techniques. [97] In this thesis, we exploited UV-Vis and emission spectroscopy, including ethidium bromide (EB) displacement assays and ITC to study the interaction of our metal complexes (Figure 3.1) and nucleic acids (Figure 3.2). [97–99]

UV-Vis absorption spectroscopy enables to investigate the binding of nucleic acids and metal complexes by monitoring variations in their absorption profiles, such as hypochromism, hyperchromism and shift in the maximum position upon binding.[97] The analysis of these changes can be used to qualitatively study the interaction or to obtain a quantitative evaluation by means of the fitting of the evolution of the UV-Vis bands over a titration. The absorption variations upon interaction can be followed on both nucleic acid or metal complex side. Indeed, on the one hand, DNA and RNA exhibit a broad band in the UV region with a maximum at 260 nm that is due to the chromophoric groups in purines and pyrimidines. It is possible to follow the changes in nucleic acid absorbance to get information on the effect that ligands have on its structure. For example, UV-Vis spectroscopy has been used to identify denaturation of DNA strands in the presence of denaturating agents. [97,99] On the other hand, metal complexes show absorption profiles that can undergo changes in the presence of nucleic acids, revealing a binding. Variations in the absorption maxima of metal complexes upon titration with nucleic acids are often used to determine binding constants by fitting these data using the Scatchard model or, in the cases where the Scatchard plots reveal a non-cooperative binding, the McGhee-von Hippel model.[100]

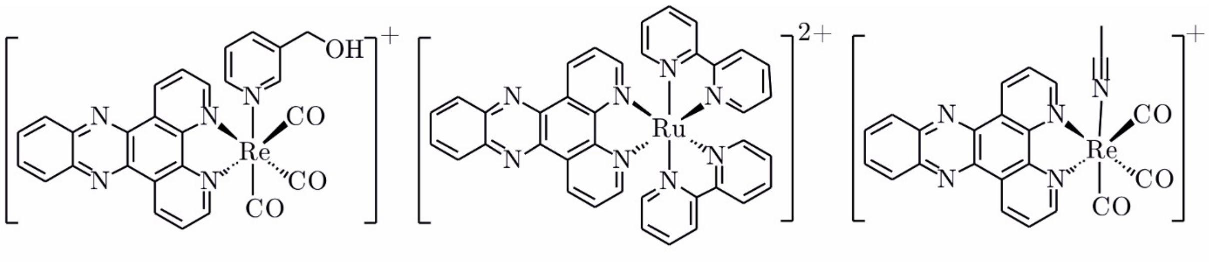

1 2 10

Figure 3.1 Chemical structure of $[Re(CO)_3(dppz)(3\text{-}CH_2OH\text{-}Py)]^+$ (1), $[Ru(bpy)_2(dppz)]^{2+}$ (2) and $[Re(CO)_3(dppz)(MeCN)]^+$ (10).

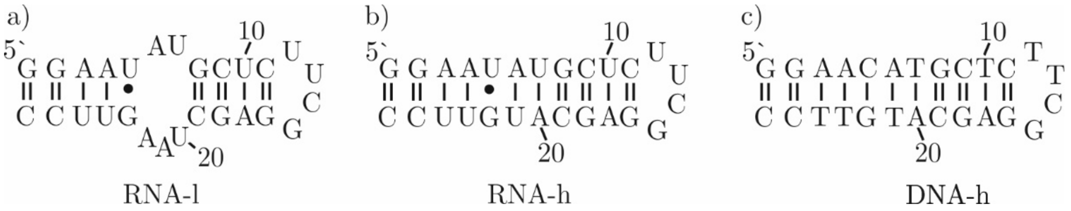

Figure 3.2 Secondary structure of a) RNA-l; b) RNA-h, b) DNA-h.

UV-Vis spectroscopy was used in this thesis to investigate the RNA binding of complex 1 and complex 10 (Figure 3.1). This last complex is an intermediate of the reaction path for the synthesis of complex 1 (Section 5.3) and it differs from the latter one in the axial ligand. Indeed, complex 1 bears a 3-CH_2OH-Py moiety, whereas complex 10 a MeCN group.

Fluorescence spectroscopy is another technique that can provide information on the binding of small molecules with nucleic acids by monitoring changes in their emission profile, such as intensity variations or spectral shifts. [97,99,101] Indeed, like in the case of UV-Vis data, plots of the maxima upon titration give qualitative insights on an interaction and their fitting can provide quantitative information. [99] For example, it is common to perform titrations of nucleic acids into solution of metallo-intercalators and use their emission enhancement upon binding to obtain a quantitative evaluation of the interaction strength, using the same analysis method mentioned above for UV-Vis data. [99] Moreover, competition assays in the presence of molecules known to bind nucleic acids like ethidium bromide, are often used to study the interaction of small ligands with nucleic acids. [97,99]

Another technique used to study this interaction is Isothermal Titration Calorimetry (ITC). This method allows a quantitative characterization of the energetic processes associated with a binding reaction. Indeed, the fitting of the heat related to an interaction can provide various thermodynamic data, such as enthalpy, entropy, binding constant and stoichiometry of the binding. [98,102,103] The ITC studies, commented in this thesis, were performed at the University of Balearic Islands by Dr. Miquel Barceló-Oliver on RNA-l and complex 1 and complex 2. As shown in Figure 3.6, the ITC experiments performed on RNA-l titrated with both complexes show similar profiles although some differences are present.

Using these latter two techniques we obtained further insights, such as stoichiometry, and a qualitative evaluation of the binding strength and the mode of interaction of complex 1 and complex 2 (Figure 3.1) with the different RNA and DNA constructs (Figure 3.2) used in this thesis.

3.1. UV-Vis experiments on complex 1 and complex 10 with RNA-l

As displayed in the example spectrum in Figure 3.3, the electronic spectra of complex 1 and complex 10, show an intense absorption maximum at around 280 nm and weaker peaks at about 380 nm. The first one originates from the ligand-centred ^{1}IL π-π* and n–π* transitions, whereas the latter ones at lower energy can be attributed to a mixture of ^{1}MLCT (dπ(Re)–π*(dppz)) and ^{1}IL transitions. [15,104] Changes in the UV absorption bands of metal complexes could be associated to nucleic acid binding, either by covalent or non-covalent binding, such as intercalation. [99,105] In the following sections, the use of UV-Vis titrations to evaluate the binding of RNA-l and complex 1 and complex 10 is described.

3.1.1. Complex 10 and RNA-l

The absorbance of complex 10, whose structure is depicted in Figure 3.1 (right), was monitored in the presence of 0.2 equivalents of RNA-l. After RNA

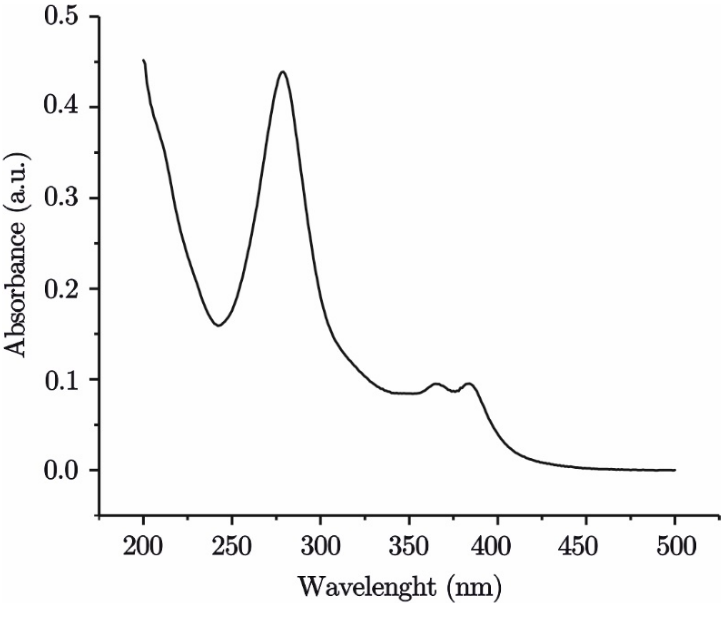

Figure 3.3 UV/Vis spectrum of a 10 μM solution of complex 1 (PBS, pH 7.2).

addition, we observed a hypochromic shift of the absorbance of the complex (Figure 3.4) that suggests that an interaction with RNA is taking place. However, as visible in Figure 3.4, the absorbance decreases continuously over the next 8 hours, suggesting that an equilibrium is not reached over the course of the experiment, thus hampering the study of this system.

It is noteworthy that the changes in the UV-Vis absorption of complex 10 could be due to two different binding modes with RNA-l, covalent or non-covalent. Indeed, the complex bears a MeCN group in axial position that was shown to be a highly reactive leaving group, easily displaced by biological material during the incubation period of cellular accumulation assays. The uptake of complex 10 is likely ruled by lipophilicity and DNA binding. [15] Hence, also in this case, the displacement of the MeCN could favour the direct coordination of complex 10 to RNA-l. This hypothesis is strengthened by the NMR studies performed on the metal ions interaction of RNA-l (Section 2.7), that show the possibility of direct coordination to N7 at different sites in this

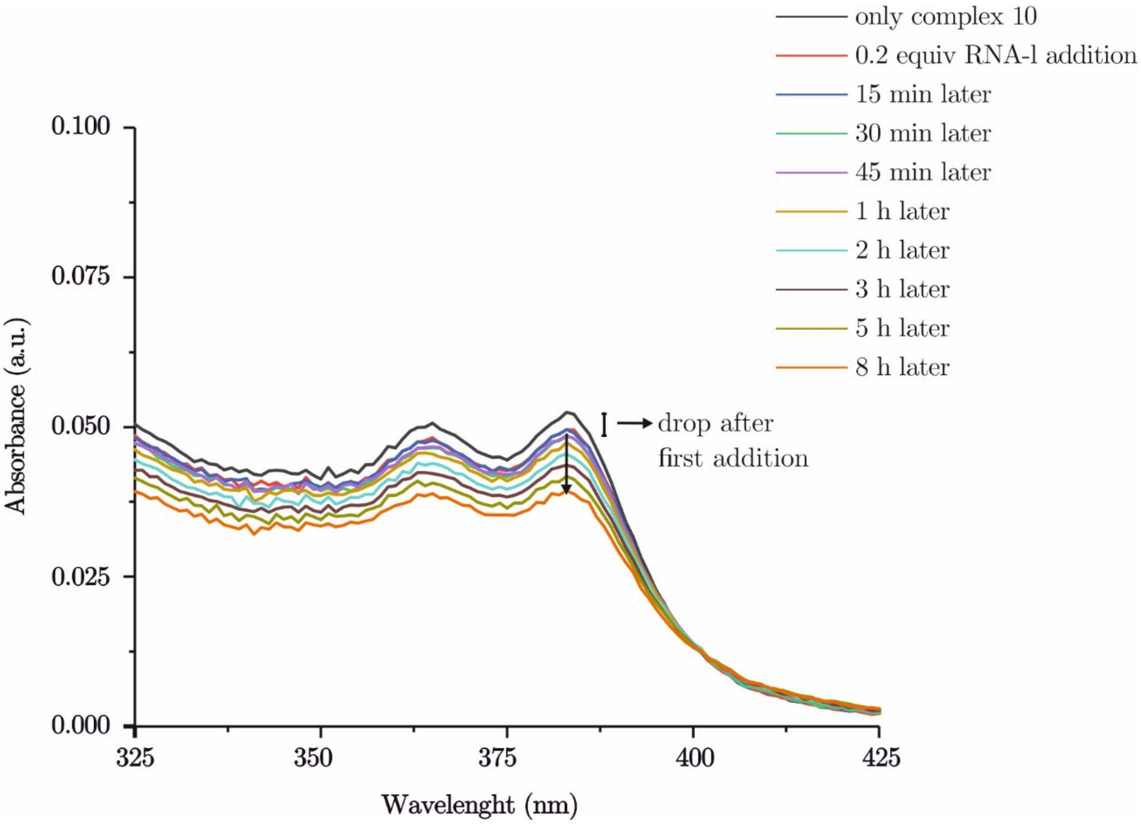

Figure 3.4 Overlay of UV/Vis spectra between 325 and 425 nm of complex 10 (PBS, pH 7.2) upon addition of 0.2 equivalents of RNA-l, recorded over 8 hours.

RNA construct. [9] Therefore, in light of these reasons the investigation of complex 10 and RNA-l was set aside.

3.1.2. Complex 1 and RNA-l

Complex 1, differently from complex 10 presented in the previous section, bears in axial position a pyridine moiety (Figure 3.1). This group was proved to be much less reactive showing, unlike complex 10, the ability of accumulating in different compartments in the cell. [15] Hence, the presence of this axial ligand should disfavour the possibility of direct binding to RNA and foster the non-covalent interaction.

On the contrary to what observed for complex 10, in this case, a single addition of RNA-l into a solution of complex 1 led to a stable absorption value

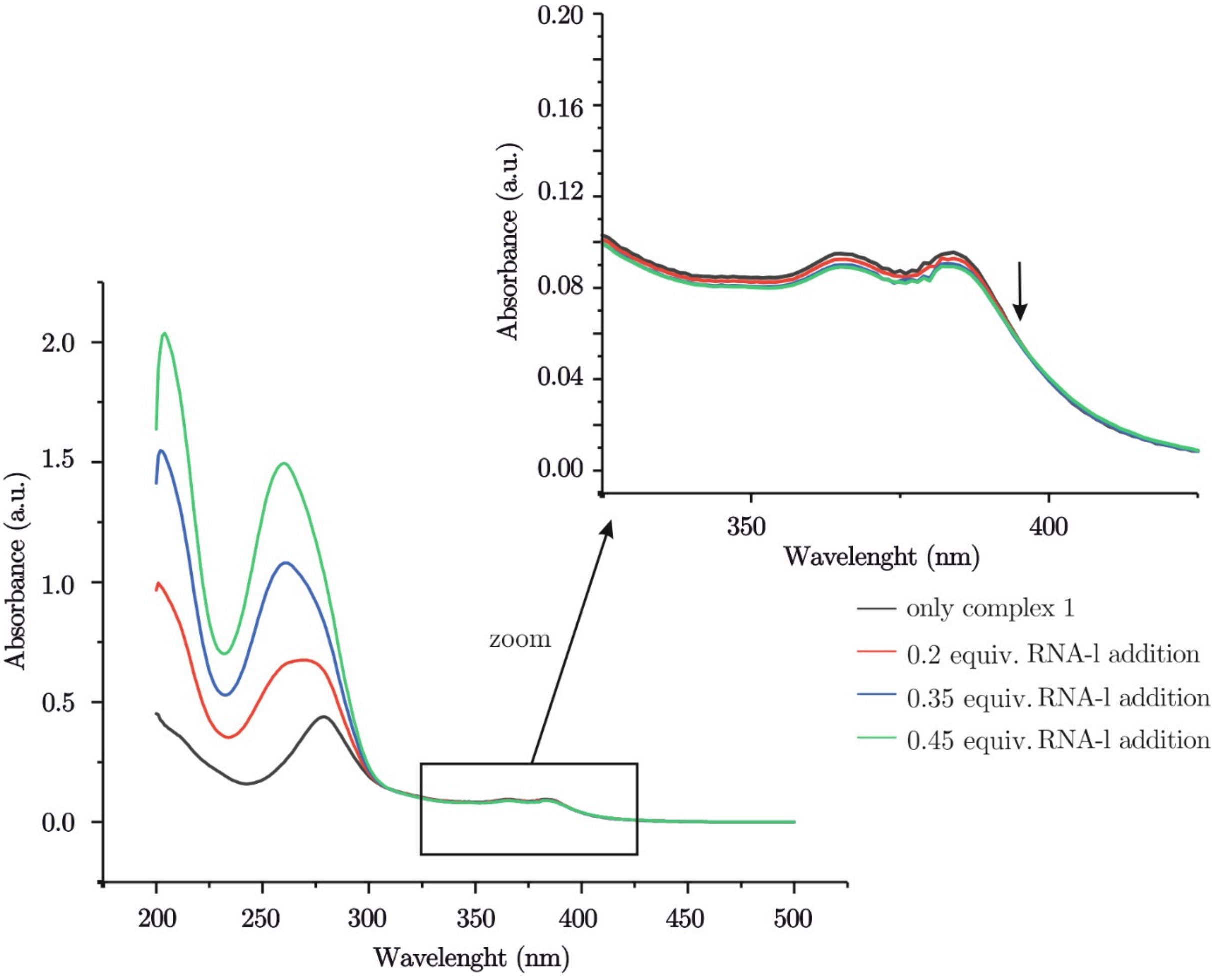

Figure 3.5 Overlay of UV/Vis spectra between 200 and 500 nm of complex 1 (9.4 µM, PBS, pH 7.2) with additions of RNA-l (0.2, 0.35, 0.45 equivalents) with zoom of the area between 325 and 425 nm.

over time, and therefore titrations were performed to study more in depth the interaction. In these experiments, RNA-l was stepwise added to complex 1, resulting in the hypochromic effect shown in the zoomed panel of Figure 3.5. This indicates that a binding between the two components of the mixture occurs. However, the decrease in absorbance at each step of the titration is very little. Assuming that the interaction occurs via the dppz moiety for both RNA and DNA we can compare the decrease in intensity observed in our case to the one reported in the literature for the binding of complex 1 with CT-DNA, [15] and suggest that the affinity for RNA is lower. Such small differences in absorbance upon binding are affected by non-negligible errors, and unfortunately not quantitative evaluation of the binding strength was obtained via UV-Vis titrations. However, although the binding of complex 1 with RNA-l results to be weaker than the one with CT-DNA, the NMR spectroscopy studies reported in Chapter 2 proved that it takes place. For this reason, the interaction was further investigated with other techniques explained in the following sections.

3.2. Isothermal Titration Calorimetry experiments

Isothermal Titration Calorimetry (ITC) is a powerful and effective technique used to study the binding of many biological systems, such as protein-protein, nucleic acid-protein, proteins or nucleic acids and small ligands. [103,106] This method is based on the measurement of the interaction heat and it offers the possibility to obtain an entire set of thermodynamic data (n, K, ΔH, ΔS) to characterize an interaction from only a single titration. [102] Indeed, this method relies on the fact that the integrated heat (q_i) at each injection step is a function of the total concentration of titrant (M_T), the binding enthalpy (ΔH), the stoichiometry (n), the fraction of saturation of the binding (F) and the cell volume (V), according to the following equation:

$$q_i = nFM_T\Delta HV \quad \text{Equation 3.1}$$

This equation is then mathematically rearranged allowing to obtain the thermodynamic data of the interaction process under investigation. [102]

The instrument consists of two cells maintained at the same temperature, one of which is the reference and the other one is the sample cell. To this last one, a

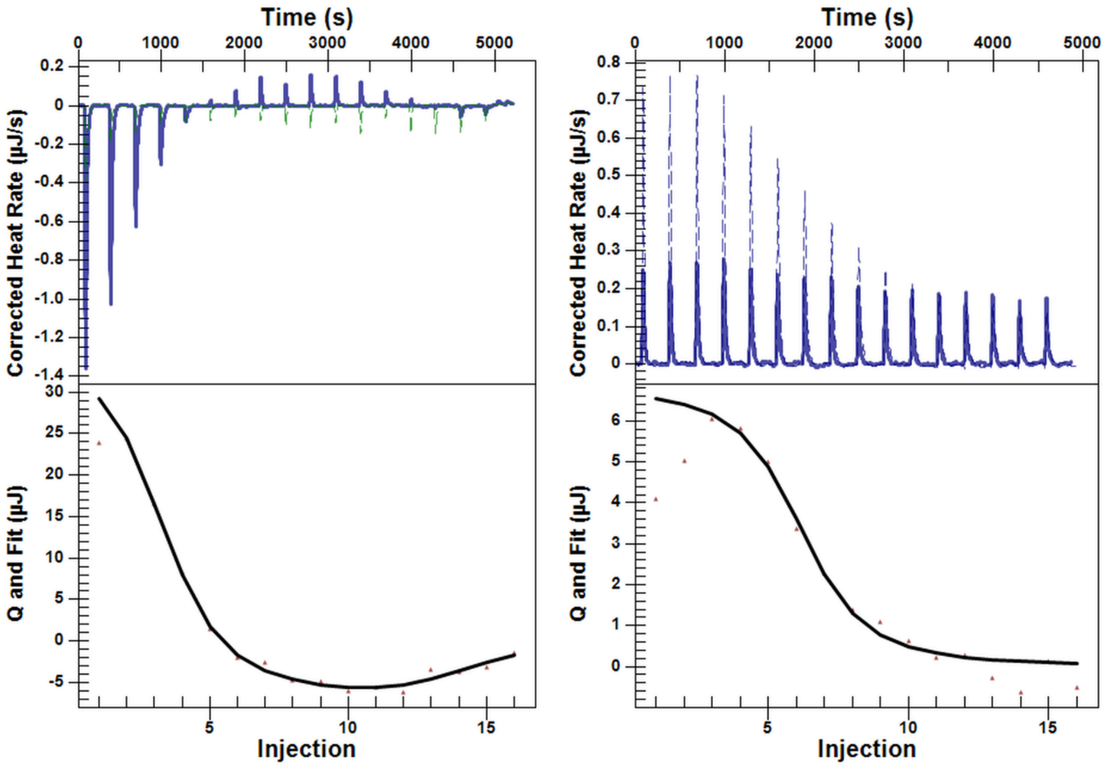

Figure 3.6 ITC data collected on RNA-l in the presence of increasing amounts of complex 1 (on the left, 25ºC, PBS with 2% DMSO, pH 7.2) and of complex 2 (on the right, 25ºC, PBS, pH 7.2).

syringe containing the titrant is connected. [103] At each addition of titrant to the sample, in case of interaction, there is a release or an absorption of heat that the instrument has to compensate to keep the two cells at equal temperature. The compensation results in a peak that can be integrated *versus* time. All the peaks at each point of the titration give rise to a curve that can be fitted with the mathematical equation that better describes its shape and the interaction expected. [107]

The ITC studies, commented in this thesis, were performed at the University of Balearic Islands by Dr. Miquel Barceló-Oliver on RNA-l and complex 1 and complex 2. As shown in Figure 3.6, the ITC experiments performed on RNA-l titrated with both complexes show similar profiles although some differences are present.

In both cases an endothermic process was detected, ascribable to the binding of the metal complex to the RNA internal loop. A second exothermic binding with lower binding affinity could be identified in the case of complex 2. Hence, the data were fitted using a one-binding site model for complex 1 and a two-binding sites model for complex 2. The second binding event is in the lower limit of detectability and could be due to an interaction at the base-paired regions. This result is in accordance with the NMR data (Section 2.8), that show a first selective binding localised at the internal loop that then is extended over the whole sequence. This second event could not be observed in the case of complex 1, most likely owing to its low binding affinity along with the presence of a 2% of DMSO in PBS that contributes to the overall heat. Although the data could be qualitatively evaluated, in both cases the low interaction affinity is likely responsible for non-negligible errors, and no quantitative data could be obtained. For this reason, further investigations are needed to obtain more reliable data for a quantitative evaluation.

However, a stoichiometry of two molecules of complex 1 per one RNA internal loop could be obtained. Interestingly, this result was obtained in two different ways, firstly adding the complex to RNA-l and then in the reverse way, by adding RNA-l into a solution of complex 1. Indeed, in the first case a stoichiometry value, $n = 2$ was found, confirmed by $n = 0.5$ in the second case. This stoichiometry value of two metal complexes per RNA internal loop was confirmed by Job plot experiments, as described in the next session.

3.3. Job plot experiments

The Job plot experiments rely on the continuous variation method and allow to determine the stoichiometry of an interaction at the equilibrium. [108,109] It is a widespread method that, thanks to its simplicity, has been widely used on different systems, such as ligands interacting with metal complexes, complexes of inorganic anions and organometallic compounds, DNA constructs and fluorescent dyes and organic hosts and other organic molecules. [110–114] To determine the stoichiometry value, the molar ratios of one species are varied while the total concentration of the two components is kept constant. The measured parameter, that can be for instance UV-Vis or infrared absorbance or emission intensity, is then plotted *versus* the mole fraction. The obtained graph

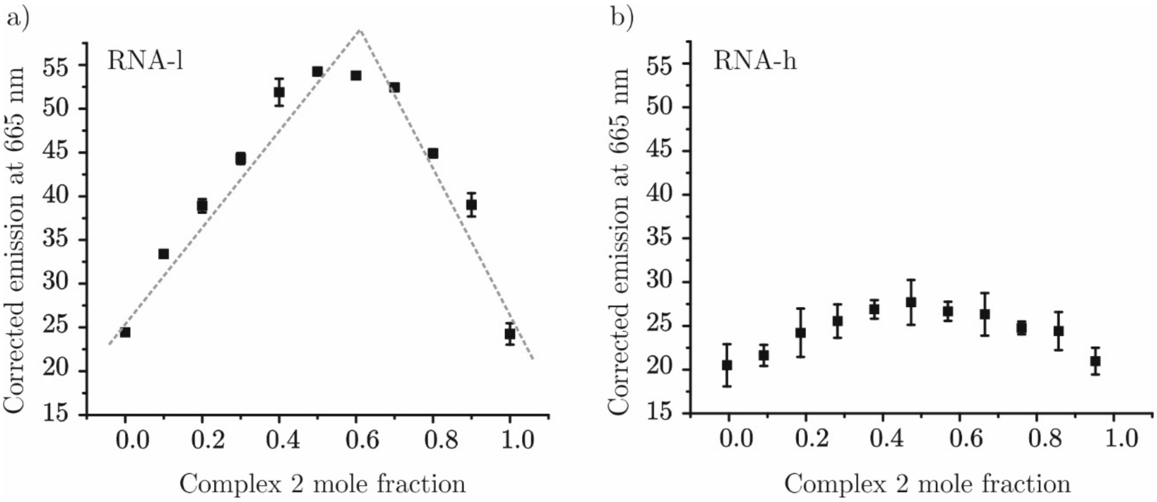

Figure 3.7 Job plot experiments of complex 2 and a) RNA-l and b) RNA-h (PBS, pH 7.2). The total molar concentration of the solutions at each point is 3 μM. The maximum in panel a) is highlighted with dashed lines.

is called Job plot and its maximum represents the stoichiometry of the interaction under investigation. [109]

In this thesis, this method was used to confirm the stoichiometry value obtained via ITC. No data could be collected on complex 1 and RNA-l, since no reliable parameters could be exploited for these experiments. Indeed, the UV-Vis absorbance data were affected by non-negligible errors and no emission could be detected upon interaction of complex 1 with RNA. This latter behaviour is not unexpected, because the luminescence restoring of Re(I)dppz complexes is already barely measurable in the presence of DNA, being less efficient than the one of the ruthenium counterparts. [15] Hence, this method was applied only to complex 2, that shows a measurable luminescence intensity and whose interaction with RNA-l was proved via NMR spectroscopy (Section 2.8) to occur in a similar manner to the one of complex 1. The ratio of complex 2 to RNA-l was varied while the total sum of both concentrations was kept constant to 3 μM and the emission at each different ratio was measured. As shown in Figure 3.7, the Job plot curve obtained shows a clear maximum that indicates a stoichiometry of two ruthenium complexes per RNA. As assumed above, based on the NMR data, complex 1 and complex 2 interact with RNA-l similarly, thus allowing us to extend the result obtained via Job plot assays for complex 2 to the binding of complex 1 and RNA-l, so confirming the ITC data.

This method was also applied for the sake of comparison on RNA-h and complex 2, as visible in Figure 3.7b. In this case, the emission intensity detected is little and the data are affected by remarkable errors, hindering a confident evaluation.

3.4. Fluorescence competition experiments

In order to qualitatively compare the binding affinities of complex 2 to DNA-h *versus* RNA-l and RNA-h, we exploited competition emission assays. In these experiments we either titrated 1 equivalent of RNA-l or RNA-h in six steps to an equimolar solution of DNA-h and complex 2 or reversely, 1 equivalent of DNA-h in six steps to an equimolar solution of RNA-l or RNA-h and complex 2.

In the first case, the addition of RNA-l or RNA-h to an equimolar mixture of DNA-h and complex 2 resulted in a decrease of the emission intensity (example in Figure 3.8a). The emission intensity of complex 2 in the presence of DNA-h is sixfold and tenfold higher than the one in the presence of RNA-l and RNA-h respectively (compare the first points of Figure 3.9a and Figure 3.9b). Hence, we

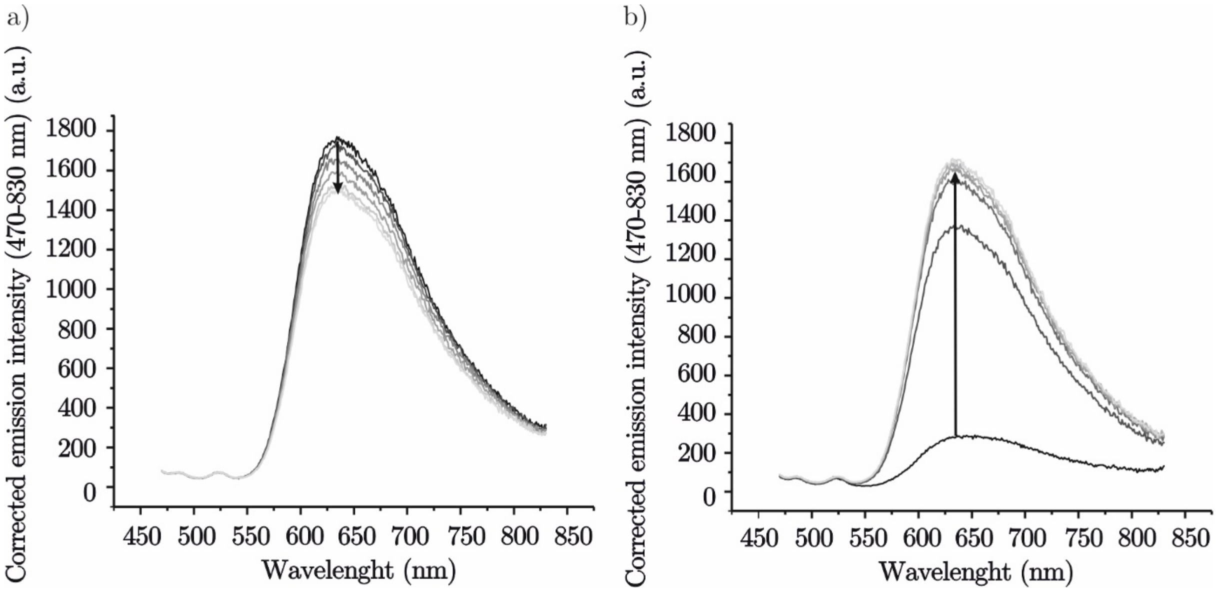

Figure 3.8 Corrected emission intensity (470-830 nm) of a) 1:1 DNA-h:complex 2 solution upon six additions of RNA-l; b) 1:1 RNA-l:complex 2 solution upon six additions of DNA-h (pH 7.2, PBS).

can consider that the emission observed during the experiment is almost exclusively due to the binding of complex 2 to DNA-h. Therefore, the decrease indicates a competition of RNA-l and RNA-h *versus* DNA-h to the binding of complex 2.

In the reverse case, the additions of DNA-h into an equimolar mixture of RNA-l or RNA-h and complex 2, lead to a strong increase in emission intensity (example in Figure 3.8b). As the emission can be mainly attributed to the interaction of complex 2 with DNA-h, this behaviour indicates that also DNA-h compete with RNA-l and RNA-h for the binding of complex 2.

To analyse these findings in more detail, we plotted the emission maximum of complex 2 over the titration *versus* the equivalents of nucleic acid added (Figure 3.9). A decrease of 30% (see experimental details in Section 6.14) is observed when 1 equivalent of RNA-l is added to an equimolar solution of DNA-h and complex 2 (black dataset in Figure 3.9a), and a complementary increase of

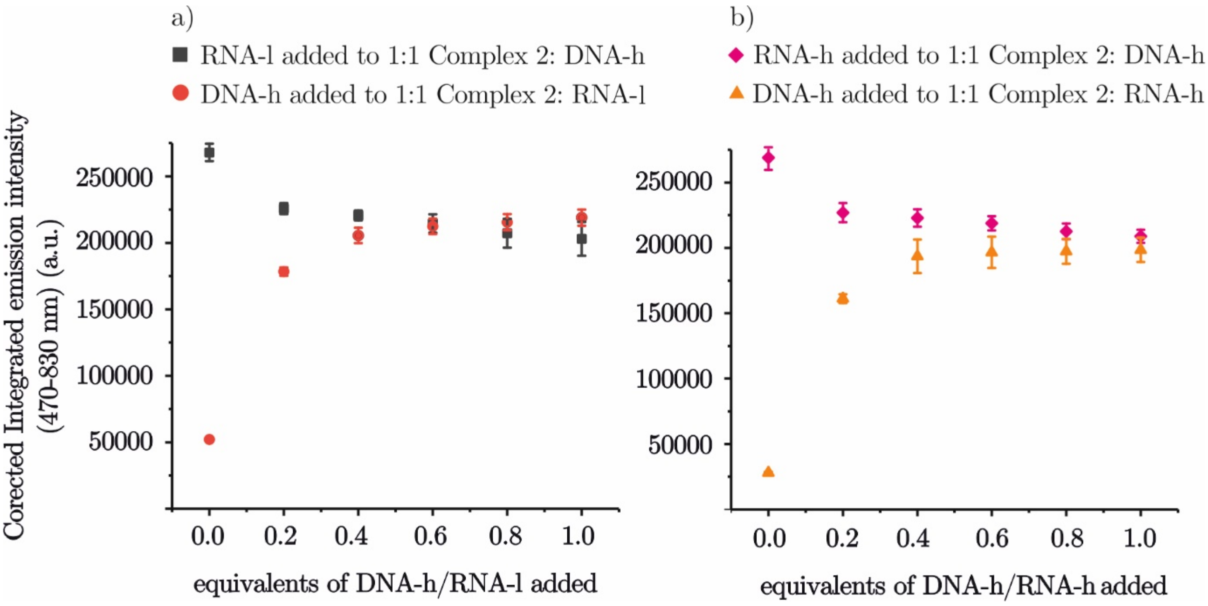

Figure 3.9 Corrected integrated emission intensity between 470 and 830 nm (PBS, pH 7.2) a) black dataset represents the emission maximum of complex 2 bound to DNA-h at different concentrations of RNA-l; red dataset represents the emission maxima of complex 2 with RNA-l at different concentration of DNA-h; b) magenta dataset represents the emission maximum of complex 2 bound to DNA-h at different concentrations of RNA-h; orange dataset represents the emission maxima of complex 2 with RNA-h at different concentration of DNA-h.

70% is visible in the reverse case (red dataset in Figure 3.9a). This result indicates that only 30% of DNA-h is displaced by RNA-l in the binding to complex 2, suggesting that the binding between DNA-h and complex 2 is stronger.

Similar data were obtained when we tested the ability of RNA-h to displace DNA-h in the binding of complex 2 (Figure 3.9b). The emission decreases of 25% (see experimental details in Section 6.14) when RNA-h is added to an equimolar mixture of DNA-h and complex 2 (magenta dataset in Figure 3.9b) and a 75% increase is observed in the reverse experiment (orange dataset in Figure 3.9b). These data indicate that 25% of DNA-h is displaced by RNA-h in the binding of complex 2 and suggests that, also in this case, the binding of the metal complex to DNA is stronger than the one with RNA.

Hence, in both cases, RNA-l and RNA-h showed to be able to compete with DNA-h to bind complex 2, although with lower strength, and to induce similar intensity decrease of the emission of complex 2 bound to DNA-h. In order to better evaluate the binding affinities of the two RNA constructs to complex 2, additional experiments on equimolar mixtures of RNA-l and complex 2 with additions of RNA-h were performed and the changes of the emission maximum upon addition were plotted (Figure 3.10). As in the previous assays, also in

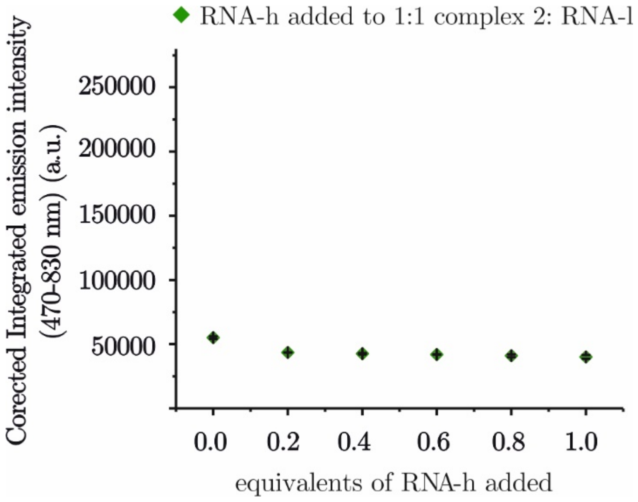

Figure 3.10 Corrected integrated emission intensity between 470 and 830 nm (PBS, pH 7.2) of complex 2 and RNA-l with additions of RNA-h. Error bars indicate standard deviations calculated for at least three replicates.

Figure 3.10 we observe a decrease of the luminescence of the complex. However, in this case the difference in emission intensity between complex 2 interacting with RNA-l and complex 2 with RNA-h is much smaller than when the metal complex emission with RNA was compared to the one with DNA-h (Figure 3.9). Hence, the emission observed at each point of the experiment is the result of both contributions, making difficult to discern between them. Therefore, no safe conclusions could be taken out of this set of experiments.

3.5. Emission titrations with complex 2 and ethidium bromide

Optical methods, such as steady state emission titrations are also widely employed to characterize the interaction of metal complexes and nucleic acids. [15,33,115] Emission titration experiments were performed using complex 2, since complex 1 does not show emission in the presence of RNA. This is not surprising as already discussed in Section 3.3. Moreover, we can also speculate

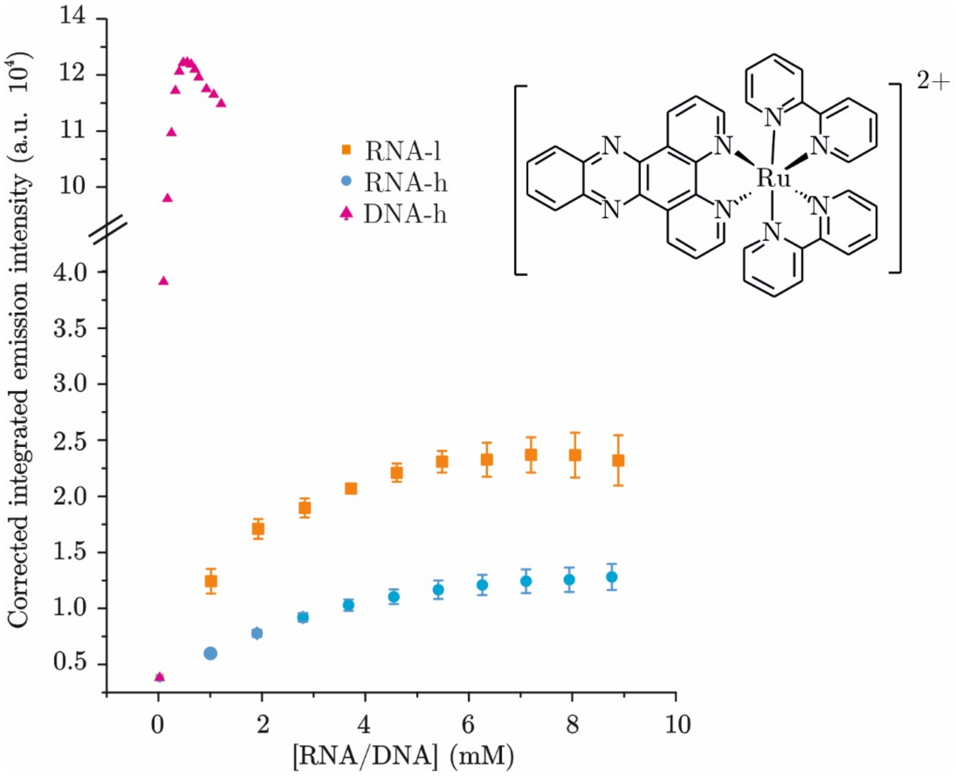

Figure 3.11 Plot of corrected integrated emission intensities of a 3 µM solution of complex 2 in the presence of increasing amounts of RNA-l (orange squares), RNA-h (light blue circles) and DNA-h (magenta triangles) in PBS, pH 7.2. Error bars indicate standard deviations calculated for at least three replicates. The emission intensity of complex 2 was integrated between 550 nm and 750 nm.

that the fast dynamics of the binding, could preclude complex 1 from spending enough time in the RNA binding pocket, thus favouring quenching of the excited state by oxygen or water molecules. Furthermore, both complexes with RNA-l are expected to interact in a similar way (Section 2.8) allowing to extend the results obtained on complex 2 to complex 1.

The emission titration experiments were performed adding stepwise RNA-l, RNA-h or DNA-h to a solution containing complex 2.

As expected based on literature data, [32,33] the emission intensity of complex 2 at 620 nm is enhanced in the presence of increasing amounts of all the three nucleic acids. However, as shown in Figure 3.11, complex 2 shows different emission intensities in the presence of the diverse constructs. It is worth to note that complex 2 in the presence of RNA-l shows higher luminescence than with RNA-h. This behaviour can be due to the presence of the internal loop that might behave as a binding pocket for the dppz moiety of complex 2, resulting in a better shielding and thus in a higher emission intensity. However, the most

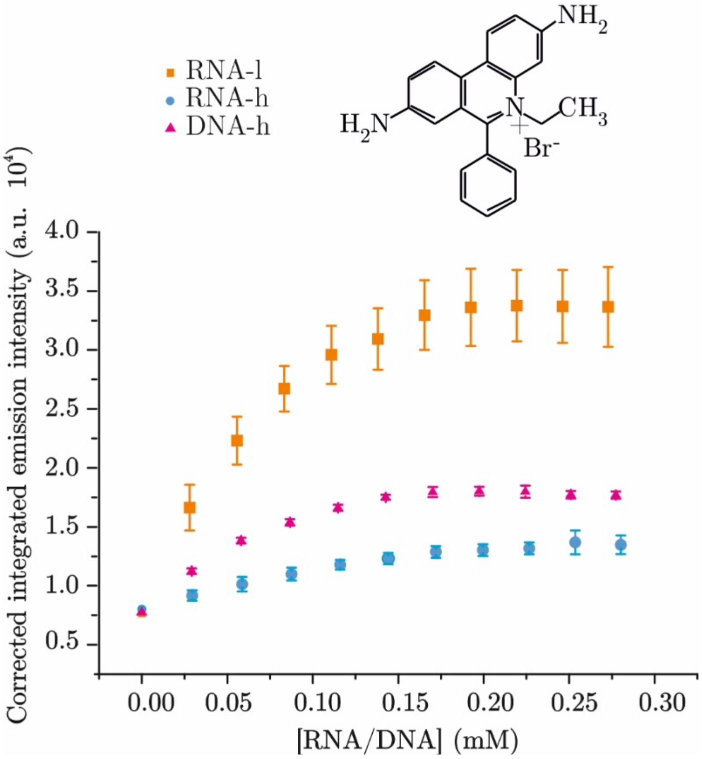

Figure 3.12 Plot of corrected integrated emission intensities of 0.1 µM ethidium bromide in the presence of increasing amounts of RNA-l (orange squares), RNA-h (light blue circles) and DNA-h (magenta triangles) in PBS, pH 7.2. The ethidium bromide emission intensity was integrated from 540 nm to 800 nm.

intense emission is observed in the presence of DNA-h, which is sixfold and tenfold higher than the one observed with RNA-l and RNA-h, respectively. It is not surprising that complex 2 shows the lowest restoring in emission with RNA-h and a much higher one in the presence of DNA-h. Indeed, it is known that classical A-form RNA does not sufficiently shield the phenazine nitrogen atoms of the dppz moiety, resulting in only little luminescence, [19] whereas B-DNA is able to offer a good screening giving rise to higher emission. [33] It is worth to note also that the emission profile observed in the presence of DNA shows a first increase, followed by a decrease in the intensity. This behaviour is likely due to different binding orientation in the interaction of Λ and Δ enantiomers of complex 2 with short DNA constructs that generates different emission profiles. [116,117] Interestingly, this is not observed in the case of RNA-l, suggesting that both enantiomeric forms of complex 2 interact in similar way with the RNA internal loop.

Emission titration experiments were also performed adding EB to our nucleic acid constructs to evaluate their ability of binding this intercalating ligand. Indeed, EB is a well acknowledged molecule that is able to intercalate into DNA and RNA structures. [15,115] Our RNA and DNA constructs were added into solutions of EB and the variations in emission intensity at 605 nm were monitored. As visible in Figure 3.12, spectra of the emission of EB at different RNA concentrations show higher intensity in the presence of RNA-l than with RNA-h, similarly to what observed in the case of complex 2 in Figure 3.11. Interestingly, in this case the interaction between DNA-h and EB leads to a recovery of luminescence, whose intensity lays between the one exhibited with RNA-l and RNA-h. Hence, our data suggest that the internal loop of RNA-l offers a flexible binding pocket that efficiently shields EB. This is not unexpected since RNA non-canonical regions were found to better allocated EB in comparison to the classical B-form DNA, [23] represented in this work by DNA-h.

3.6. Ethidium bromide displacement assays

Displacement assays with ethidium bromide [15,33] were performed aiming to evaluate the ability of complex 1 and complex 2 to compete with EB for the binding of our RNA and DNA model systems.

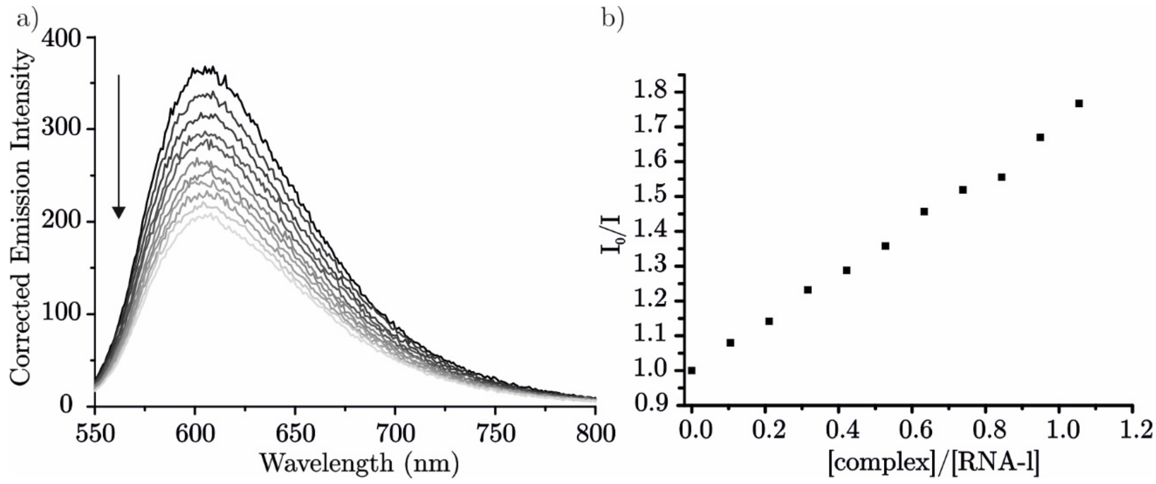

Figure 3.13 a) Example of corrected emission intensity of an equimolar solution of EB and RNA-l in the presence of increasing amount of complex 2 (pH 7.2, PBS); b) linear fitting of the emission intensity data in panel a). The arrow shows the changes in emission upon the increase of RNA-l concentration.

Equimolar solutions of the three RNA and DNA constructs and EB were prepared and then were titrated with increasing amounts of complex 1 and complex 2, resulting in a decrease of the EB luminescence, as in the example in Figure 3.13a. In all the assays EB is displaced by both complex 1 and complex 2, so suggesting that there is a contribution of intercalative binding. [23] Moreover, the drop of EB emission intensity is linear in all the cases, allowing the fitting of these data (example in Figure 3.13b) to obtain Stern-Volmer constants, K_{SV}, of these interactions, summarized in Table 3.1.

Table 3.1 Stern-Volmer constant values for complex 1 and complex 2 in the presence of the three RNA and DNA constructs.

	Complex 1	**Complex 2**
K_{SV} RNA-l	0.20(0.067)	0.73(0.011)
K_{SV} RNA-h	0.27(0.038)	0.40(0.18)
K_{SV} DNA-h	0.26(0.035)	0.65(0.074)

The K_{SV} for complex 1 with all the nucleic acids used are lower than the ones found for complex 2, suggesting that the interaction of this latter one is stronger. This difference could be ascribed to the higher charge of complex 2 or to the role played by the different ancillary ligands of the two complexes.

3.7. Conclusion

This chapter summarises the results obtained by using a combination of optical methods, such as UV-Vis and fluorescence spectroscopy, including ethidium bromide displacement assays and Job plot experiments, along with ITC to study the binding of our metal complexes and RNA and DNA constructs.

UV-Vis data were collected on complex 1 and complex 10. This latter one shows after the addition of 0.2 equivalents of RNA-l a continuous decrease of the complex absorbance. This suggests that an interaction occurs, but it does not reach the equilibrium over the time suitable for UV-Vis experiments, hampering a quantitative evaluation of the binding. Moreover, the hypochromicity observed for complex 10 can be due to the interaction with RNA-l in two different ways, a non-covalent and a covalent one. Indeed, bearing in axial position a MeCN moiety that can be displaced, [15] complex 10 might metallate RNA-l, that is also known to be prone to N7 direct coordination, as discussed in Section 2.7. [9] For these reasons, the interaction of complex 2 with RNA-l was shelved. As for complex 1, its UV-Vis profile with RNA-l suggests the presence of a stable interaction. Unlike complex 10, in this case the binding is likely due only to non-covalent interaction. Based on these reasons, titrations of RNA-l into complex 1 were performed. In these experiments, only very small differences in absorbance at each step were observed, indicating that an interaction occurs, but it is lower than the one observed in the literature for the interaction of complex 1 with CT-DNA. [15] Such little changes in the absorption values are affected by non-negligible experimental errors, so that a quantitative evaluation of these data was hindered. However, the presence of an interaction between complex 1 and complex 2 and the internal loop of RNA-l, was observed via NMR (Chapter 2) and it was further investigated using other techniques.

ITC experiments were used to study the binding between complex 1 and complex 2 and RNA-l in order to obtain quantitative data. The data obtained suffer from a general deviation and need further investigations. However, a stoichiometry value for the interaction between complex 1 and RNA-l could be proposed. It was found that two rhenium complexes can bind one RNA internal loop. Job plot assays were run to confirm the stoichiometry value obtained via ITC. They were performed only on complex 2 with RNA-l, because, unlike complex 1, its emission is measurable. Job plot experiments showed a stoichiometry of two ruthenium complexes per internal loop, that could be extended to complex 1, based on their similar interaction with RNA-l (NMR data in Chapter 2), thus confirming the stoichiometry value obtained via ITC.

Competition emission assays were used to qualitatively compare the interaction between our nucleic acid constructs and complex 2. These experiments showed that both RNA-l and RNA-h are able to displace DNA-h from complex 2, although the interaction of complex 2 with this latter one was confirmed to be stronger.

Emission assays performed titrating the three nucleic acids into samples containing complex 2, show that the emission is higher with RNA-l than with RNA-h, suggesting that the complex is better shielded from water by RNA-l. However, the emission observed in the presence of DNA-h is much higher. Interestingly, in this case the luminescence increases and then decreases during the titration. This behaviour could be due to the different interaction mode of the enantiomeric forms of complex 2. Such phenomenon was not observed for the interaction of complex 2 with RNA-l, suggesting that the different enantiomers interact with the internal loop in a similar way.

Emission assays were also done using EB to test the behaviour of our RNA and DNA model systems with intercalating agents. Also in this case, the emission of EB with RNA-l was higher than with RNA-h. Unlike the results obtained for complex 2, the emission of EB with DNA-h is lower than the one of EB in the presence of RNA-l. This finding is not surprising since it was already reported [23] that RNA non-canonical regions, such as our internal loop, can accommodate better EB than the classical B-DNA.

Ethidium bromide displacement assays allowed us to evaluate the binding of complex 1 and complex 2 towards all our three nucleic acids. In these experiments complex 2 was titrated into equimolar solution of EB and our RNA and DNA constructs. The data were then fitted to obtain the Stern-Volmer constants, that resulted lower for the binding with complex 1 than with complex 2, thus suggesting that the interaction of this second one with all our RNA and DNA sequences is stronger. This difference might be due to the higher charge of complex 2 or to the different axial ligands that the complexes bear.

Based on the data collected in this chapter, we could confirm that the interaction of complex 1 and complex 2 with RNA-l is localised at the internal loop and it occurs with a stoichiometry of two metal complexes per RNA. However, our results also suggest that the binding with DNA-h is stronger. Hence, these findings combined with the ones described in Chapter 2, showed that the binding at the internal loop represents the possibility to target RNA non-canonical structural features with metal complexes. However, this interaction is weaker than the unspecific one observed for DNA-h in the cases herein investigated. Therefore, further efforts are needed to design metal complexes that are simultaneously able to selectively bind specific RNA features and to show higher affinity for RNA binding over DNA.

4. STD NMR experiments and MD simulations on complex 1 and RNA-l

The NMR data collected on complex 1 and complex 2 with RNA-l, shown in Chapter 2, suggest that the interaction occurs via the dppz moiety and it is localized at the internal loop. Indeed, the resonances of the nucleobases in that region and the ones located close by are the most affected upon metal complex addition. Unfortunately, the NMR spectra suffer from fast dynamics and signals coalescence, hampering a precise localization of the metal complex in the internal loop region. Besides NMR, UV-Vis and emission titrations, ethidium bromide displacement assays and ITC experiments confirmed the interaction at the internal loop (Chapter 3). Moreover, a stoichiometry of two metal complexes per RNA was suggested.

In order to further characterize the binding of complex 1 and complex 2 with the RNA internal loop we used Saturation Transfer Difference (STD) NMR experiments [80] and Molecular Dynamics (MD) simulations, [118] which will be described in this chapter written in collaboration with Prof. Dr. Giampaolo Barone and Dr. Angelo Spinello (University of Palermo), who performed the MD simulations.

4.1. Saturation Transfer Difference (STD) NMR

Saturation Transfer Difference (STD) NMR is a well-established method reported in the literature to study the binding of macromolecular receptors and

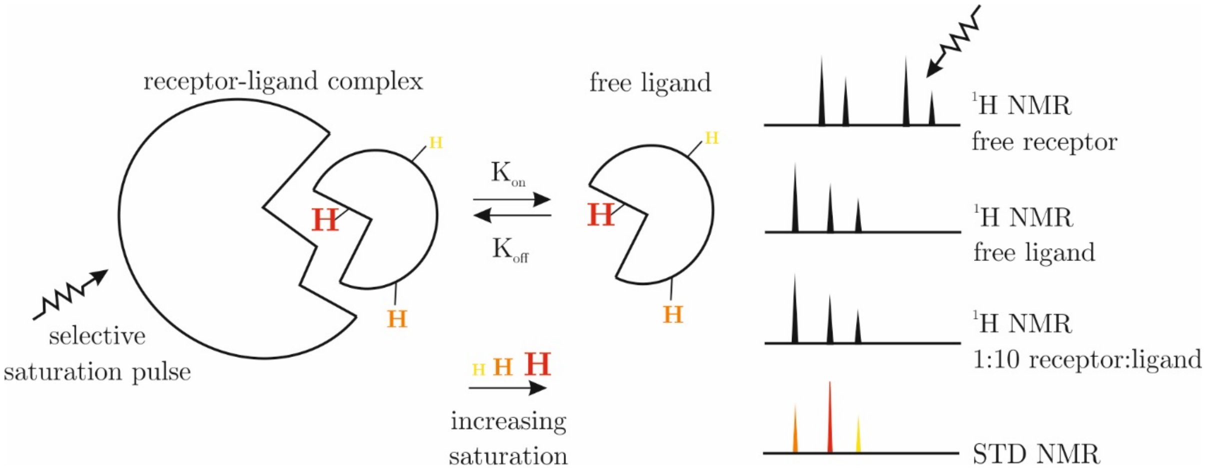

Figure 4.1 On the left, illustration of the STD NMR mechanism for a ligand in fast exchange between the bound and the free state. On the right, schematic representations of ^{1}H NMR spectra of the free receptor, of the free ligand, of the receptor and of ligand mixture and of the STD NMR.

small ligands. [80,81,119,120] In the early stages, it was used only to fast-screen the presence of an interaction for wide libraries of compounds. [80,121] Nowadays, its full potential is exploited. Indeed, it is applied to investigate the binding between small ligands and macromolecular receptors, giving information on the proximity of the protons of the ligand to the receptor and also to calculate dissociation constants. [81,82,122–124]

STD NMR relies on a subtraction of two experiments. One is called *on-resonance* and the other one is called *off-resonance.* [80,81] In the first one, a selective pulse is directed to a small region of the spectrum where only the proton resonances of the receptor are observable (Figure 4.1 upper right). Indeed, it is crucial to avoid the excitation of the protons of the ligand, because they should receive magnetization only from the receptor. In the latter experiment the selective pulse is set to an empty region where no resonances of the receptor and of the ligand are present. The final spectrum, STD NMR in Figure 4.1, is the subtraction of these two experiments and it shows exclusively the signals of the ligand which have been close enough to the receptor to receive magnetization via spin diffusion. The left part of Figure 4.1 represents the STD NMR mechanism for a ligand in fast exchange between bound and free state. In the picture, the protons of the ligand are highlighted using different font sizes according to the amount of magnetization they receive during the on-resonance experiment. Hence, the bigger is the font, the closer in space the protons of the ligand are to the receptor upon binding and the higher is the amount of magnetization received.

This experiment can be successful only if the following requirements are fulfilled by the system under investigation. [80,81]

- The receptor and the ligands have to be in fast exchange. This is essential to build up a significant population of saturated ligands, thus allowing to obtain a spectrum with a good signal to noise ratio. Indeed, if the ligand stays too long in the binding site, this will preclude other ligands to receive magnetization, thus hampering the saturation of a significant number of ligands in solution.

- The relaxation rate of the receptor magnetization represents also an important parameter. Indeed, the bigger the molecule, the faster the relaxation, resulting in a more sensitive experiment since more magnetization is transferred. For this reason, normally STD NMR studies are performed on receptors with molecular weight higher than 10 kDa. [122] However, a few studies were also reported on receptors with lower molecular weight. [125,126]
- Most of the studies have been done on systems with a dissociation constant in the range 10^{-3}-10^{-8} M. [80]

Moreover, for STD NMR experiments to be successful it is essential to use a large excess of ligands. Normally a ratio 1:10 or 1:100 between receptor and ligand is used, leading to a ^{1}H NMR spectrum in which the signals of the receptor are hardly visible. (schematic representation in Figure 4.1, right).

Summarizing all the requirements, the success of an STD NMR experiment depends on the choice of the appropriate frequency for the selective pulse, on the receptor size, on the exchange rate of the system, on the range of dissociation constant and on the use of a large excess of ligands.

We used STD NMR to identify the position of complex 1 and complex 2 upon binding of RNA-l. The two systems under investigation seem to fulfill the requirements needed for a fruitful application of the STD NMR method. Indeed, some RNA signals can be selectively excited, RNA-l is in the correct molecular weight range and dynamics seems to be fast (Section 2.8). Moreover, based on DNA interaction with similar complexes, the dissociation constant should lie in the correct range. [15,32] The only limitation could be represented in the case of complex 1 by its low water solubility that may preclude the usage of a large excess of ligands in solution.

STD NMR experiments were collected on RNA-l in the presence of a tenfold excess of complex 1 and complex 2, setting the on-resonance irradiation to 3933 Hz (5.62 ppm, region where for RNA samples H1', H5 signals are found), while the off resonance one to 21000 Hz (30 ppm). In Figure 4.2 are depicted the STD NMR experiments for complex 1 (panel a) and complex 2 (panel b), the ^{1}H NMR spectra of the mixture used in this assay and the ones of the isolated RNA-l and complexes.

In the case of complex 1, an abundant precipitation after the addition of tenfold excess of ligand was observed and the ^{1}H NMR spectrum of the mixture

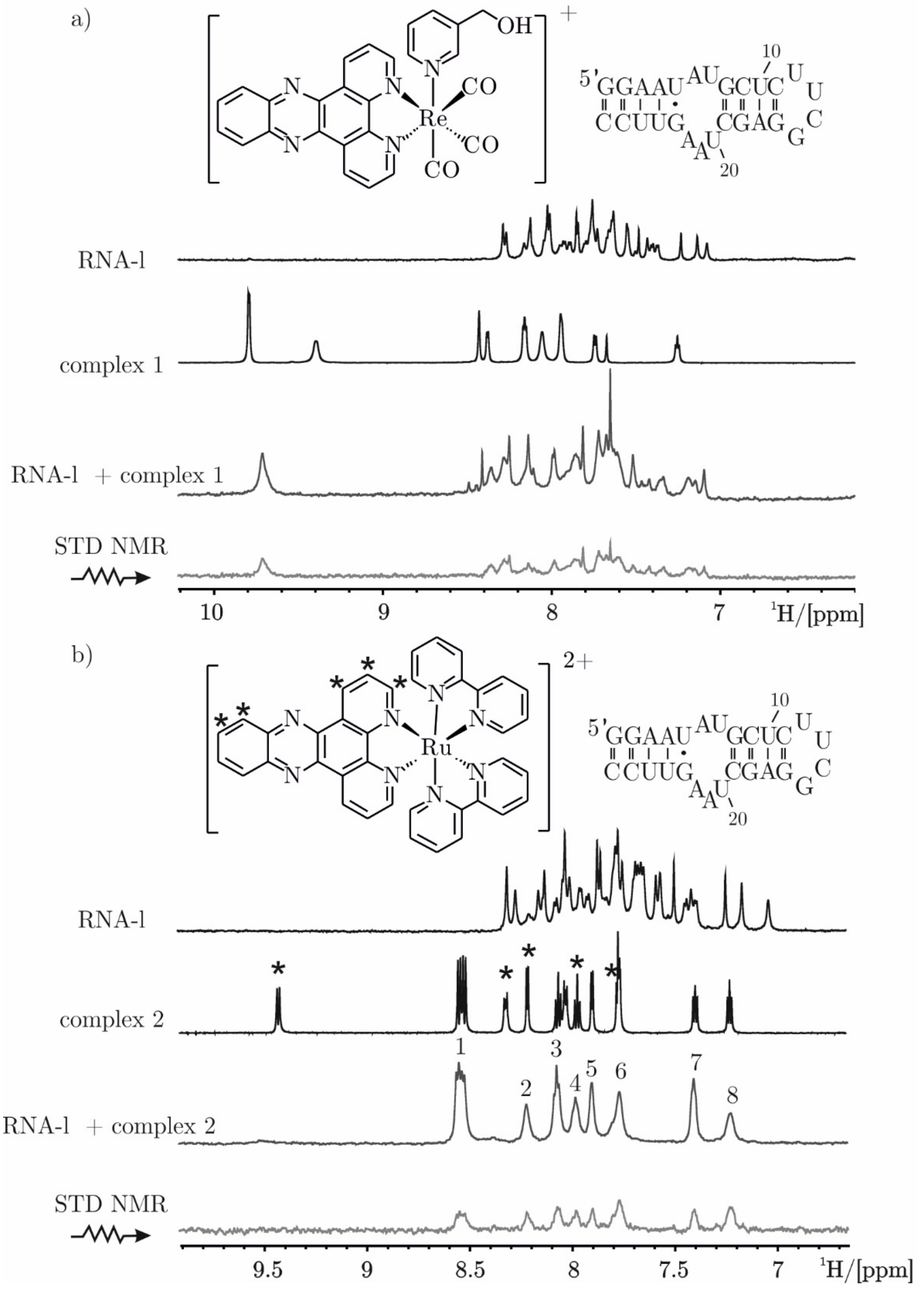

Figure 4.2 a) ^{1}H NMR spectrum of RNA-l, complex 1 and reference spectrum of 25 µM RNA-l and 350 µM complex 1 (300 K, 700 MHz); b) ^{1}H NMR spectrum of RNA-l, complex 2 and reference spectrum 25 µM RNA-l and 350 µM complex 2 (300 K, 700 MHz). In panel b, stars highlight the resonances of the protons of the dppz moiety. Numbers are used to indicate the signals of the resonances visible in the spectrum of the mixture of complex 2 and RNA-l.

shows the signals of both species (Figure 4.2a), indicating that the amount of complex 1 is not sufficient to obtain a successful STD NMR spectrum. We anyway recorded an STD NMR experiment, that did not show clear changes. Hence, these data suggest that the low water solubility of complex 1 hindered the possibility of performing STD NMR experiments.

On the contrary, only slight precipitation was observed when a tenfold excess of complex 2 was added to RNA-l. The ^{1}H NMR spectrum of this mixture shows no detectable resonances for RNA-l and intense signals for the metal complex (Figure 4.2b). Moreover, the signals of complex 2 undergo a general broadening, indicating that an interaction occurs. Some of the metal complex signals are not visible, however among the observable ones in the STD NMR spectrum, the highest degree of saturation is observed for peak 8 (100%), followed by peak 6 (83%), peak 2 (60%) and peak 4 (59%). The degree of saturation was calculated as reported in Section 6.11. Peak 8 belongs to the bipyridine, peak 6 is an overlay of protons of the dppz and the bipyridine ligand, peak 2 and peak 4 correspond to resonances of protons in the dppz moiety. Hence, as for the five signals of the protons of the dppz moiety (marked with stars in Figure 4.2b), two of them disappear upon addition of complex 2 and the remaining three show high degree of saturation in the STD NMR experiment. Therefore, our data suggest that the binding between complex 2 and RNA-l occurs with the involvement of the whole dppz moiety along with a small area of the bipyridine ligand.

4.2. MD simulations on complex 1 and RNA-l

Preliminary MD simulation studies were performed using the X-ray crystal structure of complex 1 with BF_4^-, provided by Dr. Michael P. Coogan (University of Lancaster) and the NMR solution structure of RNA-l (xp06_141, Figure 4.3a) previously solved in the laboratories of Prof. Dr. Roland K.O. Sigel. [11] This latter one was obtained employing standard simulated annealing and refinement protocols implemented in CNS [127] and Xplor-NIH [128,129]. All of the NMR experiments were recorded in 60 mM KCl, 10 µM EDTA (pH 6.8-6,7). The distance restraints used derive from [^{1}H,^{1}H]-NOESY spectra, backbone angles were restrained to standard A-RNA values in regions where the NOESY peak pattern and the base pairing suggest standard helical conformation and left unrestrained in other regions. The sugar puckers were restrained to 3' endo conformation in helical regions, to 2' endo conformation for residues showing strong H1'H2' and medium H1'H3' cross peaks in 50 ms [^{1}H,^{1}H]-TOCSY spectra, and left unrestrained otherwise. For bases in stable base pairs and helical regions chi was restrained to anti conformation. In the UUCG tetraloop, U12, U13 and C14 were restrained to anti according to the literature while G15 was restrained to syn due to strong intranucleotide H8-H1' peak. [87,130] The twenty lowest-energy structures (none of them have NOE violations > 0.2 Å nor dihedral angle violations > 5°) show an overall RMSD of 2.71 +/-1.09, while an RMSD of 0.98 +/- 0.33 is observed when the overlay is performed on the internal loop region (5-9, 18-23). [11]

Two preliminary MD structures were simulated, one in the presence of one molecule of complex 1 (Interc2_cluster1 in Figure 4.3b) and the other one in the presence of two molecules of complex 1 (cluster1_bis_long, Figure 4.3c), as

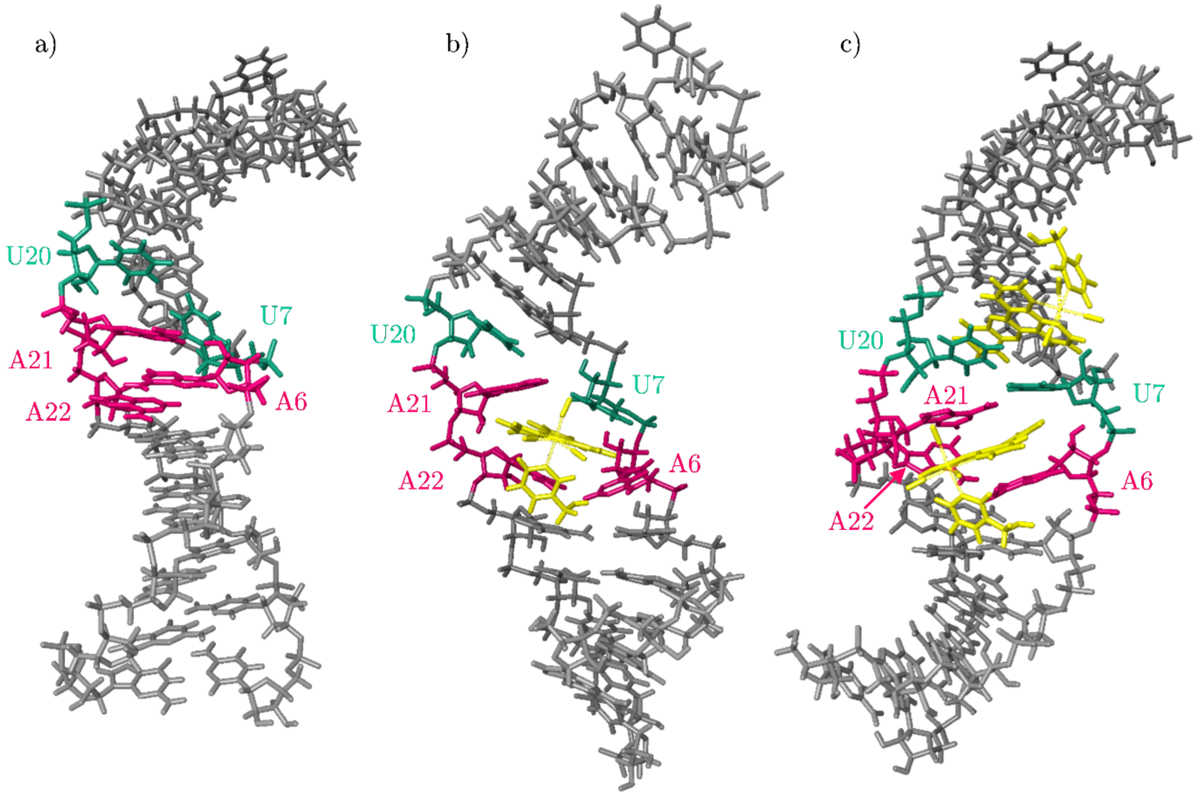

Figure 4.3 a) NMR solution structure of RNA-l (xp06_141); b) MD simulation in the presence of two molecules of complex 1 (cluster1_bis_long) and b) MD simulation in the presence of one molecule of complex 1 (Interc2_cluster1). A6, A21, A22 are highlighted in magenta, U7 and U10 in green and complex 1 in yellow.

suggested from the stoichiometry value obtained via ITC (Section 3.2 and Section 3.3).

The MD simulations were performed with GROMACS 5.0.4 [131,132] using the Amber99 force field [133] with Parmbsc0 nucleic acid torsions [134] and OL modifications [135].

The starting geometry and the partial atomic charges of complex 1 were calculated with Gaussian 09 (M. Frisch, G. Trucks, H. Schlegel, G. Scuseria, M. Robb, J. Cheeseman, et al., Gaussian 09, Revision B.01, Gaussian 09 Revis. A1 Gaussian Inc Wallingford CT. (2009)) by using the M06-2X DFT functional [136] and the dzvp basis set [137]. Other intramolecular force-field parameters were generated with ACPYPE [138] and parafreq, [139] respectively for the organic moiety and the metal centre. Finally, partial charges were obtained with electrostatic potential (ESP) fitting using the pop=CHELPG [140] keyword.

A cubic box of TIP3P water molecules was added around the RNA to a depth of 1.0 nm on each side of the solutes. Na^+ ions were added in order to neutralized the system, while other Na^+ and Cl^- ions were added to set the solution ionic strength to 0.15 M. Explicit solvent simulations were performed in the isothermal-isobaric NPT ensemble, at a temperature of 300 K, under control of a velocity rescaling thermostat. [141] The particle mesh Ewald method was used to describe long-range electrostatic interactions. [142] A time step of 2 fs was used for integration and all covalent bonds were constrained with the LINCS algorithm. There were two temperature coupling groups in these simulations: the first for the RNA and the metal complex, the second for water and ions. The preliminary MD simulations showed that the structure of the isolated metal complex is maintained in solution. Preliminary energy minimizations were run for 5000 steps with the steepest descend algorithm. During the equilibration, the metal complex/RNA system was harmonically restrained with a force constant of 1000 kJ mol^{-1} nm^{-2}, gradually relaxed into five consecutive steps of 100 ps each, to 500, 200, 100 and 50 kJ mol^{-1} nm^{-2}. Finally, 500 ns unconstrained MD simulations were performed.

The two preliminary structures obtained via molecular dynamics, one with two molecules of complex 1 (cluster1_bis_long) and the other one with one molecule of complex 1 (Interc2_cluster1), were compared to the NMR solution structure of RNA-l (xp06_141). From these preliminary studies, it seems that the one complex binds at the three stacked adenines by inserting its dppz moiety between A6 and A21 (Figure 4.3b/c). The second complex binds between the U7U20 mismatch and G8C19 base pair (Figure 4.3c).

In Appendix 14 a table with proton-proton distances based on the NOE list used for structure calculation of RNA-l for all the three structures is reported. Comparison of the proton-proton distances shows that the residues in the helical regions of RNA-l, namely G1C27, G2C26, A3U24, A4U25, C9G18, U10A17 and C11G16, are almost not influenced by the presence of complex 1, independently from the number of metal complexes. Moreover, only little changes are also observed for the residues U12, U13, C14, G15, showing that the binding of complex 1 to the internal loop does not affect the structure of the terminal loop. More significant changes (up to 7 Å, Appendix 14) are observed for the residues directly involved in the interaction at the internal loop. In particular, the inter-residue distances of the three stacked adenines A6, A21 and A22 show the most significant changes, that are highlighted in grey in Appendix 14. Especially the distances involving their H2 protons seem to strongly increase. As shown in the NMR structure in Figure 4.3a, the H2 protons of A6, A21 and A22 point inside the internal loop and therefore are very sensitive to structural changes induced by the interaction of complex 1 in this region. For example, the distance between A6H2 and A21H2 strongly increases (from around 3 Å to 6 Å in cluster1_bis_long and to around 10 Å in Interc2_cluster1). Moreover, the distance between A6H2 and A22H8 gets significantly larger (from around 5 Å to 8.5 Å in cluster1_bis_long and to around 8 Å in Interc2_cluster1). Significant variations are also visible for the distances where U7 and G8 are involved, suggesting that the interaction influences the structure of the whole internal loop. However, these distances are more affected in the MD simulation with two molecules of complex 1, rather than in the one with one complex 1 (above 2 Å and up to 5 Å for cluster1_bis_long and slightly smaller for Interc2_cluster1, Appendix 14), as U7 and G8 seems to be the second binding site.

4.3. Further [^{1}H,^{1}H]-NOESY spectra to investigate the interaction in the presence of KCl

[^{1}H,^{1}H]-NOESY spectra were recorded at 303 K in 60 mM KCl, 10 μM EDTA in the absence and in the presence of 1 equivalent of complex 1, to support the molecular dynamics simulations. These [^{1}H,^{1}H]-NOESY spectra look very similar to the ones obtained using PBS and similarly to those (Section 2.1) also in this case a different pD (6.7 and 7.0) leads to different spectra as it is visible in Figure 4.4. The most affected resonances are the ones corresponding to the nucleotides in the dynamic internal loop region of RNA-l. Indeed, in the [^{1}H,^{1}H]-NOESY spectrum at pD 7.0, the signals of protons belonging to A6, U7 and G8 are less intense and broader and the cross peak G8H8-H1', which is visible at pD 6.7, cannot be detected in these conditions.

[^{1}H,^{1}H]-TOCSY experiments performed in the same conditions were employed to confirm the assignment of H5-H6 connections.

A one-step addition of 1 equivalent of complex 1 to RNA-l was performed and the changes in chemical shifts and intensity of the resonances were evaluated.

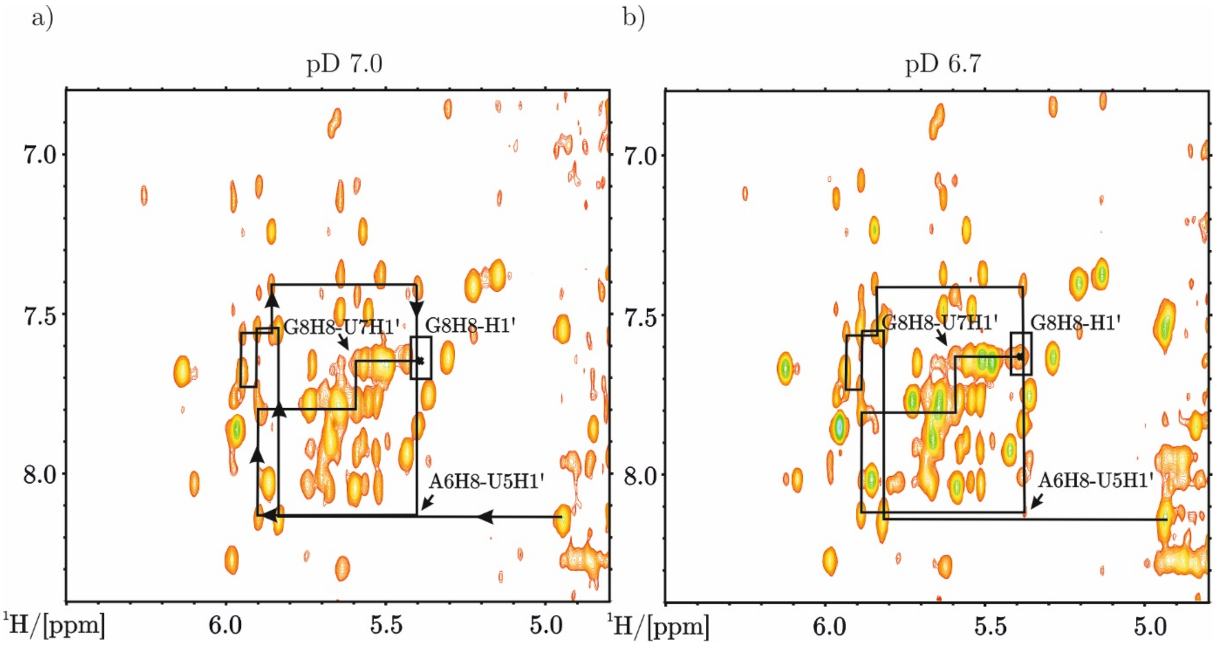

Figure 4.4 [^{1}H,^{1}H]-NOESY sequential walk region of a) RNA-l 0.35 mM, PBS, pD 7.0, 303 K, 700 MHz and b) RNA-l 0.35 mM, 60 mM KCl, 10 μM EDTA, pD 6.7, 303 K, 700 MHz.

The signals are in general broader upon metal complex addition, leading to a loss of signals, especially around the diagonal. However, the effect was not that strong as in PBS (compare Figure 2.20 and Figure 4.5). Therefore, more chemical shift variations in the area of the sequential walk region (H1' and H6/H8 proton resonances) could be followed (bar plot graph in Figure 4.5). As expected, the most influenced area is the one of the internal loop whereas the terminal loop is only slightly affected. This is in accordance with the MD simulations that propose a binding localised between A6 and A21. As visible in Figure 4.5, among H6/H8 proton chemical shift changes, the highest variations in the presence of complex 1 are visible for A6, A21 and A22 resonances. In the case of the H1' resonances, the most significant shift is observed for A6 in the internal loop region, and for U24 which is close by.

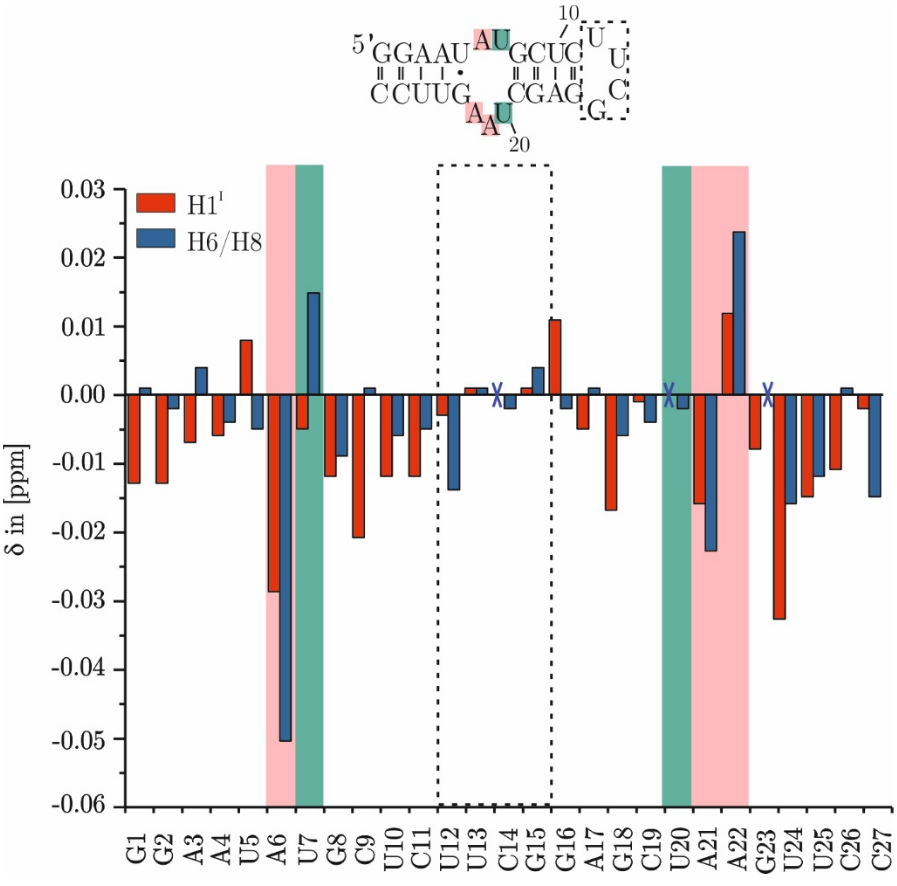

Figure 4.5 Comparison of H8/H6 and H1' chemical shift changes of RNA-l in the presence of 1 equiv. of complex 1. (0.35 mM, 60 mM KCl, 10 µM EDTA with 2% DMSO, pD 6.8, 303 K, 700 MHz). Blue crosses represent resonances whose chemical shift did not change in the presence of 1 equivalent of complex 1. The box highlights the terminal loop region of RNA-l.

We also evaluated the changes in intensity of the H1' and H6/H8 proton correlations (sequential walk connections), but no significant differences were observed, suggesting that the inter-atomic distances do not change considerably. This is in agreement with the MD simulations where no strong variations were observed for the sequential connections (Appendix 14).

Changes in the internal loop can also be monitored in the diagonal region, where the cross peaks of the aromatic stacking interactions are visible (Figure 4.6). Indeed, in the red boxes in panel a) it is possible to observe signals deriving from the stacking of A6, A21, A22 and U7 (Section 2.1). All of these signals disappear in the presence of complex 1 suggesting that the complex interacts in that position. This could be due to two reasons. On the one hand, an increase of the inter-reside distances above 5-6 Å could be responsible for such behaviour, which is in agreement with the MD simulations that show very large values for the distances involving the H2 protons of A6, A21 and A22

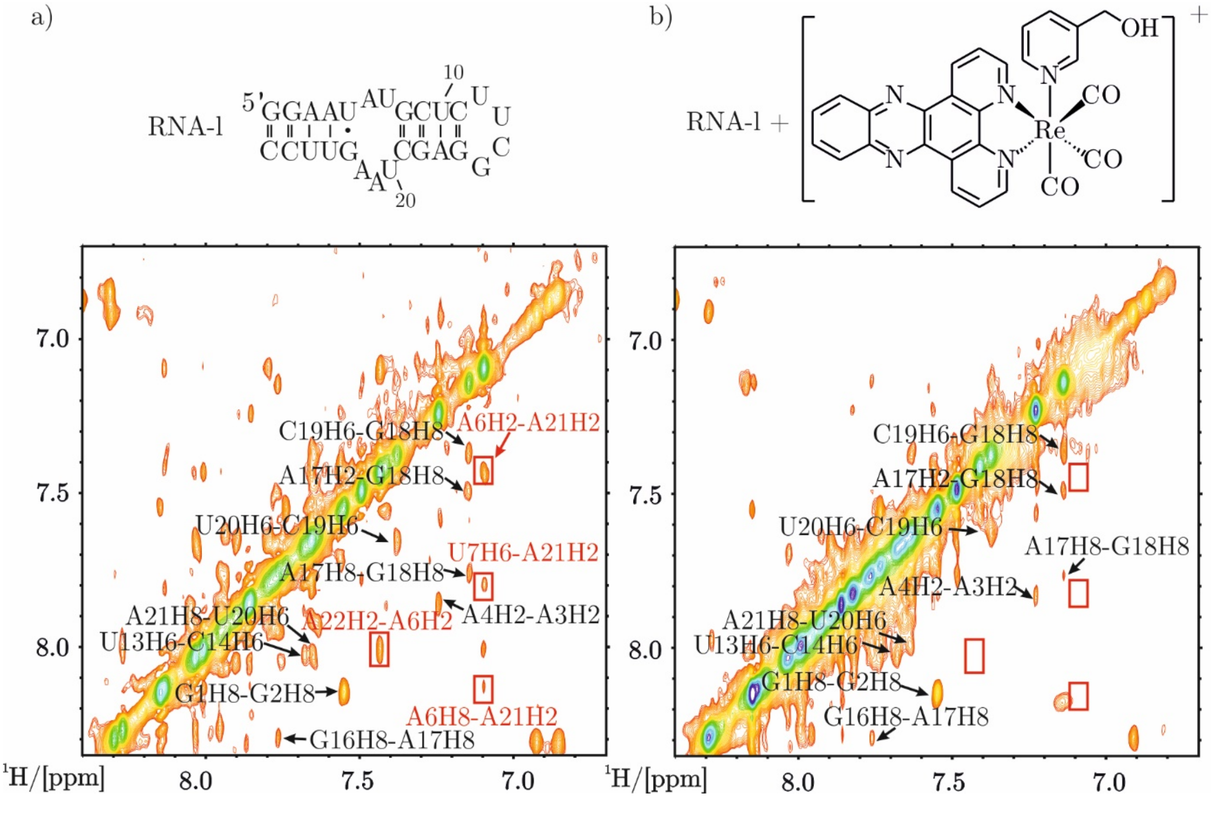

Figure 4.6 Sections of [^{1}H,^{1}H]-NOESY spectra recorded on RNA-l in the absence a) and in the presence b) of 1 equiv. of complex 1 (0.35 mM, 60 mM KCl, 10 µM EDTA, pD 7.0, 303 K, 700 MHz). The boxes indicate some of the cross peaks belonging to nucleotides that disappear upon metal complex addition.

(described in the previous section). However, as no connections between RNA-l and complex 1 were observed no useful information could be obtained from the spectra to support the exact position of the complex in the internal loop. On the other hand, the disappearance of the cross peaks could be to the high dynamics of the interaction. Therefore, we cannot safely distinguish if the loss of cross peaks is due to an increase of distances or to dynamics caused by the interaction of the complex in this area. As for all of the remaining unchanged cross peaks in Figure 4.6, they belong to the two helical regions of RNA-l. This result indicates that no binding takes place outside the internal loop region, as visible in the structures obtained by the MD simulations.

Other important information could be obtained by the area of the [^{1}H,^{1}H]-NOESY spectrum shown in Figure 4.7 (area of the H1'-H2' and H5 of pyrimidines). All of the highlighted resonances are visible both in the absence and in the presence of complex 1. They belong to the stem regions and the terminal loop, and it is not unexpected that they do not undergo changes upon metal complex addition. However, U20H5-C19H5 decreases in intensity in the presence of complex 1 (compare panel a and panel b). This could be due to an increase of the distance between the two H5 protons. As shown in Table 4.1, this is in agreement with the structure containing two rhenium complexes, that shows an increase of the distance U20H5-C19H5. On the contrary, such result is in contrast with the intermediate structure having only one molecule of complex 1.

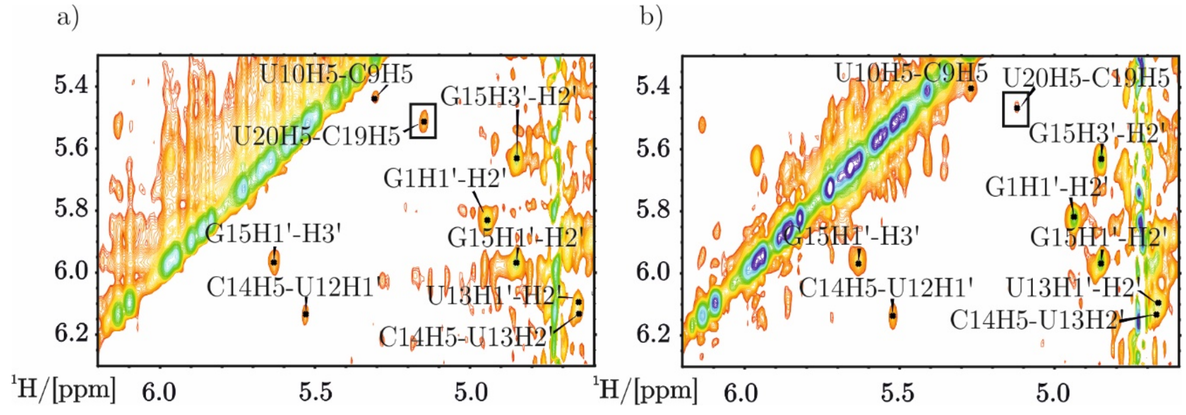

Figure 4.7 Sections of [^{1}H-^{1}H]-NOESY spectra recorded on RNA-l in the absence a) and in the presence b) of 1 equiv. of complex 1 (0.35 mM, 60 mM KCl, 10 µM EDTA, pD 7.0, 303 K, 700 MHz). The black box highlights the cross peak U20H5-C19H5.

Table 4.1 Distance between U20H5 and C19H5 in xp06_141, cluster1_bis_long and interc2_cluster1. Information extracted from Appendix 14.

	xp06_141	**cluster1_bis_long**	**interc2_cluster1**
U20H5-C19H5	4.5 Å	6.3 Å	3.6 Å

4.4. Conclusion

In this chapter the use of STD NMR experiments and MD simulations to further characterize the position of complex 1 in the RNA-l internal loop is described. Indeed, the data presented so far (Chapter 2 and Chapter 3), suggested that complex 1 interacts with the internal loop of RNA-l, but no information of its precise localisation were obtained.

STD NMR experiments were performed on complex 1 and complex 2. In the first case, the low water solubility of the rhenium complex did not allow to reach the excess of ligands in solution, that is crucial for a good STD NMR spectrum, and no useful data could be obtained. In the case of complex 2 no solubility issues were encountered and the STD experiment was successfully performed. The ^{1}H NMR spectrum of the mixture of complex 2 and RNA-l used for STD NMR shows the presence of an interaction and the loss of two peaks belonging to protons of the dppz moiety. Then the STD NMR spectrum shows that one peak belonging to a bipyridine proton is the one that received the highest amount of magnetization. However, except for this peak, the majority of the signals that displayed the highest degree of saturation are represented by the ones belonging to the protons of the dppz group. This result along with the fact that among the five resonances of the dppz protons, two are not visible in the presence of RNA-l and that the remaining three seem to be close enough to RNA-l to receive a high degree of magnetization, suggests that the whole dppz moiety along with only a portion of bipyridine is involved in the binding at the internal loop.

Preliminary MD simulations were performed on the X-ray crystal structure of complex 1 and the NMR solution structure of RNA-l, [11] taking into account the stoichiometry value of two metal complexes per RNA internal loop found in Chapter 3 (Section 3.2 and Section 3.3). In addition to the MD structure with two molecules of complex 1, an MD structure with only one molecule of complex 1 was also simulated.

The distances of the protons in both MD structures were compared to the information obtained via [^{1}H,^{1}H]-NOESY experiments. Only little changes were observed for the residues in the two helical regions and in the terminal loop, in accordance with the MD simulations proposed. The intermolecular NOE signals deriving from the stacking of the adenines in the internal loop disappeared in the [^{1}H,^{1}H]-NOESY spectrum upon addition of metal complex, due to fast dynamics (Chapter 2). This, unfortunately, precludes any evaluation of the distances among the residues in this area and its comparison with the proposed MD structures. Finally, an important information was given by the cross peak U20H5-C19H5 whose intensity decreases upon complex 1 binding. This could be the consequence of an increase of the distance between these two protons. Interestingly, this result is in accordance only with the MD simulation containing two molecules of complex 1.

5. Design and preliminary synthesis of a novel Re(I)dppz complex

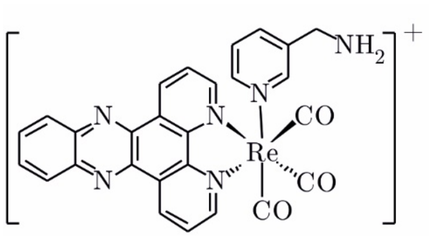

Figure 5.1 Chemical structure of $[Re(CO)_3(dppz)(3\text{-}CH_2NH_2\text{-}Py)]^+$ 12).

As revealed in the previous chapters, one of the most critical limitations connected to the usage of complex 1 is represented by its low water solubility and the need of using traces of organic solvent to favour its solubility in water. Indeed, on the one hand, the NMR experiments suffered from the low concentration likely responsible for poor signal to noise ratio. On the other hand, the presence of organic solvent interfered with ITC measurements. For these reasons, we designed, in collaboration with Dr. Michael P. Coogan, a new rhenium complex with potentially increased water solubility. In order to do that, we planned to modify the ancillary ligand without changing the dppz moiety, which is responsible for RNA interaction. Therefore, a water soluble moiety, such as an aminomethyl group, was chosen as substituent at the pyridine ring. The resulting $[Re(CO)_3(dppz)(3\text{-}CH_2NH_2\text{-}Py)]^+$ (complex 12) is protonated in physiological conditions, thus showing an enhanced water solubility with respect to the one of complex 1. Moreover, the presence of an amino group could favour RNA binding and reduce the dynamics of the interaction.

A five step reaction (Appendix 15), based on literature data [15,143–146] was used to synthesize complex 12. This preliminary synthesis was carried out along with the master student Severin Koch during a research project that I directly supervised.

5.1. Step 1 and step 2: Synthesis of dipyrido[3,2-*a*:2',3'-*c*]phenazine (7)

In the first two steps (Figure 5.2) we synthesized the dipyrido[3,2-*a*:2',3'-*c*] phenazine ligand (7), obtained by reacting 1,10-phenanthroline-5,6-dione (5) with the commercially available o-phenyldiamine (6). [145]

Compound 5 was obtained by oxidation of compound 4 in the presence of potassium bromide in a mixture of nitric and sulfuric acid with a yield of 79%. [145] The IR analysis (Appendix 16) and ^1H NMR spectrum (Appendix 17) confirmed the formation of the desired compound. [143,147] In this last one, the six aromatic

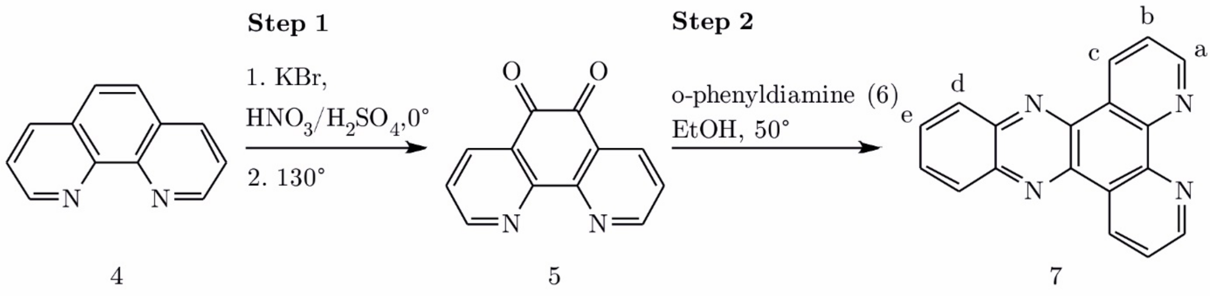

Figure 5.2 Reaction scheme for the synthesis of dipyrido[3,2-a:2',3'-c]phenazine (7).

protons of the phenanthroline moiety are observed at 9.13 ppm, 8.52 ppm and 7.60 ppm (doublets). No other remarkable peaks were observed, suggesting that the compound was pure and could be used for the next reaction step without further purification.

Compound 7 was synthesized by the reaction between compound 5 and compound 6, with a yield of 80%. [143,144] It was characterized by ^{1}H NMR and ^{13}C NMR experiments. The ^{1}H NMR spectrum (Appendix 18) shows all the expected resonances: at 9.65 ppm, 9.28 ppm and 7.80 ppm (a, b and c in Figure 5.2, doubles of doublets) and at 8.36 ppm and 7.93 ppm (d and e in Figure 5.2, doubles of doublets). [143] ^{13}C signals (Appendix 19) are comparable to the ones reported in the literature. [148] Compound 7 was then used for the next reaction step without further purification.

5.2. Step 3: Synthesis of bromotricarbonyldipyrido[3,2-*a*:2',3'-*c*] phenazinerhenium (9)

Bromotricarbonyldipyrido[3,2-*a*:2',3'-*c*]phenazinerhenium(I) (9) was obtained by reacting compound 7 and bromopentacarbonylrhenium(I) (5) (Figure 5.3). [146]

The ligand substitution was confirmed by IR spectroscopy (Appendix 20) (CO stretching at 2025 cm^{-1}, 1930 cm^{-1} and 1885 cm^{-1}) in agreement with literature data. [146] Moreover, the formation of the desired complex was confirmed by ^{1}H NMR (Appendix 21). [146] The protons of the dppz moiety are found at 9.82 ppm, 9.56 ppm 8.18 ppm (a, b and c, broad doublets) and 8.49 ppm, 8.26 ppm (d and e, doublet of doublets). The spectrum shows only traces of impurities (around 5%), thus the complex was used for the next reaction step without further purification.

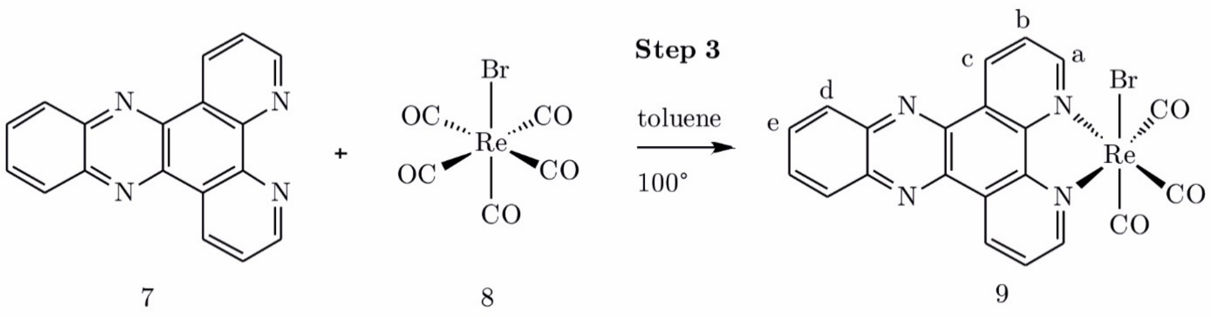

Figure 5.3 Reaction scheme for the synthesis of bromotricarbonyldipyrido [3,2-a:2',3'-c]phenazinerhenium(I) (9).

5.3. Step 4: Synthesis of acetonitriletricarbonyldipyrido[3,2-a:2',3'c] phenazinerhenium(I)tetrafluoroborate (10)

In this step of the synthesis, depicted in Figure 5.4, the bromide group of complex 9 is substituted by acetonitrile in the presence of silvertetrafluoroborate to form acetonitriletricarbonyldipyrido[3,2-*a*:2',3'-*c*]phenazinerhenium(I) tetrafluoroborate (10). [15]

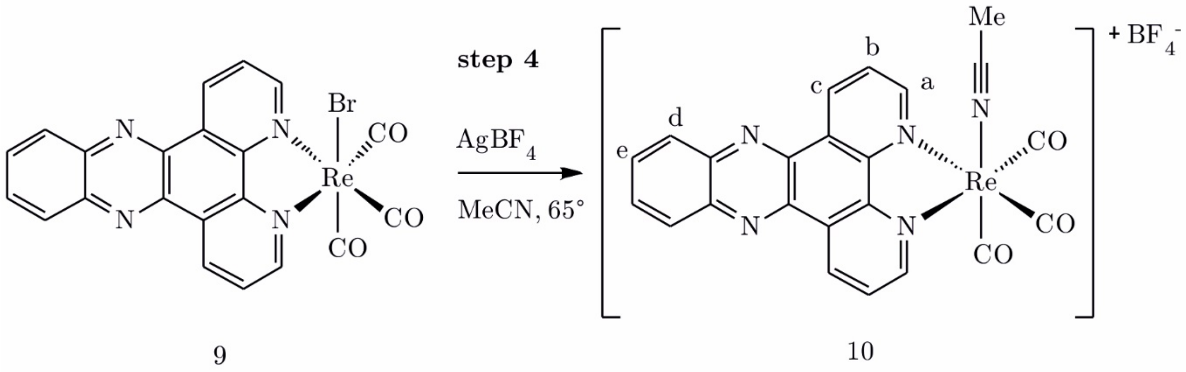

Figure 5.4 Reaction scheme for the synthesis of acetonitriletricarbonyldipyrido [3,2-*a*:2',3'-*c*]phenazinerhenium(I)-tetrafluoroborate (10).

The desired complex was obtained with a yield of 85%. [15] The identity of complex 10 was confirmed by IR spectroscopy (Appendix 22), ^{1}H NMR (Appendix 23) and ^{13}C NMR (Appendix 24) experiments. In addition, [^{1}H,^{13}C]-HSQC, [^{1}H,^{13}C]-HMBC and [^{1}H,^{1}H]-COSY experiments (Appendix 25, Appendix 26 and Appendix 27) were recorded to confirm what observed in the 1D spectra.

The IR spectrum shows the signals of the CO stretching at 2035 cm^{-1} and 1920 cm^{-1}. The ^{1}H NMR spectrum (Appendix 23) shows all the expected signals: at 9.81 ppm, 9.48 ppm, 8.18 ppm (a, b and c, doublet of doublets) and at 8.41 ppm and 8.12 ppm (d and e, doublet of doublets). [15] Two quaternary ^{13}C signals are not observed under our experimental conditions, while the visible resonances are in agreement with the literature (Appendix 24). [15]

5.4. Step 5: Synthesis of 3-picolylammoniumtricarbonyldipyrido [3,2-*a*:2',3'*c*]phenazinerhenium(I) (12)

As shown in Figure 5.5, the last reaction step involves the substitution of the MeCN group of complex 10 by 3-picolylamine (11a) to form the target compound, namely 3-picolylaminetricarbonyldipyrido[3,2-*a*:2',3'-*c*] phenazinerhenium(I) (12). This reaction step is based on similar reported ligand substitutions. [15]

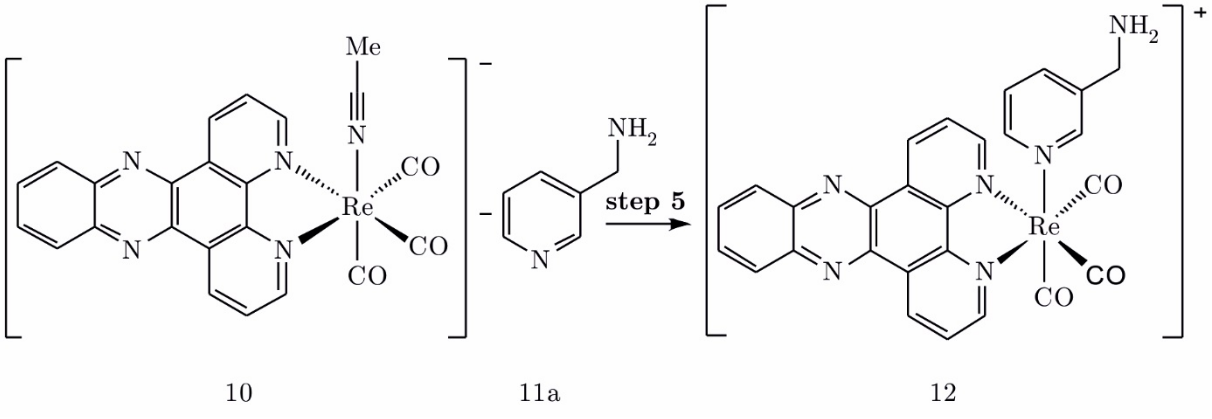

Figure 5.5 Synthesis of 3-picolylammoniumtricarbonyldipyrido[3,2-*a*:2',3'*c*] phenazinerhenium(I).

As summarized in Table 5.1, the influence of several different parameters, such as solvent, temperature, reaction time, ratio between reactants and protection of the amino group have been tested for the step 5. In the discussion of the results, we will refer to the reaction trials using the numbering of Table 5.1.

Trials 1-5 were performed reacting compound 11a with complex 10 varying solvent, reaction time, temperature and ratio of the reactants. As visible in Figure 5.6, the ^{1}H NMR spectrum of the reaction mixture (trial 1 after 16 hours of reaction) shows more signals than the ones expected for complex 12, and weak signals corresponding to the starting material.

Table 5.1 Reaction parameters tested for the reaction step 5 to form complex 12.

	Solvent	**Temperature (°C)**	**Total reaction time (h)**	**Ratio (10:8)**	**Protection of compound 11a**
1	Chloroform	50	16.0	1:1.3	No
2	Chloroform	65	27.0	1:1.2	No
3	Chloroform	50	96.0	1:1.5	No
4	Toluene	50	43.0	1:1.2	No
5	Methanol	55	22.5	1:1.2	No
6	Chloroform	50	4.00	1:1.2	Yes
7	Methanol	55	141	1:1.2	Yes
8	Methanol	55	47.0	1:3	Yes
9	Methanol	55	24.0	1:6	Yes

These data suggest that the reaction is not completed, and a mixture of species is formed. Although some of the reaction conditions were changed, similar ^{1}H NMR spectra were obtained.

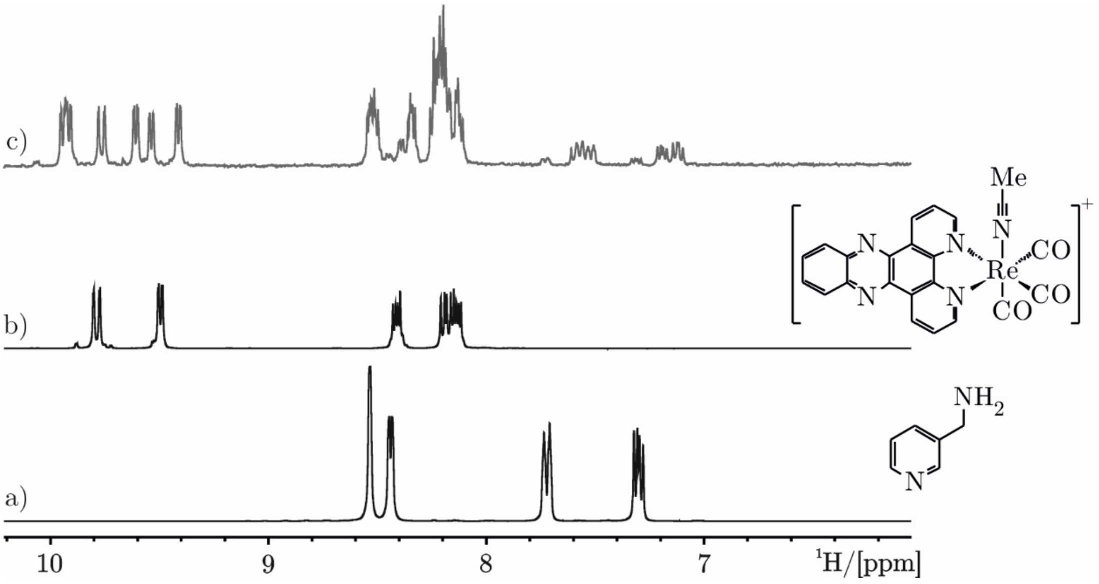

Figure 5.6 a) ^{1}H NMR spectrum of commercially available picolylamine; b) ^{1}H NMR spectrum of complex 10; c) ^{1}H NMR spectrum of the reaction mixture of reaction n.1 (the numbering is in Table 5.1) after 16 hours. (CD_3CN, 300 K, 400 MHz).

According to the nature of the starting material, three reaction products could be obtained.

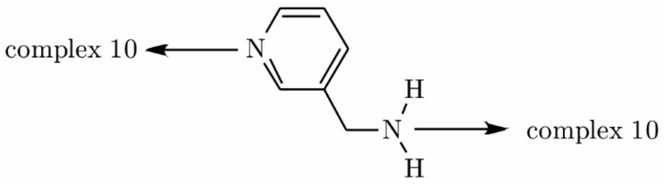

Figure 5.7 Available sites for reaction of compound 11a represented with arrows.

Compound 11a, as shown in Figure 5.7, is a pyridine substituted with a primary amine, and as such, it can react with complex 10 following three different reaction paths: (i) via the nitrogen of the pyridine, (ii) via the nitrogen of the primary amine or (iii) via both nitrogen atoms bridging two metal centres. [149]

In order to favour the coordination via the nitrogen of the pyridine ring and to obtain the desired product, we protected the primary amine of compound 11a. The protection was performed via protonation, treating compound 11a with ammoniumhexafluorophosphate to form the corresponding 3-picolylammonium salt in Figure 5.8.

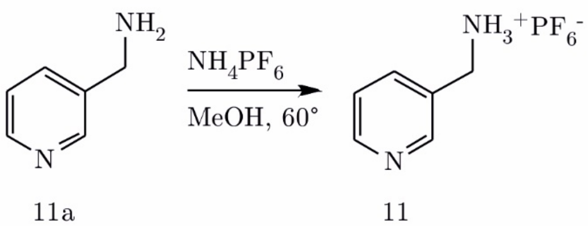

11a 11

Figure 5.8 Protection reaction of compound 11a to obtain compound 11.

The release of ammonia gas, checked with pH paper, and the precipitation of a white solid during the protection reaction indicated the formation of compound 11 (96% yield). This was further confirmed via NMR. Indeed, the ^{1}H NMR spectrum of compound 11 shows the presence of the $–NH_3^+$ group at 3.40 ppm (Appendix 28) and a significant downfield shift of the aromatic resonances with respect to the spectrum of compound 11a (Figure 5.9), in agreement with the behaviour of proton resonances of amines for protonation reactions reported in the literature. [150] Furthermore, the presence of the hexafluorophosphate counter ion was confirmed by ^{19}F NMR (Appendix 29) that shows the fluoride peak at -72.94 ppm as a doublet with a ^{31}P-^{19}F coupling constant of 706 Hz, in accordance with the literature. [151]

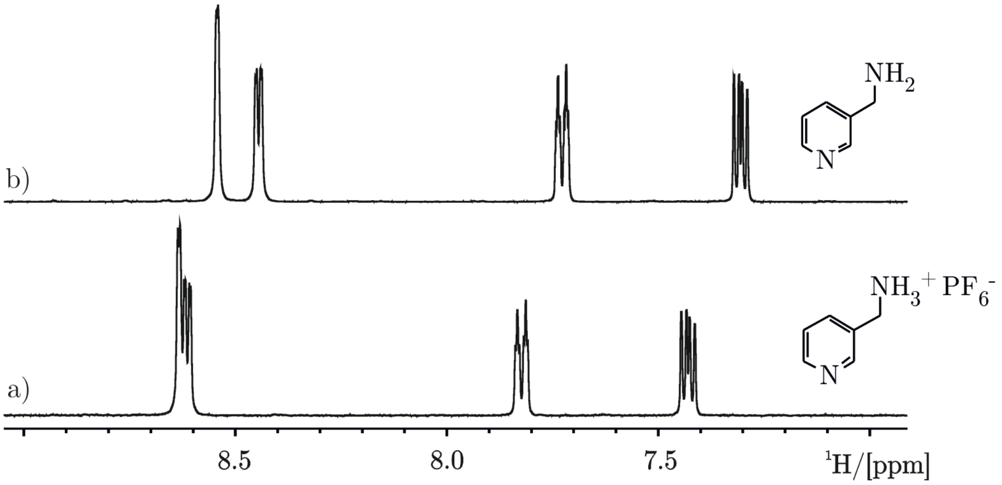

Figure 5.9 a) ^{1}H NMR spectrum of 3-picolylamine ammonium salt; b) ^{1}H NMR spectrum of 3-picolylamine. (CD$_3$CN, 300 K, 400 MHz).

Trials 6-9 were then performed using compound 11 and the reaction took place as depicted in Figure 5.10.

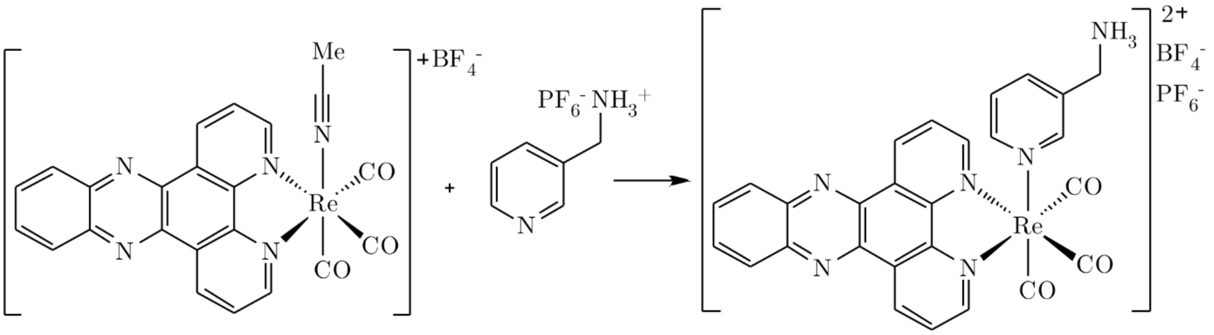

10

11

12

Figure 5.10 Synthesis of 3-picolylammoniumtricarbonyldipyrido[3,2-*a*:2',3'*c*] phenazinerhenium(I)tetrafluoroboratehexafluorophosphate (12).

In trial 6, the reaction was performed in chloroform and its evolution was monitored by ^{1}H NMR experiments (Figure 5.11).

After the addition of compound 11 to complex 10 in chloroform at room temperature, the ^{1}H NMR spectrum (Figure 5.11c) shows only the peaks corresponding to the dppz moiety of complex 10 and the signals belonging to the salt of picolylamine are barely visible. This behaviour indicates that compound 11 is poorly soluble in chloroform at room temperature. Hence, the reaction mixture was heated up to 50°C. After 4 hours of reaction, the ^{1}H NMR spectrum shows the signals of the dissolved compound 11, but no changes in the resonances of complex 10 and no formation of new species were observed (Figure 5.11d). The reaction was then stopped.

We changed solvent to favour the solubility of compound 11. Trials 7-9 were performed in methanol testing different reaction time and ratio of reactants, showing in all the cases the formation of complex 12. In trial 7 the reaction was run for 141 hours using a 1.2 excess of compound 11. ^{1}H NMR showed signals of the target compound and of the unreacted complex 10 (around 25%) (arrows in Figure 5.12c). Hence, in trial 8, the excess of compound 11 was increased and the reaction time reduced to 47 hours. The ^{1}H NMR of the reaction mixture

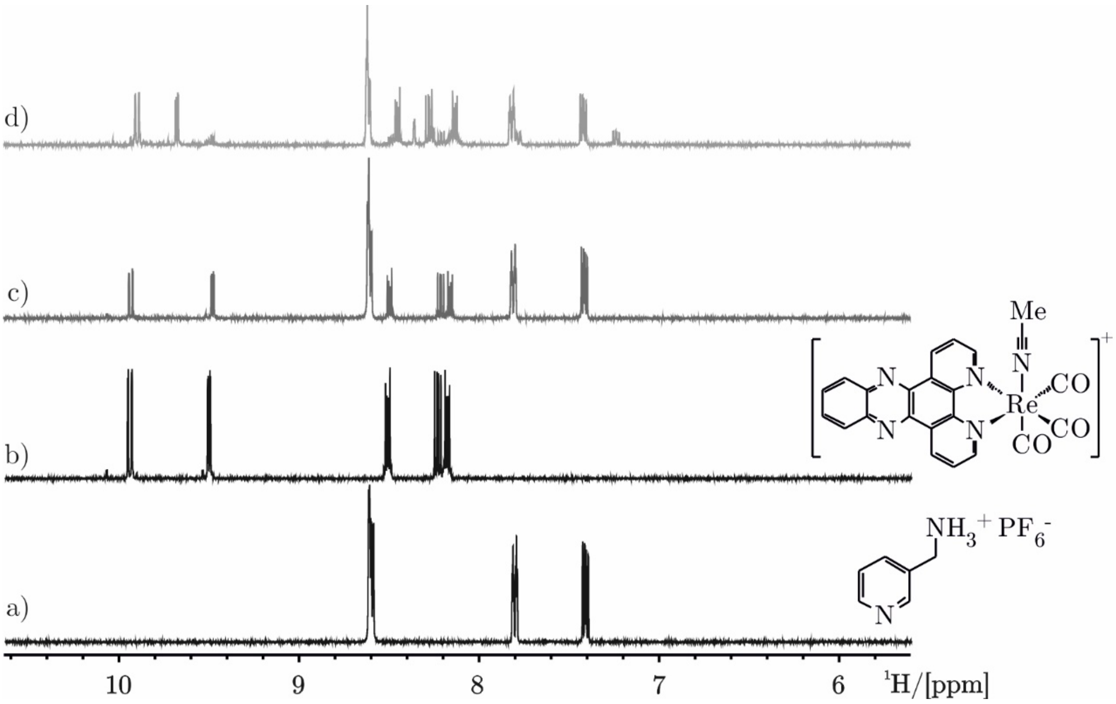

Figure 5.11 a) ^{1}H NMR spectrum of compound 11; b) ^{1}H NMR spectrum of complex 10; c) ^{1}H NMR spectrum immediately after the addition of compound 11 to complex 10 (at room temperature); d) ^{1}H NMR spectrum of the reaction mixture after 4 hours at 50°C. (CD_3CN, 300 K, 400 MHz).

(Figure 5.12d) shows similar yield but in this case weaker signals for complex 10 ($<$15%). In trial 9 the excess of compound 11 was further increased to sixfold and the reaction performed for 24 hours leading to a comparable result. The product was washed with water to remove the excess of unreacted compound 11 and characterized via NMR spectroscopy (Figure 5.13, Appendix 30, Appendix 31, Appendix 32, Appendix 33) and MS analysis. (Appendix 34).

The ^{1}H NMR spectrum (Figure 5.13) shows all of the expected resonances: the resonances of the protons of the dppz at 9.92 ppm, 9.67 ppm, 8.29 ppm, 8.47 ppm and 8.15 ppm (a, doublet, b, multiplet, c, doublet, e and d, doublets) and the ones of the pyridine ring at 8.39 ppm, 8.29 ppm, 7.82 ppm and 7.29 ppm (1, singlet, 3, doublet, 4, triplet, 5 multiplet) and the signal counting for methylene protons at 3.93 ppm (singlet, Appendix 30). ESI-MS measurement showed two signals, m/z = 661 ($[M - H]^+$) and 553 ($[M - C_6H_9N_2]^+$) (Appendix 34, the additional peaks were not assigned).

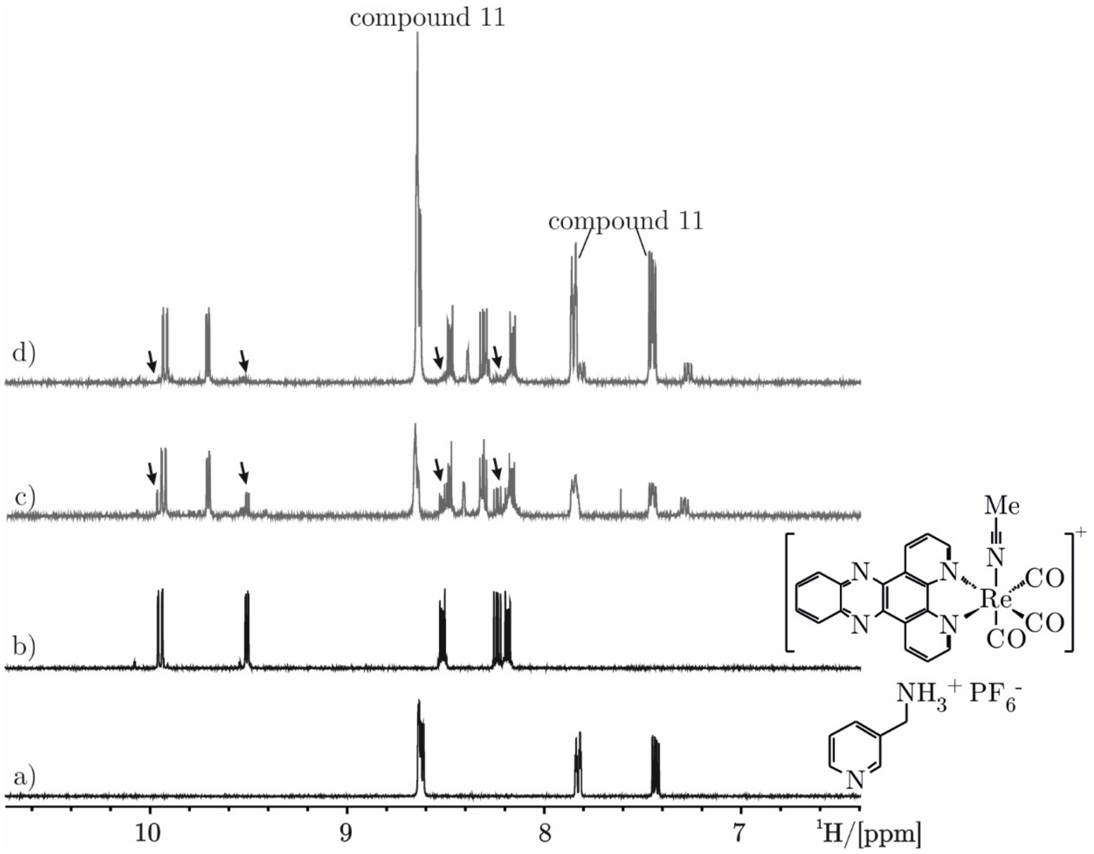

Figure 5.12 a) ^{1}H NMR spectrum of compound 11; b) ^{1}H NMR spectrum of complex 10; c) ^{1}H NMR spectrum of the reaction mixture of trial 7 after 141 hours; d) ^{1}H NMR spectrum of the reaction mixture of trial 8 after 47 hours. (CD_3CN, 300 K, 400 MHz).

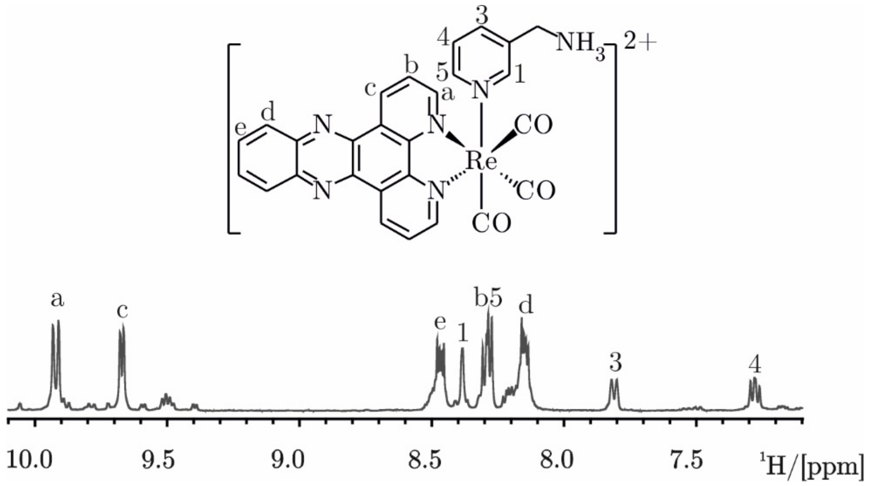

Figure 5.13 ^1H NMR of 3-picolylammoniumtricarbonyldipyrido [3,2-*a*:2',3'*c*]phenazinerhenium(I)tetrafluoroboratehexafluorophosphate (CD_3CN, 300 K, 400 MHz) with assignment. Besides the signals of the main species, also a 15% of complex 10 and 5% of other by products are visible.

Preliminary water solubility tests were performed on the product obtained without further purification. No improved water solubility was shown, calling for further design of new Re(I)dppz complexes with different water soluble pendants, such as for example histidine [152] or urea linked pyridine-PEG systems. [153]

5.5. Conclusion

A novel Re(I)dppz complex was designed with a (3-aminomethyl)pyridine moiety in axial position. This ancillary ligand was chosen to potentially improve the water solubility with respect to the one of complex 1. Its synthesis, based on literature data, [15,32,143–145,152,154] consists of 5 reaction steps. Several reaction conditions, such as different solvents, temperatures, reaction times, ratio between the starting materials and protection of the (3-aminomethyl)pyridine ligand were tested for the last reaction step. Complex 12 was synthesized and characterized via NMR spectroscopy and MS analysis. Its water solubility was preliminarily tested and no significant increase was observed, highlighting the need of further design to obtain a more water soluble Re(I)dppz complex.

6. Materials and methods

6.1. Chemicals and materials

All chemicals were purchased from either Fluka-Sigma-Aldrich (Buchs, Switzerland) or Brunschwig Chemie (Basel, Switzerland) at puriss p.a. or biograde.

DNA templates for RNA *in vitro* transcription were obtained from Microsynth (Balgach, Switzerland). The nucleotide 5'-triphosphates (NTPs) were purchased from Carl Roth GmbH (Karlsruhe, Germany), except for ATP from GE Healthcare (Glattbrugg, Switzerland). ^{15}N-labeled NTPs were purchased from Silantes GmbH (München, Germany). Tris(hydroxymethyl)-aminomethane (TRIS), 4-(2-hydroxyethyl)piperazine-1-ethansulfonic acid (HEPES), ethylenediaminetetraacetic acid (EDTA), sodium chloride, potassium chloride, dithiothreitol (DTT), Triton^{TM} X-100 used for the transcription were purchased from Sigma-Aldrich, whereas the T7 polymerase was homemade. The RNA purification was done on denaturing polyacrylamide gels prepared using AccuGel (40% (w/v), 29:1 Acrylamide-Bisacrylamide) from National Diagnostics (Hessle, UK) and urea (UltraPure) from EUROBIO (Les Ulis, France). Ammonium persulfate (APS) and N,N,N,N tetramethylendiamine (TEMED) used for gel polimerization were purchased from Carl Roth GmbH and Co (Karlsruhe, Germany) and from Sigma-Aldrich respectively. 10x TBE buffer (0.89 M Tris Borate at pH 8.3, 0.2 M Na_2EDTA) bought from National Diagnostics (Atlanta, USA) was used to obtain 1x TBE buffer then used in the electrophoresis apparatus.

Dephosphorylated RNA samples were obtained using alkaline phosphatase, calf intestinal (CIAP) from Promega Corporation (USA).

$[Re(CO)_3(dppz)(3\text{-}CH_2OH\text{-}Py)]OTf$ ($3\text{-}CH_2OH\text{-}Py$ = 3-hydroxymethyl pyridine; OTf = trifluoromethane-sulfonate) (complex 1) was synthesized according to published literature by the group of Dr. Michael P. Coogan (Lancaster University, UK). [154] $[Ru(bpy)_2(dppz)](NO_3)_2$ (dppz = dipyrido [3,2-a:2',3'-c]phenazine) (complex 2) was synthesized following standard procedures in our laboratories. [32] $[Ru(bpy)_3]Cl_2$ (bpy = 2,2'-bipyridine) (complex 3) was obtained from Sigma-Aldrich and used as received. The concentration of the solutions containing complex 1 and complex 2 was confirmed by UV-Vis using the following extinction coefficients, calculated in PBS: ε_{384} 10180 [$M^{-1}cm^{-1}$] (for complex 1), ε_{372} 15290 [$M^{-1}cm^{-1}$] (for complex 2). Complex 3 solutions were obtained by dissolving a weighed amount of complex and the concentration was confirmed by comparing the intensity of its resonances to the ones of RNA in the ^{1}H NMR spectrum.

All the chemicals for synthesis were purchased at Fluka-Sigma-Aldrich and used as received.

Deutereted solvents for Nuclear Magnetic Resonance experiments, such as D_2O (100%), DMSO-d6 (99,8%), CD_3CN (99,8%) and $CDCl_3$ (99,8%) were purchased from ARMAR CHEMICALS (Doettlingen, Switzerland).

6.2. Buffers and solutions

15% denaturing gel solution - In 1 L total volume: 420 g of Urea (7 M concentration), 100 mL of 10x TBE, 275 mL of 29:1 Acryl-Bisacryl, and filtered and autoclaved deionized water. The solution is further filtered before usage.

Transcription buffer - 40 mM Tris-HCl (pH 7.5), 40 mM DTT, 2 mM spermidine, 0.01 % Triton X-100.

Denaturing loading buffer - 11.7 M urea, 40 mM Tris-HCl (pH 7.5), 0.1% xylene cyanol (XC), 0.1% bromophenol blue (BB), 230 mM sucrose, 0.8 mM EDTA pH 8.0.

Urea loading buffer - 11.8 M Urea, 8.3% sucrose, 42 mM Tris-HCl (pH 7.5), 0.8 mM EDTA (pH 8.0), 0.08% (w/v) dye xylene cyanol (XC) and bromophenol blue (BB). The buffer was stored at 4°C in the dark before usage.

10x TBE buffer for electrophoresis and electroelution - 0.89 M Tris-HCl (pH 8.3), 0.89 M boric acid, 0.002 M EDTA. This buffer was diluted to 1x with deionized water, and autoclaved before usage.

CIAP buffer used for desphosphorilation - 50 mM Tris-HCl at pH 9.3, 1 mM $MgCl_2$, 0.1 mM $ZnCl_2$ and 1 mM spermidine.

6.3. Instrumentation and software

All solutions were prepared using deionized water obtained from a TKA GenPure water purification system (TKA Wasseraufbereitungssysteme in

Niederelbert, Germany), then filtered with 0.22 µm Steritop bottle top filters (Merck Millipore in Billerica, MA, USA) and autoclaved in order to ensure RNase free conditions.

The PAGE gels were visualized by means of a Bio-Vision system from Vilber (Eberhardzell, Germany). The RNA was recovered from the gel by means of an electroelution apparatus using Whatman® Elutrap System with BT1 and BT2 membranes. The samples were desalted using Vivaspin centrifugal devices (Sartorius Stedim biotech, Aubagne, France) if obtained via *in vitro* transcription, whereas HPLC purified samples were desalted using NAP™ columns from GE Healthcare (Switzerland). The pH was determined using a Metrohm 605 pH-meter with a Minitrode glass electrode from Hamilton. The Centrifuges Sorvall RC 6 Plus from Thermo Fischer Scientific (Reinach, Switzerland) using rotors SA-600 and Eppendorf 5804R with rotor A-4-44 were used during the transcription process.

The RNA extinction coefficients were calculated using the online tool of the website http://eu.idtdna.com/calc/analyzer (OligoAnalyzer 3.1), whereas the values indicated by Microsynth were used for all the DNA constructs. All of the UV-Vis measurements were recorded on a PerkinElmer Lambda 25 or 850 spectrometer with PerkinElmer UV WinLab software using a quartz cuvette with 10 mm path length or a Nanodrop 2000 instrument from Thermo Scientific.

All of the emission spectra were carried out on a Varian Cary Eclipse with Cary Eclipse Win FLR software.

ITC experiments were performed by Dr. Miquel Barceló-Oliver (University of Balearic Islands, Spain) on a Nano ITC low volume calorimeter from TA Instruments and the data were analysed using the NanoAnalyze Software v3.1.2.

All of the NMR experiments were performed on the following spectrometer: Bruker AV300 MHz spectrometer equipped with a QNP probe, Bruker AV400 MHz spectrometer equipped with a QNP probe, Bruker AV500 MHz spectrometer equipped with a BBO TCI z-axis pulsed field gradient CryoProbe®, Bruker DRX-500 spectrometer equipped with a BBO probe, Bruker AV600 MHz spectrometer equipped with a TCI z-axis pulsed field gradient CryoProbe® and Bruker AV700 MHz spectrometer equipped with a

CP-TXI z-axis pulsed field gradient CryoProbe®. The NMR data were then processed using TopSpin 3.1 from Bruker and analysed using Sparky (http://www.cgl.ucsf.edu/home/sparky/).

ESI-MS measurements were performed on a Bruker Daltonics HCT ESI-MS spectrometer.

Maestro 10.5 released by Schrödinger was used to visualize pdb files.

CorelDRAW X7 (version 17.1.0.572) was used to make the pictures of this thesis.

6.4. DNA and RNA constructs

The following RNA constructs were transcribed:

- RNA-l:

  5′-GGAAUAUGCUCUUCGGAGCUAAGUUCC-3′

  Mw = 8610 Da, ε_{260nm} = 266 [$mM^{-1}cm^{-1}$].

- RNA-h:

  5′-GGAAUAUGCUCUUCGGAGCAUGUUCC-3′

  Mw = 8281 Da, ε_{260nm} = 254 [$mM^{-1}cm^{-1}$].

using the following top strand (TS) and original template (OT) DNA templates:

- OT(*met*)$_{\text{RNA-l}}$:

  5′-*GG*AACTTAGCTCCGAAGAGCATATTCCTATAGTGAGTCGTATTAATTTC-3′

  Mw = 15084.8 Da, ε_{260nm} = 487 [$mM^{-1}cm^{-1}$].

- TS$_{\text{RNA-l}}$:

  5′-GAAATTAATACGACTCACTATAGGAATATGCTCTTCGGAGCTAAGTTCC-3′

  Mw = 15062.8, ε_{260nm} = 493 [$mM^{-1}cm^{-1}$].

- OT(*met*)$_{\text{RNA-h}}$:

  5′-*GG*AACATGCTCCGAAGAGCATATTCCTATAGTGAGTCGTATTAATTTC-3′

  Mw = 14782.6 Da, ε_{260nm} = 479 [$mM^{-1}cm^{-1}$].

- TS$_{\text{RNA-h}}$:

  5′-GAAATTAATACGACTCACTATAGGAATATGCTCTTCGGAGCATGTTCC-3′

  Mw = 14711.6 Da, ε_{260nm} = 479 [$mM^{-1}cm^{-1}$].

According to published literature, [155] in order to prevent RNA 3'-heterogeneity the DNA templates contain 2'-methoxy modifications (identified with a *G* in italics in the sequences above) at the two terminal nucleotides of the 5'-end.

Moreover, a DNA construct, named DNA-h, was used in this study:

- DNA-h:

  5'- GGA ACA TGC TCT TCG GAG CAT GTT CC- 3'

  Mw = 7962 Da, ε_{260} [$mM^{-1}cm^{-1}$] = 244.

6.5. Preparation of RNA samples

All the RNA samples were transcribed *in vitro* using double stranded DNA and homemade T7-RNA polymerase. [51,156] The transcriptions were normally run for a time range between 3 and 15 hours at 37°C applying a constant shaking at 300 rpm and resulted in similar yields. The transcription mixture contained 5-7 mM of each NTP, 0.5-1.0 µM of the double stranded DNA template (Microsynth), 0.1% Triton X-100, 15-30 mM $MgCl_2$ and transcription buffer (TXN) containing 40 mM TRIS-HCl (pH 7.5), 40 mM DTT, 2 mM spermidine (Table 6.1). The transcription was followed by ethanol precipitation performed adding threefold the sample volume of cold ethanol and 1/20 parts of sample volume of 5 M NaCl. The precipitate was spun down via centrifugation at 4°C (30 min, 9500 rpm) and the supernatant removed.

After transcription, the RNA samples were purified by electrophoresis using a 15% PAGE. The sample was then extracted from the gel by electroelution and precipitated in ethanol (see above). Subsequently, the RNA was desalted using Vivaspin centrifugal devices with 3 kDa cut-off via several washing steps, at first with a 1 M KCl solution at pH 8 and afterwards with ultrapure water until neutral pH was reached. Specifically, 3-5 steps of washing using KCl promoted the removal of Tris, deriving from the TBE buffer used in the electrophoresis step. The sample was then lyophilized, stored at -20°C and re-dissolved in buffer, when needed. The transcription yield of RNA-l was generally higher (ca. 400 nmol from 5 mL of transcription mixture were obtained) than the one of RNA-h (ca. 100 nmol from 5 mL of transcription mixture were obtained).

At the end of the procedure the concentration of the RNA samples was determined via UV-Vis.

Table 6.1 The optimal transcription conditions were determined for every RNA construct on small scale transcriptions varying one parameter per time and judging via UV shadowing the intensity of the resulting band on polyacrylamide gels. * the amount of polymerase was adapted according to its activity, normally between 20-50 µl per mL of transcription mixture; ** amount of water to be filled up to 5 mL of total volume.

Transcription mixture (5 mL)	**RNA-l**	**RNA-h**
TXN buffer	1 mL	1 mL
GTP	5 mM	7 mM
ATP	5 mM	7 mM
CTP	5 mM	7 mM
UTP	5 mM	7 mM
Triton X-100	0.01%	0.01%
OT strand	0.5 µM	1 µM
TS strand	0.5 µM	1 µM
MgCl2	30 mM	15 mM
T7 Polymerase	*	*
Water	**	**

6.6. Preparation of DNA samples

The DNA construct was bought at Microsynth desalted or HPLC purified. In the first case, it was purified on a 15% PAGE, electroeluted and desalted, following the same procedure described for the RNA samples. In the second case, the samples were desalted using NAP^{TM} columns. After the purification step, the concentration of the DNA samples was determined via UV-Vis.

6.7. Preparation of dephosphorylated RNA samples

The RNA dephosphorylation was performed using alkaline phosphatase. About 200 nmol of RNA were dissolved in 22 mL of Tris-HCl at pH 8 and 2.5 mL of CIAP buffer. Each solution was afterwards divided in 2 aliquots and 250 µl of CIAP (1U/µL) each were added. These mixtures were then incubated in water at 37°C for 15 minutes and afterwards at 56°C for additional 15 minutes. After this first incubation cycle, 250 µl of CIAP (1U/µL) were further added to each solution and the incubation was repeated following the same procedure, first at 37°C and then at 56°C. The enzyme activity was stopped by the addition of 1 M EDTA to reach a final concentration of 0.1 mM EDTA and the solutions were lyophilized. The RNA samples were then purified on 15% PAGE, recovered via electroelution and desalted, as previously described. The yield of dephosphorylation and recovery was ca. 22-26%. The samples were checked via ^{31}P NMR experiments as reported in Appendix 8.

6.8. Sample preparation for NMR spectroscopy

Samples for NMR studies were prepared via transcription using natural abundance or ^{15}N enriched nucleotides, and then dissolved in PBS or 60 mM KCl and 10 µM EDTA in H_2O/D_2O (9:1) or 100% D_2O according to the needs and placed into 5 mm Shigemi tubes. The pH/pD was kept for every sample between 6.8 and 7.2 and if needed, adjusted with 0.1 mM DCl or HCl and 0.1 mM NaOD or NaOH. UV-Vis measurements were used to determine the RNA concentration (normally between 0.1 and 0.5 mM) before all of the NMR measurements. Each sample was annealed at 90-95°C for 3-5 minutes and cooled in ice before any NMR experiment.

6.9. NMR spectroscopy

^{1}H chemical shifts were directly referenced to external DSS (0.2%, pH 7.5) and ^{15}N were indirectly referenced to ^{1}H of DSS, ^{31}P spectra were referenced to external 85% H_3PO_4, [157] and ^{113}Cd NMR spectra were referenced to external 0.1 M $Cd(ClO_4)_2$. [158]

1D ^{1}H NMR experiments were recorded on the RNA samples and the metal complexes for routine checks either in D_2O or in H_2O/D_2O (9:1) using excitation sculpting, presaturation or watergate pulse scheme to suppress the water signal.

1D ^{31}P NMR were acquired using a power-gated decoupling sequence (with 30-degree flip angle) to check the absence of triphosphate groups in RNA dephosphorylated samples.

[^{1}H,^{1}H]-NOESY (Nuclear Overhauser SpectroscopY) and [^{1}H,^{1}H]-TOCSY (Total Correlation SpectroscopY) experiments were performed on RNA samples prepared with natural abundance nucleotides in D_2O. They were used to assign non-exchangeable protons and were recorded at 293 and 303 K with 250 ms and 50 ms as mixing times, respectively. The water suppression was obtained by employing a water presaturation pulse scheme.

[^{1}H,^{1}H]-NOESY spectra were recorded in H_2O/D_2O (9:1) at 278 and 293 K using 150 ms of mixing times and a watergate pulse scheme for water suppression to assign imino proton resonances.

Heteronuclear 2D experiments were performed on RNA samples prepared employing ^{15}N enriched nucleotides. ^{2}J-[^{1}H,^{15}N]-HSQC (Heteronuclear Single Quantum Coherence) experiments at 303 K were used to assess the purine nitrogen atoms, such as N1, N3, N7 and N9.

DOSY (Diffusion-Ordered Spectroscopy) experiments were used to screen the ability of the different metal complexes to bind to RNA-l comparing the RNA diffusion coefficients in the presence and in the absence of metal complex. They were acquired using the standard Bruker pulse program ledbpgp2s_es and a diffusion time (Δ) and gradient length (δ) equals to 300 ms and 2 ms respectively. The gradient strength was incremented from 11 to 31 G/cm in 30 steps and each FID had at least 96 transients with 32768 data points in F2 dimension. The data analysis was done on Topspin 3.1 using the standard 2D DOSY processing protocol with logarithmic scale in the F1 dimension (diffusion coefficient).

STD (Saturation Transfer Difference) NMR experiments were recorded using the stddiffesgp.2 Bruker standard sequence to obtain more information on the metal complex protons involved in the binding to RNA. The *on-resonance* irradiation of the RNA-l was performed at 3933 Hz (700 MHz instrument), while the *off-resonance* irradiation was set at 21000 Hz (700 MHz instrument), where no resonances of the RNA were observed.

[^{1}H,^{1}H]-COSY, [^{1}H,^{13}C]-HSQC and [^{1}H,^{13}C]-HMBC (Heteronuclear Multiple Bond Correlation) standard experiments were acquired to assign the resonances of complex 1 (Appendix 35, Appendix 36, Appendix 37) and to characterize the newly synthesised products (Chapter 5)

6.10. NMR characterisation of the free species in solution: RNA and DNA constructs, complex 1, complex 2 and complex 3

All the RNA and DNA constructs, likewise the metal complexes used, were at first characterized in their free form.

Complex 1 is only slightly soluble in PBS in the presence of 2% of DMSO (the maximum concentration in our conditions is about 0.2 mM). For this reason, its ^{13}C resonances were assigned in either pure DMSO, using a 9.3 mM sample, or in PBS in the presence of 30% DMSO, using a 2.5 mM sample. ^{1}H and ^{13}C resonances in the two cases are reported in Appendix 35 and ^{1}H NMR, [^{1}H,^{13}C]-HSQC and [^{1}H,^{13}C]-HMBC spectra used for the characterization are reported in Appendix 36 and Appendix 37.

1D ^{1}H NMR spectra of complex 1 were also recorded at lower concentration in PBS, in the presence of 2% of DMSO. An example spectrum is reported in Appendix 38. ^{1}H NMR (PBS in D_2O): 9.77 (dd, J = 5.2, 1.2, 2H); 9.45 (m, 2H); 8.40 (d, J = 1.2, ^{1}H); 8.35 (dd, J = 6.2, 0.7, 1H); 8.16 (dd, J = 8.6, 5.4, 2H); 8.10 (broad signal, 2H); 7.95 (m, 2H); 7.71 (d, J = 8.6, 1H); 7.22 (dd, J = 8.6, 6.5, 1H) (Appendix 38).

Complex 2 characterization was obtained in PBS via ^{1}H NMR. ^{1}H NMR (PBS in D_2O): 9.43 (d, J = 8.9, 2H); 8.38-8.28 (m, 6H); 8.04 (d, J = 5.40, 2H); 7.94 (m, 2H); 7.89 (t, J = 8.5, 2H); 7.79 (t, J = 8.5, 2H); 7.74 (d, J = 5.5, 2H); 7.66 (t, J = 5.8, 2H); 7.59 (d J = 6.0, 2H); 7.21 (t, J = 6.9, 2H); 7.02 (t, J = 6.9, 2H) (Appendix 39). [159]

Complex 3 was characterized by means of ^{1}H NMR experiments. ^{1}H NMR (PBS in D_2O): 8.30 (d, J = 8.7, 2H); 7.81 (t, J = 8.7, 2H); 7.60 (d, J = 6.0, 2H); 7.13 ppm (t, J = 7.0, 2H) (Appendix 40). [159]

Concerning RNA-l and RNA-h, the aromatic and H1' proton resonances in the area of the sequential walk were assigned by means of [^{1}H,^{1}H]-NOESY and confirmed by means of [^{1}H,^{1}H]-TOCSY spectra performed in PBS (Appendix 1 and Appendix 3). The imino proton resonances of RNA-l, RNA-h and DNA-h were assigned via [^{1}H,^{1}H]-NOESY in PBS prepared in a 9:1 mixture of H_2O/D_2O (Appendix 2). Purine N7, N1, N9 and N3 ^{15}N chemical shifts were assigned through ^{2}J-[^{1}H,^{15}N]-HSQC experiments (Appendix 4) Moreover, ^{1}H NMR experiments on RNA-l samples prepared in the presence of different amount of DMSO in PBS (up to 30%) were performed (Figure 2.6) to evaluate the influence of the organic solvent on the RNA structure.

6.11. NMR interaction studies

The interaction studies were performed recording either 1D ^{1}H NMR, [^{1}H,^{1}H]-NOESY, [^{1}H,^{1}H]-TOCSY or ^{2}J-[^{1}H,^{15}N]-HSQC spectra on a RNA sample in the absence and in the presence of metal complex in order to localise the binding site and evaluate the RNA structural changes in the presence of the metal complex. A typical titration experiment was carried out on a 0.1-0.5 mM sample of nucleic acid in 180 or 220 μL with additions of metal complex solution (0.5-2 μL) in the NMR Shigemi tube. Complex 1 solutions were freshly prepared for every titration in a range of 5-10 mM in pure DMSO. The sample at the end of the titrations had a final DMSO content up to 4%. 11-12.5 mM solutions of complex 2 and complex 3 in PBS prepared in D_2O were used for the additions.

DOSY (Diffusion-Ordered Spectroscopy) experiments were carried out to screen the ability of the different metal complexes to bind to RNA-l comparing the RNA diffusion coefficients in the presence and in the absence of metal complex. DOSY spectra were collected on PBS solutions prepared in 100% D_2O of 0.35 mM RNA-l at 303 K, pD 7.0 in the presence of 1 equivalent of complex 1, complex 2 and complex 3.

STD (Saturation Transfer Difference) NMR experiments were used as complementary method to better understand which part of the metal complex was involved in the interaction. A typical STD NMR spectrum was obtained on 25 μM RNA-l sample with a fifteenfold excess of complex 1 or complex 2 (350 μM). The experiments were performed in 60 mM KCl, 10 μM EDTA at pD 6.7/6.9 at 300 K for complex 1, while for complex 2 in PBS at pD 6.8 and at 300 K. All of the STD NMR experiments were recorded on a 700 MHz spectrometer using the stddiffesgp.2 Bruker standard sequence. The on-resonance irradiation of the RNA-l was performed at 3933 Hz (5.62 ppm), while the off-resonance irradiation was set at 21000 Hz (30 ppm), where no resonances of the RNA were observed. The degree of saturation in percentage was calculated setting to 100% the peak that showed the lowest loss of intensity comparing the ^{1}H NMR spectrum of the mixture and the STD NMR one.

6.12. Isothermal Titration Calorimetry (ITC) assays

A typical ITC experiment was carried out on the calorimeter stabilized at either 25°C or 30°C for at least one hour. The sample and the reference cell were filled with 250 μL of solution and the titrant was added to the samples cell in 16 injections of 3.03 μL using a collection time of 300 s between consecutive additions. All of the experiments were carried out in triplicate at 25°C or/and 30°C. The data fitting was done using NanoAnalyze v3.1.2.

All the experiments performed on complex 1 were done in PBS in the presence of 2% DMSO, because of its poor water solubility, whereas for complex 2 they were carried out in pure PBS. Concerning complex 1 the experiments were recorded using a ~15 μM RNA or DNA solution in the sample cell and a ~200 μM solution of complex 1 used as titrant. On the contrary, in the case of complex 2, the experiments were performed with the sample cell filled with a ~45 μM RNA or DNA solution in PBS, while the titration syringe was loaded a ~1000 μM solution of complex 2 in PBS. Measurements of the dilution heat were performed injecting the titrant into the buffer following the same procedure described above. These data were then subtracted to the experimental peaks leading to corrected peak areas afterwards plotted *versus* concentration of titrant stepwise injected. The curves obtained were then fitted to the selected type of process.

6.13. Job plot experiments

Job plot or method of continuous variation experiments were used to obtain the stoichiometry of the interaction between complex 2 and RNA-l and RNA-h. In a typical Job plot assay, the total molar concentration was kept constant at 3 μM while the mole fractions of complex 2 and RNA were changed. Emission spectra were collected at the eleven different molar ratios. The stock solutions used in this experiment were respectively 82.5 μM for complex 2, 100 μM for RNA-l, and 98 μM for RNA-h.

6.14. Emission experiments and ethidium bromide (EB) displacement assays

All of the emission spectra were recorded in PBS with 50 mM NaCl at pH 7.1 at room temperature and the data obtained were multiplied by standard correction factors to obtain corrected intensity values. All of the experiments were performed in triplicate or more.

The concentration of RNA and DNA stock solutions was usually 100-1000 μM and was measured via UV-Vis, while the one of the stock solutions of the metal complexes was in a range of 100-500 μM. These latter solutions were prepared in PBS for complex 2 and complex 3, whereas in the case of complex 1 a 2% of acetonitrile was added. The concentration was checked via UV-Vis in the case of complex 1 and complex 2, while in the case of complex 3 by means of 1D ^{1}H NMR as described in Section 6.1. EB stock solutions were obtained weighing an amount of compound in order to prepare a 60-70 μM concentration in PBS and afterwards diluted to 0.1 μM.

A typical emission titration consisted in the addition of RNA or DNA to a solution of complex 2 (3.0-3.5 μM) or EB (0.1 μM) until a metal complex to nucleic acid ratio of 1 to 3 was obtained. Complex 2 was kept below 3.5 μM to avoid aggregation due to π-π stacking of the aromatic units. [160,161] All of the emission experiments were collected between 550 and 750 nm for complex 2 with $\lambda_{ex} = 444$ nm and from 540 to 800 nm in the case of EB with $\lambda_{ex} = 512$ nm.

EB fluorescence displacement assays were carried out on 5-12 μM equimolar mixtures of EB and RNA or DNA. Complex 1 or complex 2 was then stepwise added until an EB to metal complex ratio of 1:1 was obtained. The emission experiments were collected from 540 to 800 nm with 512 nm as excitation wavelength. The spectra were corrected using standard correction curves. Stern-Volmer quenching constants were obtained via the following equation:

$$\frac{I_0}{I} = 1 + K_{SV} r \quad \text{Equation 6.1}$$

where I_o and I correspond to the fluorescence intensities in the absence and the presence of metal complex, K_{SV} represents the linear Stern-Volmer quenching constant and r is the ratio of the metal complex total concentration to the one of nucleic acid.

Emission experiments were also performed to obtain a qualitative evaluation of the binding strength of RNA/DNA and complex 2. In a typical assay a 10-11 µM sample of complex 2 in PBS was treated with 1 equivalent of DNA-h and then titrated with RNA-l or RNA-h. The emission of complex 2 was stepwise monitored between 470 and 830 nm using as excitation wavelength 444 nm. The percentage of intensity decrease, $I\%$ is calculated using the following formula:

$$I\% = \frac{(I_{max} - I)}{(I_{max} - I_{min})} * 100 \qquad \text{Equation 6.2}$$

where I_{max} is the maximum emission intensity, I corresponds to the intensity at each point of the titration and I_{min} is the minimum emission intensity. For example, for the experiment performed starting with a 1:1 solution of DNA-h and complex 2, I% is calculated as follows: I_{max} is the emission intensity of the 1:1 solution of DNA-h and complex 2 (first point of black dataset in Figure 3.9a of Chapter 3), I is the emission at the each addition of RNA-l and I_{min} is the emission intensity of a 1:1 solution of RNA-l and complex 2 (first point of the red dataset in Figure 3.9a of Chapter 3).

6.15. UV-Vis experiments

All of the UV-Vis experiments were carried out on 8-14 µM solutions of complex 1 and complex 10 in PBS at pH 7.1 with 2% of acetonitrile at room temperature. During the titration the concentration of RNA-l was varied from 0 to a maximum of 5 equivalents. As a consequence of nucleic acid additions, the complex concentration varied of a maximum of 2% and as such, this change was considered negligible.

6.16. Synthesis of $[Re(CO)_3(dppz)(3\text{-}CH_2NH_3\text{-}Py)]^{2+}$

$[Re(CO)_3(dppz)(3\text{-}CH_2NH_3\text{-}Py)]XY$ ($3\text{-}CH_2NH_3\text{-}Py$ = 3-picolylammonium; X is tetrafluoroborate, BF_4^- and Y is hexafluorophosphate, PF_6^-) was obtained via a 5 steps reaction (Appendix 15) based on literature procedures. [15,143–146]

6.16.1. Step 1: Synthesis of 1,10-phenanthroline-5,6-dione (5)

1,10-phenanthroline (4) (3.00 g, 16.6 mmol) and KBr (3.00 g, 25.2 mmol) were slowly dropped into an ice-cold mixture of HNO_3/H_2SO_4 (30 mL of 100% HNO_3 and 30 mL of 96% H_2SO_4). At complete addition, the mixture was heated at 130°C for 3.5 hours. The reaction mixture was cooled down at room temperature, diluted in ice (300 g) and partially neutralized with NaOH (5 M, 400 mL) till pH 5, while cooling in ice. The compound was extracted with CH_2Cl_2 (5x 100 mL), the organic phase washed with brine (3x 100 mL) and dried with $MgSO_4$. The solvent was evaporated *in vacuo* to give the oxidized product 5, that appears like an orange solid (2.74 g, 13.0 mmol, 79%).

ATR-IR: 3065 cm^{-1}, (w, arom. C-H), 1685 cm^{-1} (s, C=O), 1577 cm^{-1} (m, C=C), 1560 cm^{-1} (m, C=C) (Appendix 16). [143]

^1H NMR ($CDCl_3$): 9.13 (dd, J = 4.7, 1.8, 2H); 8.47 (dd, J = 7.9, 1.8, 2H); 7.60 (dd, J = 7.9, 4.7, 2H) (Appendix 17). [143,147]

6.16.2. Step 2: Synthesis of dipyrido[3,2-a:2',3'-c]phenazine (7)

Compound 5 was further reacted with o-phenyldiamine (6) (0.65 g, 6.00 mmol) at 55°C in EtOH (400 mL) for 2.5 hours and stirred at room temperature for further 16 hours. Then, the volume was reduced *in vacuo* and the compound precipitated with a mixture of 1:9 of $MeOH/H_2O$ (100 mL) and filtered. The light-yellow solid was recrystallized in MeOH to give compound 7 as a milky powder (1.07 g, 3.8 mmol, 80%).

^1H NMR ($CDCl_3$): 9.65 (dd, J = 8.1, 1.8, 2H); 9.28 (dd, J = 4.5, 1.8, 2H); 8.36 (dd, J = 6.5, 3.4, 2H); 7.93 (dd, J = 6.5, 3.4, 2H); 7.80 (dd, J = 8.1, 4.5, 2H) (Appendix 18). [143]

^{13}C NMR ($CDCl_3$): 152.70; 148.5; 142.69; 141.30; 134.02; 130.86; 129.74; 127.80; 124.35 (Appendix 19). [148]

6.16.3. Step 3: Synthesis of bromotricarbonyldipyrido[3,2a:2',3'c] phenazinerhenium(I) (9)

Bromopentacarbonylrhenium(I) (8) (0.51 g, 1.3 mmol) and compound 7 (0.36 g, 1.3 mmol) were mixed and dry toluene was added. The mixture was heated to sub-reflux (100°C) for 30 min. The colour of the mixture turned to pale yellow after cooling at room temperature. The precipitate was filtered giving complex 9 as a yellow solid (0.71 g, 1.1 mmol, 89%).

ATR-IR (only carbonyls region): 2025 cm^{-1} (s, stretching CO), 1930 cm^{-1} (s, stretching CO), 1885 cm^{-1} (s, stretching CO) (Appendix 20). [146]

^{1}H NMR (DMSO): 9.82 (d, J = 8.0, 2H); 9.56 (d, J = 4.6, 2H); 8.49 (dd, J = 6.4, 3.3, 2H); 8.26 (dd, J = 8.1, 5.3, 2H); 8.18 (dd, J = 6.3, 3.4, 2H) (Appendix 21). [146]

6.16.4. Step 4: Synthesis of acetonitriletricarbonyldipyrido[3,2-a:2',3'c] phenazinerhenium(I)tetrafluoroborate (10)

Complex 9 (0.35 g, 0.6 mmol) was dissolved in MeCN (10 mL). $AgBF_4$ (0.15 g, 0.8 mmol) was added and the mixture heated at sub-reflux (65°C) for 19 hours in the dark. After cooling to room temperature, the solvent was evaporated until a minimum volume and the product was precipitated with diethyl ether. The compound was filtered to obtain complex 10 as an orange solid (0.32 g, 0.5 mmol, 85%).

ATR-IR: 2035 cm^{-1} (s, stretching CO), 1920 cm^{-1} (s, stretching CO) (Appendix 22).

^{1}H NMR (CD_3CN): 9.81 (dd, J = 8.3, 1.4, 2 arom. H); 9.48 (dd, J = 5.3, 1.4, 2 arom. H); 8.41 (dd, J = 6.6, 3.4, 2H); 8.18 (dd, J = 8.3, 5.3, 2H); 8.12 (dd, J = 6.6, 3.4, 2H); 1.94 (s, 3 H, CH3) (Appendix 23, Appendix 25).

^{13}C NMR (CD_3CN): 156.88; 150.60; 143.79; 140.15; 137.65; 133.74; 131.67; 130.62; 129.05; 3.89; 1.32 (Appendix 24, Appendix 26, Appendix 27). [15]

6.16.5. Step 5: Synthesis of 3-picolylammoniumtricarbonyldipyrido [3,2-*a*:2',3'*c*]phenazinerhenium(I)tetrafluoroborate hexafluorophosphate (12)

To synthesize complex 12 was necessary the synthesis of 3-picolylammoniumhexafluorophosphate (11). NH_4PF_6 (0.18 g, 1.1 mmol) was dissolved in dried MeOH (3 mL) and 3-Picolylamine was dropwise added. The mixture was heated to 60°C for 1.5 hours in an open flask. The evaporation of

NH_3 was checked testing the vapours with pH paper. At complete solvent evaporation, the resulting precipitate was cooled to room temperature and dried *in* vacuo to give compound 11 as white solid (2.7 g, 1.1 mmol, 96%).

^{1}H NMR (CD_3CN): 8.61 (*d*, *J* = 2.1, 1 arom. H); 8.59 (*dd*, *J* = 4.8, 1.6, 1 arom. H); 7.80 (*ddd*, *J* = 7.9, 2.3, 1.7, 1 arom. H); 7.40 (*ddd*, *J* = 7.9, 4.8, 0.8, 1 arom. H); 4.10 (*s*, 2H, CH_2); 3.37 (*s*, 3H, NH_3) (Appendix 28). [150]

^{19}F NMR (CD_3CN): -72.94 (*d*, *J* = 706.3) (Appendix 29). [151]

Complex 10 (0.03 g, 0.05 mmol) and compound 11 (0.04 g, 0.14 mmol) were mixed in MeOH (3 mL). The mixture was heated to 55°C for 48 hours. The solvent was evaporated to a minimum volume and the complex precipitated via addition of water. The product was filtered to give complex 12 as a yellow solid, with traces (<5%) of impurities (9 mg, 0.012 mmol, 26%).

^{1}H NMR (CD_3CN): 9.92 (dd, J = 8.3, 1.4, 2H); 9.67 (dd, J = 5.3, 1.4, 2H); 8.47 (dd, J = 6.5, 3.5, 2H); 8.39 (d, J = 2.1, 1H); 8.29 (dd, J = 8.3, 5.3, 2H); 8.24 – 8.18 (m, 1H); 8.15 (dd, J = 6.7, 3.4, 2H); 7.82 (d, J = 8.1, 1H); 7.29 (dd, J = 8.0, 5.8, 1H); 3.93 (s, 2H, CH_2) (Appendix 30, Appendix 31, assignment provided in Figure 5.13).

^{13}C NMR (CD_3CN): 156.70; 154.15; 153.49; 150.42; 143.92; 141.99; 140.25; 138.12; 133.85; 133.74; 132.08; 130.67; 129.69; 129.04; 127.75; 41.23; 1.32 (Appendix 32, Appendix 33).

MS (ESI): m/z = 661 ($[M - H]^+$), 553 ($[M - C_6H_9N_2]^+$) (Appendix 34, the additional peaks were not attributed). Exact m/z = 662. The spectrum was recorded in positive and negative mode under the following conditions: injection rate 3 µL/min, nebulizer P = 10 psi, dry gas flow rate 5 L/min, gas T = 350°C using LCMS grade solvents.

7. Summary

In the last decades, the number of studies on the interaction of metal complexes with nucleic acids grew steadily. [1,2,7] Metal complexes can be exploited as diagnostic and therapeutic agents having as target the most important biological macromolecules in the cell, such as proteins, DNA and RNA. The latter one is a very challenging and interesting molecule owing to its involvement in many biological processes and its structural variety. [3–6] Indeed, compared to DNA, RNA can adopt a complex structure, which includes, besides double helical regions, bulges, hairpins and junctions that can offer specific binding sites for small molecules. [14,49] Interactions of metal complexes with RNA and DNA can occur via covalent or non-covalent binding. [2,7,16,17]

In this thesis we investigated the non-covalent interaction of metal complexes and metal ions with RNA aiming at obtaining insights in their binding properties that can be used for a rational design of structure-selective probes. As model system, we used a 27 nucleotides long RNA construct (RNA-l in Figure 7.1a), whose NMR structure in solution was solved in the group of Prof. Dr. Roland K.O. Sigel. [11] This construct derives from the ζ region of domain 1 of the group II intron ai5γ from *Saccharomyces cerevisiae* that together with the κ element forms the κ-ζ region. The latter one, correctly structured, allows the interaction with domain 5 which is the basis of the catalytic activity of the whole intron.

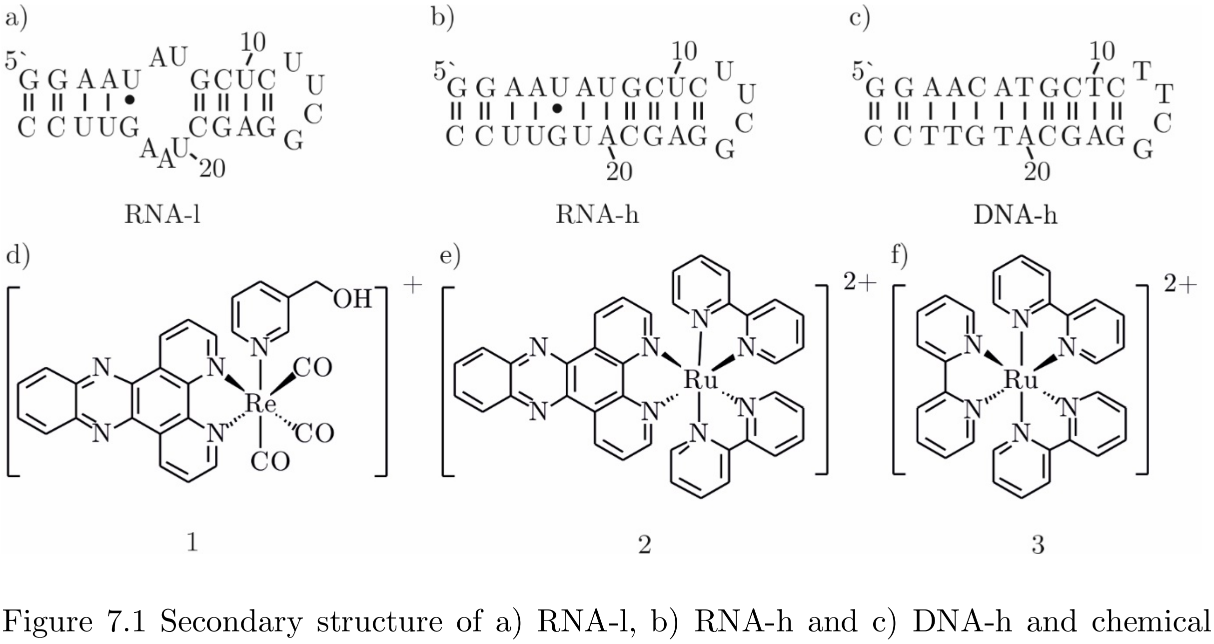

Figure 7.1 Secondary structure of a) RNA-l, b) RNA-h and c) DNA-h and chemical structures of d) $[Re(CO)_3(dppz)(3\text{-}CH_2OH\text{-}py)]^+$ (1), e) $[Ru(bpy)_2(dppz)]^{2+}$ (2) and f) $[Ru(bpy)_3]^{2+}$ (3).

RNA-l possesses a great potential as probe for different secondary structural features that are common in RNA, because it contains a GU wobble, a terminal loop and an internal loop. The last one is a very interesting secondary structural element in RNA as internal loops are reported for their potential to act as selective binding pockets for small molecules. [4,14,50]

We studied the binding of RNA-l with $[Re(CO)_3(dppz)(3\text{-}CH_2OH\text{-}py)]^+$ (complex 1, Figure 7.1d), whose ability to act as potential bio-imaging agent was reported by the group of Dr. Michael P. Coogan (University of Lancaster, United Kingdom). [15] Previous studies on similar complexes with the general formula $[Re(CO)_3(dppz)(X)]^+$ (where X can be a wide variety of ligands) showed that they interact with CT-DNA and accumulate in DNA and RNA rich-regions in the cell. In particular, among the pool of similar complexes, complex 1 showed one of the highest binding constant with DNA, most likely thanks to the presence of the hydroxymethyl group that can favour hydrogen bonding with DNA. These interesting data and the lack of information on RNA binding of metal complexes were the starting point of our study. Besides RNA-l, we also used two additional oligonucleotide sequences, RNA-h (Figure 7.1b) and DNA-h (Figure 7.1c). The first one is a 26 nucleotides long RNA construct very similar to RNA-l but without the internal loop, employed to better understand the role of this feature in the interaction with complex 1. The second one is a DNA analogous of RNA-l used to understand the differences in RNA and DNA binding of complex 1. Moreover, we used $[Ru(bpy)_2(dppz)]^{2+}$ (complex 2, Figure 7.1e), and $[Ru(bpy)_3]^{2+}$ (complex 3, Figure 7.1f) as additional metal complexes to investigate in more detail the role of the dppz moiety in the binding to RNA-l.

RNA binding sites for metal ions and metal complexes: an NMR study

Metal ions are essential for RNA as they help to obtain a distinct complex three-dimensional fold that is often a prerequisite to fulfil its function, and moreover they can also be directly involved in the catalytic activity of RNAs called ribozymes. [60]

Metal ion binding sites in RNA can represent potential metal complex binding sites, hence NMR studies on the interaction of Mg(II), Cd(II) and cobalt(III)hexammine with RNA-l were used to predict the binding behaviour of complex 1. The NMR data on the metal ion binding sites are from a recent publication [9] from Bartova *et al.* of which I am a co-author. Our results suggest that two regions are mainly influenced by the presence of metal ions. One is the 5'-end triphosphate that in the presence of Cd(II) showed the formation of Cd(II) induced macrochelates. [9] The second area is the internal loop. Indeed, small chemical shift changes in this region upon addition of the three metal ions suggest overall electrostatic interaction at this site. These findings were confirmed by Mn(II) line broadening experiments that showed that the 5'-end and the internal loop are the most influenced regions.

With these data at hand, we started to study the interaction of complex 1 and RNA-l via 1D ^{1}H NMR titrations in water. The imino proton resonances observed in these experiments reflect the stability of the base pairs of RNA and are sensitive to structural changes or direct interaction upon addition of metal complex. The spectra of RNA-l upon stepwise additions of complex 1 (Figure 7.2, left) show that mainly one specific resonance is influenced, namely G8H1, that broadens strongly. This signal belongs to a residue in the internal loop suggesting a binding close by. On the contrary, 1D ^{1}H NMR titrations of

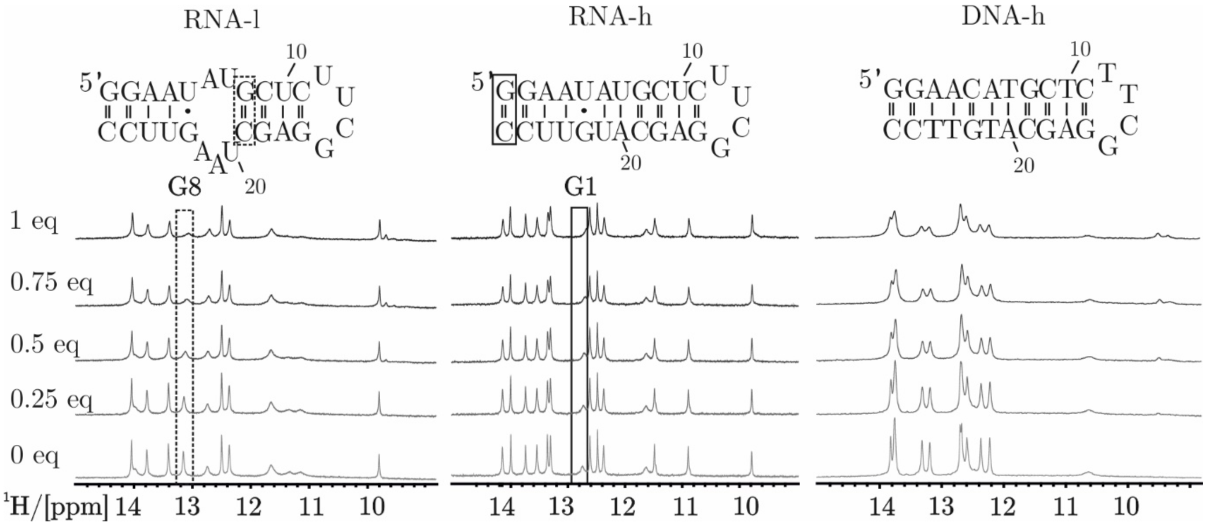

Figure 7.2 Overlay of ^{1}H spectra (imino region) of RNA-l, RNA-h and DNA-h recorded in the presence of increasing amounts of complex 1 (0.2 mM, PBS with 2% DMSO, pH 7, 293K, 700 MHz). The squares indicate the base pairs, whose intensities are significantly reduced upon addition of complex 1.

RNA-h, the RNA construct without the internal loop, with complex 1 show only an effect at the 5'-end (Figure 7.2, middle), most likely due to the fact that the first base pairs of a sequence are generally less tight and might offer a binding site for the metal complex. This result suggests that the presence of the internal loop is essential for the RNA binding. 1D ^{1}H NMR titrations of the analogous DNA-h with complex 1 show a very different behaviour (Figure 7.2, right), as almost all its imino resonances are influenced, indicating an unspecific overall binding.

Once we observed a selective interaction between complex 1 and RNA-l, we decided to investigate the role of the dppz moiety in the binding, as this group is well known for its ability to behave as an intercalating unit. [19,32] To understand its involvement in the binding to the RNA internal loop, we performed additional 1D ^{1}H NMR titration experiments in D_2O of RNA-l using complex 1, complex 2 and complex 3. In the presence of both complex 1 and complex 2, that bear the dppz moiety, we observed a strong influence on the resonances of the H2 protons of the three adenines A6, A21, and A22 in the internal loop. These results confirmed the specific binding of the two complexes to the internal loop region and, moreover, they indicated the involvement of the dppz moiety in the interaction. This was supported by what obtained for complex 3, which does not bear the dppz unit, and does not show an interaction with RNA-l.

More in depth studies were performed using 2D experiments, such as [^{1}H,^{1}H]-NOESY, [^{1}H,^{1}H]-TOCSY and [^{1}H,^{15}N]-HSQC that confirmed the presence of an interaction at the internal loop. However, fast dynamics and disappearance of the resonances belonging to this region did not allow to obtain further insights on the position of the metal complex in the binding site using NMR spectroscopy.

Optical studies and ITC experiments

The class of $[Re(CO)_3(dppz)(X)]^+$ derivatives, which includes complex 1, was shown in the literature to possess characteristic UV profiles that reveal hypochromicity in the presence of DNA. [15] Furthermore, these kind of complexes are weakly emissive in aqueous media with a significant enhancement of emission intensity upon addition of DNA. [15] Data deriving from titrations of metal complex solutions with nucleic acid can be plotted to obtain a qualitative evaluation of the binding and can be fitted to provide quantitative information. Hence, we exploited various optical methods aiming at a quantitative evaluation of the binding.

UV-Vis titrations were performed following the changes of the absorption profile of complex 1 in the presence of increasing amounts of RNA-l. This led to a hypochromic effect on the absorption bands of complex 1 that could be due to the involvement of its aromatic ligands in the binding with RNA. However, the changes in absorbance observed upon interaction were very little, suggesting that the RNA binding is lower compared to the one reported in literature for CT-DNA. [15] Moreover, such small variations are affected by non-negligible experimental error, hindering a reliable quantitative evaluation of these data. Hence, another technique was applied in order to quantify the binding.

ITC is a method that offers the possibility to obtain an entire set of thermodynamic data, such as stoichiometry, binding constant, enthalpy and entropy, of an interaction via measurements of the heat released during a titration. [102] In our case the data were collected on both complex 1 and complex 2 with RNA-l that showed a similar behaviour in the NMR studies. These measurements were performed by Dr. Miquel Barceló-Oliver (University of Balearic Islands). In both cases, an interaction was detected, but the low affinity resulted in significant errors. Therefore, no quantitative data could be obtained, and further investigation is needed. However, a stoichiometry value of two molecules of complex 1 per RNA internal loop could be confidently proposed.

To confirm this stoichiometry, Job plot assays were performed (Figure 7.3). In these experiments the emission of complex 2 was measured at different molar ratios of metal complex to RNA-l or RNA-h with a constant total concentration of the two components. These assays were performed using only complex 2 since no emission was observed for complex 1 in the presence of RNA. This is not surprising, because the luminescence restoring of Re(I)dppz complexes is already barely measurable in the presence of DNA, being much less efficient than the ruthenium analogue complexes. [50] A clear maximum at a 1:2 ratio was observed for RNA-l and complex 2, indicating that two ruthenium complexes interact

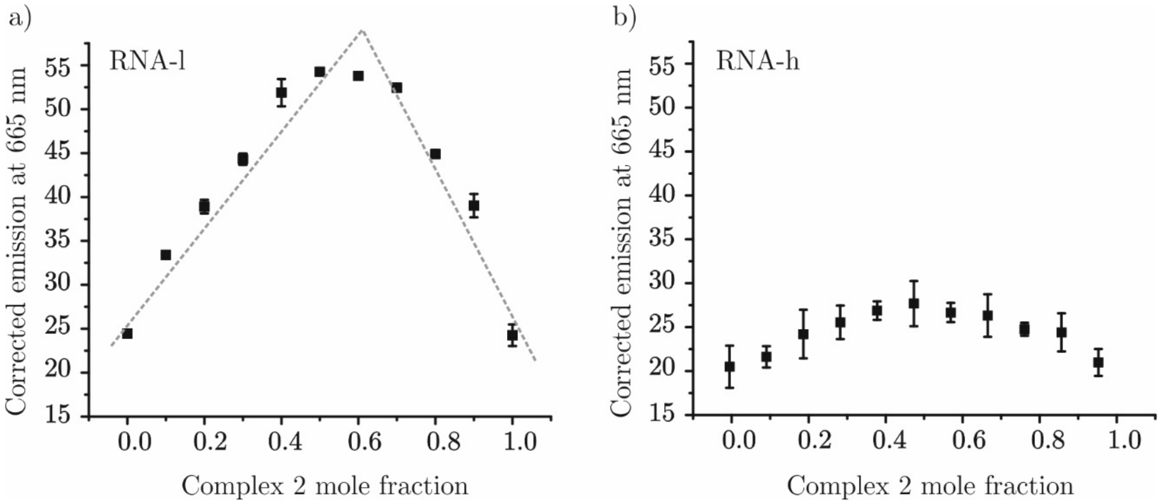

Figure 7.3 Job plot experiments of complex 2 and a) RNA-l and b) RNA-h (PBS, pH 7.2). The total molar concentration of the solutions at each point is 3 µM. The maximum in panel a) is highlighted with dashed lines.

with this RNA, thus confirming the ITC results. By contrast, the emission intensity detected for complex 2 and RNA-h, was only very little and the data are affected by remarkable errors, preventing a confident evaluation.

Although a binding constant could not be calculated using the previously discussed methods, a qualitative evaluation of the binding strength was obtained via emission competition experiments of equimolar solutions of DNA-h and complex 2 adding RNA-l or RNA-h. For each step the emission maximum was then plotted versus the concentration of RNA added. The results show a decrease of emission indicating that both RNA-l and RNA-h are able to compete with DNA-h for the binding to complex 2, although this last one between DNA-h and complex 2 resulted stronger.

In general, the ability of complex 2 of restoring its emission upon binding to nucleic acids could be also employed to qualitatively and quantitatively assess its interaction monitoring the changes in emission upon titration of nucleic acids. In the case of our short nucleic acid sequences, only a qualitative evaluation was possible, since the model generally applied for data fitting relies on the assumption that the nucleic acid molecule is an infinite system. [100]

Emission titrations on solutions of complex 2 adding our RNA and DNA constructs were performed. In all of the cases we observed an increase of emission indicating the presence of an interaction. The restored emission upon binding was higher for RNA-l than for RNA-h, suggesting that the first RNA offers better shielding conditions. For DNA-h, the emission was much higher than the one observed for both RNA models. However, it is worth to note that the emission profile observed in the presence of DNA shows first an increase followed by a decrease in intensity. This suggests the presence of different interactions due to diverse binding modes of the two enantiomeric forms of complex 2. [117] Such behaviour was not observed in the case of RNA-l, indicating that in this case their binding to the internal loop occurs in a similar way.

Moreover, emission titrations were performed using ethidium bromide (EB). This small ligand is very well known in the literature because it interacts with double helical RNAs and DNAs, thereby showing strong fluorescence enhancement upon intercalative binding. [115] For this reason, studying its behaviour with our sequences could give information on the binding preferences.

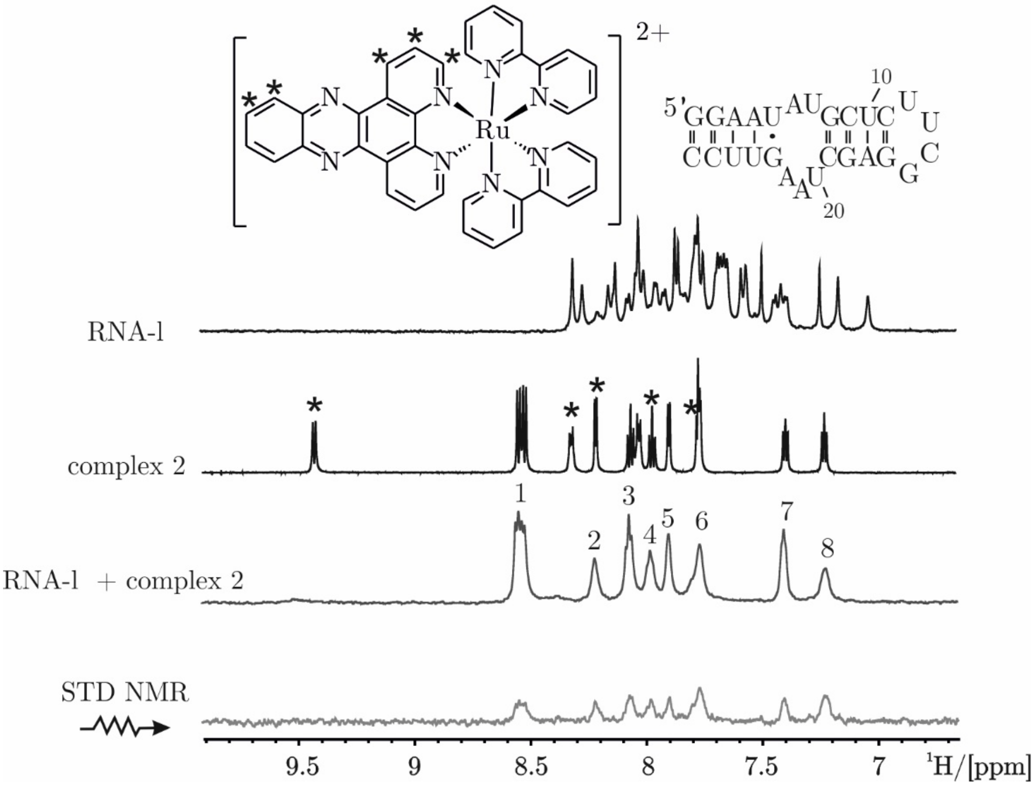

Figure 7.4 ^{1}H NMR spectrum of RNA-l, complex 2 and reference spectrum of 25 µM RNA-l and 350 µM complex 1 (300 K, 700 MHz). Stars highlight the proton resonances of the dppz moiety. Numbers are used to indicate the signals of the resonances visible in the spectrum of the mixture of complex 2 and RNA-l.

These experiments were performed with all the three RNA and DNA constructs showing an increase of the EB emission maximum. However, its emission is higher with RNA-l than with RNA-h and the one in the presence of DNA-h lies in between the one observed with RNA-l and RNA-h. These results suggest that our RNA internal loop allocates and shields EB in a better way than RNA-h and DNA-h.

Ethidium bromide was also used in emission displacement assays to evaluate the ability of complex 2 and complex 1 to compete with EB for the binding to our nucleic acid sequences. The emission of an equimolar solution of EB and RNA or DNA was evaluated titrating either complex 1 or complex 2 to this mixture. The observed decrease in intensity could indicate that there is a contribution of intercalative binding. These data could be fitted allowing to calculate Stern-Volmer (K_{SV}) constants. In general, the K_{SV} calculated for complex 2 in the presence of all the three constructs are higher than in the case of complex 1, thus suggesting a stronger interaction. This result might be due to the influence of the higher charge of complex 2 or to the difference in axial ligands between the two complexes.

STD NMR experiments and MD simulations

To obtain more insights on the positions of the metal complex in the RNA internal loop, STD (Saturation Transfer Difference) NMR experiments were performed. This technique relies on the transfer of magnetization from a receptor (RNA-l) to a ligand (metal complex) in an experiment performed in excess of the latter one. RNA-l was irradiated at 3933 Hz (5.62 ppm), thus avoiding the resonances of the complex. In the STD NMR experiment we observe only the signals of the ligand protons that are close enough in space to RNA-l to receive magnetization via spin diffusion. Due to the low water solubility of complex 1, STD NMR experiments could be performed successfully only on complex 2 and RNA-l. The ^{1}H NMR spectrum of the sample used for STD NMR proves that an interaction occurs, since in the presence of RNA-l, a general broadening of the proton resonances of complex 2 was observed, along with the disappearance of some of the signals of protons belonging to the dppz moiety (all resonances of the dppz protons are marked with stars in Figure 7.4). We then evaluated the degree of saturation of the resonances in the STD NMR spectrum. The highest saturated peak belongs to a proton of the bipyridine ring (peak 8), however the rest of the peaks that show high degrees of saturation belong to the dppz ligand (peaks 6, 4 and 2 in order of descending degree of saturation). The fact that among the five resonances belonging to protons of the dppz group, two are not visible in the presence of RNA-l and that the remaining three seem to be close enough to RNA-l to receive a high degree of magnetization, implies that the whole dppz ligand is responsible for the interaction with the RNA internal loop, including a minor contribution of the bipyridine.

Preliminary MD (Molecular Dynamic) simulations were performed by Prof. Dr. Giampaolo Barone and Dr. Angelo Spinello (University of Palermo) with the aim of obtaining a more precise positioning of the metal complex in the internal loop. Preliminary MD simulations were performed on the X-ray crystal structure of complex 1 and the NMR solution structure of RNA-l (Figure 7.5). [11]

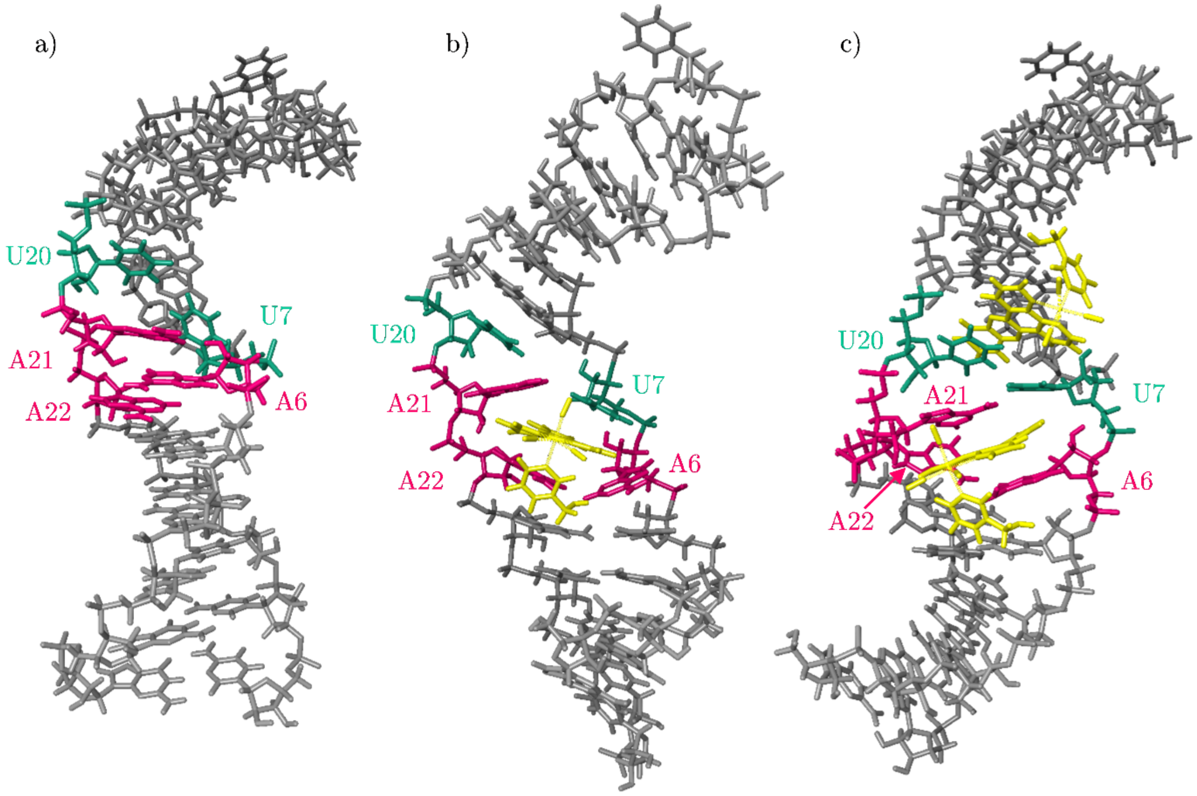

Figure 7.5 a) NMR solution structure of RNA-l (xp06_141); b) MD simulation in the presence of two molecules of complex 1 (cluster1_bis_long) and b) MD simulation in the presence of one molecule of complex 1 (Interc2_cluster1). A6, A21, A22 are highlighter in magenta, U7 and U10 in green and complex 1 in yellow.

Two MD structures were simulated, one in the presence of one molecule of complex 1 and the other one in the presence of two molecules of complex 1, as suggested from the stoichiometry value obtained via ITC (Section 3.2 and Section 3.3). From these preliminary studies, it seems that one complex binds at the three stacked adenine by inserting its dppz moiety between A6 and A21 and the second one binds between the U7U20 mismatch and the G8C19 base pair.

[^{1}H,^{1}H]-NOESY experiments on RNA-l and complex 1 were used to support the MD simulations. In accordance with the MD structures, no significant changes were observed for the proton resonances of the helical region and of the terminal loop. The NOE signals that are due to the stacking of the adenines in the internal loop disappeared upon addition of complex 1, confirming that the interaction is localised in this area and that the system is in fast exchange (Chapter 2). Unfortunately, this hampers any evaluation of the distances between the residues in this area and their comparison with the proposed MD structures. Finally, an interesting information was obtained by comparing the cross peak U20H5-C19H5 in the absence and in the presence of complex 1. Indeed, its intensity decreases upon binding of complex 1, suggesting an increase of the distance between the two residues, which is in agreement with the MD structure containing two molecules of complex 1.

Synthesis of a novel Re(I)dppz complex

To overcome the water solubility issues encountered in the study of the RNA and DNA binding properties of complex 1, we designed a novel Re(I)dppz complex (complex 12 in Figure 7.6). This contains a rhenium-dppz core, responsible for the emission and the interaction with the nucleic acids and the tricarbonyl moiety that was also kept unchanged. Hence, we acted on the pyridine ligand to modulate the water solubility by changing the original 3-hydroxymethyl group to a 3-aminomethyl one. The modification at the pyridine ligand and the increased overall charge of the complex could not only have a positive influence on the water solubility but could also strengthen the binding, and therefore help to overcome the issue of the fast dynamics.

The synthesis consists of 5 reaction steps. [15,143–146] Among them, steps 1-4 were already reported in the literature, whereas step 5 was based on similar

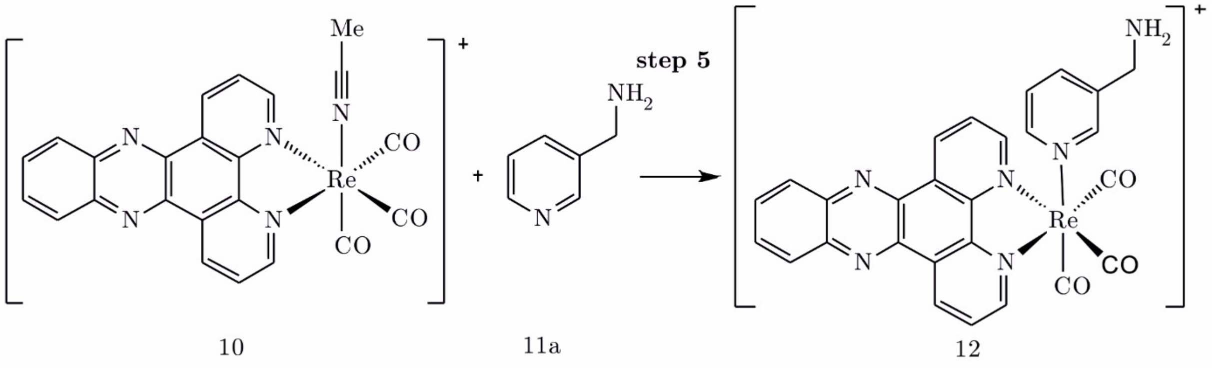

Figure 7.6 Reaction step of acetonitriletricarbonyldipyrido[3,2-*a*:2',3'-*c*] phenazinerhenium(I)-tetrafluoroborate (10) and 3-picolylamine (11a) for the synthesis of 3-picolylammoniumtricarbonyldipyrido[3,2-*a*:2',3'*c*] phenazinerhenium(I) (12).

procedures (reaction scheme in Figure 7.6). Therefore, an optimization of different parameters such as solvent, temperature, reaction time and ratio between the starting materials, was needed. Moreover, a critical issue of this last substitution reaction consists in controlling the reactivity of the 3-picolylamine. Indeed, this compound can react following three different reaction paths: (i) via the nitrogen of the pyridine, (ii) via the nitrogen of the primary amine or (iii) via both nitrogen atoms bridging two metal centres. [149] Hence, we protected the amino group of the pyridine ligand to obtain only the product formed by metal coordination of the nitrogen of the pyridine ring. This protection was achieved by the protonation of the 3-picolylamine forming the corresponding ammonium salt.

Complex 12 was characterized via NMR spectroscopy and MS analysis. Solubility tests in water showed that the newly synthesized complex does not show an increased water solubility, calling for the design of further complexes with water soluble pendants, such as for example histidine [152] or urea linked pyridine-PEG systems. [153]

Conclusion

In this thesis we investigated the non-covalent interaction of complex 1 and RNA-l. The latter one is part of domain 1 of the *Sc.*ai5γ group II intron, it is 27 nucleotides long and it contains several common secondary structural features in RNA. In particular, it includes in its structure an 11 nucleotides long asymmetric internal loop. This motif is especially interesting since internal loops are known to act as preferential interaction sites for small molecules. [4,14,50] Our results confirmed the ability of the internal loop to act as specific binding pocket, since a preferential binding of complex 1 to this site was observed. This finding was supported by additional experiments using RNA-h, that does not contain this loop, and complex 1, in which no selective interaction was found. Moreover, our data indicated that the dppz moiety is involved in the binding and that the interaction occurs with a stoichiometry of two metal complexes per RNA. Unfortunately, no quantitative data on the binding could be obtained.

However, still some critical points need to be overcome to obtain a good selective binding agent for RNA. One of them is represented by the low water solubility of complex 1. We tried to overcome this limitation by synthesizing a novel complex with a differently substituted axial ligand, but unfortunately the newly formed compound did not show improved solubility in aqueous media. Another critical point is related to the interaction of complex 1 with our RNA internal loop. Although the binding is selective, it is still less strong that the unspecific one observed with DNA. Hence, further efforts are needed to obtain metal complexes with suitable photophysical properties, which are water soluble, and bind selectively to RNA secondary structural elements with higher affinity than to DNA. These properties are the basis to successfully apply these complexes as RNA structure-selective binding probes for a diagnostic and therapeutic purpose.

8. Zusammenfassung

In den letzten Jahrzehnten ist die Anzahl an Studien über Wechselwirkungen zwischen Metallkomplexen und Nukleinsäuren stetig gestiegen. [1,2,7] Metallkomplexe können sowohl als diagnostische wie auch als therapeutische Mittel verwendet werden, um gezielt die wichtigsten biologische Moleküle wie Proteine, DNA und RNA zu binden. Die RNA ist in vielen wichtigen biologischen Prozessen direkt beteiligt und somit eine besonders interessante, durch ihre strukturelle Vielfalt gleichzeitig aber auch eine sehr anspruchsvolle Zielstruktur. [3–6] Im Gegensatz zu DNA, kann RNA viele verschiedene sekundäre Strukturen wie zum Beispiel Haarnadelstrukturen, asymetrische interne Loops ("bulges") oder Verzweigung annehmen, welche spezifische Bindestellen für kleine Moleküle darstellen können. [14,49] Interaktionen zwischen Metallkomplexen und RNA können sowohl kovalent als auch nicht-kovalent sein. [2,7,16,17]

In dieser Arbeit untersuchten wir die nicht-kovalente Interaktion zwischen Metallkomplexen und Metallionen mit RNA, um mit den gewonnenen Erkenntnissen strukturselektive Moleküle auf rationelle Art und Weise zu erzeugen. Wir benutzten ein 27 Nukleotid langes RNA Konstrukt (RNA-l in Abbildung 8.1a) als Modellsystem, dessen NMR Struktur in Lösung bereits in der Gruppe von Prof. Dr. Roland K.O. Sigel bestimmt wurde. [11] Dieses Konstrukt leitet sich von der ζ Region der Domäne 1 des Gruppe II Introns ai5γ

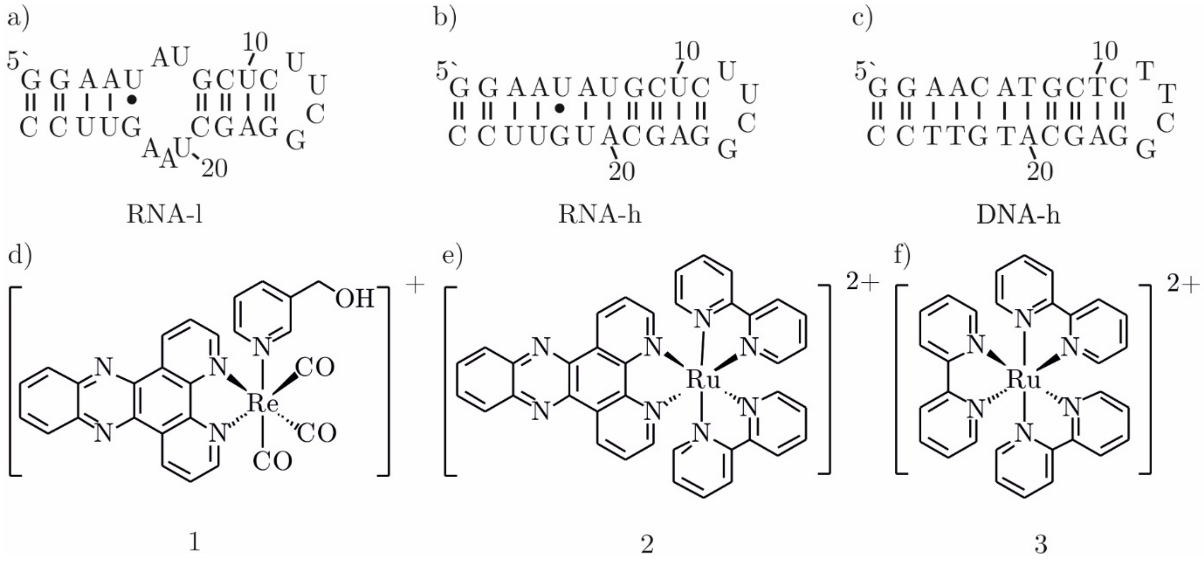

Abbildung 8.1 Sekundärstruktur von a) RNA-l, b) RNA-h und c) DNA-h und die chemische Strukturen von d) $[Re(CO)_3(dppz)(3\text{-}CH_2OH\text{-}py)]^+$ (1), e) $[Ru(bpy)_2(dppz)]^{2+}$ (2) und f) $[Ru(bpy)_3]^{2+}$ (3).

von *Saccharomyces cerevisiae* ab, welches Zusammen mit dem κ Element die κ-ζ Region bildet. Ist die κ-ζ Region korrekt gefaltet, ermöglicht sie die Interaktion mit Domäne 5 und führt zur katalytischen Aktivität des Introns. [8–10] Das RNA-l Konstrukt ist ein sehr geeignetes Modellsystem, da es ein GU Wobble-Paar, einen terminalen und einen internen Loop enthält, alles Sekundärstrukturen die typischerweise in RNA vorkommen. Der interne Loop ist ein sehr interessantes Strukturelement der RNA, das für sein Potential als selektive Bindgungsstelle für kleine Moleküle bekannt ist. [4,14,50]

Wir haben das Bindungsverhalten zwischen RNA-l und des Metallkomplexes $[Re(CO)_3(dppz)(3\text{-}CH_2OH\text{-}py)]^+$ (Komplex 1, Abbildung 8.1d) untersucht, dessen Eigenschaft als potentielles Mittel für das Bioimaging-Verfahren durch die Gruppe von Dr. Michael P. Coogan (Universität Lancaster, Grossbritanien) beschrieben wurde. [15] Frühere Studien über ähnliche Komplexe mit der generellen Formel $[Re(CO)_3(dppz)(X)]^+$ (wobei X eine grosse Vielzahl verschiedener Liganden sein kann) haben gezeigt, dass diese mit CT-DNA interagieren und dass sie sich in DNA- und RNA-reichen Regionen der Zelle ansammeln. Gerade Komplex 1 weist eine der höchsten Bindungskonstanten mit DNA auf, die wahrscheinlich durch die Hydroxymethylgruppe bedingt ist, welche Wasserstoffbrücken mit der DNA bilden kann. Diese interessante Tatsache, sowie die nur spärlich vorhandenen Informationen über RNA Wechselwirkungen mit Metallkomplexen waren der Ausgangspunkt für unsere Studie. Neben RNA-l haben wir noch zwei weitere Oligonukleotid Sequenzen benutzt, RNA-h (Abbildung 8.1b) und DNA-h (Abbildung 8.1c). RNA-h ist ein 26 Nukleotid langes RNA Konstrukt, sehr ähnlich wie RNA-l, aber ohne den internen Loop, um die Funktion des internen Loops in der Interaktion mit Komplex 1 besser zu erforschen. DNA-h ist die analoge DNA Sequenz zu RNA-h und wurde verwendet, um Unterschiede zwischen DNA und RNA in der Bindung von Komplex 1 zu ermitteln. Um den Einfluss der dppz Einheit in der Bindung zu RNA-l besser zu verstehen, haben wir ausserdem zwei weitere Komplexe, $[Ru(bpy)_2(dppz)]^{2+}$ (Komplex 2, Abbildung 8.1e), und $[Ru(bpy)_3]^{2+}$ (Komplex 3, Abbildung 8.1f), verwendet.

RNA Bindungsstellen für Metall-Ionen und Komplexe: eine NMR Studie

Metallionen sind für RNA ein integraler Bestandteil, da sie nicht nur im Faltungsprozess zu einer funktionsfähigen drei-dimensionalen Struktur beteiligt sind, sondern auch direkt in die Aktivität katalytischer RNA, sogennanter Ribozyme, involviert sein können. [60] Da RNA-Metallionenbindungsstellen generell auch potentielle Bindungsstellen für Metallkomplexe sein können, haben wir die Wechselwirkung von Mg(II), Cd(II) und Cobalt(III)hexammin mit RNA-l mittels NMR Spektrospopie untersucht. Die NMR Daten sind aus einer kürzlich erschienenen Publikation von Bartova *et al.* in der ich als Co-Author beteiligt war. Unsere Daten zeigen, dass hauptsächlich zwei Regionen der RNA durch die Metallionen beeinflusst werden. Zum einen das 5'-Ende, dessen Triphosphat mit Cd(II) Makrochelate bildet, und zum anderen der interne Loop. Die Zugabe der drei Metallionentypen führte zu kleinen Änderungen der chemischen Verschiebung von Resonanzen des internen Loops, was eine elektrostatische Interaktion an dieser Stelle vermuten lässt. Diese Resultate wurden durch zusätzliche Linienverbreiterungsexperimente mit Mn(II) belegt, da auch hier hauptsächlich die Resonanzen des 5'-Endes und des internen Loops den grössten Effekt zeigten.

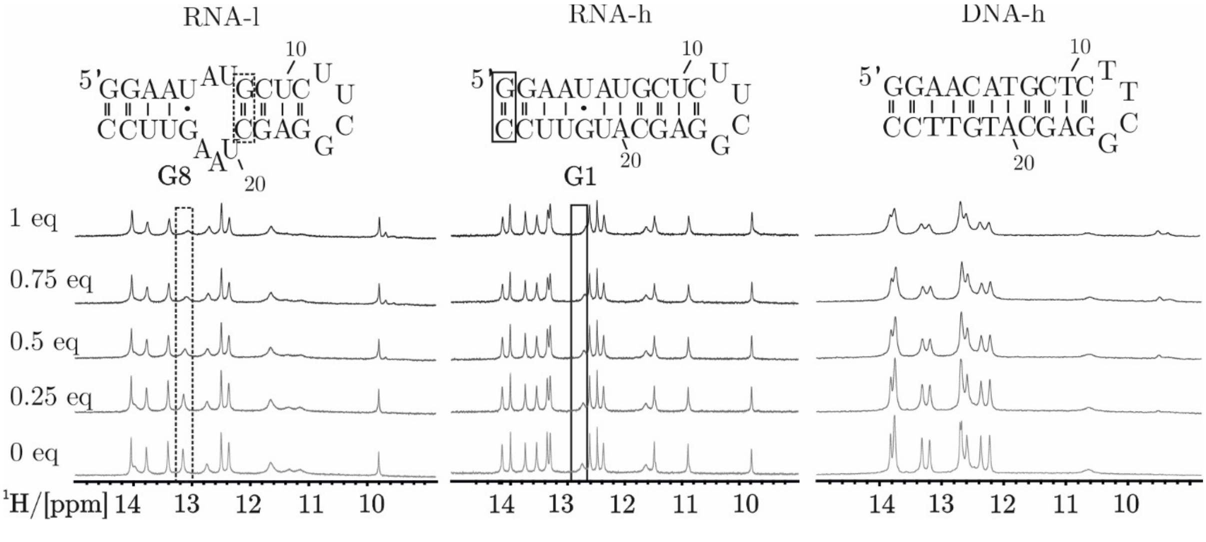

Abbildung 8.2 Überlagerung von ^{1}H Spektren (imino Region) von RNA-l, RNA-h und DNA-h aufgenommen bei steigenden Konzentrationen von Komplex 1 (0.2 mM, PBS mit 2% DMSO, pH 7, 293K, 700 MHz). Der Rahmen gibt an welches Basenpaar durch die Zugabe von Komplex 1 am meisten beeinflusst wurde.

Auf Grundlage dieser Daten wurde die Interaktion zwischen Komplex 1 und RNA-mittels 1D ^{1}H NMR Titrationen in Wasser untersucht. Die Iminoresonanzen, die in diesem Experiment aufgenommen werden, geben Auskunft über die Stabilität der Basenpaare und reagieren sehr empfindlich auf strukturelle Änderungen oder direkte Interaktionen mit dem Metallkomplex. Die schrittweise Zugabe von Komplex 1 zu RNA-l beeinflusste hauptsächlich eine spezifische Resonanz, G8H1, welches sich extrem verbreiterte (Abbildung 8.2, rechts). Diese Resonanz gehört zu einem Nukleotid des internen Loops und deutet auf eine Bindingsstelle nahe dieses Loops hin. Im Gegensatz dazu, zeigte RNA-h, das Konstrukt ohne internen Loop, nur einen kleinen Effekt am 5‘-Ende (Abbildung 8.2, mittig). Das erste Basenpaar einer Sequenz ist normalerweise nicht so stabil, wie der Rest und bietet sich wahrscheinlich somit als Bindungsstelle für den Metallkomplex an. Die 1D ^{1}H NMR NMR-Daten des DNA-h Konstruktes zeigen ein komplett anderes Verhalten (Abbildung 8.2, links). Es verbreitern sich alle Resonanzen, was wahrscheinlich durch eine unspezifische globale Bindung hervorgerufen wird.

Nachdem wir eine spezifische Interaktion des Komplex 1 am internen Loop der RNA-l gefunden hatten, wollten wir die Rolle des dppz-Restes in dieser Bindung genauer untersuchen. Der dppz-Rest ist dafür bekannt als interkalierende Einheit zu agieren. Wir haben dazu zusätzlich ^{1}H NMR Titrationen in D_2O mit Komplex 1, Komplex 2 und Komplex 3 (Abbildung 8.1e und Abbildung 8.1f) durchgeführt. In Anwesenheit von Komplex 1 und Komplex 2, beide besitzen den dppz-Rest, haben wir einen starken Einfluss auf die H2 Protonen der drei Adenine A6, A21 und A22 gefunden. Dieses Resultat bestätigt die vorherigen Daten und zeigt, dass die dppz-Einheit direkt an der Bindung beteiligt ist. Zusätzlich unterstützt wird dieses Resultat durch die Tatsache, dass für Komplex 3 keine Interaktion mit RNA-l gefunden wurde.

Weiterführende 2D NMR-Experimente wie [^{1}H,^{1}H]-NOESY, [^{1}H,^{1}H]-TOCSY und [^{1}H,^{15}N]-HSQC haben die Interaktion am internen Loop bestätigt. Allerdings lässt die schnelle Dynamik und das Verschwinden der Resonanzen in dieser Region, keine weitere Charakterisierung mittels NMR zu.

Optische Studien und ITC Experimente

Die Gruppe der $[Re(CO)_3(dppz)(X)]^+$ Metallkomplexe, zu der auch Komplex 1 gehört, hat ein charakteristisches UV-Profil, dass in Anwesenheit von DNA Hypochromie aufweist. Ausserdem zeigt diese Gruppe von Komplexen in wässriger Lösung nur eine schwache Emmission, die aber bei Zugabe von DNA stark zunimmt. [15] Die Auswertung photospektroskopischer Titrationen von Metallkomplexen mit Nukleinsäuren kann nicht nur eine qualitatives Bild über die Interaktion geben, sondern kann auch dafür benutzt werden um die Bindungskonstante quantitativ zu bestimmen. Wir haben aus diesem Grund verschiedene optische Methoden verwendet mit dem Ziel die Bindungskonstante zu quantifizieren.

Wir haben UV/Vis Titrationen von Komplex 1 mit RNA-l durchgeführt und die Änderung des Absorptionsprofils des Komplexes beobachtet. Dabei haben wir einen hypochromen Effekt der Absorptionsbande von Komplex 1 gefunden, was auf eine Beteiligung der aromatischen Liganden hinweist. Da jedoch die Absorptionsänderung im Vergleich zu DNA sehr gering ist, ist vermutlich die Bindungsstärke an RNA kleiner als die Bindungsstärke die für CT-DNA gefunden wurde. [15] Demzufolge haben wir versucht mit Hilfe anderer Methoden die Bindungskonstante zu bestimmen.

ITC ist eine Methode mit der gleichzeitig eine Menge verschiedener Daten, wie Stöchiometrie, Bindungskonstante, Enthalpie und Entropie durch Messung der freiwerdender Wärme, während der Interaktion zweier Moleküle bestimmt werden kann. ITC Messungen wurden sowohl von Komplex 1 und Komplex 2 mit RNA-l von Dr. Miquel Barceló-Oliver (University of Balearic Islands, Spanien) durchgeführt. Beide Komplexe haben im NMR eine sehr ähnliche Verhalten mit RNA-l gezeigt. In beiden Fällen konnte zwar eine Wechselwirkung detektiert werden, die freiwerdene Wärme war aber sehr gering und die Daten mit grossen Fehlern behaftet, so dass keine quantitative Auswertung vorgenommen werden konnte. Es konnte aber mit einer gewisssen Sicherheit ein stöchiometrischer Wert von 2 Molekülen Komplex 1 pro internem Loop der RNA bestimmt werden.

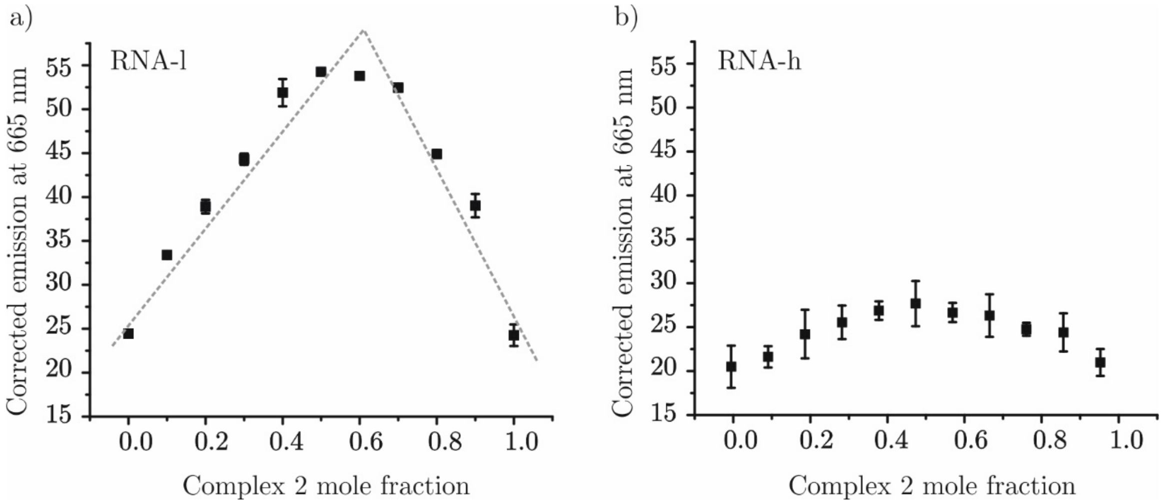

Abbildung 8.3 Jobscher Plot von Komplex 2 mit a) RNA-l und b) RNA-h (PBS, pH 7.2). Die totale molare Konzentration der Lösungen an jedem Punkt ist 3 µM. Das Maximum in Panel a) ist durch die gestrichelte Linie verdeutlicht.

Um die Stöchiometrie zu validieren wurde zusätzlich die Jobsche Methode eingesetzt (Abbildung 8.3). In diesen Experimenten wird die Emission von Komplex 2 in Abhängigkeit verschiedener RNA/Komplex Verhältnisse gemessen, wobei die Gesamtkonzentration beider Reaktionspartner konstant gehalten wird. Die Experimente konnten nur mit Komplex 2 und RNA-l bzw. RNA-h durchgeführt werden, da die Lumineszenz des Re(I)dppz-Komplexes selbst mit DNA kaum messbar war, ganz im Gegensatz zu den analogen Ru(II))dppz-Komplexen.[50] Für RNA-l und Komplex 2 haben wir ein klares Maximum beobachtet was das 2:1 Komplex - RNA Verhältnis der ITC Daten bestätigt. Im Gegensatz dazu wurde für RNA-h und Komplex 2 kein klares Maximum detektiert. Ausserdem war die Intensität der Emission so gering und mit grossem Fehler behaftet, dass keine genauere Auswertung möglich war.

Da wir die Bindungskonstante nicht quantifizieren konnten, haben wir Emission-Konkurrenz-Experimente eingesetzt, um die Interaktionsstärke zwischen Komplex 2 und unseren DNA und RNA Konstrukten zumindest qualitativ abschätzen zu können. Dazu wurden zu eine 1:1 Mischung von DNA-h und Komplex 2 schrittweise RNA-l oder RNA-h gegeben und anschliessend das Emissionsmaximum gegen die RNA Konzentration aufgetragen. In beiden Fällen wurde eine Abnahme der Emission beobachtet, was zeigt dass sowohl RNA-l wie auch RNA-h mit der DNA um Komplex 2 konkurrieren können. Die Abnahme der Emission war für RNA-l etwas grösser als wie bei RNA-h.

Generell kann die Eigenschaft von Komplex 2 in Anwesenheit von Nukleinsäuren stark zu emittieren benutzt werden, um die Bindungseigenschaften qualitativ und quantitativ zu bestimmen. Es ist aber für sehr kurze Nukleinsäurekonstrukte, wie in unserem Fall, nur eine qualitative Auswertung möglich, da das generell verwendete Fitting-Modell für unendlich lange Systeme ausgelegt ist. [100] Emissions-Titrationen wurden für Komplex 2 mit all unseren RNA und DNA Konstrukten durchgeführt. Nach Zugabe aller Konstrukte ist die Emission angestiegen, was eine Wechselwirkung bestätigt. Für RNA-l war der Anstieg etwas stärker als für RNA-h, was darauf hindeutet, dass die dppz-Einheit in RNA-h besser abgeschirmt wird. Der Emissionsanstieg war im Fall der DNA-h viel grösser als für RNA-l und RNA-h und der Kurvenverlauf war leicht anders. Am Anfang kam es zu einem starken Anstieg gefolgt von einem schwachen aber stetigen Abfall. Dieses Verhalten deutet auf verschiedene Bindungsgeometrien der zwei Enantiomere hin, die sich konzentrationsabhängig verhalten. [117] Da im Fall von RNA-l nicht so ein Verlauf gefunden wurde, zeigt dass beide Enantiomere wahrscheinlich sehr ähnlich mit dem internen Loop interagieren.

Die Emission von Ethidiumbromid (EB) wurde ebenfalls mit den drei RNA und DNA Konstrukten gemessen. Dieses kleine Molekül ist dafür bekannt sehr gut in doppelsträngige RNA und DNA zu interkalieren und dabei einen riesigen Anstieg der Emission zu erfahren. Alle Experimente mit den drei Konstrukten hatten einen Anstieg der Emissionsbande von EB zur Folge. Die Emission war für RNA-l am grössten, gefolgt von DNA-h und RNA-h, und zeigt das EB im internen Loop besser abgeschirmt wird als in helikalen Bereichen.

EB wurde auch in EB-Austausch Experimenten benutzt, welche die Möglichkeit bieten zu analysieren, wieviel EB durch Komplex 2 und Komplex 1 ersetzt wird. Die Emission von einer 1:1 Mischung von EB mit RNA oder DNA wurde unter Zugabe von Komplex 1 oder Komplex 2 evaluiert. Die beobachtete Abnahme suggeriert, dass die Bindung zu einem gewissen Grad interkalativ ist. Die Emissionsintensität ist linear abnehmend und ermöglichte das Berechnen der Stern-Volmer (K_{SV}) Konstanten. Generell ist der K_{SV} Wert für Komplex 2 mit allen unserer DNA und RNA Konstrukten höher wie der für Komplex 1, was auf eine stärkere Interaktion schliessen lässt. Dies kann an der höheren Ladung des Komplexes, oder an den verschiedenen axialen Liganden liegen.

STD NMR Experimente und MD Simulationen

Um weiterführende Information über die genaue Position des Komplexes im internen Loop zu erhalten, haben wir STD (Saturation Transfer Difference) NMR-Experimente durchgeführt. Diese Methode basiert auf dem Transfer von Magnetisierung von einem Rezeptor (RNA-l) zu einem Liganden (Metallkomplex), wobei der Ligand im grossen Überschuss vorliegt. Die RNA-l wurde bei einer Resonanz von 3933 Hz (5.62 ppm) angeregt, damit die Resonanzen des Komplexes nicht auch mit angeregt wurden. In diesen STD NMR-Experimenten werden nur Signale des Liganden beobachtet, die räumlich gesehen nah genug an der RNA-l sind, um Magnetisierung durch Spin-Diffusion zu erhalten. Aufgrund der geringen Wasserlöslichkeit von Komplex1, konnten nur Experimente mit Komplex 2 und RNA-l erfolgreich durchgführt werden. Das 1D ^{1}H NMR Spektrum der Probe, die für die STD NMR-Experimente benutzt wurde, zeigt dass es zu einer Interaktion zwischen RNA-l und Komplex 2 kommt, da alle Protonen des Komplexes sich verbreitern und einige Protonresonanzen der dppz-Einheit komplett verschwinden (alle Resonanzen die zur dppz-Einheit gehören sind in Abbildung 7.5 mit einem Stern markiert). Anschliessend haben wir den Sättigungsanteil der Resonanzen im STD NMR-Spektrum bestimmt (Abbildung 8.4). Die gesättigste Resonanz gehört zu einem Proton des Bipyridinringes (Peak 8). Alle andere Resonanzen die eine Sättigung zeigen, gehören zur dppz-Einheit (Peak 6, 4 und 2, geordnet nach dem Sättigungsanteil). Die Tatsache, dass von den fünf dppz-Resonanzen zwei nicht sichtbar sind und die anderen drei eine Sättigung zeigen, impliziert dass die gesamte dppz-Einheit in der Wechselwirkung mit dem internen Loop beteiligt ist und zu einem geringen Teil auch der Bipyridinring.

MD-Simulationen (Molecular dynamic simulations) wurden von Prof. Dr. Giampaolo Barone and Dr. Angelo Spinello (University of Palermo) durchgeführt mit dem Ziel eine genauere Angabe über die Positionierung des

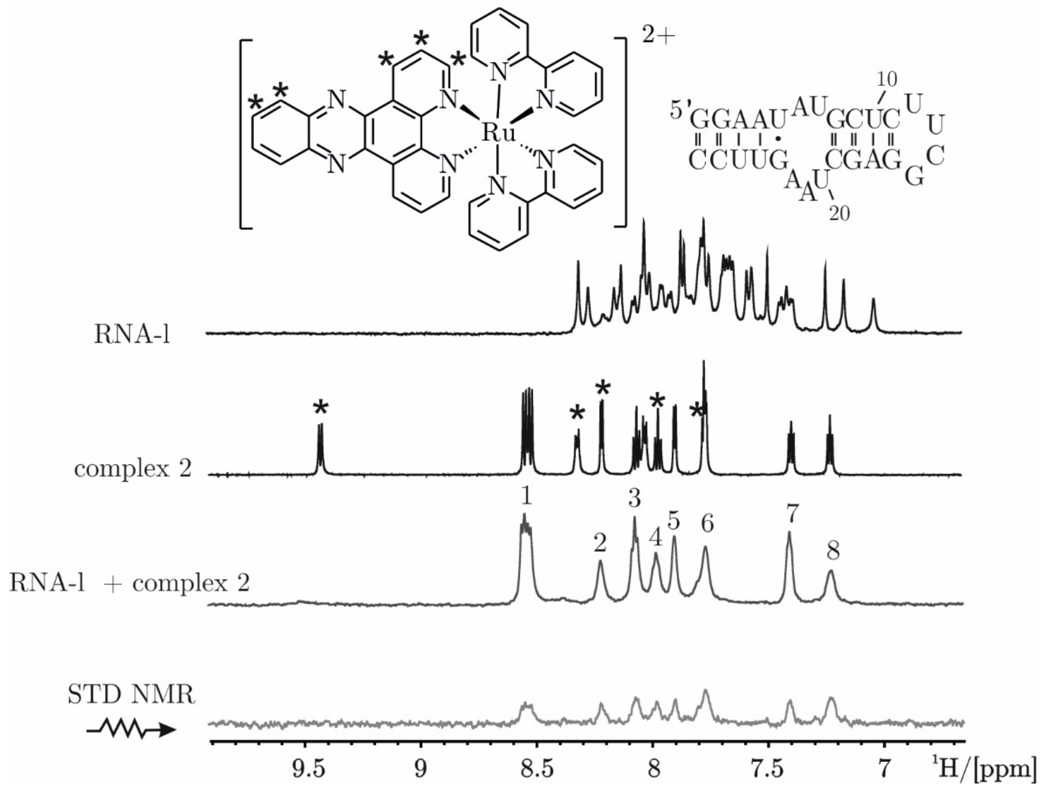

Abbildung 8.4 ^{1}H NMR Spektrum von RNA-l, Komplex 2 und das Referenzspektrum von 25 μM RNA-l und 350 μM Komplex 1 (300 K, 700 MHz). Die Resonanzen der dppz-Protonen sind mit Sternen markiert, während die Nummern die sichtbaren Resonanzen der Komplex 2/RNA-l Mischung kennzeichnen.

Komplexes zu erhalten. Erste MD-Simulationen wurden ausgehend von der Kristallstruktur des Komplex 1 und der NMR Struktur von RNA-l (Abbildung 8.5) durchgeführt. [11] Zwei verschiedene MD-Strukturen wurden simuliert, eine in Gegenwart von nur einem Komplexmolekül und eine in Gegenwart von zwei Molekülen. wobei generell laut der ITC Daten von einer Stöchiometrie von zwei Metallkomplexen pro RNA ausgegangen werden kann. (Abschnitt 3.2 und Abschnitt 3.3).

Die vorläufigen MD-Strukturen suggerieren, dass ein Komplex bei den drei gestapelten Adeninen bindet in dem es seine dppz-Einheit zwischen A6 und A21 schiebt, während sich der zweite Komplex zwischen die U7U20-Mispaarung und dem G8C19 Basenpaar einlagert.

Um die Daten der MD-Simulationen zu stützen, wurden zusätzlich [^{1}H,^{1}H]-NOESY Spektren von RNA-l und Komplex 1 aufgenommen. In

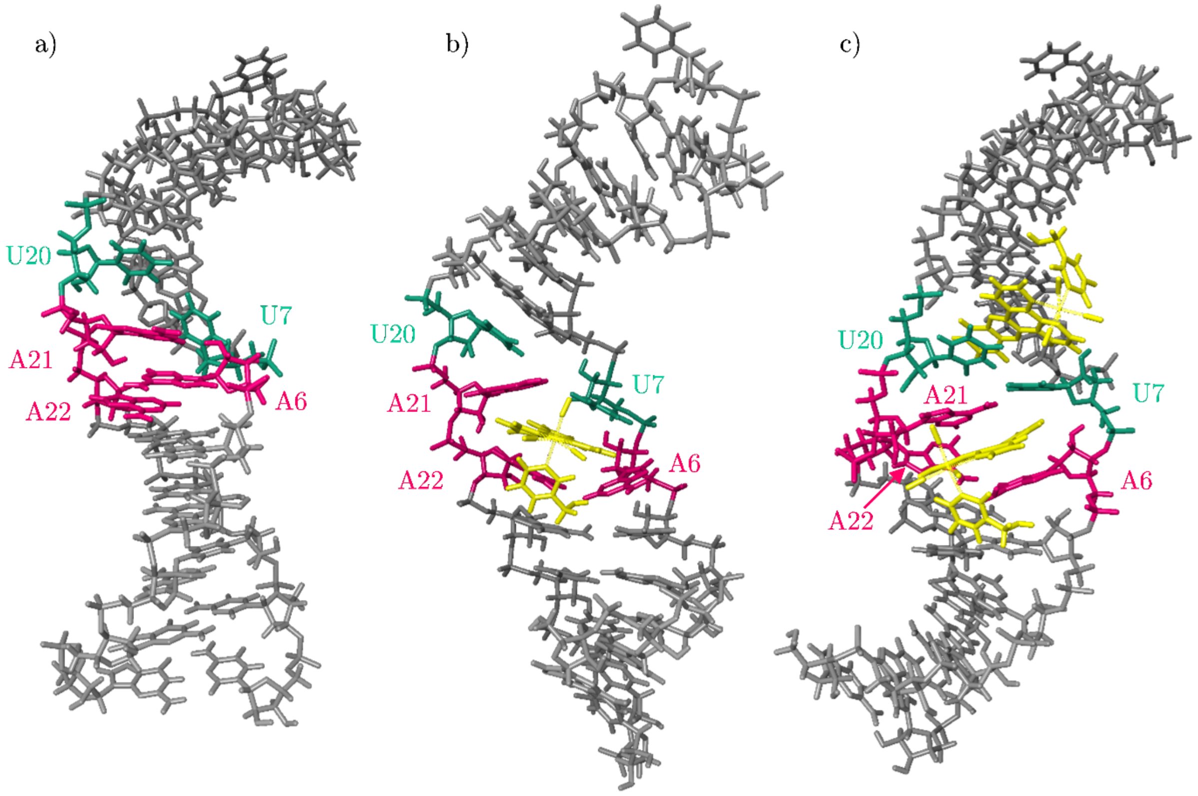

Abbildung 8.5 a) NMR Struktur von RNA-l; b) MD Simulation mit zwei Molekülen Komplex 1; c) MD Simulation mit einem Molekül Komplex 1. Die Farben zeigen den internen Loop, in Magenta A6, A21 und A22, während U7 und U20 in grün dargestellt sind. Komplex 1 ist gelb eingefärbt.

Übereinstimmung mit den MD-Simulationen wurde keine signifikante Änderung der Protonenresonanzen gefunden, die zur Helix-Region oder des terminalen Loops gehören. Hingegen sind NOE Signale zwischen den drei gestapelten Adeninen im internen Loop nach Zugabe von Komplex 1 verschwunden. Das beweist, dass die Interaktion in dieser Region stattfindet und das System sich im schnellen Austausch befindet. (Kapitel 2). Unglücklicherweise, ist es so nicht möglich die Distanzen zwischen den einzelnen Nukleotiden in dieser Region mit den Distanzen der MD Strukturen zu vergleichen. Zu guter Letzt haben wir aber noch ein interessantes Verhalten der U20H5-C19H5 Korrelation gefunden. Seine Intensität nimmt nämlich durch Zugabe von Komplex 1 ab, was darauf schliessen lässt, dass die Distanz zwischen den Nukleotiden zunimmt. Dieser Verhalten ist in Überseinstimmung mit MD-Simulationen der RNA-l Struktur mit zwei Molekülen des Komplexes 1.

Synthese eines neuen Re(I)dppz Komplexes

Um das Problem der schlechten Wasserlöslichkeit von Komplex 1 zu lösen, wurde ein neuer Re(I)dppz Komplex entworfen. Dieser Komplex enthält die dppz-Einheit, welche für die Emissionseigenschaften und die Wechselwirkung mit Nukleinsäuren verantwortlich ist, und auch die drei Carbonylgruppen bleiben unverändert. Wir haben nur den axialen Pyridinliganden modifiziert, um eine höhere Wasserlöslichkeit des Komplexes zu erreichen. Dazu wurde die 3-Hydroxymethylgruppe zu 3-Aminomethyl abgeändert (Komplex 12 in Abbildung 8.6, rechts). Die Veränderung am Pyridinliganden sowie die Erhöhung der Gesamtladung könnte nicht nur einen positiven Einfluss auf die Wasserlöslichkeit, sondern auch auf die Bindungseigenschaften haben und so eventuell das Problem der zu schnellen Dynamik lösen. Die Synthese besteht aus 5 Schritten. [15,143–146] Schritt 1-4 wurden wie in der Literatur beschrieben durchgeführt, aber bei Schritt 5 mussten verschiedene Parameter wie Temperatur, Reaktionszeit und Lösungsmittel, sowie das Verhältnis zwischen Ausgangsmaterialien optimiert werden. Ein kritischer Schritt in der letzten Substitutionsreaktion war ausserdem die Reaktivität von 3-Picolyamin zu kontrollieren. Diese Verbindung kann nämlich auf drei verschiedene Arten reagieren, (i) über den Stickstoff des Pyridins, (ii) über den Stickstoff des primären Amins oder (iii) über beide Stickstoffe und dabei zwei Metalle verbrücken. [149] Wir haben die Aminogruppe des Pyridinliganden geschützt, um sicher zu stellen, dass nur das Stickstoffatom des Pyridinringes an das Metall koordiniert. Die Gruppe konnte durch Protonierung zum Ammoniumsalz

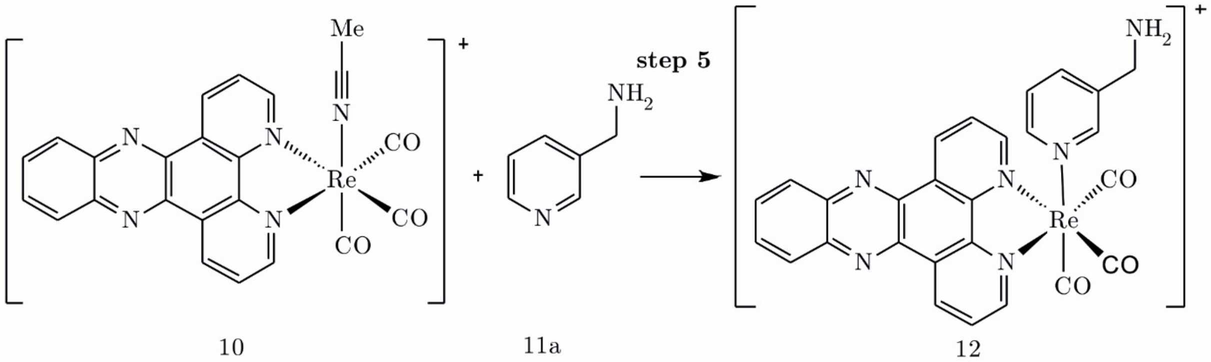

Abbildung 8.6 Reaktionsschritte von $[Re(CO)_3(dppz)(MeCN)][BF_4]$ (10) und 3-Picolylamin (11a) für die Synthese von $[Re(CO)_3(dppz)(3\text{-}CH_2NH_2\text{-}py)]^+$ (12).

erfolgreich geschützt werden. Komplex 12 wurde nach der Synthese mittels NMR und MS Analyse charakterisiert. Löslichkeitsversuche zeigten aber, dass der neue Komplex keine verbesserte Wasserlöslichkeit aufweist, was das Design weiterer Komplexe notwendig macht, wie zum Beispiel Histidin [152] oder Harnstoffverlinkte Pyridin-PEG Systeme. [153]

Schlussfolgerung

In dieser Arbeit haben wir die nicht-kovalente Interaktion von Komplex 1 und RNA-l untersucht. Die RNA ist Teil der Domäne 1 des Gruppe II Introns von *Sc.*ai5γ, ist 27 Nukleotid lang und enthält verschiedene Strukturelemente typisch für RNA. Gerade der 11 nt lange asymetrischen internen Loop ist ein besonders interessantes Motiv, da es bekannt dafür ist, besonders für kleine Moleküle ein präferierte Bindungsstelle zu sein. [4,14,50] In dieser Arbeit konnten wir diesen Befund bestätigen, da der interne Loop auch für Komplex 1 eine spezifische Bindungsstelle darstellte. Unsere Ergebnisse konnten wir durch zusätzliche Untersuchungen mit dem Nukleinsäurekonstrukt RNA-h, welches keinen internen Loop enthält, bestätigen, da wir keine selektive Wechselwirkung mit Komplex 1 gefunden haben. Weiterhin haben unsere Daten gezeigt, dass die dppz-Einheit in der Wechselwirkung involviert ist und dass die Interaktion mit einer Stöchiometrie von zwei Metallkomplexen pro RNA stattfindet. Leider war es uns nicht möglich quantitative Daten über die Bindungsstärke zu erhalten.

Um tatsäclich Metallkomplexe, die selektive an RNA binden zu erhalten, müssen noch einige Hindernisse überwunden werden. Wie bei Komplex 1 gesehen, ist ein Problem die Wasserlöslichkeit. Dieses Punkt haben wir versucht zu lösen, indem wir einen neuen Metallkomplex mit einem leicht variierten axialen Liganden synthetisiert haben. Leider zeigte dieser Komplex aber keine erhöhte Wasserlöslichkeit. Ein weiterer kritischer Punkt muss bezüglich der Wechselwirkung von Komplex 1 mit dem internen RNA Loop gemacht werden. Obwohl die Bindung selektiv ist, ist die Bindungsstärke geringer als die unspezifische Bindung zu DNA. Um Komplexe mit guten photophysikalischen Eigenschaften, welche gleichzeitig auch wasserlöslich sind und selektiv und stärker an RNA Sekundärstrukturelemente als an DNA binden, zu bekommen, ist noch viel Arbeit notwendig. Nur wenn all diese Eigenschaften in einem

Molekül vereint sind, ist eine Verwendung als diagnostisches und therapeutisches Mittel dieser Komplexe realistisch.

Appendices

Appendix 1 H1' sugar and aromatic proton chemical shifts of RNA-l (PBS, pD 6.8, 303 K, 700 MHz).

RNA-l	**δ [ppm] H1'**	**δ [ppm] H6/H8**	**δ [ppm] H2/H5**	**RNA-l**	**δ [ppm] H1'**	**δ [ppm] H6/H8**	**δ [ppm] H2/H5**
G1	5.83	8.14	-	**G15**	5.96	7.85	-
G2	5.90	7.56	-	**G16**	4.44	8.3	-
A3	5.94	7.74	7.24	**A17**	5.97	7.47	7.49
A4	5.86	4.56	7.84	**G18**	5.64	7.15	-
U5	5.386	7.426	5.24	**C19**	5.52	7.38	5.15
A6	5.891	8.115	7.42	**U20**	5.56	7.66	5.53
U7	5.597	7.8	5.62	**A21**	5.72	8.02	7.00
G8	5.415	7.64	-	**A22**	5.96	8.25	8.00
C9	5.52	7.64	5.30	**G23**	5.70	7.96	-
U10	5.58	7.94	5.43	**U24**	5.53	7.76	5.35
C11	5.55	7.76	5.64	**U25**	5.67	8.05	5.59
U12	5.53	7.78	5.74	**C26**	5.57	7.90	5.68
U13	6.10	8.02	5.85	**C27**	5.74	7.66	5.48
C14	5.95	7.67	6.14				

Appendix 2 ^{1}H imino proton chemical shifts of RNA-l, RNA-h and DNA-h (0.1-0.2 mM, PBS, pH 7-7.2, 278-293 K, 700 MHz) Imino resonances were assigned using [^{1}H-^{1}H]-NOESY experiments recorded in water and confirmed by the assignment of [^{1}H-^{1}H]-NOESY spectra recorded in PBS/D$_2$O. Assignments of resonances marked with * were confirmed using experiments in 60 mM KCl, and literature data. [5]

RNA-l	**δ [ppm] NH1/NH3**	**RNA-h**	**δ [ppm] NH1/NH3**	**DNA-h**	**δ [ppm] NH1/NH3**
G1	12.79	**G1**	12.78	**G1**	12.60
G2	12.42	**G2**	12.43	**G2**	12.54
A3	-	**A3**	-	**A3**	-
A4	-	**A4**	-	**A4**	-
U5	11.50*	**U5**	11.55	**C5**	-
A6	-	**A6**	-	**A6**	-
U7	n.a.	**U7**	13.38	**T7**	13.25
G8	13.27	**G8**	12.66	**G8**	12.35
C9	-	**C9**	-	**C9**	-
U10	14.12	**U10**	14.08	**T10**	13.69
C11	-	**C11**	-	**C11**	-
U12	11.76*	**U12**	11.74	**T12**	n.a.
U13	n.a.	**U13**	n.a.	**T13**	n.a.
C14	-	**C14**	-	**C14**	-
G15	9.84	**G15**	9.81	**G15**	n.a.
G16	12.54	**G16**	12.52	**G16**	12.61
A17	-	**A17**	-	**A17**	-
G18	13.39	**G18**	13.34	**G18**	12.53
C19	-	**C19**	-	**C19**	-
U20	-	**A20**	-	**A20**	-
A21	-	**A21**	-	**A21**	-
A22	-	**G22**	10.94	**G22**	12.11
G23	11.23*	**U23**	14.19	**T23**	13.71
U24	14.13	**U24**	13.81	**T24**	13.72
U25	13.86	**C25**	-	**C25**	-
C26	-	**C26**	-	**C26**	-
C27	-				

Appendix 3 ^{1}H chemical shift assignment of RNA-h (0.14 mM, PBS, pH 6.8, 298 K, 700 MHz).

RNA-h	**δ [ppm] H1'**	**δ [ppm] H2'**	**δ [ppm] H6/H8**	**δ [ppm] H2/H5**	**RNA-h**	**δ [ppm] H1'**	**δ [ppm] H2'**	**δ [ppm] H6/H8**	**δ [ppm] H2/H5**
G1	5.827	4.945	8.157	-	**C14**	5.941	4.093	7.677	6.131
G2	5.901	4.686	7.555	-	**G15**	5.969	4.849	7.862	-
A3	5.956	4.670	7.767	7.270	**G16**	4.437	-	8.304	-
A4	5.848	4.627	7.605	7.803	**A17**	5.971	4.706	7.762	-
U5	5.239	4.175	7.523	5.348	**G18**	5.632	4.441	7.176	-
A6	5.979	4.497	8.358	7.284	**C19**	5.983	4.463	7.606	5.147
U7	5.797	4.643	7.671	5.095	**A20**	5.476	4.317	8.057	7.360
G8	5.562	4.532	7.674	-	**U21**	5.806	4.480	7.701	5.225
C9	5.478	4.367	7.598	5.221	**G22**	5.492	4.485	7.730	-
U10	5.553	4.561	7.912	5.397	**U23**	5.464	4.353	7.726	5.188
C11	5.546	4.314	7.771	5.633	**U24**	5.647	4.477	8.025	5.559
U12	5.53	3.735	7.773	5.735	**C25**	5.576	4.207	7.901	5.648
U13	6.108	4.651	8.025	5.865	**C26**	5.719	3.981	7.659	5.478

Appendix 4 ^{1}H and ^{15}N chemical shift assignment of the purines of ^{15}N labelled RNA-l (0.18 mM, PBS, pD 6.8, 303 K, 600 MHz).

RNA-l	**H8 δ [ppm]**	**N7 δ [ppm]**	**H2 δ [ppm]**	**N1 δ [ppm]**	**N3 δ [ppm]**
G1	8.15	231.96	-	-	-
G2	7.56	233.73	-	-	-
A3	7.74	230.21	7.25	221.32	212.87
A4	7.58	231.42	7.85	222.56	213.81
A6	8.12	232.85	7.40	223.54	216.21
G8	7.67	233.74	-	-	-
G15	7.86	231.93	-	-	-
G16	8.29	233.55	-	-	-
A17	7.75	229.29	7.49	221.77	212.65
G18	7.15	234.46	-	-	-
A21	8.02	232.70	7.07	225.45	216.26
A22	8.23	232.52	7.98	223.71	216.74
G23	7.97	234.77	-	-	-

Appendix 5 ^{2}J-[^{1}H,^{15}N]-HSQC on ^{15}N labelled sample of RNA-l titrated with increasing amounts of Mg(II) (0.9 mM, 60 mM KCl, pD 6.8, 300 K, 700 MHz). Squares indicate line broadening and coloured arrows indicate a significant induced shift upon addition of Mg(II). [9]

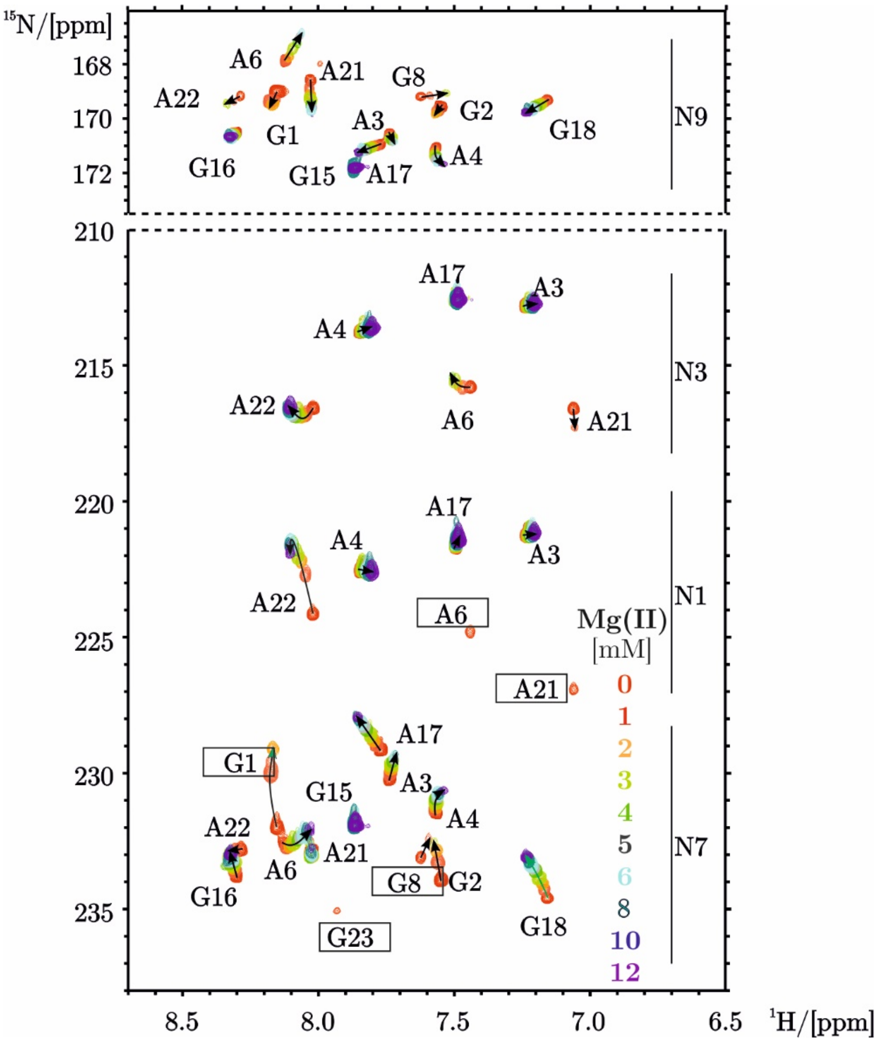

Appendix 6 ^{2}J-[^{1}H,^{15}N]-HSQC on ^{15}N labelled sample of RNA-l titrated with increasing amounts of cobalt(III)hexammine (0.55 mM, 60 mM KCl, pD 6.8, 300 K, 700 MHz). Squares indicate line broadening and arrows indicate induced shift upon addition of cobalt(III)hexammine. [9]

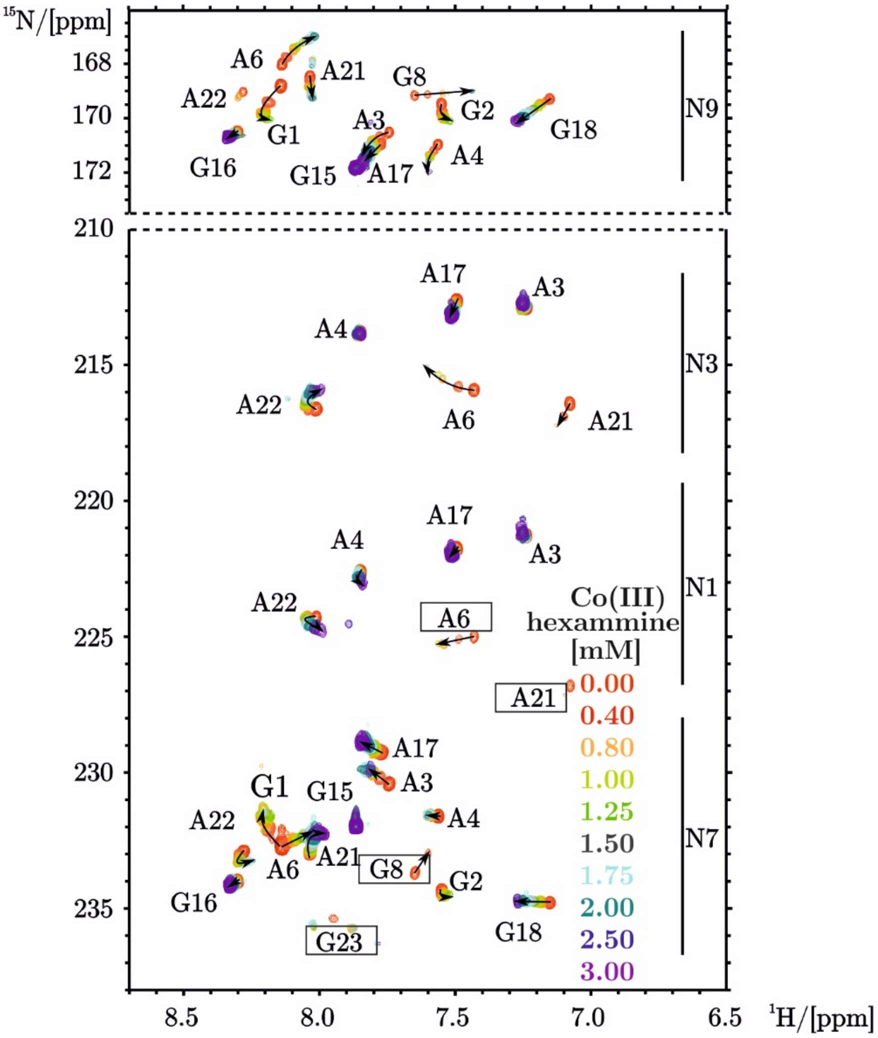

Appendix 7 Stackplots of ^{31}P NMR spectra in the region between -1 and 2 ppm. a) RNA-l titrated with increasing amounts of Mg(II) (0.49 mM, 60 mM KCl, pD 7.0, 300 K, 500 MHz); b) RNA-l titrated with increasing amounts of cobalt(III)hexammine (0.42 mM, 60 mM KCl, pD 7.0, 300 K, 500 MHz); c) RNA-l titrated with increasing amounts of Cd(II) (0.45 mM, 60 mM KClO4, pD 6.9, 300 K, 500 MHz).

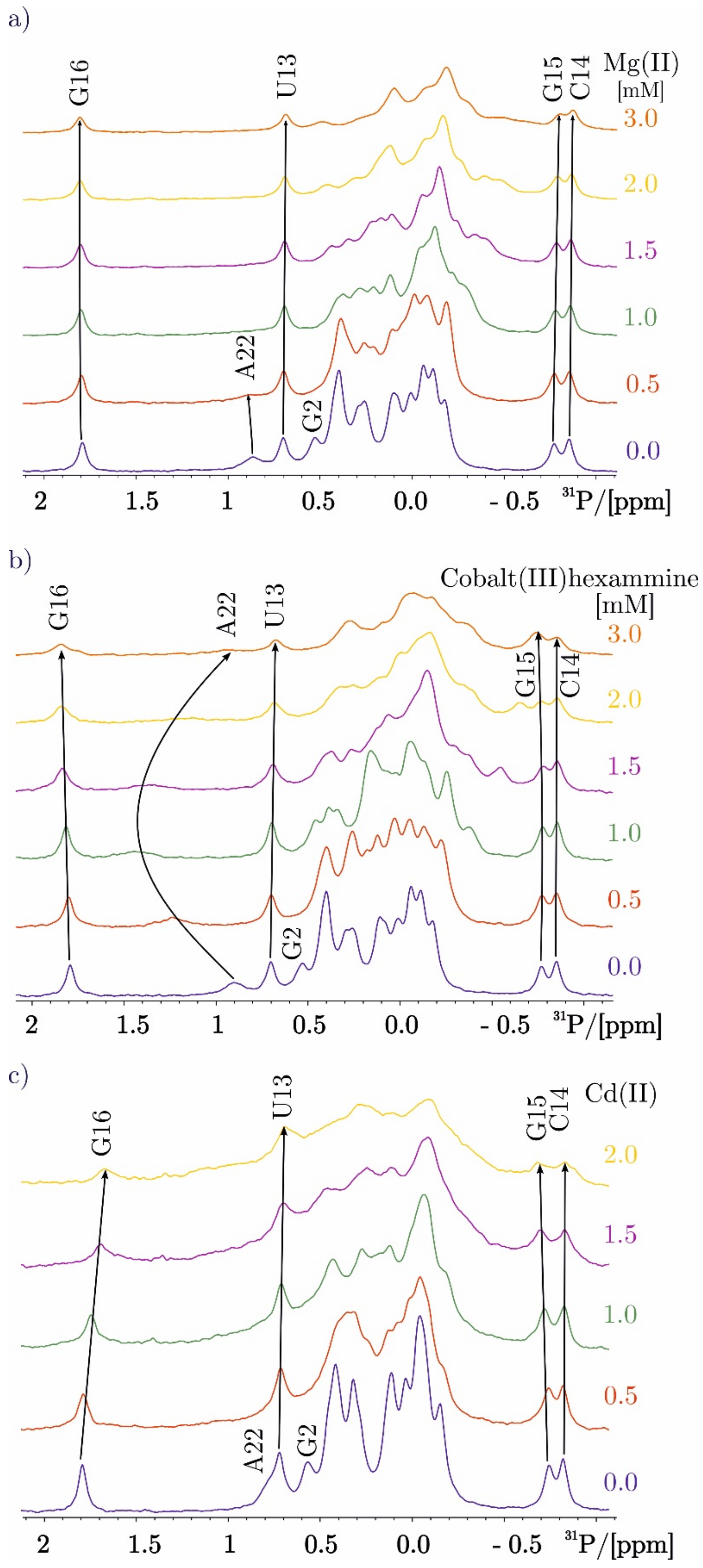

Appendix 8 ^{31}P NMR of RNA-l, dephosphorylated RNA-l and dephosphorylated RNA-h (0.10-0.14 mM, PBS, pD 6.9, 303 K, 500 MHz).

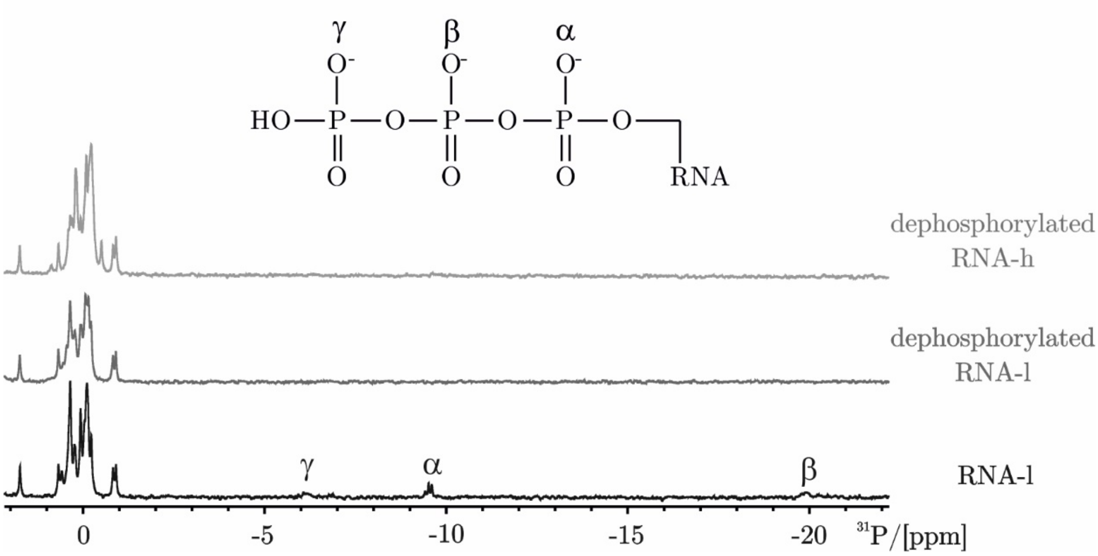

Appendix 9 ^{1}H spectra (aromatic proton region) of RNA-l in the presence of 0.25 equivalents of complex **1** (0.09 mM, PBS, pH 6.8, 293 K, 700 MHz).

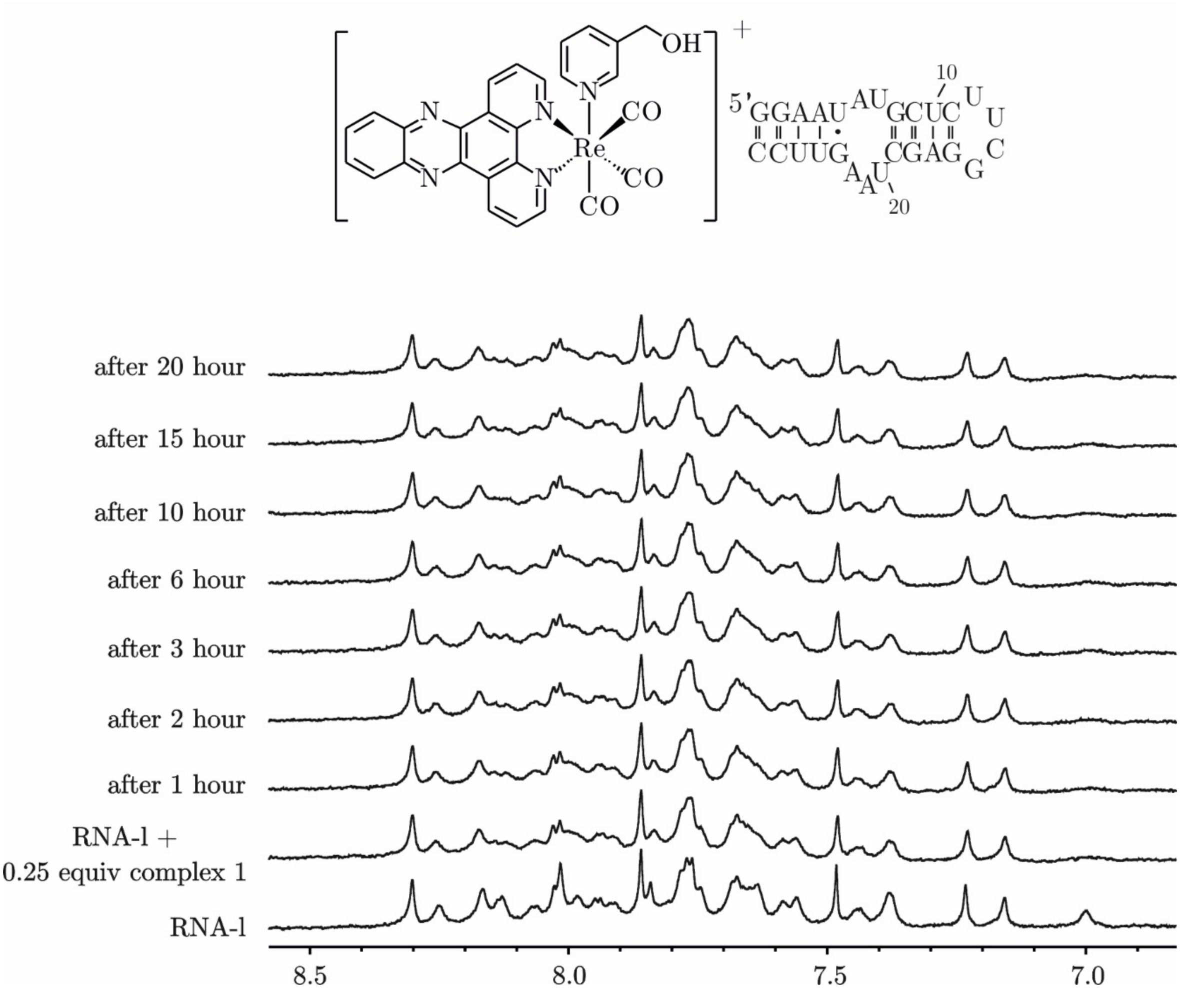

Appendix 10 ^{1}H spectra (aromatic proton region) of RNA-1 in the presence of 0.25 equivalents of complex 2 (0.09 mM, PBS, pH 6.8, 293 K, 700 MHz).

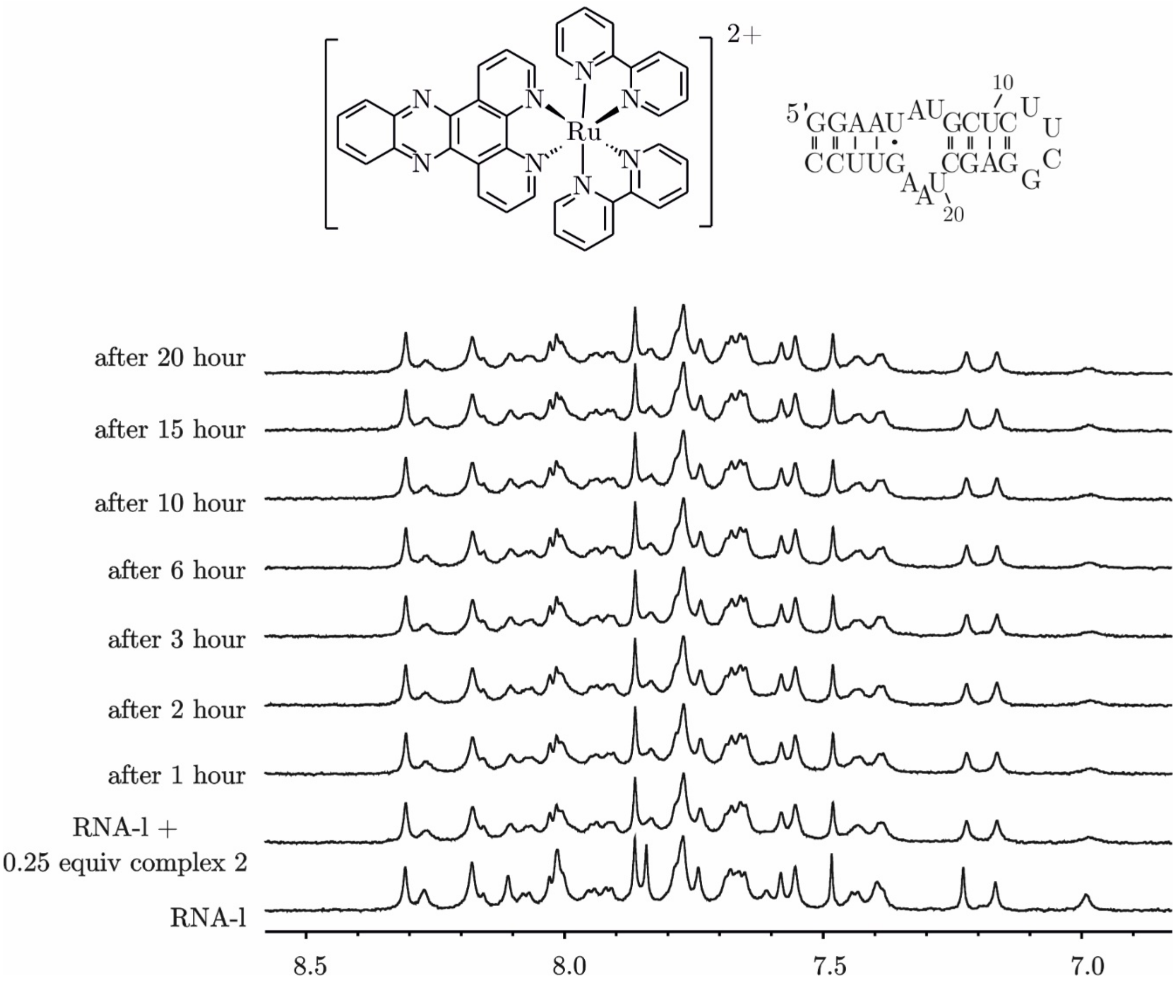

Appendix 11 Sections of [^{1}H-^{1}H]-NOESY spectra recorded on RNA-l in the absence (left) and in the presence (right) of 1 equivalent of complex 2 (0.34 mM, PBS, pD 6.8, 303 K, 700 MHz). The boxes indicate some of the cross peaks belonging to nucleotides in the internal loop that either disappear or broaden upon metal complex addition.

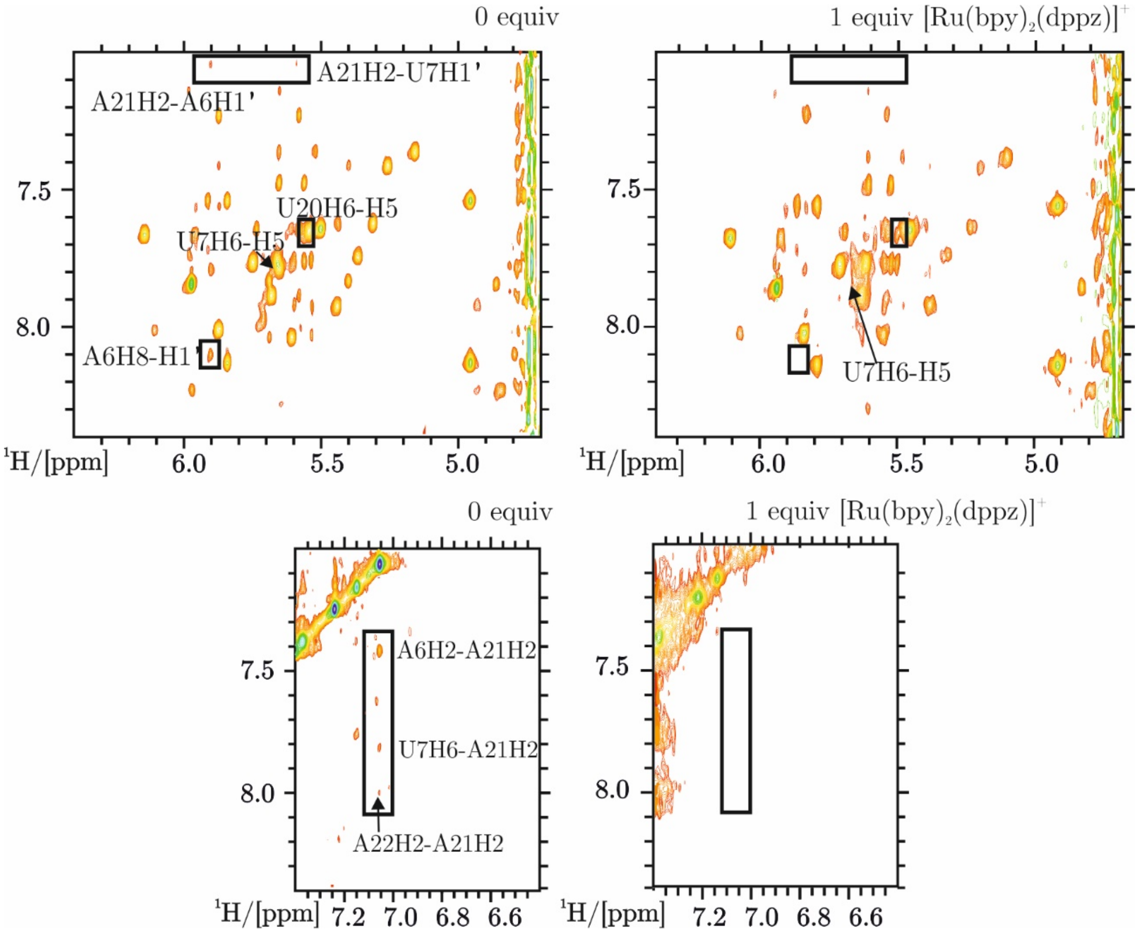

Appendix 12 Portions of [^{1}H,^{1}H]-TOCSY spectra recorded on RNA-l in the absence (left) and in the presence (right) of 1 equivalent of complex 2 (0.35 mM, PBS, pD 6.8, 303 K, 700 MHz). The boxes indicate some of the cross peaks belonging to nucleotides in the internal loop that either disappear or broaden upon metal complex addition.

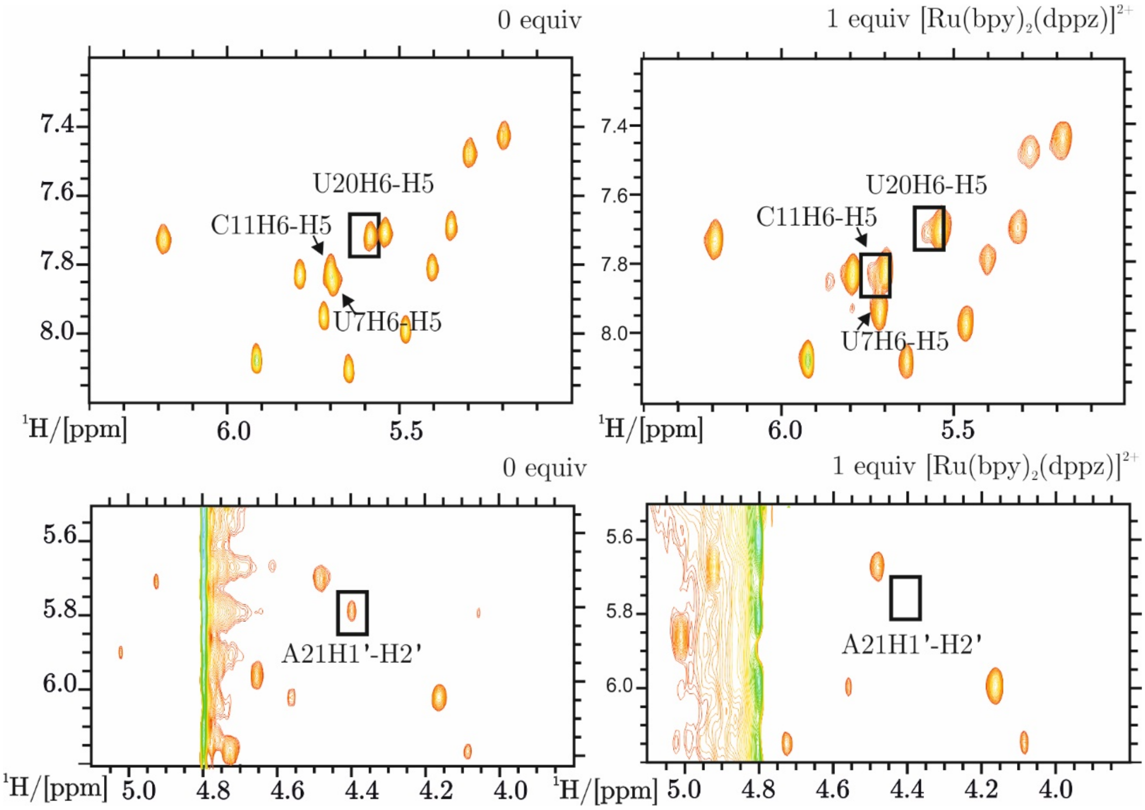

Appendix 13 ^{1}H spectra (imino proton region) of dephosphorylated samples of RNA-l in panel a) and RNA-h in panel b) in the presence of increasing amounts of complex 1 (0.14 mM, PBS, pH 6.9, 293 K, 700 MHz).

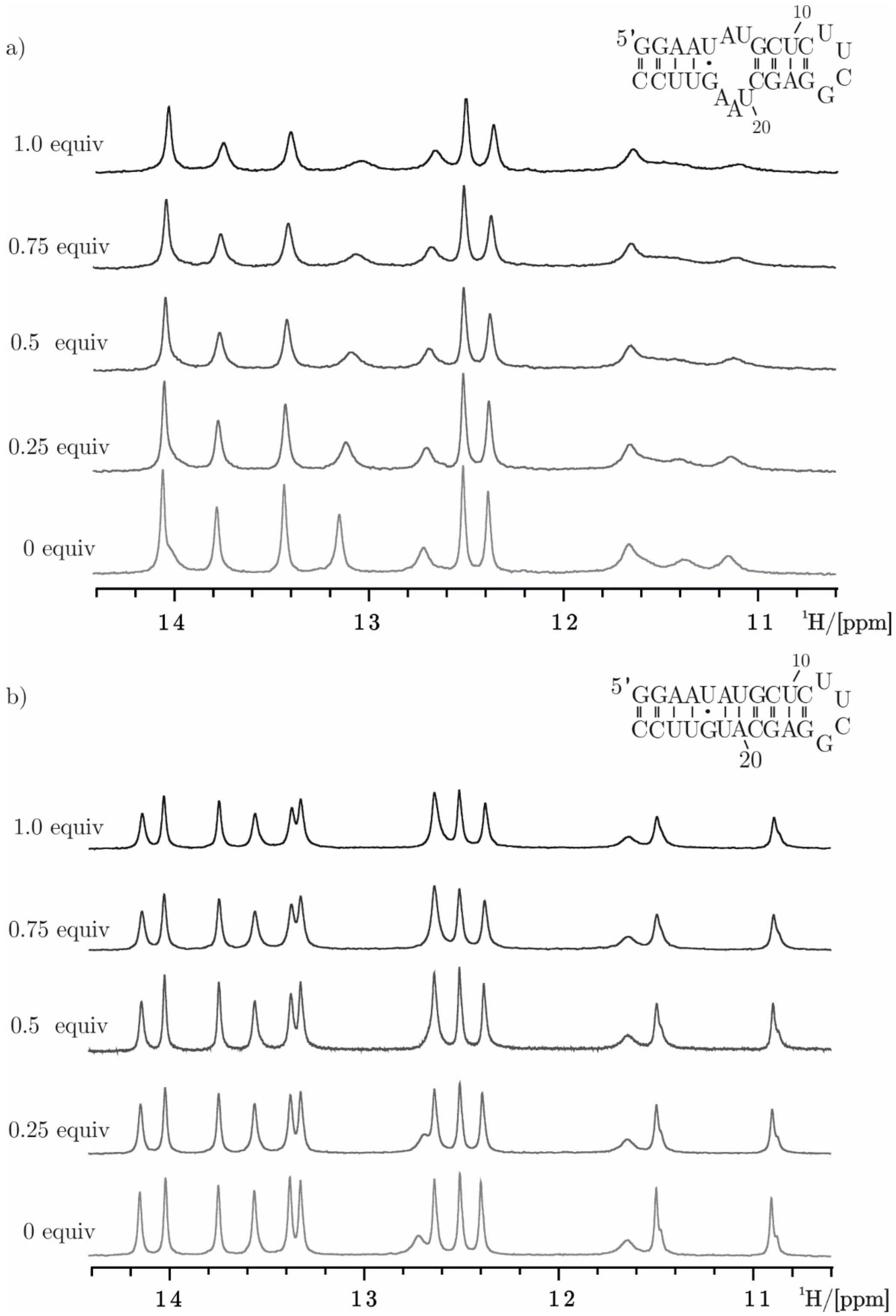

Appendix 14 Distances derived from xp06_141, NMR solution structure of RNA-l (column 1), and from MD simulations, 141_interc2_cluster1 represents RNA-l with one molecule of complex 1 (column 2) and cluster1_bis_long with two molecules of complex 1 (column 3). In the last two columns of the table it is reported the difference of the distances between column 1 and 2 and column 1 and 3. Strong changes are highlighted in grey.

				1	2	3		
residue	**proton**	**residue**	**proton**	**RNA-l (Å)**	**RNA-l+ 1 complex (Å)**	**RNA-l+ 2 complexes (Å)**	**1-2 (Å)**	**1-3 (Å)**
1	**H1'**	**1**	**H2'**	2.74	2.81	2.76	0.07	0.02
1	**H1'**	**1**	**H3'**	3.86	3.92	3.8	0.06	-0.06
1	**H1'**	**1**	**H4'**	3.68	3.21	3.21	-0.47	-0.47
1	**H1'**	**1**	**H5''**	5.22	5.19	5.21	-0.03	-0.01
1	**H1'**	**1**	**H5'**	4.71	4.7	4.7	-0.01	-0.01
1	**H2'**	**1**	**H3'**	2.41	2.38	2.62	-0.03	0.21
1	**H2'**	**1**	**H4'**	3.9	3.8	3.74	-0.1	-0.16
1	**H2'**	**1**	**H5''**	4.89	4.89	5.15	0	0.26
1	**H2'**	**1**	**H5'**	5.34	5.34	5.5	0	0.16
1	**H2'**	**2**	**H5''**	4.56	4.91	4.12	0.35	-0.44
1	**H2'**	**2**	**H5'**	3.29	3.93	2.67	0.64	-0.62
1	**H5'**	**1**	**H5''**	1.77	1.7	1.71	-0.07	-0.06
1	**H8**	**1**	**H1'**	3.73	3.28	3.74	-0.45	0.01
1	**H8**	**1**	**H2'**	4.05	4.47	4.15	0.42	0.1
1	**H8**	**1**	**H3'**	2.81	4.34	2.99	1.53	0.18
1	**H8**	**1**	**H4'**	3.94	4.56	4.53	0.62	0.59
1	**H8**	**1**	**H5''**	3.36	5.08	4.77	1.72	1.41
1	**H8**	**1**	**H5'**	3.1	4.32	4.25	1.22	1.15
1	**H8**	**2**	**H8**	4.23	5.65	4.62	1.42	0.39
2	**H1'**	**1**	**H2'**	3.72	3.99	4.35	0.27	0.63
2	**H1'**	**2**	**H2'**	2.84	2.75	2.59	-0.09	-0.25
2	**H1'**	**2**	**H3'**	3.89	3.77	3.67	-0.12	-0.22
2	**H1'**	**2**	**H4'**	3.27	3.16	3.38	-0.11	0.11
2	**H1'**	**2**	**H5''**	5.15	5.15	5.25	0	0.1
2	**H3'**	**2**	**H2'**	2.4	2.46	2.37	0.06	-0.03
2	**H5'**	**2**	**H5''**	1.77	1.68	1.88	-0.09	0.11
2	**H8**	**1**	**H1'**	4.54	4.95	4.6	0.41	0.06
2	**H8**	**1**	**H2'**	2.15	2.26	2.21	0.11	0.06
2	**H8**	**1**	**H3'**	2.52	3.03	3.43	0.51	0.91
2	**H8**	**2**	**H1'**	3.62	3.61	3.78	-0.01	0.16
2	**H8**	**2**	**H2'**	4.14	4	4.11	-0.14	-0.03
2	**H8**	**2**	**H3'**	3.46	3	3.02	-0.46	-0.44
2	**H8**	**2**	**H4'**	4.44	4.38	4.38	-0.06	-0.06
2	**H8**	**2**	**H5''**	4.46	4.56	4.52	0.1	0.06
2	**H8**	**2**	**H5'**	4	4.35	3.88	0.35	-0.12

3	**H1'**	**3**	**H2'**	2.77	2.75	2.64	-0.02	-0.13
3	**H1'**	**3**	**H3'**	3.87	3.68	3.72	-0.19	-0.15
3	**H1'**	**3**	**H4'**	3.59	3.39	3.22	-0.2	-0.37
3	**H1'**	**3**	**H5''**	5.22	5.13	5.19	-0.09	-0.03
3	**H2**	**3**	**H1'**	4.69	4.85	4.54	0.16	-0.15
3	**H2**	**4**	**H1'**	4.51	2.89	4.05	-1.62	-0.46
3	**H2**	**4**	**H2'**	6.68	5.37	6.31	-1.31	-0.37
3	**H2**	**25**	**H1'**	5.4	5.42	5.47	0.02	0.07
3	**H2**	**25**	**H2'**	5.48	5.64	5.24	0.16	-0.24
3	**H2**	**26**	**H1'**	4.47	4.62	3.75	0.15	-0.72
3	**H2**	**26**	**H2'**	6.55	6.59	5.93	0.04	-0.62
3	**H8**	**2**	**H1'**	5.04	4.72	4.84	-0.32	-0.2
3	**H8**	**2**	**H2'**	2.22	2.1	2.35	-0.12	0.13
3	**H8**	**2**	**H3'**	3.18	3	3.21	-0.18	0.03
3	**H8**	**2**	**H8**	5.81	4.73	5.12	-1.08	-0.69
3	**H8**	**3**	**H1'**	3.75	3.63	3.92	-0.12	0.17
3	**H8**	**3**	**H2'**	3.98	4.14	4.01	0.16	0.03
3	**H8**	**3**	**H3'**	2.84	2.96	2.64	0.12	-0.2
3	**H8**	**3**	**H4'**	4.09	4.37	4.42	0.28	0.33
3	**H8**	**3**	**H5''**	3.6	4.19	4.31	0.59	0.71
3	**H8**	**3**	**H5'**	3.36	4.06	3.86	0.7	0.5
3	**H8**	**4**	**H8**	5.56	4.49	4.7	-1.07	-0.86
4	**H1'**	**3**	**H2'**	3.8	3.87	4.4	0.07	0.6
4	**H1'**	**4**	**H2'**	2.77	2.7	2.83	-0.07	0.06
4	**H1'**	**4**	**H3'**	3.88	3.91	3.77	0.03	-0.11
4	**H1'**	**4**	**H4'**	3.59	3.57	3.24	-0.02	-0.35
4	**H1'**	**4**	**H5''**	5.2	5.18	5.16	-0.02	-0.04
4	**H1'**	**5**	**H1'**	6.01	6.19	6.06	0.18	0.05
4	**H1'**	**5**	**H5**	6.12	6.34	6.29	0.22	0.17
4	**H2**	**3**	**H2**	4.56	5.24	5.32	0.68	0.76
4	**H2**	**4**	**H1'**	4.73	4.56	4.59	-0.17	-0.14
4	**H2**	**4**	**H2'**	4.84	4.18	4.87	-0.66	0.03
4	**H2**	**5**	**H1'**	4.11	3.14	4.31	-0.97	0.2
4	**H2**	**24**	**H1'**	5.63	4.66	5.43	-0.97	-0.2
4	**H2**	**25**	**H1'**	4.5	5.82	4.51	1.32	0.01
4	**H8**	**3**	**H1'**	4.98	4.69	4.89	-0.29	-0.09
4	**H8**	**3**	**H2'**	2.23	2.19	2.61	-0.04	0.38
4	**H8**	**3**	**H3'**	3.29	2.5	3.55	-0.79	0.26
4	**H8**	**4**	**H1'**	3.73	3.71	3.66	-0.02	-0.07
4	**H8**	**4**	**H2'**	4.03	3.94	3.54	-0.09	-0.49
4	**H8**	**4**	**H3'**	2.94	3.31	2.62	0.37	-0.32
4	**H8**	**4**	**H4'**	4.11	4.36	4.13	0.25	0.02
4	**H8**	**4**	**H5''**	3.57	3.93	4.12	0.36	0.55
4	**H8**	**4**	**H5'**	3.44	3.76	3.55	0.32	0.11
4	**H8**	**5**	**H5**	4.61	4.36	4.42	-0.25	-0.19
4	**H8**	**5**	**H6**	5.44	5.18	5.44	-0.26	0
5	**H1'**	**4**	**H2'**	4.12	4.29	4.27	0.17	0.15
5	**H1'**	**5**	**H2'**	2.79	2.78	2.78	-0.01	-0.01

5	**H1'**	**5**	**H3'**	3.88	3.78	3.88	-0.1	0
5	**H1'**	**5**	**H4'**	3.51	3.03	3.2	-0.48	-0.31
5	**H1'**	**5**	**H5**	5.35	5.46	5.44	0.11	0.09
5	**H1'**	**5**	**H5''**	5.21	5.12	5.04	-0.09	-0.17
5	**H5**	**4**	**H2'**	3.87	4.39	3.9	0.52	0.03
5	**H5**	**4**	**H3'**	3.16	3.83	3.86	0.67	0.7
5	**H5**	**5**	**H2'**	5.23	4.68	4.78	-0.55	-0.45
5	**H5**	**5**	**H3'**	4.43	4.43	4.7	0	0.27
5	**H6**	**4**	**H1'**	5.32	5.69	5.86	0.37	0.54
5	**H6**	**4**	**H2'**	2.57	3.12	3.05	0.55	0.48
5	**H6**	**4**	**H3'**	3.2	3.26	3.87	0.06	0.67
5	**H6**	**4**	**H5''**	5.74	5.47	6.67	-0.27	0.93
5	**H6**	**5**	**H1'**	3.62	3.83	3.68	0.21	0.06
5	**H6**	**5**	**H2'**	3.69	3.1	2.98	-0.59	-0.71
5	**H6**	**5**	**H3'**	2.54	2.23	2.4	-0.31	-0.14
5	**H6**	**5**	**H4'**	3.86	4.25	4.13	0.39	0.27
5	**H6**	**5**	**H5**	2.41	2.38	2.45	-0.03	0.04
5	**H6**	**5**	**H5''**	3.5	4.27	3.93	0.77	0.43
5	**H6**	**5**	**H5'**	3.31	4.24	4	0.93	0.69
6	**H1'**	**5**	**H2'**	4.36	4.7	5.49	0.34	1.13
6	**H1'**	**6**	**H2'**	3.07	2.77	2.88	-0.3	-0.19
6	**H1'**	**6**	**H3'**	3.89	3.86	4.17	-0.03	0.28
6	**H1'**	**6**	**H4'**	3.53	3.52	3.56	-0.01	0.03
6	**H1'**	**6**	**H5''**	4.84	5.21	5.37	0.37	0.53
6	**H1'**	**7**	**H2'**	5.69	7.6	6.45	1.91	0.76
6	**H1'**	**7**	**H3'**	5.89	6.97	7.42	1.08	1.53
6	**H2**	**6**	**H1'**	4.53	4.25	4.39	-0.28	-0.14
6	**H2**	**6**	**H2'**	6.44	6.23	6.74	-0.21	0.3
6	**H2**	**7**	**H1'**	4.44	8.54	9.36	4.1	4.92
6	**H2**	**21**	**H1'**	3.64	10.77	8.72	7.13	5.08
6	**H2**	**21**	**H2**	3.24	9.53	5.7	6.29	2.46
6	**H2**	**21**	**H2'**	4.1	9.86	11.42	5.76	7.32
6	**H2**	**22**	**H1'**	4	7.5	8.65	3.5	4.65
6	**H2**	**23**	**H1'**	6.8	6.19	5.12	-0.61	-1.68
6	**H3'**	**6**	**H2'**	2.42	2.46	2.34	0.04	-0.08
6	**H3'**	**6**	**H4'**	2.65	2.95	2.89	0.3	0.24
6	**H3'**	**6**	**H5''**	2.27	2.53	2.95	0.26	0.68
6	**H3'**	**6**	**H5'**	3.56	3.54	3.74	-0.02	0.18
6	**H8**	**5**	**H1'**	5	6.2	6.05	1.2	1.05
6	**H8**	**5**	**H2'**	2.22	3.6	3.64	1.38	1.42
6	**H8**	**5**	**H3'**	3.23	4.69	4.96	1.46	1.73
6	**H8**	**5**	**H6**	5.14	5.98	6.22	0.84	1.08
6	**H8**	**6**	**H1'**	3.85	3.96	3.88	0.11	0.03
6	**H8**	**6**	**H2'**	2.68	2.94	2.45	0.26	-0.23
6	**H8**	**6**	**H3'**	4.47	2.08	2.87	-2.39	-1.6
6	**H8**	**6**	**H4'**	4.49	4.51	4.75	0.02	0.26

6	**H8**	**6**	**H5''**	3.77	3.95	4.8	0.18	1.03
6	**H8**	**6**	**H5'**	3.79	4.46	4.73	0.67	0.94
6	**H8**	**7**	**H5**	6.65	3.57	6.48	-3.08	-0.17
6	**H8**	**7**	**H6**	6.08	4.72	6.44	-1.36	0.36
6	**H8**	**21**	**H2**	5.81	10.5	8.82	4.69	3.01
6	**H8**	**22**	**H2**	6.01	7.12	9.59	1.11	3.58
7	**H1'**	**6**	**H1'**	3.15	6.09	6.15	2.94	3
7	**H1'**	**6**	**H2'**	5.93	5	6.13	-0.93	0.2
7	**H1'**	**7**	**H2'**	2.78	2.76	3.11	-0.02	0.33
7	**H1'**	**7**	**H3'**	3.87	3.94	3.68	0.07	-0.19
7	**H1'**	**7**	**H4'**	3.52	3.35	3.16	-0.17	-0.36
7	**H1'**	**7**	**H5''**	4.47	5.3	4.72	0.83	0.25
7	**H5**	**6**	**H1'**	4.53	4.78	6.59	0.25	2.06
7	**H5**	**6**	**H2'**	4.21	2.51	5.03	-1.7	0.82
7	**H5**	**6**	**H3'**	4.5	4.06	7.04	-0.44	2.54
7	**H5**	**7**	**H2'**	5.72	4.91	4.4	-0.81	-1.32
7	**H5**	**7**	**H3'**	5.15	4.4	6.59	-0.75	1.44
7	**H5**	**7**	**H5''**	4.29	6.16	7.32	1.87	3.03
7	**H6**	**6**	**H1'**	2.96	4.62	5.9	1.66	2.94
7	**H6**	**6**	**H2**	6.01	7.78	9.45	1.77	3.44
7	**H6**	**6**	**H2'**	3.96	2.19	4.33	-1.77	0.37
7	**H6**	**6**	**H3'**	3.7	4.06	6.01	0.36	2.31
7	**H6**	**7**	**H1'**	3.26	3.54	3.55	0.28	0.29
7	**H6**	**7**	**H2'**	4.38	3.42	2.03	-0.96	-2.35
7	**H6**	**7**	**H3'**	3.71	2.53	4.22	-1.18	0.51
7	**H6**	**7**	**H4'**	4.17	3.92	5.06	-0.25	0.89
7	**H6**	**7**	**H5**	2.41	2.42	2.4	0.01	-0.01
7	**H6**	**7**	**H5''**	2.64	4.02	4.98	1.38	2.34
7	**H6**	**7**	**H5'**	4.27	3.57	5.02	-0.7	0.75
7	**H6**	**8**	**H8**	4.83	6.28	5.82	1.45	0.99
7	**H6**	**21**	**H2**	3.2	6.76	8.93	3.56	5.73
8	**H1'**	**7**	**H2'**	3.46	5.91	6.03	2.45	2.57
8	**H1'**	**8**	**H2'**	2.81	2.65	2.9	-0.16	0.09
8	**H1'**	**8**	**H3'**	3.88	3.75	3.81	-0.13	-0.07
8	**H1'**	**8**	**H4'**	3.38	3.35	3.07	-0.03	-0.31
8	**H1'**	**8**	**H5''**	5.19	5.19	5.13	0	-0.06
8	**H8**	**6**	**H1'**	7.02	10.23	9.39	3.21	2.37
8	**H8**	**6**	**H2**	7.78	12.39	12.49	4.61	4.71
8	**H8**	**7**	**H1'**	4.64	4.51	3.28	-0.13	-1.36
8	**H8**	**7**	**H2'**	2.23	2.87	4.84	0.64	2.61
8	**H8**	**7**	**H3'**	2.2	4.94	4.42	2.74	2.22
8	**H8**	**8**	**H1'**	3.67	3.79	3.77	0.12	0.1
8	**H8**	**8**	**H2'**	4.08	4.3	3.81	0.22	-0.27
8	**H8**	**8**	**H3'**	3.22	3.05	2.93	-0.17	-0.29
8	**H8**	**8**	**H4'**	4.33	4.42	4.47	0.09	0.14
8	**H8**	**8**	**H5''**	4.22	4.53	4.61	0.31	0.39
9	**H1'**	**8**	**H2'**	4.81	4.78	4.16	-0.03	-0.65
9	**H1'**	**9**	**H2'**	2.77	2.73	2.66	-0.04	-0.11

9	**H1'**	**9**	**H3'**	3.87	3.66	3.72	-0.21	-0.15
9	**H1'**	**9**	**H4'**	3.57	3.3	3.21	-0.27	-0.36
9	**H1'**	**9**	**H5''**	5.22	5.12	5.11	-0.1	-0.11
9	**H5**	**8**	**H1'**	4.84	5.4	6.53	0.56	1.69
9	**H5**	**8**	**H2'**	2.34	3.74	4.17	1.4	1.83
9	**H5**	**8**	**H3'**	2.76	4	4.67	1.24	1.91
9	**H5**	**9**	**H2'**	5.38	5.34	5.22	-0.04	-0.16
9	**H5**	**9**	**H3'**	4.5	4.37	4.5	-0.13	0
9	**H5**	**9**	**H5''**	5.48	6.34	6.21	0.86	0.73
9	**H6**	**8**	**H1'**	5	4.78	5.89	-0.22	0.89
9	**H6**	**8**	**H2'**	2.29	2.33	3.06	0.04	0.77
9	**H6**	**8**	**H3'**	3.49	3.68	4.19	0.19	0.7
9	**H6**	**9**	**H1'**	3.56	3.7	3.78	0.14	0.22
9	**H6**	**9**	**H2'**	3.9	3.84	3.59	-0.06	-0.31
9	**H6**	**9**	**H3'**	2.74	2.43	2.29	-0.31	-0.45
9	**H6**	**9**	**H4'**	3.81	4.1	4.25	0.29	0.44
9	**H6**	**9**	**H5**	2.44	2.47	2.43	0.03	-0.01
9	**H6**	**9**	**H5''**	3.43	4.02	3.9	0.59	0.47
9	**H6**	**10**	**H5**	5.3	4.28	3.48	-1.02	-1.82
10	**H1'**	**9**	**H2'**	3.49	4.04	3.78	0.55	0.29
10	**H1'**	**10**	**H2'**	2.76	2.79	2.81	0.03	0.05
10	**H1'**	**10**	**H3'**	3.85	3.81	3.69	-0.04	-0.16
10	**H1'**	**10**	**H4'**	3.58	3.09	3.14	-0.49	-0.44
10	**H1'**	**10**	**H5''**	5.2	5.11	5.12	-0.09	-0.08
10	**H5**	**9**	**H2'**	3.58	4.39	3.87	0.81	0.29
10	**H5**	**9**	**H3'**	3.45	4.02	4.04	0.57	0.59
10	**H5**	**9**	**H5**	5.69	3.67	3.09	-2.02	-2.6
10	**H5**	**10**	**H1'**	5.32	5.34	5.28	0.02	-0.04
10	**H5**	**10**	**H2'**	5.38	5.01	5.32	-0.37	-0.06
10	**H5**	**10**	**H3'**	4.38	4.43	4.64	0.05	0.26
10	**H5**	**10**	**H5''**	5.3	6.29	6.51	0.99	1.21
10	**H6**	**9**	**H1'**	4.94	5.08	4.66	0.14	-0.28
10	**H6**	**9**	**H2'**	2.2	2.63	2.28	0.43	0.08
10	**H6**	**9**	**H3'**	3.32	3.23	3.47	-0.09	0.15
10	**H6**	**9**	**H6**	5.54	4.55	4.24	-0.99	-1.3
10	**H6**	**10**	**H1'**	3.57	3.64	3.56	0.07	-0.01
10	**H6**	**10**	**H2'**	3.88	3.64	3.71	-0.24	-0.17
10	**H6**	**10**	**H3'**	2.64	2.62	2.53	-0.02	-0.11
10	**H6**	**10**	**H4'**	3.78	4.21	4.13	0.43	0.35
10	**H6**	**10**	**H5**	2.41	2.33	2.46	-0.08	0.05
10	**H6**	**10**	**H5''**	3.31	4.15	4.18	0.84	0.87
10	**H6**	**11**	**H6**	4.29	5.79	4.53	1.5	0.24
11	**H1'**	**10**	**H2'**	3.77	4.52	4.25	0.75	0.48
11	**H1'**	**11**	**H2'**	2.87	2.66	2.79	-0.21	-0.08
11	**H1'**	**11**	**H3'**	3.9	3.78	3.81	-0.12	-0.09
11	**H1'**	**11**	**H4'**	3.16	3.16	3.05	0	-0.11
11	**H1'**	**11**	**H5''**	5.1	5.17	5.1	0.07	0
11	**H1'**	**11**	**H5'**	4.52	4.8	4.61	0.28	0.09

11	**H2'**	**11**	**H3'**	2.39	2.43	2.53	0.04	0.14
11	**H5**	**10**	**H2'**	4.14	3.34	4.08	-0.8	-0.06
11	**H5**	**10**	**H3'**	3.71	4.06	4.21	0.35	0.5
11	**H5**	**10**	**H5**	3.35	4.86	3.6	1.51	0.25
11	**H5**	**11**	**H2'**	5.29	5.09	5.13	-0.2	-0.16
11	**H5**	**11**	**H3'**	5.08	4.57	4.74	-0.51	-0.34
11	**H5**	**12**	**H5**	3.94	3.86	3.51	-0.08	-0.43
11	**H5'**	**11**	**H5''**	1.77	1.76	1.71	-0.01	-0.06
11	**H6**	**10**	**H1'**	4.53	5.37	5.11	0.84	0.58
11	**H6**	**10**	**H2'**	2.15	2.67	2.54	0.52	0.39
11	**H6**	**10**	**H3'**	2.84	4.03	3.38	1.19	0.54
11	**H6**	**10**	**H5**	4.91	6.6	5.26	1.69	0.35
11	**H6**	**11**	**H1'**	3.51	3.68	3.69	0.17	0.18
11	**H6**	**11**	**H2'**	3.85	3.31	3.72	-0.54	-0.13
11	**H6**	**11**	**H3'**	3.19	2.27	2.72	-0.92	-0.47
11	**H6**	**11**	**H4'**	4.19	4.14	4.29	-0.05	0.1
11	**H6**	**11**	**H5**	2.44	2.5	2.39	0.06	-0.05
11	**H6**	**11**	**H5''**	4.41	4.04	4.55	-0.37	0.14
11	**H6**	**11**	**H5'**	3.61	4.05	4.12	0.44	0.51
12	**H1'**	**11**	**H2'**	3.65	3.94	4.3	0.29	0.65
12	**H1'**	**12**	**H2'**	2.78	2.71	2.89	-0.07	0.11
12	**H1'**	**12**	**H3'**	3.87	3.71	3.85	-0.16	-0.02
12	**H1'**	**12**	**H4'**	3.52	3.36	3.32	-0.16	-0.2
12	**H1'**	**12**	**H5''**	4.65	5.17	5.06	0.52	0.41
12	**H3'**	**12**	**H2'**	2.41	2.41	2.18	0	-0.23
12	**H3'**	**12**	**H4'**	2.99	3.01	2.86	0.02	-0.13
12	**H4'**	**12**	**H2'**	3.86	3.86	3.9	0	0.04
12	**H5**	**11**	**H2'**	4.49	4.13	4.22	-0.36	-0.27
12	**H5**	**11**	**H3'**	3.64	3.86	3.95	0.22	0.31
12	**H5**	**12**	**H2'**	5.54	4.72	4.58	-0.82	-0.96
12	**H5**	**12**	**H3'**	4.81	3.76	4.89	-1.05	0.08
12	**H5**	**12**	**H5''**	4.28	5.65	6.31	1.37	2.03
12	**H5'**	**12**	**H2'**	5.12	5.56	5.15	0.44	0.03
12	**H6**	**11**	**H1'**	5.21	4.98	5.15	-0.23	-0.06
12	**H6**	**11**	**H2'**	2.64	2.42	2.57	-0.22	-0.07
12	**H6**	**11**	**H3'**	2.88	3.26	3.36	0.38	0.48
12	**H6**	**11**	**H5**	4.95	5.09	4.94	0.14	-0.01
12	**H6**	**12**	**H1'**	3.45	3.69	3.71	0.24	0.26
12	**H6**	**12**	**H2'**	4.12	3.57	3.19	-0.55	-0.93
12	**H6**	**12**	**H3'**	3.19	2.16	2.92	-1.03	-0.27
12	**H6**	**12**	**H4'**	3.97	3.88	4.27	-0.09	0.3
12	**H6**	**12**	**H5**	2.41	2.34	2.36	-0.07	-0.05
12	**H6**	**12**	**H5''**	2.49	3.68	4.08	1.19	1.59
12	**H6**	**14**	**H5**	6.44	4.96	6.17	-1.48	-0.27
13	**H1'**	**13**	**H2'**	3.08	3.03	2.91	-0.05	-0.17
13	**H1'**	**13**	**H3'**	3.86	3.67	3.74	-0.19	-0.12
13	**H1'**	**13**	**H4'**	3.35	2.39	3.18	-0.96	-0.17
13	**H1'**	**13**	**H5'**	4.83	4.37	4.64	-0.46	-0.19

13	**H1'**	**13**	**H5''**	4.85	4.6	4.95	-0.25	0.1
13	**H1'**	**14**	**H5'**	4.15	5.3	4.81	1.15	0.66
13	**H1'**	**14**	**H5''**	5.13	6.1	6.23	0.97	1.1
13	**H2'**	**12**	**H2'**	3.41	4.06	4.04	0.65	0.63
13	**H2'**	**13**	**H3'**	2.41	2.11	2.32	-0.3	-0.09
13	**H2'**	**14**	**H2'**	5.38	6.58	6.39	1.2	1.01
13	**H3'**	**12**	**H2'**	4.62	3.75	4.68	-0.87	0.06
13	**H3'**	**14**	**H4'**	5.76	4.99	5.39	-0.77	-0.37
13	**H3'**	**14**	**H5''**	4.51	4.27	4.73	-0.24	0.22
13	**H3'**	**14**	**H5'**	3.84	3.01	3.67	-0.83	-0.17
13	**H5**	**12**	**H2'**	4.39	6.32	5.76	1.93	1.37
13	**H5**	**12**	**H4'**	2.99	3.66	2.69	0.67	-0.3
13	**H5**	**12**	**H5''**	5.79	5.25	4.34	-0.54	-1.45
13	**H5**	**13**	**H1'**	5.43	5.44	5.42	0.01	-0.01
13	**H5**	**13**	**H2'**	4.37	4.45	4.64	0.08	0.27
13	**H5**	**13**	**H3'**	6.52	6.42	6.72	-0.1	0.2
13	**H5''**	**12**	**H2'**	4.38	4.13	4.91	-0.25	0.53
13	**H5'**	**12**	**H2'**	5.54	4.85	5.44	-0.69	-0.1
13	**H5'**	**13**	**H5''**	1.78	1.74	1.74	-0.04	-0.04
13	**H6**	**12**	**H1'**	4.89	4.85	4.85	-0.04	-0.04
13	**H6**	**12**	**H2'**	3.41	4.47	4.65	1.06	1.24
13	**H6**	**12**	**H4'**	4.05	3.4	3.52	-0.65	-0.53
13	**H6**	**12**	**H6**	6.73	6.59	6.85	-0.14	0.12
13	**H6**	**13**	**H1'**	3.72	3.69	3.65	-0.03	-0.07
13	**H6**	**13**	**H2'**	2.28	2.29	2.63	0.01	0.35
13	**H6**	**13**	**H3'**	4.17	4.05	4.39	-0.12	0.22
13	**H6**	**13**	**H4'**	4.51	4.59	4.52	0.08	0.01
13	**H6**	**13**	**H5**	2.41	2.45	2.47	0.04	0.06
13	**H6**	**13**	**H5''**	3.92	5.19	4.54	1.27	0.62
13	**H6**	**13**	**H5'**	4.12	4.95	3.71	0.83	-0.41
13	**H6**	**14**	**H5**	4.2	5.94	5.5	1.74	1.3
13	**H6**	**14**	**H6**	5.27	6.14	6.09	0.87	0.82
14	**H1'**	**12**	**H2'**	6.31	6.43	5.64	0.12	-0.67
14	**H1'**	**13**	**H3'**	5.85	5.9	5.71	0.05	-0.14
14	**H1'**	**14**	**H2'**	3.06	3.01	3.02	-0.05	-0.04
14	**H1'**	**14**	**H3'**	3.9	3.7	3.78	-0.2	-0.12
14	**H1'**	**14**	**H4'**	3.53	3.1	3.24	-0.43	-0.29
14	**H1'**	**14**	**H5**	5.42	5.39	5.4	-0.03	-0.02
14	**H1'**	**14**	**H5''**	5.03	4.94	4.88	-0.09	-0.15
14	**H1'**	**14**	**H5'**	4.61	4.76	4.62	0.15	0.01
14	**H1'**	**15**	**H5'**	5.34	5.31	5.57	-0.03	0.23
14	**H1'**	**15**	**H5''**	3.9	3.99	4.23	0.09	0.33
14	**H2'**	**12**	**H2'**	6.53	6.24	6.58	-0.29	0.05
14	**H2'**	**14**	**H4'**	3.84	3.54	3.93	-0.3	0.09
14	**H2'**	**14**	**H5''**	3.72	3.48	3.8	-0.24	0.08
14	**H2'**	**14**	**H5'**	3.97	3.85	4.31	-0.12	0.34
14	**H3'**	**14**	**H4'**	2.66	2.86	2.9	0.2	0.24
14	**H3'**	**14**	**H5''**	2.6	2.59	2.49	-0.01	-0.11

14	**H3'**	**14**	**H5'**	3.73	3.81	3.74	0.08	0.01
14	**H4'**	**14**	**H5'**	2.48	2.47	2.32	-0.01	-0.16
14	**H5**	**12**	**H1'**	5.59	4.94	5.71	-0.65	0.12
14	**H5**	**12**	**H2'**	2.89	2.34	3.27	-0.55	0.38
14	**H5**	**12**	**H3'**	4.09	3.73	4.62	-0.36	0.53
14	**H5**	**13**	**H2'**	2.99	5.08	4.18	2.09	1.19
14	**H5**	**13**	**H3'**	2.37	3.75	3	1.38	0.63
14	**H5**	**13**	**H4'**	4.52	5.41	4.87	0.89	0.35
14	**H5**	**13**	**H5''**	2.43	2.94	2.66	0.51	0.23
14	**H5**	**13**	**H5'**	4.15	4.01	4.06	-0.14	-0.09
14	**H5**	**14**	**H2'**	4.36	4.62	4.67	0.26	0.31
14	**H5**	**14**	**H3'**	6.46	6.81	6.62	0.35	0.16
14	**H5**	**14**	**H4'**	6.65	6.5	6.7	-0.15	0.05
14	**H5**	**14**	**H5''**	6.15	6.7	6.6	0.55	0.45
14	**H6**	**12**	**H2'**	4.5	3.48	4.35	-1.02	-0.15
14	**H6**	**13**	**H1'**	5.24	6.2	5.84	0.96	0.6
14	**H6**	**13**	**H2'**	3.15	4.44	3.83	1.29	0.68
14	**H6**	**13**	**H3'**	2.16	2.6	2.32	0.44	0.16
14	**H6**	**13**	**H4'**	4.83	5	4.87	0.17	0.04
14	**H6**	**13**	**H5''**	3.93	2.93	3.76	-1	-0.17
14	**H6**	**13**	**H5'**	5.54	4.61	5.28	-0.93	-0.26
14	**H6**	**14**	**H1'**	3.71	3.69	3.71	-0.02	0
14	**H6**	**14**	**H2'**	2.29	2.8	2.77	0.51	0.48
14	**H6**	**14**	**H3'**	4.08	4.67	4.34	0.59	0.26
14	**H6**	**14**	**H4'**	4.32	4.14	4.38	-0.18	0.06
14	**H6**	**14**	**H5**	2.44	2.4	2.42	-0.04	-0.02
14	**H6**	**14**	**H5''**	3.89	4.41	4.25	0.52	0.36
14	**H6**	**14**	**H5'**	3.21	3.52	3.64	0.31	0.43
15	**H1'**	**14**	**H4'**	4.52	4.89	4.58	0.37	0.06
15	**H1'**	**14**	**H5''**	5.07	5.42	4.57	0.35	-0.5
15	**H1'**	**14**	**H5'**	4.71	4.95	4.12	0.24	-0.59
15	**H1'**	**15**	**H2'**	2.85	2.82	2.79	-0.03	-0.06
15	**H1'**	**15**	**H3'**	3.9	3.94	3.86	0.04	-0.04
15	**H1'**	**15**	**H4'**	3.26	3.3	3.11	0.04	-0.15
15	**H1'**	**15**	**H5''**	4.77	4.68	4.47	-0.09	-0.3
15	**H1'**	**16**	**H1'**	5.95	5.53	5.79	-0.42	-0.16
15	**H1'**	**16**	**H4'**	5.55	4.98	5.99	-0.57	0.44
15	**H2'**	**14**	**H4'**	5.2	4.87	5.44	-0.33	0.24
15	**H2'**	**15**	**H4'**	3.83	3.99	3.74	0.16	-0.09
15	**H2'**	**15**	**H5''**	4.43	3.88	4.46	-0.55	0.03
15	**H2'**	**16**	**H1'**	3.73	2.93	4.01	-0.8	0.28
15	**H2'**	**16**	**H2'**	5.42	4.65	5.87	-0.77	0.45
15	**H2'**	**16**	**H3'**	4.59	4.98	4.94	0.39	0.35
15	**H2'**	**16**	**H4'**	3.41	2.52	3.34	-0.89	-0.07
15	**H2'**	**16**	**H5'**	2.36	4.83	2.49	2.47	0.13
15	**H2'**	**16**	**H5''**	3.85	5.03	4.11	1.18	0.26
15	**H3'**	**14**	**H4'**	3.87	3.98	4.15	0.11	0.28
15	**H3'**	**16**	**H1'**	5.23	3.64	4.3	-1.59	-0.93

15	**H3'**	**16**	**H3'**	5.36	5.07	4.41	-0.29	-0.95
15	**H3'**	**16**	**H5'**	3.59	4.31	3.21	0.72	-0.38
15	**H3'**	**16**	**H5''**	4.68	4.18	4.21	-0.5	-0.47
15	**H3'**	**15**	**H2'**	2.39	2.29	2.31	-0.1	-0.08
15	**H3'**	**15**	**H4'**	3.01	2.99	3.11	-0.02	0.1
15	**H3'**	**15**	**H5''**	2.27	1.99	2.6	-0.28	0.33
15	**H3'**	**15**	**H5'**	3.28	2.73	2.69	-0.55	-0.59
15	**H4'**	**14**	**H4'**	4.15	4.43	4.02	0.28	-0.13
15	**H4'**	**14**	**H5'**	5.87	5.83	4.94	-0.04	-0.93
15	**H4'**	**14**	**H5''**	5.74	5.51	4.47	-0.23	-1.27
15	**H5''**	**14**	**H4'**	2.53	2.52	1.96	-0.01	-0.57
15	**H5''**	**14**	**H5''**	4.86	4.8	4.01	-0.06	-0.85
15	**H5''**	**14**	**H5'**	4.71	4.77	4	0.06	-0.71
15	**H5'**	**14**	**H4'**	3.62	3.86	3.58	0.24	-0.04
15	**H5'**	**14**	**H5''**	5.69	5.64	5.19	-0.05	-0.5
15	**H5'**	**14**	**H5'**	5.96	6.04	5.54	0.08	-0.42
15	**H8**	**14**	**H4'**	5.14	4.85	5.98	-0.29	0.84
15	**H8**	**14**	**H5''**	4.79	4.62	6.31	-0.17	1.52
15	**H8**	**14**	**H5'**	4.02	3.78	5.15	-0.24	1.13
15	**H8**	**15**	**H1'**	2.49	2.28	2.62	-0.21	0.13
15	**H8**	**15**	**H2'**	4.12	4.16	3.13	0.04	-0.99
15	**H8**	**15**	**H3'**	5.43	5.44	4.87	0.01	-0.56
15	**H8**	**15**	**H4'**	5.57	5.1	5.5	-0.47	-0.07
15	**H8**	**15**	**H5''**	6.25	5.71	6.02	-0.54	-0.23
15	**H8**	**15**	**H5'**	7.03	6.57	6.93	-0.46	-0.1
15	**H8**	**16**	**H1'**	5.73	6.09	4.5	0.36	-1.23
16	**H8**	**15**	**H2'**	2.88	5.68	4.32	2.8	1.44
16	**H8**	**15**	**H3'**	2.63	4.99	2.62	2.36	-0.01
16	**H8**	**16**	**H1'**	3.7	3.8	3.95	0.1	0.25
16	**H8**	**16**	**H2'**	4.1	3.82	4.02	-0.28	-0.08
16	**H8**	**16**	**H3'**	2.97	2.55	2.73	-0.42	-0.24
16	**H8**	**16**	**H4'**	4.04	4.32	4.43	0.28	0.39
16	**H8**	**16**	**H5''**	3.5	2.47	4.03	-1.03	0.53
16	**H8**	**16**	**H5'**	3.3	4.12	4.11	0.82	0.81
16	**H8**	**17**	**H8**	4.86	3.72	5.15	-1.14	0.29
17	**H1'**	**16**	**H1'**	5.92	5.59	5.45	-0.33	-0.47
17	**H1'**	**16**	**H2'**	4.24	4.04	4.01	-0.2	-0.23
17	**H1'**	**17**	**H2'**	2.83	2.7	2.74	-0.13	-0.09
17	**H1'**	**17**	**H3'**	3.89	3.69	3.55	-0.2	-0.34
17	**H1'**	**17**	**H4'**	3.3	3.25	3.17	-0.05	-0.13
17	**H1'**	**17**	**H5''**	5.16	5.02	5.23	-0.14	0.07
17	**H2**	**11**	**H1'**	3.69	4.56	3.86	0.87	0.17
17	**H2**	**17**	**H1'**	4.72	4.53	4.89	-0.19	0.17
17	**H2**	**17**	**H2'**	4.92	4.48	4.66	-0.44	-0.26
17	**H2**	**18**	**H1'**	3.72	3.5	3.59	-0.22	-0.13
17	**H2**	**18**	**H2'**	6.01	5.44	5.79	-0.57	-0.22
17	**H2**	**18**	**H8**	5.8	4.86	5.04	-0.94	-0.76
17	**H2**	**19**	**H5**	7.82	6.84	8.09	-0.98	0.27

17	**H8**	**16**	**H1'**	4.69	4.83	5.01	0.14	0.32
17	**H8**	**16**	**H2'**	2.19	2.67	2.36	0.48	0.17
17	**H8**	**16**	**H3'**	3.11	3.14	3.56	0.03	0.45
17	**H8**	**17**	**H1'**	3.73	3.88	3.74	0.15	0.01
17	**H8**	**17**	**H2'**	3.91	3.76	4.37	-0.15	0.46
17	**H8**	**17**	**H3'**	3.11	2.76	2.77	-0.35	-0.34
17	**H8**	**17**	**H4'**	4.4	4.64	4.25	0.24	-0.15
17	**H8**	**17**	**H5''**	4.42	4.28	4.3	-0.14	-0.12
17	**H8**	**17**	**H5'**	3.72	4.28	3.87	0.56	0.15
17	**H8**	**18**	**H8**	5.77	4.73	5.09	-1.04	-0.68
18	**H1'**	**17**	**H2'**	3.96	4.22	4.28	0.26	0.32
18	**H1'**	**18**	**H2'**	2.77	2.65	2.79	-0.12	0.02
18	**H1'**	**18**	**H3'**	3.87	3.76	3.91	-0.11	0.04
18	**H1'**	**18**	**H4'**	3.55	3.25	3.36	-0.3	-0.19
18	**H1'**	**18**	**H5''**	5.19	5.01	5.24	-0.18	0.05
18	**H1'**	**19**	**H5**	5.24	5.78	6.52	0.54	1.28
18	**H2'**	**18**	**H3'**	2.41	2.53	2.38	0.12	-0.03
18	**H8**	**17**	**H1'**	4.9	4.88	5.33	-0.02	0.43
18	**H8**	**17**	**H2'**	2.19	2.3	3	0.11	0.81
18	**H8**	**17**	**H3'**	3.6	3.55	3.46	-0.05	-0.14
18	**H8**	**18**	**H1'**	3.74	3.97	3.83	0.23	0.09
18	**H8**	**18**	**H2'**	3.96	3.89	3.44	-0.07	-0.52
18	**H8**	**18**	**H3'**	2.84	2.67	2.43	-0.17	-0.41
18	**H8**	**18**	**H4'**	4.11	4.5	4.27	0.39	0.16
18	**H8**	**18**	**H5''**	3.58	4.37	4.04	0.79	0.46
18	**H8**	**18**	**H5'**	3.52	4.09	3.96	0.57	0.44
18	**H8**	**19**	**H5**	3.71	4.04	4.6	0.33	0.89
19	**H1'**	**18**	**H2'**	4.11	3.91	4.43	-0.2	0.32
19	**H1'**	**19**	**H2'**	2.78	2.75	2.9	-0.03	0.12
19	**H1'**	**19**	**H3'**	3.88	3.82	3.78	-0.06	-0.1
19	**H1'**	**19**	**H4'**	3.52	3.08	2.99	-0.44	-0.53
19	**H1'**	**19**	**H5''**	5.23	5.22	5.03	-0.01	-0.2
19	**H5**	**18**	**H2'**	3.15	3.89	4.26	0.74	1.11
19	**H5**	**18**	**H3'**	2.63	4.11	4.54	1.48	1.91
19	**H5**	**19**	**H2'**	5.25	5.52	4.41	0.27	-0.84
19	**H5**	**19**	**H3'**	4.44	4.94	4.6	0.5	0.16
19	**H5**	**19**	**H5''**	5.8	6.52	6.56	0.72	0.76
19	**H6**	**18**	**H1'**	4.96	4.84	5.76	-0.12	0.8
19	**H6**	**18**	**H2'**	2.2	2.32	3.05	0.12	0.85
19	**H6**	**18**	**H3'**	2.94	3.45	3.98	0.51	1.04
19	**H6**	**18**	**H8**	5.14	4.65	5.09	-0.49	-0.05
19	**H6**	**19**	**H1'**	3.61	3.57	3.72	-0.04	0.11
19	**H6**	**19**	**H2'**	3.73	4.07	2.8	0.34	-0.93
19	**H6**	**19**	**H3'**	2.57	3.09	2.42	0.52	-0.15
19	**H6**	**19**	**H4'**	3.85	4.17	4.3	0.32	0.45
19	**H6**	**19**	**H5**	2.44	2.33	2.39	-0.11	-0.05
19	**H6**	**19**	**H5''**	3.64	4.32	4.25	0.68	0.61
19	**H6**	**19**	**H5'**	3.03	3.99	4.3	0.96	1.27

20	**H1'**	**19**	**H2'**	2.99	4.17	5.79	1.18	2.8
20	**H1'**	**20**	**H2'**	2.78	2.81	2.81	0.03	0.03
20	**H1'**	**20**	**H3'**	3.88	3.82	3.79	-0.06	-0.09
20	**H1'**	**20**	**H4'**	3.52	3.05	3.19	-0.47	-0.33
20	**H1'**	**20**	**H5''**	4.98	5.03	5.12	0.05	0.14
20	**H5**	**19**	**H2'**	4	4.42	3.99	0.42	-0.01
20	**H5**	**19**	**H3'**	4.09	3.53	5.04	-0.56	0.95
20	**H5**	**19**	**H5**	4.8	3.59	6.33	-1.21	1.53
20	**H5**	**20**	**H2'**	5.44	5.22	4.96	-0.22	-0.48
20	**H5**	**20**	**H3'**	4.69	4.35	4.46	-0.34	-0.23
20	**H6**	**19**	**H1'**	5.01	4.92	6.37	-0.09	1.36
20	**H6**	**19**	**H2'**	2.29	2.58	4.12	0.29	1.83
20	**H6**	**19**	**H3'**	3.34	2.78	5.12	-0.56	1.78
20	**H6**	**19**	**H5**	5.85	5.08	7.81	-0.77	1.96
20	**H6**	**19**	**H6**	5.02	4.37	6.67	-0.65	1.65
20	**H6**	**20**	**H1'**	3.51	3.69	3.72	0.18	0.21
20	**H6**	**20**	**H2'**	3.99	3.76	3	-0.23	-0.99
20	**H6**	**20**	**H3'**	2.99	2.51	2.07	-0.48	-0.92
20	**H6**	**20**	**H4'**	3.92	3.96	4.12	0.04	0.2
20	**H6**	**20**	**H5**	2.41	2.45	2.46	0.04	0.05
20	**H6**	**20**	**H5''**	3.03	4.08	3.82	1.05	0.79
21	**H1'**	**20**	**H2'**	3.98	4.57	5.18	0.59	1.2
21	**H1'**	**20**	**H3'**	6.11	6.86	7.18	0.75	1.07
21	**H1'**	**21**	**H2'**	3.07	2.88	3.04	-0.19	-0.03
21	**H1'**	**21**	**H3'**	3.87	3.8	3.63	-0.07	-0.24
21	**H1'**	**21**	**H4'**	3.48	3.54	3.24	0.06	-0.24
21	**H1'**	**21**	**H5''**	4.68	5.12	4.76	0.44	0.08
21	**H2**	**5**	**H2'**	7.03	12.65	9.8	5.62	2.77
21	**H2**	**6**	**H1'**	3.21	8.84	7.45	5.63	4.24
21	**H2**	**6**	**H2'**	4.49	8.09	8.61	3.6	4.12
21	**H2**	**6**	**H3'**	5.77	10.5	10.76	4.73	4.99
21	**H2**	**7**	**H1'**	3.42	4.16	9.06	0.74	5.64
21	**H2**	**7**	**H2'**	4.9	4.92	10.52	0.02	5.62
21	**H2**	**7**	**H5**	3.26	7.38	7.67	4.12	4.41
21	**H2**	**21**	**H1'**	4.5	4.19	4.71	-0.31	0.21
21	**H2**	**21**	**H2'**	6.44	5.92	7.01	-0.52	0.57
21	**H2**	**22**	**H1'**	6.04	7.37	4.38	1.33	-1.66
21	**H2'**	**21**	**H3'**	2.42	2.25	2.19	-0.17	-0.23
21	**H5'**	**21**	**H5''**	1.77	1.79	1.71	0.02	-0.06
21	**H8**	**6**	**H2**	5.07	12.08	10.67	7.01	5.6
21	**H8**	**20**	**H1'**	5.76	5.75	5.77	-0.01	0.01
21	**H8**	**20**	**H2'**	2.98	3.08	3.38	0.1	0.4
21	**H8**	**20**	**H3'**	3.66	4.48	5.14	0.82	1.48
21	**H8**	**20**	**H6**	6.01	6.3	5.85	0.29	-0.16
21	**H8**	**21**	**H1'**	3.86	3.96	3.8	0.1	-0.06
21	**H8**	**21**	**H2'**	2.71	3.14	2.35	0.43	-0.36
21	**H8**	**21**	**H3'**	4.53	2.08	4.52	-2.45	-0.01
21	**H8**	**21**	**H4'**	4.57	4.37	5.48	-0.2	0.91

21	**H8**	**21**	**H5''**	3.57	3.91	5.16	0.34	1.59
21	**H8**	**21**	**H5'**	4.18	4.13	5.31	-0.05	1.13
22	**H1'**	**21**	**H1'**	4.45	5.68	4.07	1.23	-0.38
22	**H1'**	**21**	**H2'**	5.02	5.19	6.34	0.17	1.32
22	**H1'**	**22**	**H2'**	2.95	2.85	2.74	-0.1	-0.21
22	**H1'**	**22**	**H3'**	3.96	3.81	3.58	-0.15	-0.38
22	**H1'**	**22**	**H4'**	2.96	3.07	3.13	0.11	0.17
22	**H1'**	**22**	**H5''**	4.41	5.14	5.12	0.73	0.71
22	**H1'**	**22**	**H5'**	4.96	4.88	4.53	-0.08	-0.43
22	**H2**	**6**	**H1'**	3.44	3.45	7.31	0.01	3.87
22	**H2**	**6**	**H2**	3.44	3.13	4.89	-0.31	1.45
22	**H2**	**7**	**H1'**	3.17	7.08	9.12	3.91	5.95
22	**H2**	**8**	**H1'**	7.3	12.42	8.12	5.12	0.82
22	**H2**	**21**	**H2**	4.62	8.71	2.51	4.09	-2.11
22	**H2**	**22**	**H1'**	4.55	4.7	4.58	0.15	0.03
22	**H2**	**22**	**H2'**	5.77	4.78	5.13	-0.99	-0.64
22	**H2**	**23**	**H1'**	4.52	3.76	3.82	-0.76	-0.7
22	**H2'**	**22**	**H4'**	3.87	3.65	3.78	-0.22	-0.09
22	**H2'**	**22**	**H5''**	4.57	4.71	4.92	0.14	0.35
22	**H3'**	**22**	**H4'**	2.99	2.95	3.01	-0.04	0.02
22	**H3'**	**22**	**H5''**	2.96	2.65	2.95	-0.31	-0.01
22	**H3'**	**22**	**H5'**	2.39	3.67	3.59	1.28	1.2
22	**H8**	**6**	**H2**	4.81	8.07	8.54	3.26	3.73
22	**H8**	**21**	**H1'**	5.39	4.6	2.37	-0.79	-3.02
22	**H8**	**21**	**H2'**	3.47	2.35	4.92	-1.12	1.45
22	**H8**	**21**	**H3'**	3.76	4.31	4.5	0.55	0.74
22	**H8**	**21**	**H4'**	6.22	5.8	3.74	-0.42	-2.48
22	**H8**	**21**	**H5''**	5.31	6.88	5.88	1.57	0.57
22	**H8**	**21**	**H5'**	6.88	7.55	5.93	0.67	-0.95
22	**H8**	**21**	**H8**	6.04	5.29	6.08	-0.75	0.04
22	**H8**	**22**	**H1'**	3.83	3.74	3.75	-0.09	-0.08
22	**H8**	**22**	**H2'**	3.12	4.12	4.09	1	0.97
22	**H8**	**22**	**H3'**	3.26	3.26	2.87	0	-0.39
22	**H8**	**22**	**H4'**	4.65	4.36	4.48	-0.29	-0.17
22	**H8**	**22**	**H5''**	3.36	4.36	4.61	1	1.25
22	**H8**	**22**	**H5'**	4.41	4.26	4.23	-0.15	-0.18
22	**H8**	**23**	**H5'**	7.39	7.26	6.04	-0.13	-1.35
22	**H8**	**23**	**H8**	5.24	5.3	4.11	0.06	-1.13
23	**H1'**	**22**	**H1'**	4.53	5.31	5.65	0.78	1.12
23	**H1'**	**22**	**H2'**	5.19	3.97	4.1	-1.22	-1.09
23	**H1'**	**23**	**H2'**	2.81	2.71	2.85	-0.1	0.04
23	**H1'**	**23**	**H3'**	3.87	3.67	3.95	-0.2	0.08
23	**H1'**	**23**	**H4'**	3.39	3.25	2.9	-0.14	-0.49
23	**H1'**	**23**	**H5''**	5.19	5.09	5.06	-0.1	-0.13
23	**H1'**	**23**	**H5'**	4.71	4.86	4.49	0.15	-0.22
23	**H3'**	**23**	**H2'**	2.41	2.17	2.32	-0.24	-0.09
23	**H8**	**6**	**H2**	6.92	7.33	7.03	0.41	0.11
23	**H8**	**22**	**H1'**	3.95	4.9	5.51	0.95	1.56

23	**H8**	**22**	**H2'**	2.18	2.1	3.61	-0.08	1.43
23	**H8**	**22**	**H3'**	4.05	3.26	3.73	-0.79	-0.32
23	**H8**	**22**	**H4'**	5.05	5.45	6.56	0.4	1.51
23	**H8**	**22**	**H5''**	6.53	5.79	6.56	-0.74	0.03
23	**H8**	**23**	**H1'**	3.79	3.89	3.75	0.1	-0.04
23	**H8**	**23**	**H2'**	3.74	3.76	3.65	0.02	-0.09
23	**H8**	**23**	**H3'**	2.69	2.98	3.27	0.29	0.58
23	**H8**	**23**	**H4'**	4.27	4.56	4.5	0.29	0.23
23	**H8**	**23**	**H5''**	3.96	4.3	4.93	0.34	0.97
23	**H8**	**23**	**H5'**	3.91	4.21	4.53	0.3	0.62
23	**H8**	**24**	**H5**	4.4	5.14	4.21	0.74	-0.19
23	**H8**	**24**	**H6**	5.09	5.81	5.51	0.72	0.42
24	**H1'**	**23**	**H2'**	4.22	5.2	4.05	0.98	-0.17
24	**H1'**	**24**	**H2'**	2.83	2.86	2.78	0.03	-0.05
24	**H1'**	**24**	**H3'**	3.88	3.85	3.73	-0.03	-0.15
24	**H1'**	**24**	**H4'**	3.3	3.26	3.15	-0.04	-0.15
24	**H1'**	**24**	**H5''**	5.15	5.24	5.12	0.09	-0.03
24	**H5**	**23**	**H1'**	5.8	5	5.73	-0.8	-0.07
24	**H5**	**23**	**H2'**	3.53	3.09	3.19	-0.44	-0.34
24	**H5**	**23**	**H3'**	3.9	4.64	3.37	0.74	-0.53
24	**H5**	**23**	**H4'**	6.69	6.83	6.13	0.14	-0.56
24	**H5**	**24**	**H2'**	5.2	4.89	5.16	-0.31	-0.04
24	**H5**	**24**	**H3'**	4.66	4.45	4.22	-0.21	-0.44
24	**H5**	**24**	**H5''**	6.07	6.33	6.12	0.26	0.05
24	**H6**	**23**	**H1'**	4.89	4.33	5.49	-0.56	0.6
24	**H6**	**23**	**H2'**	2.19	2.29	2.67	0.1	0.48
24	**H6**	**23**	**H3'**	3.61	4.21	3.66	0.6	0.05
24	**H6**	**23**	**H4'**	5.72	5.69	5.8	-0.03	0.08
24	**H6**	**24**	**H1'**	3.59	3.58	3.74	-0.01	0.15
24	**H6**	**24**	**H2'**	3.7	3.55	3.53	-0.15	-0.17
24	**H6**	**24**	**H3'**	2.74	2.66	2.1	-0.08	-0.64
24	**H6**	**24**	**H4'**	4.07	4.07	4.01	0	-0.06
24	**H6**	**24**	**H5**	2.41	2.39	2.3	-0.02	-0.11
24	**H6**	**24**	**H5''**	3.89	4.16	3.99	0.27	0.1
24	**H6**	**25**	**H5**	5.1	4.67	3.49	-0.43	-1.61
25	**H1'**	**24**	**H1'**	5.02	5.75	6.17	0.73	1.15
25	**H1'**	**24**	**H2'**	3.9	4.64	4.37	0.74	0.47
25	**H1'**	**25**	**H2'**	2.79	2.93	2.93	0.14	0.14
25	**H1'**	**25**	**H3'**	3.86	3.85	3.66	-0.01	-0.2
25	**H1'**	**25**	**H4'**	3.46	3.22	2.94	-0.24	-0.52
25	**H1'**	**25**	**H5''**	5.18	5.14	4.96	-0.04	-0.22
25	**H1'**	**26**	**H1'**	5.37	5.8	5.64	0.43	0.27
25	**H5**	**24**	**H2'**	3.4	2.8	3.82	-0.6	0.42
25	**H5**	**24**	**H3'**	3.83	4.11	4.09	0.28	0.26
25	**H5**	**24**	**H5**	5.43	4.6	3.11	-0.83	-2.32
25	**H5**	**25**	**H2'**	5.32	4.84	4.73	-0.48	-0.59
25	**H5**	**25**	**H3'**	4.52	4.78	4.44	0.26	-0.08
25	**H5**	**26**	**H5**	4.48	4.18	3.8	-0.3	-0.68

25	**H6**	**24**	**H1'**	4.93	4.88	4.33	-0.05	-0.6
25	**H6**	**24**	**H2'**	2.19	2.28	1.98	0.09	-0.21
25	**H6**	**24**	**H3'**	3.61	3.92	3.3	0.31	-0.31
25	**H6**	**24**	**H6**	5.47	5.61	3.93	0.14	-1.54
25	**H6**	**25**	**H1'**	3.57	3.48	3.66	-0.09	0.09
25	**H6**	**25**	**H2'**	3.82	3.26	3.58	-0.56	-0.24
25	**H6**	**25**	**H3'**	2.7	2.64	2.71	-0.06	0.01
25	**H6**	**25**	**H4'**	3.92	4.06	4.27	0.14	0.35
25	**H6**	**25**	**H5**	2.41	2.54	2.41	0.13	0
25	**H6**	**25**	**H5''**	3.55	3.9	4.47	0.35	0.92
25	**H6**	**26**	**H5**	4.23	4.13	4.25	-0.1	0.02
25	**H6**	**26**	**H6**	5.06	5.24	5.18	0.18	0.12
26	**H1'**	**25**	**H2'**	3.61	4.64	4.26	1.03	0.65
26	**H1'**	**26**	**H2'**	2.78	2.84	2.82	0.06	0.04
26	**H1'**	**26**	**H3'**	3.87	3.68	3.91	-0.19	0.04
26	**H1'**	**26**	**H4'**	3.51	3.19	3.35	-0.32	-0.16
26	**H1'**	**26**	**H5''**	5.19	5.05	5.23	-0.14	0.04
26	**H1'**	**26**	**H5'**	4.78	4.48	4.88	-0.3	0.1
26	**H1'**	**27**	**H1'**	6.67	5.54	6.87	-1.13	0.2
26	**H1'**	**27**	**H4'**	7.24	6.21	6.6	-1.03	-0.64
26	**H3'**	**26**	**H2'**	2.41	2.28	2.45	-0.13	0.04
26	**H5**	**25**	**H2'**	3.48	2.76	3	-0.72	-0.48
26	**H5**	**25**	**H3'**	3	4.02	3.72	1.02	0.72
26	**H5**	**26**	**H2'**	5.4	5.32	5.4	-0.08	0
26	**H5**	**26**	**H3'**	4.59	4.72	4.97	0.13	0.38
26	**H5**	**26**	**H5''**	5.56	6.43	6.15	0.87	0.59
26	**H5**	**27**	**H5**	4.22	3.63	3.83	-0.59	-0.39
26	**H6**	**25**	**H1'**	4.97	5.02	4.86	0.05	-0.11
26	**H6**	**25**	**H2'**	2.19	2.31	2.04	0.12	-0.15
26	**H6**	**25**	**H3'**	2.97	3.95	3.58	0.98	0.61
26	**H6**	**26**	**H1'**	3.54	3.6	3.45	0.06	-0.09
26	**H6**	**26**	**H2'**	3.94	3.61	3.82	-0.33	-0.12
26	**H6**	**26**	**H3'**	2.85	2.51	2.99	-0.34	0.14
26	**H6**	**26**	**H4'**	3.89	4.19	4.1	0.3	0.21
26	**H6**	**26**	**H5**	2.44	2.45	2.42	0.01	-0.02
26	**H6**	**26**	**H5''**	3.52	4.11	3.96	0.59	0.44
26	**H6**	**26**	**H5'**	3.38	3.93	3.89	0.55	0.51
26	**H6**	**27**	**H5**	4.03	3.64	4.29	-0.39	0.26
26	**H6**	**27**	**H6**	5.4	4.5	4.65	-0.9	-0.75
27	**H1'**	**26**	**H2'**	4.62	4.01	4.74	-0.61	0.12
27	**H1'**	**27**	**H2'**	2.79	2.8	3.04	0.01	0.25
27	**H1'**	**27**	**H3'**	3.86	3.66	3.71	-0.2	-0.15
27	**H1'**	**27**	**H4'**	3.48	3.27	2.94	-0.21	-0.54
27	**H1'**	**27**	**H5'**	4.62	4.67	4.67	0.05	0.05
27	**H1'**	**27**	**H5''**	5.22	5.09	4.87	-0.13	-0.35
27	**H3'**	**27**	**H2'**	2.41	2.43	2.4	0.02	-0.01
27	**H5**	**26**	**H2'**	2.98	3.73	4.14	0.75	1.16
27	**H5**	**26**	**H3'**	2.9	3.84	4.48	0.94	1.58

27	**H5**	**27**	**H1'**	5.33	5.27	5.35	-0.06	0.02
27	**H5**	**27**	**H2'**	5.28	5.25	4.13	-0.03	-1.15
27	**H5**	**27**	**H3'**	4.49	4.43	6.48	-0.06	1.99
27	**H6**	**26**	**H1'**	5.02	4.94	4.9	-0.08	-0.12
27	**H6**	**26**	**H2'**	2.25	2.29	2.43	0.04	0.18
27	**H6**	**26**	**H3'**	3.22	3.34	3.47	0.12	0.25
27	**H6**	**27**	**H1'**	3.59	3.65	3.69	0.06	0.1
27	**H6**	**27**	**H2'**	3.77	3.7	2.32	-0.07	-1.45
27	**H6**	**27**	**H3'**	2.62	2.32	4.39	-0.3	1.77
27	**H6**	**27**	**H4'**	3.89	4.11	4.69	0.22	0.8
27	**H6**	**27**	**H5**	2.44	2.45	2.37	0.01	-0.07
27	**H6**	**27**	**H5''**	3.69	3.94	4.85	0.25	1.16
27	**H6**	**27**	**H5'**	3.2	3.76	4.26	0.56	1.06
1	**H1'**	**1**	**H1**	5.99	6.17	6.15	0.18	0.16
2	**H1**	**1**	**H1**	4.3	4.14	4.44	-0.16	0.14
2	**H1'**	**1**	**H1**	5.42	5.01	4.85	-0.41	-0.57
2	**H2'**	**2**	**H1**	5.72	5.68	5.75	-0.04	0.03
2	**H21**	**2**	**H1**	2.19	2.23	2.35	0.04	0.16
2	**H22**	**2**	**H1**	3.46	3.56	3.57	0.1	0.11
3	**H2**	**2**	**H1**	4.52	4.04	4.27	-0.48	-0.25
3	**H2**	**25**	**H3**	2.66	2.83	2.49	0.17	-0.17
3	**H61**	**25**	**H3**	2.71	2.35	2.84	-0.36	0.13
3	**H62**	**2**	**H1**	4.83	4.01	4.15	-0.82	-0.68
3	**H62**	**3**	**H61**	1.75	1.8	1.75	0.05	0
3	**H62**	**25**	**H3**	4.2	4.03	4.36	-0.17	0.16
4	**H1'**	**25**	**H3**	6.65	4.41	5.3	-2.24	-1.35
4	**H2**	**5**	**H3**	5.44	5.05	4.48	-0.39	-0.96
4	**H2**	**23**	**H1**	5.04	5.47	4.15	0.43	-0.89
4	**H2**	**24**	**H3**	2.83	2.79	3.27	-0.04	0.44
4	**H2**	**25**	**H3**	4.63	3.62	4.17	-1.01	-0.46
4	**H61**	**24**	**H3**	2.66	3.79	2.46	1.13	-0.2
4	**H61**	**25**	**H3**	5.13	5.03	4.38	-0.1	-0.75
4	**H62**	**4**	**H61**	1.75	1.75	1.78	0	0.03
4	**H62**	**5**	**H3**	4.81	3.55	3.81	-1.26	-1
4	**H62**	**23**	**H1**	5.92	5.75	5.87	-0.17	-0.05
4	**H62**	**24**	**H3**	4.19	5.36	4.14	1.17	-0.05
5	**H3**	**23**	**H1**	2.14	4.1	2.82	1.96	0.68
6	**H1'**	**23**	**H1**	5.15	6.78	6.67	1.63	1.52
6	**H8**	**5**	**H3**	5.98	7.1	7.67	1.12	1.69
6	**H8**	**8**	**H1**	12.35	15.95	13.73	3.6	1.38
8	**H21**	**8**	**H1**	2.19	2.18	2.09	-0.01	-0.1
8	**H22**	**8**	**H1**	3.46	3.51	3.42	0.05	-0.04
8	**H22**	**8**	**H1**	3.46	3.51	3.42	0.05	-0.04
9	**H1'**	**8**	**H1**	7.02	5.39	5.7	-1.63	-1.32
9	**H41**	**8**	**H1**	3.7	3.19	3.63	-0.51	-0.07
9	**H41**	**10**	**H3**	4.99	4.13	4.46	-0.86	-0.53
9	**H41**	**18**	**H1**	1.84	1.83	2.64	-0.01	0.8
9	**H41**	**19**	**H41**	4.12	3.23	3.43	-0.89	-0.69

9	**H42**	**9**	**H41**	1.75	1.7	1.77	-0.05	0.02
9	**H42**	**10**	**H3**	6.01	5.07	5.44	-0.94	-0.57
9	**H42**	**18**	**H1**	3.43	3.4	4.21	-0.03	0.78
9	**H5**	**8**	**H1**	5.71	4.23	6.26	-1.48	0.55
9	**H5**	**9**	**H41**	3.68	3.59	3.66	-0.09	-0.02
9	**H5**	**9**	**H42**	2.43	2.35	2.43	-0.08	0
9	**H5**	**18**	**H1**	4.7	4.69	5.17	-0.01	0.47
9	**H6**	**9**	**H41**	5.36	5.34	5.3	-0.02	-0.06
9	**H6**	**18**	**H1**	5.65	5.75	5.9	0.1	0.25
10	**H3**	**16**	**H1**	4.76	4.2	4.71	-0.56	-0.05
10	**H3**	**18**	**H1**	4.28	3.66	3.36	-0.62	-0.92
10	**H5**	**10**	**H3**	4.2	4.19	4.19	-0.01	-0.01
10	**H6**	**18**	**H1**	6.59	5.18	5.61	-1.41	-0.98
11	**H2'**	**16**	**H1**	4.94	5.51	5.35	0.57	0.41
11	**H41**	**10**	**H3**	4.42	2.83	4.31	-1.59	-0.11
11	**H41**	**12**	**H3**	3.76	4.37	2.57	0.61	-1.19
11	**H41**	**16**	**H1**	3.01	2.33	2.62	-0.68	-0.39
11	**H42**	**10**	**H3**	4.36	3.24	4.07	-1.12	-0.29
11	**H42**	**11**	**H41**	1.75	1.76	1.75	0.01	0
11	**H42**	**12**	**H3**	3.67	4.61	3.33	0.94	-0.34
11	**H42**	**16**	**H1**	4.48	3.89	4.09	-0.59	-0.39
11	**H5**	**10**	**H3**	4.02	4.6	4.11	0.58	0.09
11	**H5**	**11**	**H41**	3.68	3.75	3.73	0.07	0.05
11	**H5**	**11**	**H42**	2.43	2.61	2.43	0.18	0
11	**H5**	**12**	**H3**	4.81	5.04	4.77	0.23	-0.04
11	**H5**	**16**	**H1**	5.34	4.97	5.15	-0.37	-0.19
11	**H6**	**11**	**H41**	5.37	5.32	5.45	-0.05	0.08
12	**H1'**	**12**	**H3**	4.64	4.34	4.31	-0.3	-0.33
12	**H1'**	**15**	**H1**	3.76	3.15	2.24	-0.61	-1.52
12	**H1'**	**15**	**H21**	4.93	5.14	3.93	0.21	-1
12	**H1'**	**16**	**H1**	3.24	4.91	4.59	1.67	1.35
12	**H1'**	**16**	**H21**	3.48	3.37	3.91	-0.11	0.43
12	**H1'**	**16**	**H22**	4.47	3.57	4.31	-0.9	-0.16
12	**H2'**	**15**	**H1**	3.67	3.73	4.29	0.06	0.62
12	**H2'**	**15**	**H21**	5.23	5.28	5.19	0.05	-0.04
12	**H2'**	**16**	**H1**	5.7	6.72	6.85	1.02	1.15
12	**H3**	**15**	**H1**	5.11	3.69	4.14	-1.42	-0.97
12	**H5**	**12**	**H3**	4.2	4.3	4.26	0.1	0.06
12	**H5**	**16**	**H1**	6.74	6.43	6.14	-0.31	-0.6
12	**H6**	**12**	**H3**	4.77	4.75	4.79	-0.02	0.02
13	**H2'**	**15**	**H1**	3.81	4.93	4.24	1.12	0.43
13	**H3'**	**15**	**H1**	5.46	4.67	5.65	-0.79	0.19
14	**H1'**	**12**	**H3**	5.32	5.34	4.27	0.02	-1.05
14	**H1'**	**15**	**H1**	4.51	4.93	4.72	0.42	0.21
14	**H2'**	**15**	**H1**	5.93	6.15	6.82	0.22	0.89
14	**H41**	**14**	**H42**	1.75	1.75	1.77	0	0.02
14	**H5**	**12**	**H3**	5.32	4.56	6.94	-0.76	1.62
14	**H5**	**14**	**H41**	3.68	3.61	3.7	-0.07	0.02

14	**H5**	**14**	**H42**	2.42	2.4	2.33	-0.02	-0.09
14	**H5**	**15**	**H1**	4.82	4.85	6.18	0.03	1.36
14	**H5**	**15**	**H21**	6.12	5.57	6.55	-0.55	0.43
14	**H6**	**15**	**H1**	4.41	4	5.32	-0.41	0.91
15	**H1'**	**15**	**H1**	6.98	7.09	7.07	0.11	0.09
15	**H2'**	**15**	**H1**	5.74	5.66	6.77	-0.08	1.03
15	**H21**	**12**	**H3**	4.72	3.32	2.88	-1.4	-1.84
15	**H21**	**13**	**H6**	7.01	8.45	7.69	1.44	0.68
15	**H21**	**15**	**H1**	2.18	2.33	2.31	0.15	0.13
15	**H21**	**16**	**H1**	4.49	5.15	4.45	0.66	-0.04
16	**H1**	**12**	**H3**	5.49	4.12	3.72	-1.37	-1.77
16	**H1**	**15**	**H1**	4.56	5.04	4.51	0.48	-0.05
16	**H21**	**16**	**H1**	2.2	2.36	2.07	0.16	-0.13
16	**H22**	**15**	**H1**	5.74	3.84	4.35	-1.9	-1.39
16	**H22**	**16**	**H1**	3.46	3.5	3.32	0.04	-0.14
16	**H22**	**16**	**H21**	1.75	1.74	1.76	-0.01	0.01
16	**H2'**	**16**	**H1**	5.91	6.17	5.23	0.26	-0.68
16	**H8**	**15**	**H1**	5.18	6.5	5.71	1.32	0.53
17	**H1'**	**16**	**H1**	5.43	4.6	4.53	-0.83	-0.9
17	**H1'**	**16**	**H21**	4.24	3.95	3.55	-0.29	-0.69
17	**H2**	**10**	**H3**	3	3.17	2.91	0.17	-0.09
17	**H2**	**16**	**H1**	4.8	3.57	4.45	-1.23	-0.35
17	**H2**	**18**	**H1**	5.07	5.47	5.26	0.4	0.19
17	**H2'**	**16**	**H1**	6.98	5.88	6.21	-1.1	-0.77
17	**H61**	**10**	**H3**	2.44	2.4	2.43	-0.04	-0.01
17	**H62**	**10**	**H3**	4	3.89	3.96	-0.11	-0.04
17	**H8**	**16**	**H1**	5.42	5.53	4.86	0.11	-0.56
18	**H1**	**8**	**H1**	3.76	3.51	3.43	-0.25	-0.33
18	**H21**	**18**	**H1**	2.19	2.25	2.37	0.06	0.18
18	**H22**	**18**	**H1**	3.46	3.57	3.53	0.11	0.07
18	**H22**	**18**	**H21**	1.75	1.8	1.76	0.05	0.01
18	**H8**	**8**	**H1**	7.01	8.58	7.8	1.57	0.79
19	**H1'**	**8**	**H1**	5.69	5.1	5.11	-0.59	-0.58
19	**H41**	**8**	**H1**	1.95	2.68	2.33	0.73	0.38
19	**H41**	**18**	**H1**	4.39	4.14	4.04	-0.25	-0.35
19	**H42**	**8**	**H1**	3.6	4.21	3.77	0.61	0.17
19	**H42**	**19**	**H41**	1.75	1.78	1.74	0.03	-0.01
19	**H5**	**8**	**H1**	4.93	5.13	4.9	0.2	-0.03
19	**H5**	**18**	**H1**	6.22	4.48	5.86	-1.74	-0.36
19	**H5**	**19**	**H41**	3.68	3.69	3.74	0.01	0.06
19	**H5**	**19**	**H42**	2.42	2.44	2.47	0.02	0.05
19	**H6**	**8**	**H1**	5.91	5.7	5.68	-0.21	-0.23
19	**H6**	**18**	**H1**	6.9	4.94	6.43	-1.96	-0.47
19	**H6**	**19**	**H41**	5.37	5.26	5.44	-0.11	0.07
20	**H5**	**8**	**H1**	5.75	5.46	7.37	-0.29	1.62
20	**H6**	**8**	**H1**	6.23	4.88	8.3	-1.35	2.07
22	**H2**	**5**	**H3**	4.37	6.65	8.72	2.28	4.35
22	**H2**	**23**	**H1**	3.03	4.63	7.08	1.6	4.05

23	**H21**	**5**	**H3**	4.12	3.63	5.1	-0.49	0.98
23	**H21**	**23**	**H1**	2.19	2.27	2.36	0.08	0.17
23	**H21**	**24**	**H3**	4.88	3.17	4.42	-1.71	-0.46
24	**H3**	**23**	**H1**	4.23	3.81	3.36	-0.42	-0.87
24	**H3**	**25**	**H3**	4.5	3.96	4.52	-0.54	0.02
24	**H5**	**23**	**H1**	6.01	4.3	6.75	-1.71	0.74
24	**H5**	**24**	**H3**	4.2	4.21	4.26	0.01	0.06
25	**H1'**	**25**	**H3**	4.54	4.55	4.62	0.01	0.08
25	**H3**	**2**	**H1**	4.47	4.48	4.5	0.01	0.03
25	**H5**	**2**	**H1**	6.99	7.22	6.98	0.23	-0.01
26	**H1'**	**2**	**H1**	5.05	5.58	5.35	0.53	0.3
26	**H2'**	**2**	**H1**	4.97	5.66	5.4	0.69	0.43
26	**H41**	**1**	**H1**	5.06	5.13	5.5	0.07	0.44
26	**H41**	**2**	**H1**	3	2.13	2.23	-0.87	-0.77
26	**H41**	**25**	**H3**	4.55	3.27	3.74	-1.28	-0.81
26	**H42**	**2**	**H1**	4.49	3.53	3.88	-0.96	-0.61
26	**H42**	**25**	**H3**	5	3.73	3.92	-1.27	-1.08
26	**H42**	**26**	**H41**	1.75	1.72	1.82	-0.03	0.07
26	**H42**	**26**	**H6**	4.64	4.61	4.66	-0.03	0.02
26	**H5**	**2**	**H1**	5.38	4.81	5.04	-0.57	-0.34
26	**H5**	**26**	**H41**	3.68	3.62	3.73	-0.06	0.05
27	**H1'**	**1**	**H1**	5.04	5.04	4.77	0	-0.27
27	**H41**	**1**	**H1**	2.84	2.7	2.56	-0.14	-0.28
27	**H42**	**1**	**H1**	4.34	4.12	4.18	-0.22	-0.16
27	**H42**	**27**	**H41**	1.75	1.73	1.75	-0.02	0
27	**H42**	**27**	**H6**	4.64	4.74	4.92	0.1	0.28
27	**H5**	**1**	**H1**	5.27	4.93	5.21	-0.34	-0.06
27	**H5**	**2**	**H1**	4.93	4.77	4.38	-0.16	-0.55
27	**H5**	**27**	**H41**	3.68	3.65	3.84	-0.03	0.16
27	**H5**	**27**	**H42**	2.42	2.5	2.85	0.08	0.43
27	**H6**	**2**	**H1**	5.74	5.59	5.01	-0.15	-0.73

Appendix 15 Synthesis scheme of complex 12.

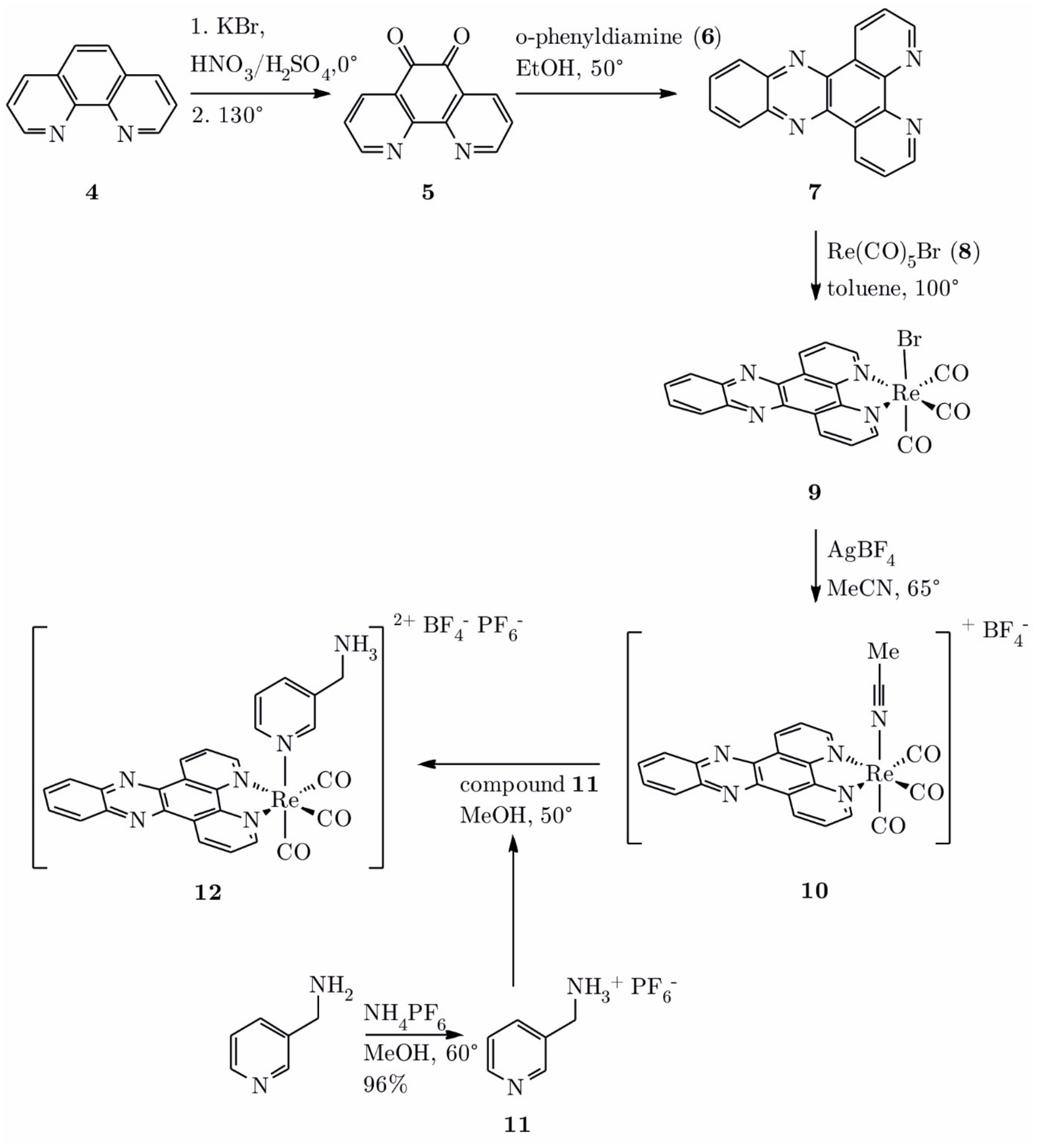

Appendix 16 ATR-IR of 1,10-phenanthroline-5,6-dione.

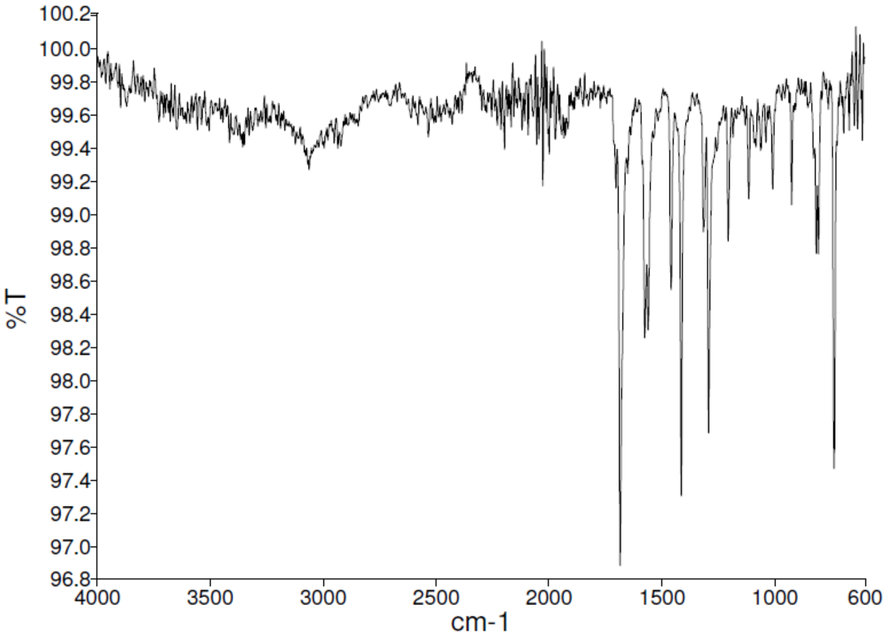

Appendix 17 ^{1}H NMR spectrum of 1,10-phenanthroline-5,6-dione ($CDCl_3$, 300 K, 300 MHz).

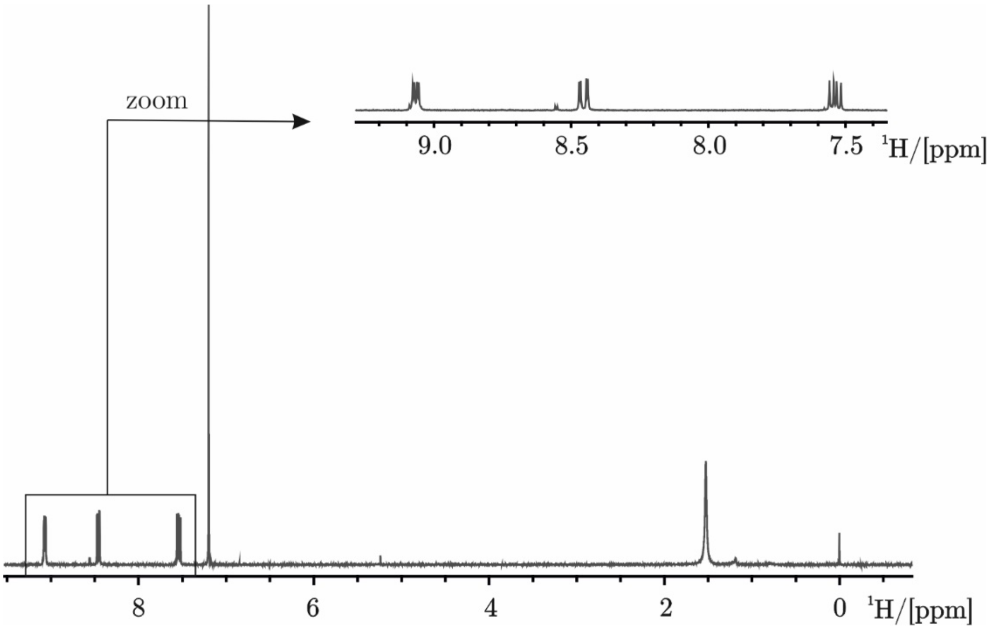

Appendix 18 ^{1}H NMR spectrum of dipyrido[3,2-a:2',3'-c]phenazine (CDCl$_3$, 300 K, 400 MHz).

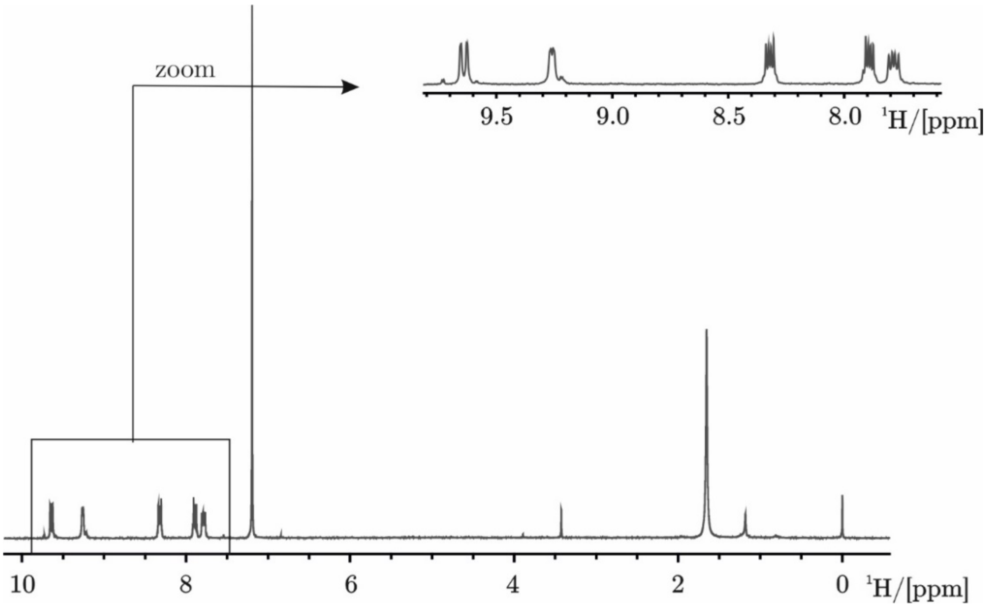

Appendix 19 ^{13}C NMR spectrum of dipyrido[3,2-a:2',3'-c]phenazine (CDCl$_3$, 300 K, 400 MHz).

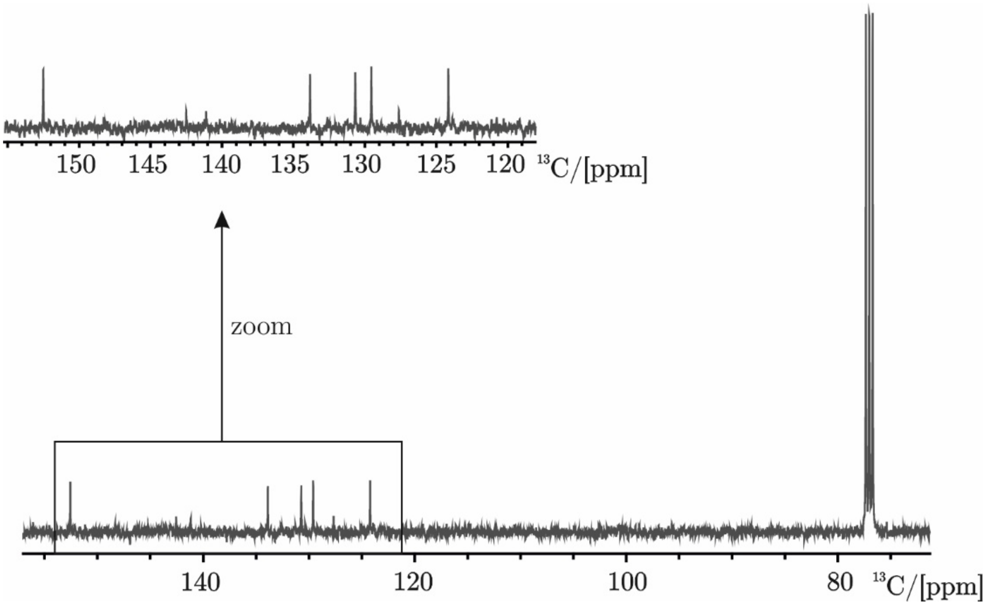

Appendix 20 ATR-IR of bromotricarbonyldipyrido[3,2a:2',3'c]phenazinerhenium(I).

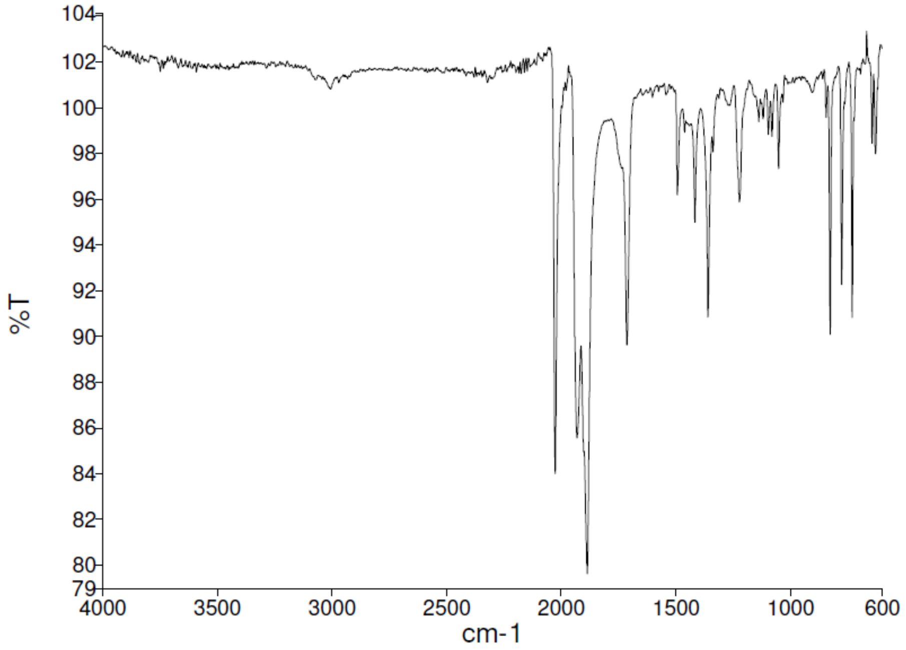

Appendix 21 ^{1}H NMR spectrum of bromotricarbonyldipyrido[3,2a:2',3'c] phenazinerhenium(I) (DMSO, 298 K, 300 MHz).

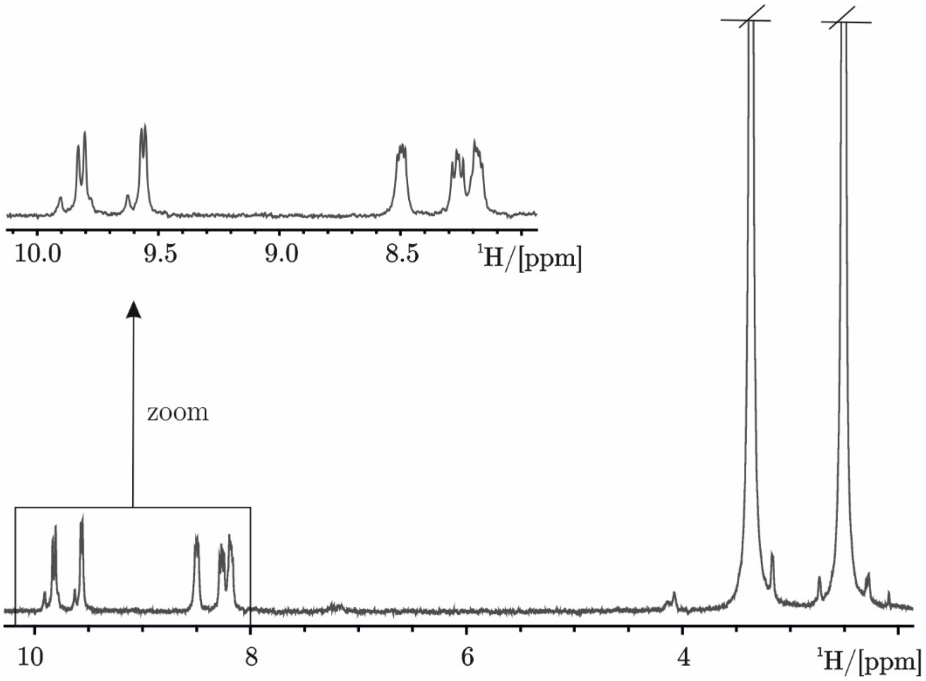

Appendix 22 ATR-IR of acetonitriletricarbonyldipyrido[3,2-a:2',3'c] phenazinerhenium(I)tetrafluoroborate.

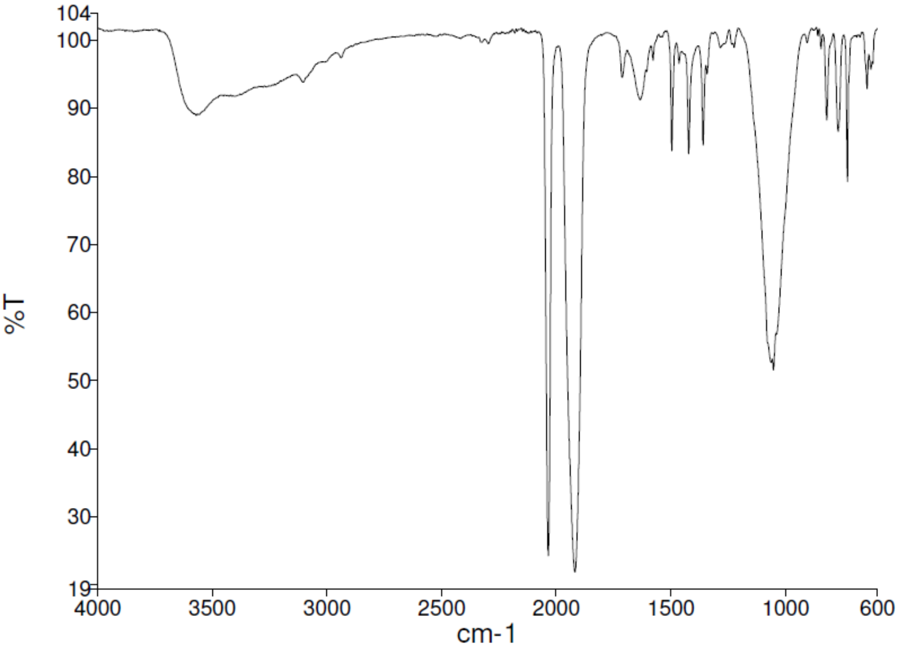

Appendix 23 ^{1}H NMR of acetonitriletricarbonyldipyrido[3,2-a:2',3'c] phenazinerhenium(I)tetrafluoroborate (CD_3CN, 300 K, 400 MHz).

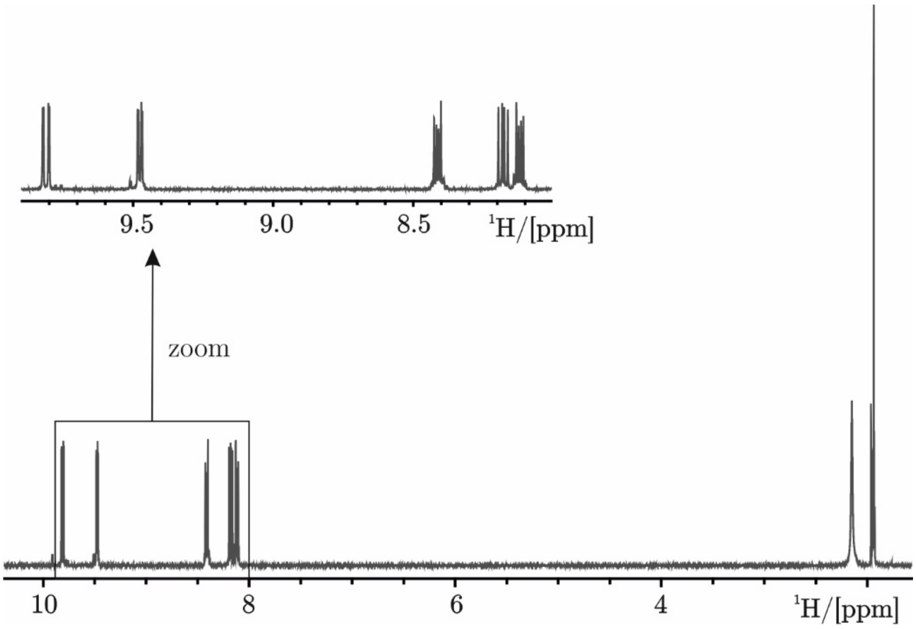

Appendix 24 ^{13}C NMR of acetonitriletricarbonyldipyrido[3,2-a:2',3'c] phenazinerhenium(I)tetrafluoroborate (CD_3CN, 300 K, 400 MHz).

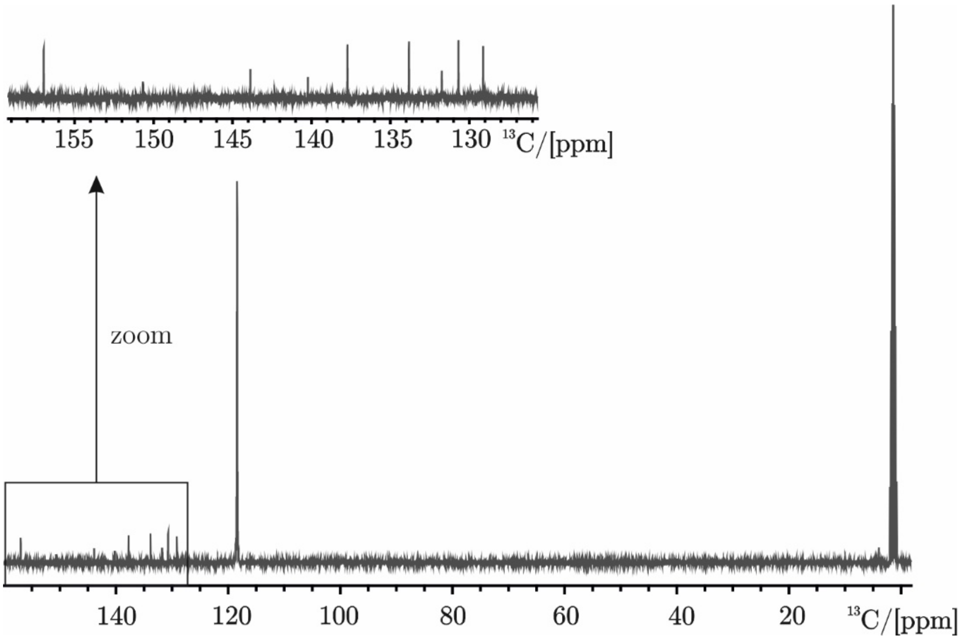

Appendix 25 [^{1}H,^{1}H]-COSY NMR of acetonitriletricarbonyldipyrido[3,2-a:2',3'c] phenazinerhenium(I)tetrafluoroborate (CD_3CN, 300 K, 400 MHz).

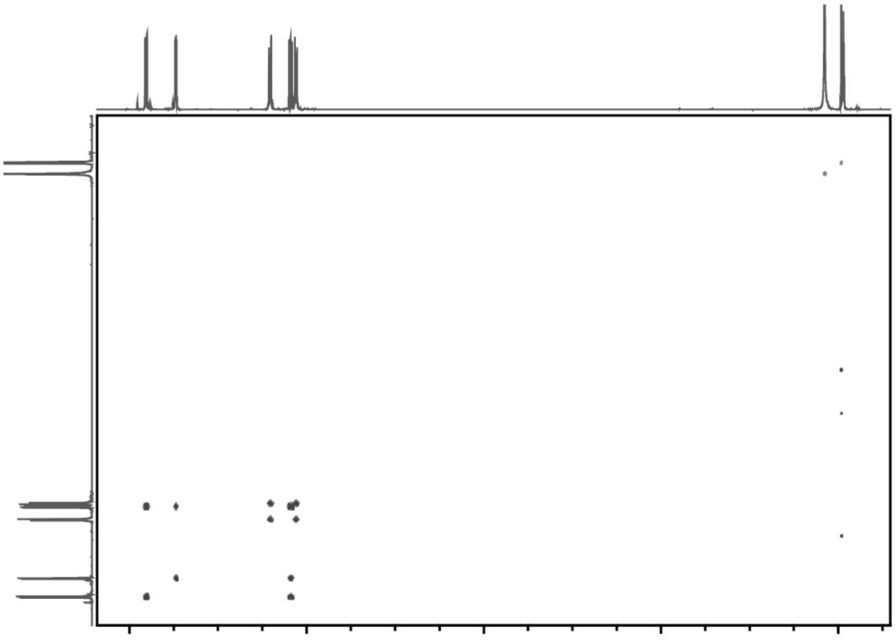

Appendix 26 [^{1}H,^{13}C]-HSQC NMR of acetonitriletricarbonyldipyrido[3,2-a:2',3'c] phenazinerhenium(I)tetrafluoroborate (CD_3CN, 300 K, 400 MHz).

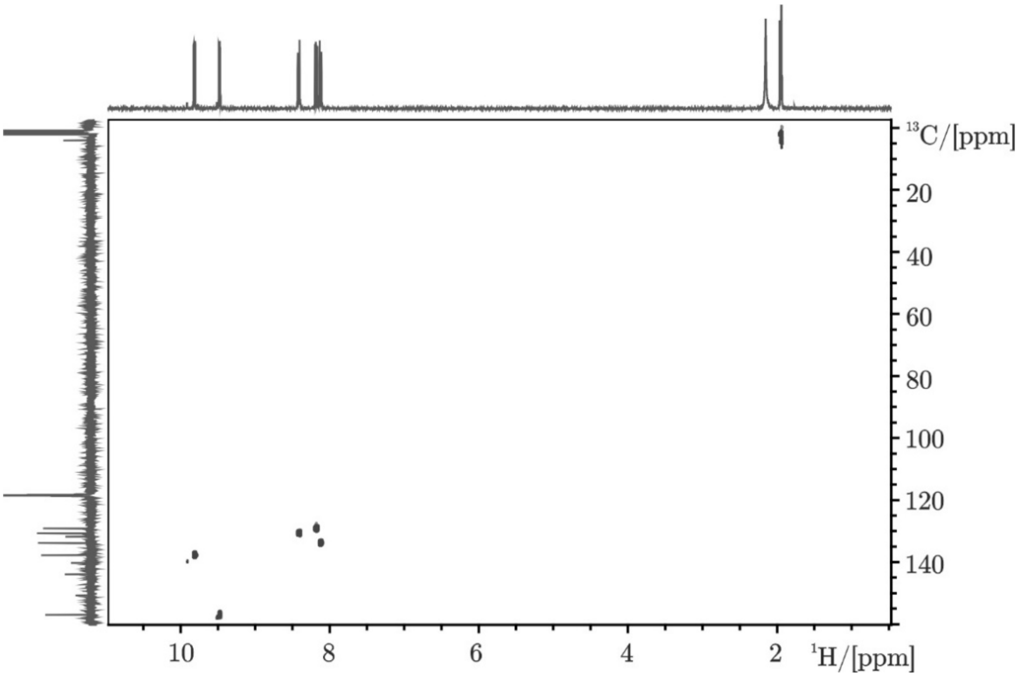

Appendix 27 [^{1}H,^{13}C]-HMBC NMR of acetonitriletricarbonyldipyrido[3,2-a:2',3'c] phenazinerhenium(I)tetrafluoroborate (CD_3CN, 300 K, 400 MHz).

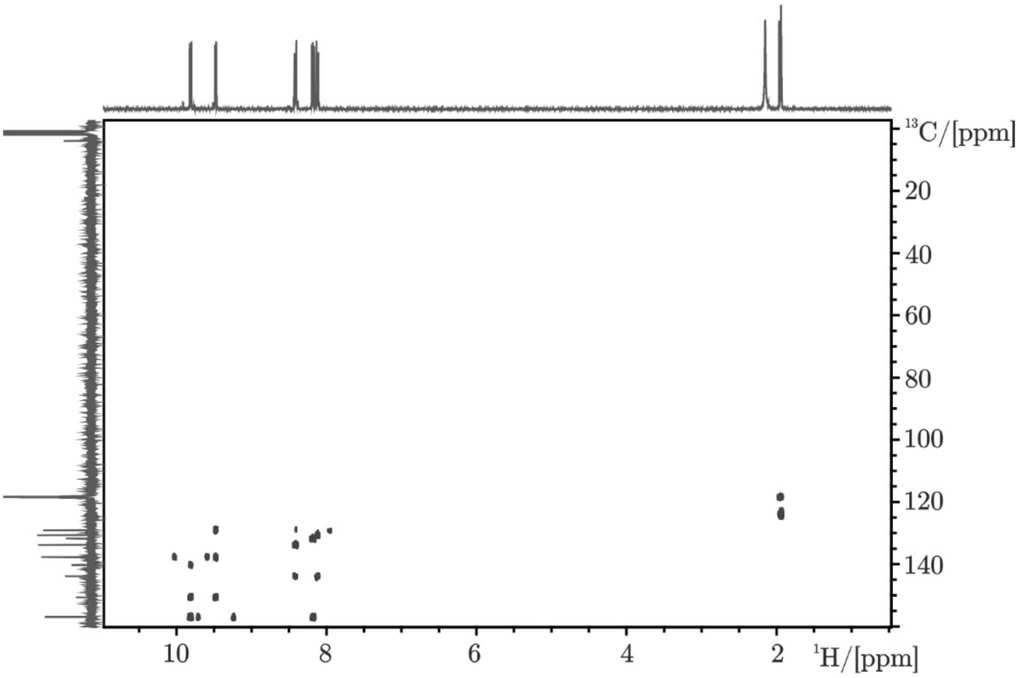

Appendix 28 ^{1}H NMR of 3-picolylammonium hexafluorophosphate (CD_3CN, 300 K, 400 MHz).

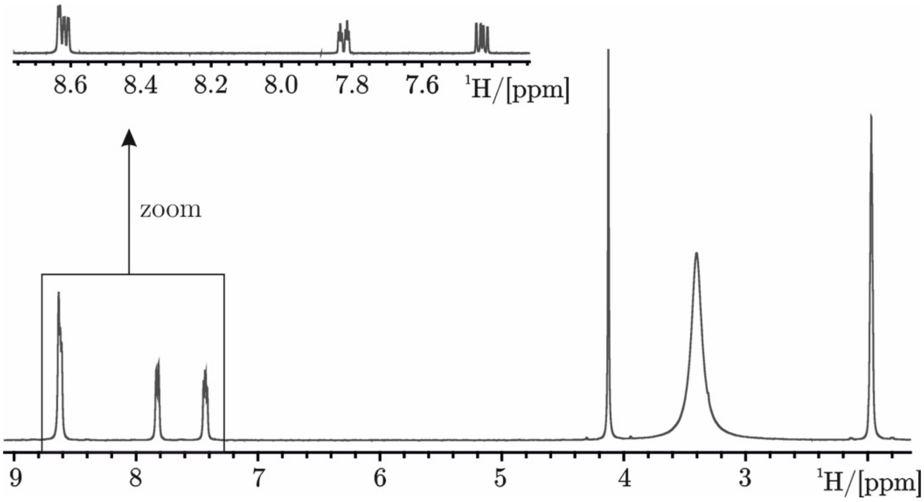

Appendix 29 ^{19}F NMR of 3-picolylammonium hexafluorophosphate (CD_3CN, 300 K, 400 MHz).

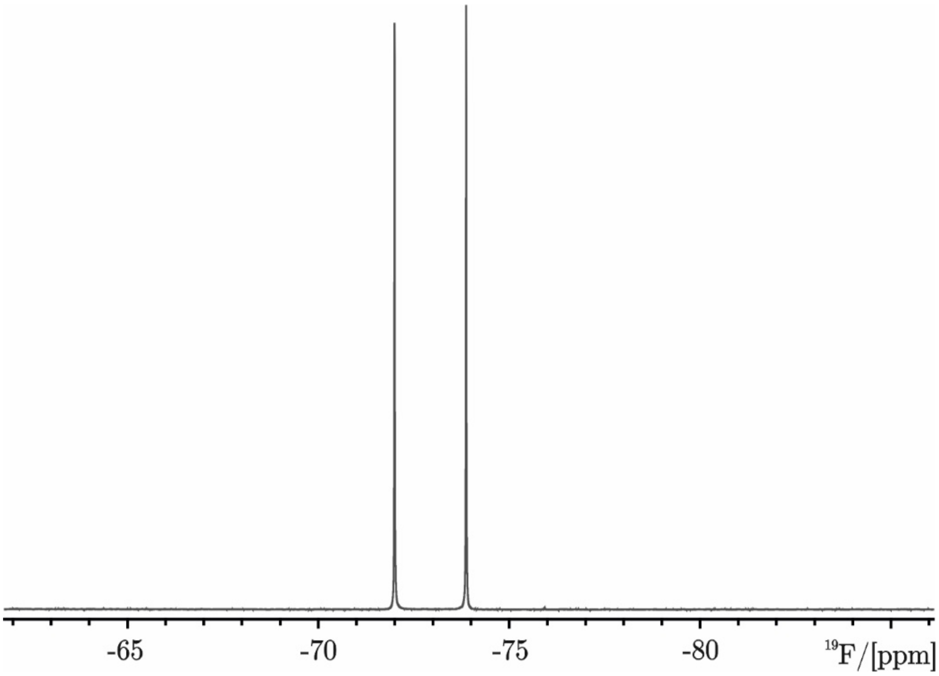

Appendix 30 ^{1}H NMR of 3-picolylammoniumtricarbonyldipyrido[3,2-*a*:2',3'*c*] phenazinerhenium(I)tetrafluoroboratehexafluorophosphate (CD_3CN, 300 K, 400 MHz).

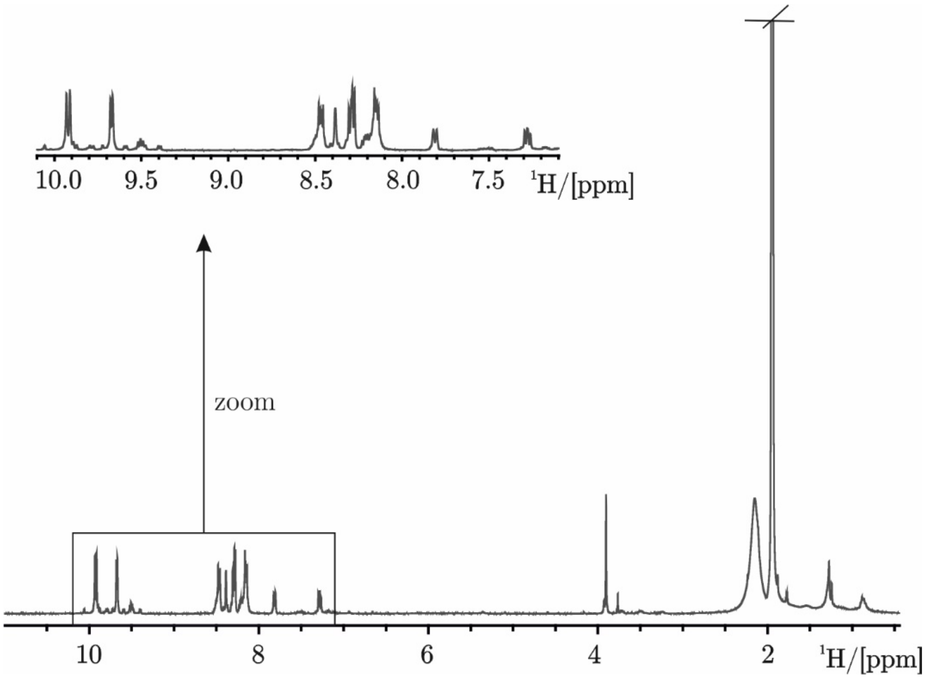

Appendix 31 [^{1}H,^{1}H]-COSY NMR of 3-picolylammoniumtricarbonyldipyrido [3,2-*a*:2',3'*c*]phenazinerhenium(I)tetrafluoroboratehexafluorophosphate (CD_3CN, 300 K, 400 MHz).

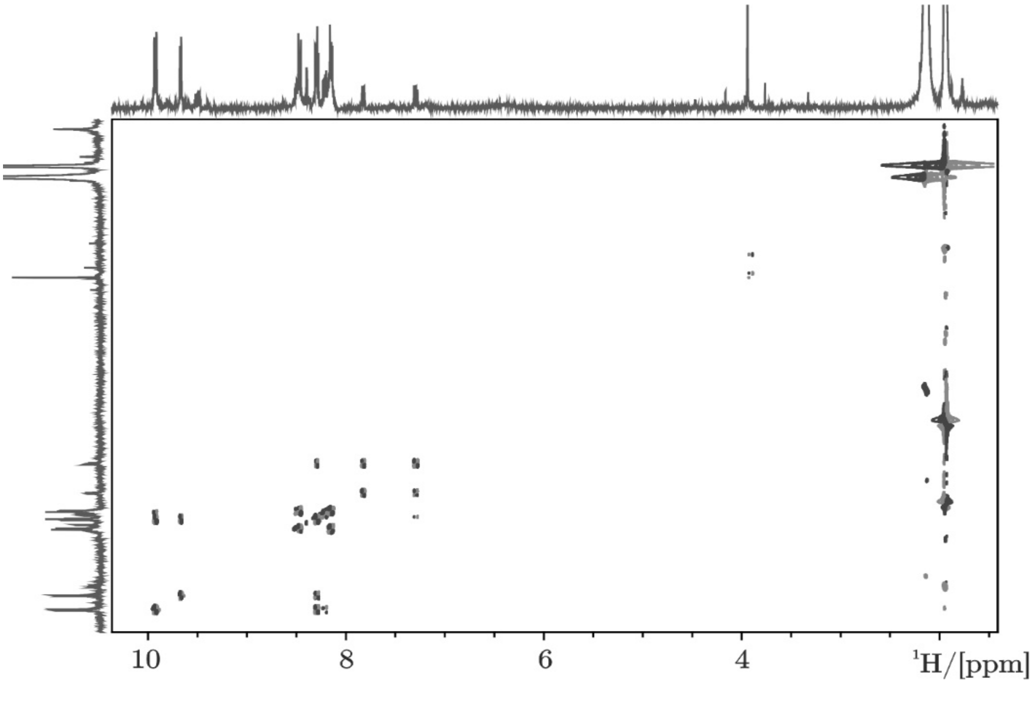

Appendix 32 [^{1}H,^{13}C]-HSQC NMR of 3-picolylammoniumtricarbonyldipyrido [3,2-*a*:2',3'*c*]phenazinerhenium(I)tetrafluoroboratehexafluorophosphate (CD_3CN, 300 K, 400 MHz).

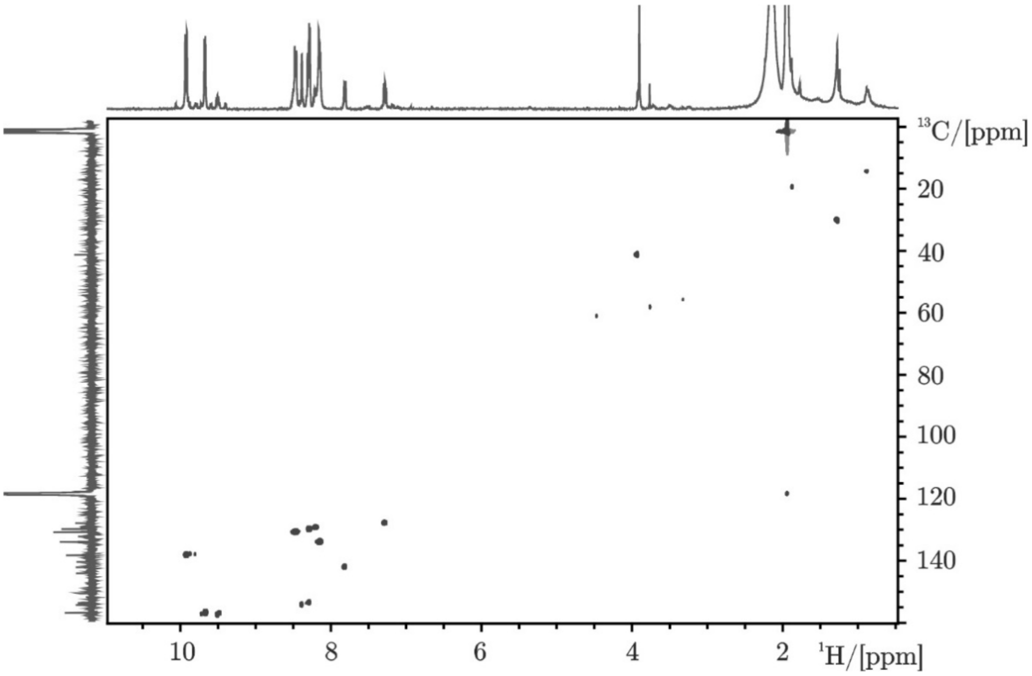

Appendix 33 [^{1}H,^{13}C]-HMBC NMR of 3-picolylammoniumtricarbonyldipyrido [3,2-*a*:2',3'*c*]phenazinerhenium(I)tetrafluoroboratehexafluorophosphate (CD_3CN, 300 K, 400 MHz).

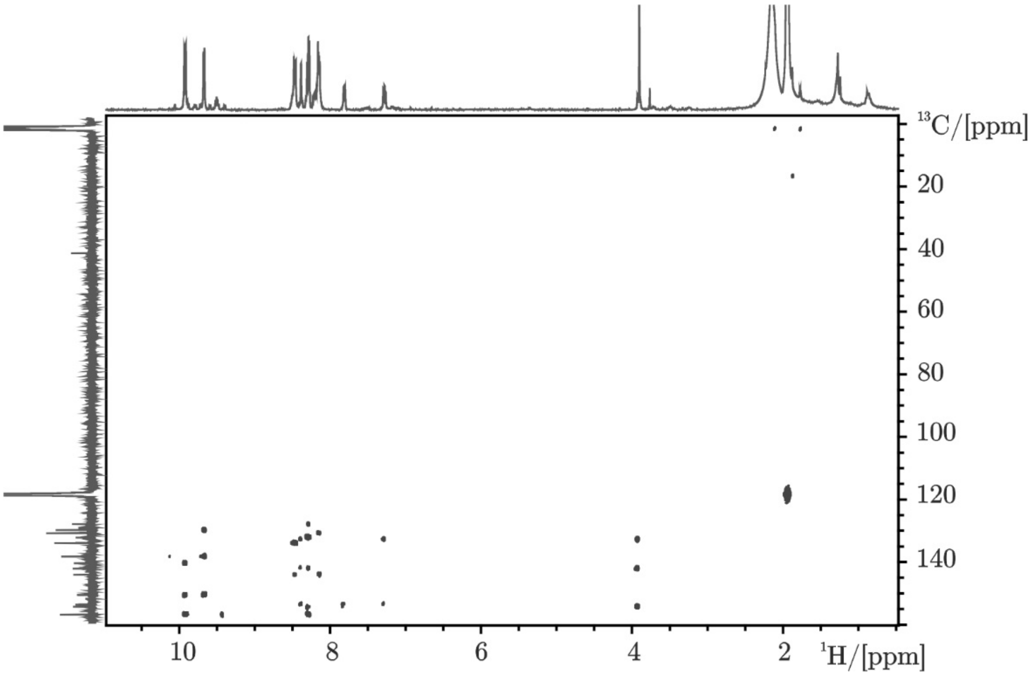

Appendix 34 MS (ES+) of 3-picolylammoniumtricarbonyldipyrido[3,2-*a*:2',3'*c*] phenazinerhenium(I)tetrafluoroboratehexafluorophosphate.

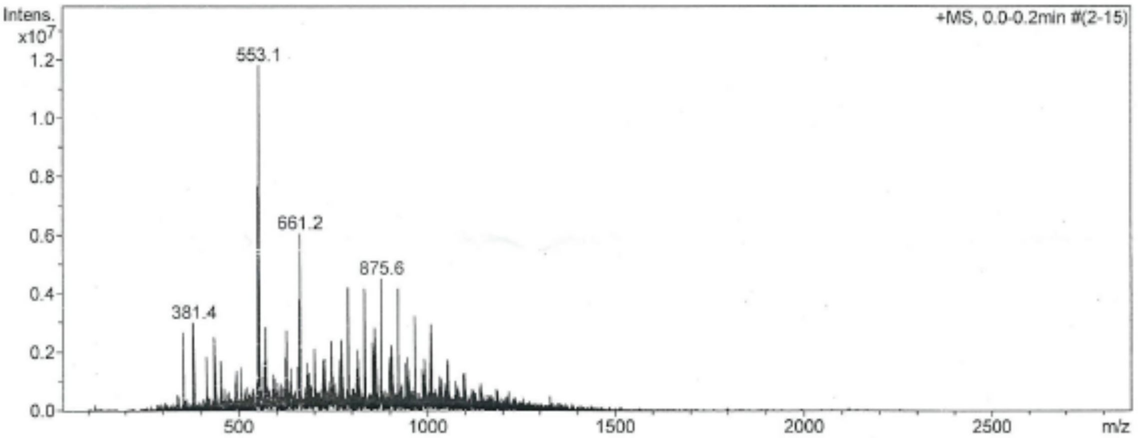

Appendix 35 ^{1}H and ^{13}C chemical shift assignment of complex 1 in DMSO and PBS with 30% of DMSO. The red coding to identify the protons refers to Appendix 36.

	DMSO		**PBS+30% DMSO**	
Complex 1	**δ [ppm] ^{1}H**	**δ [ppm] ^{13}C**	**δ [ppm] ^{1}H**	**δ [ppm] ^{13}C**
1	8.55	153.08	8.49	152.88
2	-	144.36	-	142.76
3	7.87	141.32	7.83	141.37
4	7.40	129.49	7.37	129.30
5	8.42	153.47	8.47	153.72
a	9.90	149.09	9.83	158.46
b	8.46	131.94	8.19	131.32
c	9.95	140.00	9.20	139.21
d	8.26	135.83	7.89	135.79
e	7.56	132.60	7.89	135.79
f	-	145.22	-	144.58
g	-	142.77	-	-
h	-	133.72	-	132.23
i	-	152.53	-	151.28

Appendix 36 a) structure of complex 1 with number/letter code to identify the resonances; b) ^{1}H NMR of complex 1 (2.5 mM, PBS with 30% DMSO, 298 K, 500 MHz).

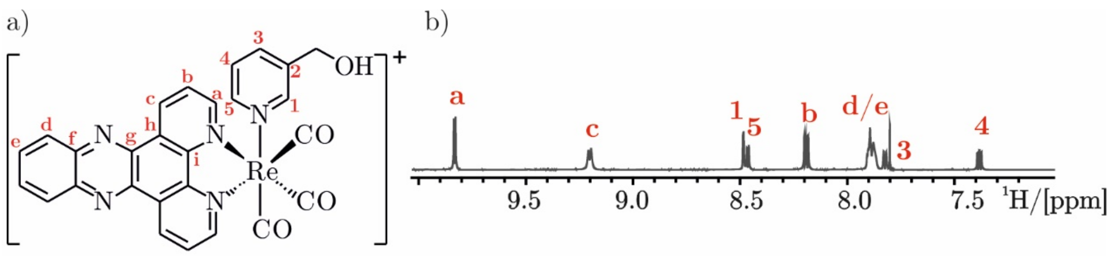

Appendix 37 a) [^{1}H,^{13}C]-HMBC of [Re(CO)$_3$(dppz)(3-CH$_2$OH-py)]$^+$ in PBS/30% DMSO; b) Overlay of [^{1}H,^{13}C]-HSQC in blue and [^{1}H,^{13}C]-HMBC of [Re(CO)$_3$(dppz)(3-CH$_2$OH-py)]$^+$ in red in DMSO.

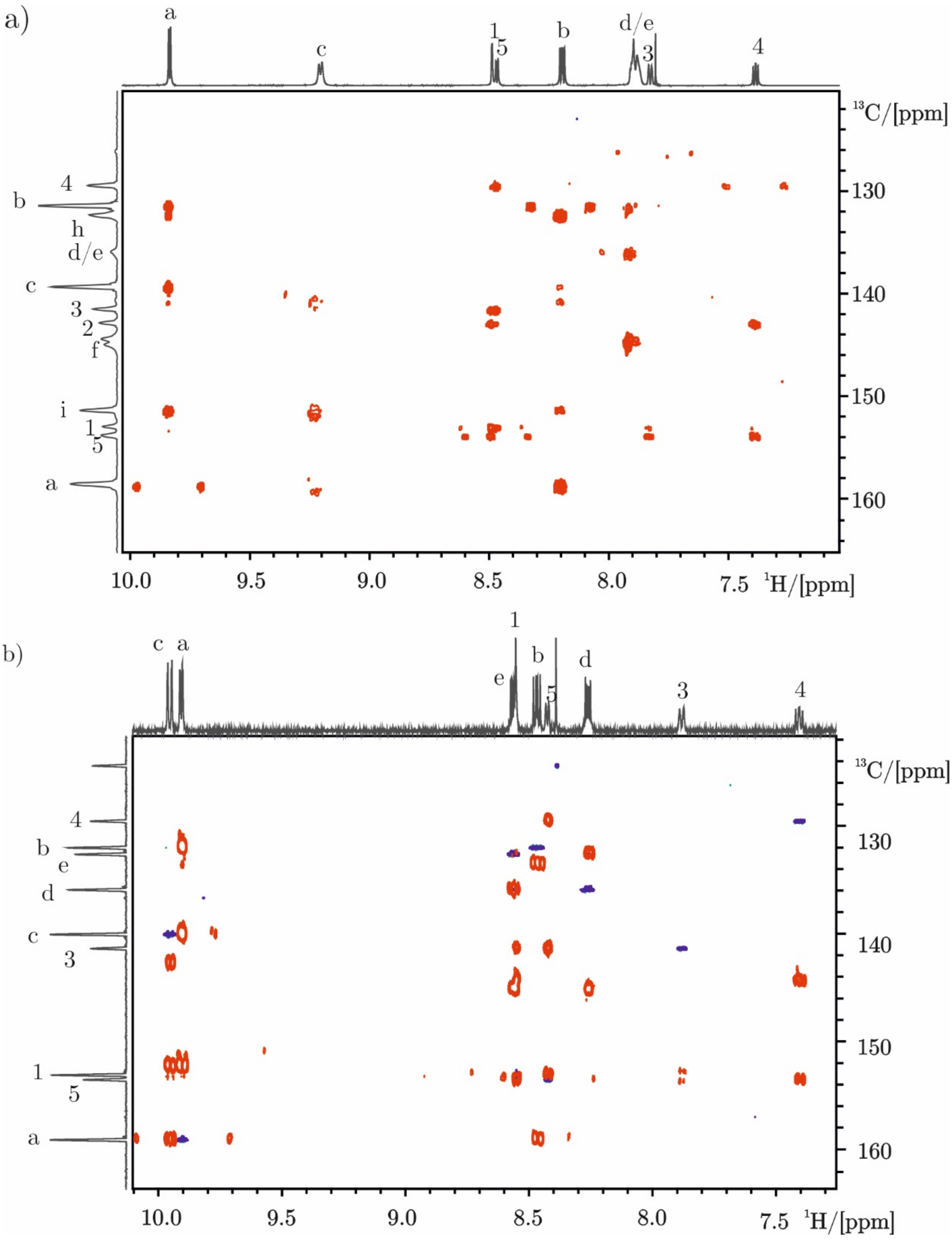

Appendix 38 ^{1}H NMR (aromatic region) of [Re(CO)$_3$(dppz)(3-CH$_2$OH-py)]OTf (PBS with 2% DMSO, 298K, 600 MHz).

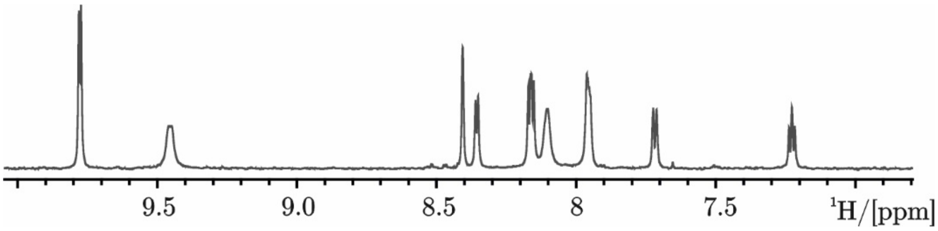

Appendix 39 ^{1}H NMR (aromatic region) of rac-[Ru(bpy)$_2$)dppz)](NO$_3$)$_2$ (PBS, 293K, 700 MHz).

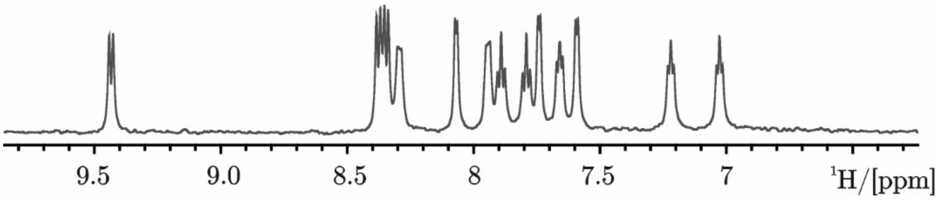

Appendix 40 ^{1}H NMR (aromatic region) of [Ru(bpy)$_3$]Cl$_2$ (PBS, 293K, 700 MHz).

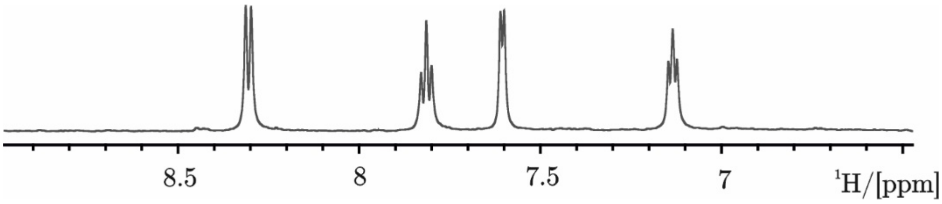

References

1. D.-L. Ma, H.-Z. He, K.-H. Leung, D. S.-H. Chan, and C.-H. Leung, Bioactive luminescent transition-metal complexes for biomedical applications, *Angew. Chem. Int. Ed.* **2013**, 52, 7666–7682.
2. M. J. Hannon, Supramolecular DNA recognition, *Chem. Soc. Rev.* **2007**, 36, 280–295.
3. J. L. Childs-Disney and M. D. Disney, Approaches to validate and manipulate RNA targets with small molecules in cells, *Annu. Rev. Pharmacol. Toxicol.* **2016**, 56, 123–140.
4. L. Guan and M. D. Disney, Recent advances in developing small molecules targeting RNA, *ACS Chem. Biol.* **2012**, 7, 73–86.
5. P. A. Sharp, The centrality of RNA, *Cell* **2009**, 136, 577–580.
6. R. F. Gesteland, T. R. Cech, and J. F. Atkins, The RNA world, Third Edition, Cold Spring Harbor Press, **2006**.
7. E. Alberti, M. Zampakou, and D. Donghi, Covalent and non-covalent binding of metal complexes to RNA, *J. Inorg. Biochem.* **2016**, 163, 278–291.
8. S. Bartova, M. Pechlaner, D. Donghi, and R. K. O. Sigel, Studying metal ion binding properties of a three-way junction RNA by heteronuclear NMR, *J. Biol. Inorg. Chem.* **2016**, 21, 319–328.
9. S. Bartova, E. Alberti, R. K. O. Sigel, and D. Donghi, Metal ion binding to an RNA internal loop, *Inorg. Chim. Acta* **2016**, 452, 104–110.
10. D. Donghi, M. Pechlaner, C. Finazzo, B. Knobloch, and R. K. O. Sigel, The structural stabilization of the three-way junction by Mg(II) represents the first step in the folding of a group II intron, *Nucleic Acids Res.* **2013**, 41, 2489–2504.
11. M. Pechlaner, Solution structure of the two core elements of group II introns and their interplay with metal ions, *PhD dissertation*, University of Zurich, **2013**.
12. C. Waldsich and A. M. Pyle, A folding control element for tertiary collapse of a group II intron ribozyme, *Nat. Struct. Mol. Biol.* **2007**, 14, 37–44.
13. C. Waldsich and A. M. Pyle, A kinetic intermediate that regulates proper folding of a group II intron RNA, *J. Mol. Biol.* **2008**, 375, 572–580.
14. J. L. Fiore and D. J. Nesbitt, An RNA folding motif: GNRA tetraloop-receptor interactions, *Quart. Rev. Biophys.* **2013**, 46, 223–264.

15. F. L. Thorp-Greenwood, M. P. Coogan, L. Mishra, N. Kumari, G. Rai, and S. Saripella, The importance of cellular localisation of probes: synthesis, photophysical properties, DNA interactions and cellular imaging properties of rhenium dppz complexes with known cellular localisation vectors, *New J. Chem.* **2012**, 36, 64–72.
16. F. R. Keene, J. A. Smith, and J. G. Collins, Metal complexes as structure-selective binding agents for nucleic acids, *Coord. Chem. Rev.* **2009**, 253, 2021–2035.
17. B. J. Pages, D. L. Ang, E. P. Wright, and J. R. Aldrich-Wright, Metal complex interactions with DNA, *Dalton. Trans.* **2015**, 44, 3505–3526.
18. R. A. Alderden, M. D. Hall, and T. W. Hambley, The discovery and development of cisplatin, *J. Chem. Educ.* **2006**, 83, 728–734.
19. B. M. Zeglis, V. C. Pierre, and J. K. Barton, Metallo-intercalators and metallo-insertors, *Chem. Commun.* **2007**, 4565–4579.
20. C. S. Chow and F. M. Bogdan, A Structural basis for RNA−ligand interactions, *Chem. Rev.* **1997**, 97, 1489–1514.
21. C. S. Chow, P. R. Cunningham, K. Lee, M. Meroueh, J. SantaLucia, and S. Varma, Photoinduced cleavage by a rhodium complex at G·U mismatches and exposed guanines in large and small RNAs, *Biochimie* **2002**, 84, 859–868.
22. N. W. Luedtke, J. S. Hwang, E. C. Glazer, D. Gut, M. Kol, and Y. Tor, Eilatin Ru(II) complexes display anti-HIV activity and enantiomeric diversity in the binding of RNA, *Chembiochem* **2002**, 3, 766–771.
23. N. W. Luedtke, The DNA and RNA specificity of eilatin Ru(II) complexes as compared to eilatin and ethidium bromide, *Nucleic Acids Res.* **2003**, 31, 5732–5740.
24. J. Boer, K. F. Blount, N. W. Luedtke, L. Elson-Schwab, and Y. Tor, RNA-selective modification by a platinum(II) complex conjugated to amino- and guanidinoglycosides, *Angew. Chem. Int. Ed.* **2005**, 44, 927–932.
25. M. P. Coogan and V. Fernández-Moreira, Progress with, and prospects for, metal complexes in cell imaging, *Chem. Commun.* **2014**, 50, 384–399.
26. K. K.-W. Lo, A. W.-T. Choi, and W. H.-T. Law, Applications of luminescent inorganic and organometallic transition metal complexes as biomolecular and cellular probes, *Dalton. Trans.* **2012**, 41, 6021–6047.

27. V. Fernández-Moreira, F. L. Thorp-Greenwood, and M. P. Coogan, Application of d^6 transition metal complexes in fluorescence cell imaging, *Chem. Commun.* **2010**, 46, 186–202.
28. C. A. Puckett and J. K. Barton, Methods to explore cellular uptake of ruthenium complexes, *J. Am. Chem. Soc.* **2007**, 129, 46–47.
29. M. R. Gill and J. A. Thomas, Ruthenium(II) polypyridyl complexes and DNA-from structural probes to cellular imaging and therapeutics, *Chem. Soc. Rev.* **2012**, 41, 3179–3192.
30. C. M. Dupureur and J. K. Barton, Use of selective deuteration and ^{1}H NMR in demonstrating major groove dinding of Δ-$[Ru(phen)_2dppz]^{2+}$ to $d(GTCGAC)_2$, *J. Am. Chem. Soc.* **1994**, 116, 10286–10287.
31. C. Hiort, P. Lincoln, and B. Norden, DNA binding of Δ- and Λ-$[Ru(phen)_2DPPZ]^{2+}$, *J. Am. Chem. Soc.* **1993**, 115, 3448–3454.
32. A. E. Friedman, J. C. Chambron, J. P. Sauvage, N. J. Turro, and J. K. Barton, A molecular light switch for DNA: $Ru(bpy)_2(dppz)^{2+}$, *J. Am. Chem. Soc.* **1990**, 112, 4960–4962.
33. A. J. McConnell, H. Song, and J. K. Barton, Luminescence of $[Ru(bpy)_2(dppz)]^{2+}$ bound to RNA mismatches, *Inorg. Chem.* **2013**, 52, 10131–10136.
34. V. W.-W. Yam, K. K.-W. Lo, K.-K. Cheung, and R. Y.-C. Kong, Synthesis, photophysical properties and DNA binding studies of novel luminescent rhenium(I) complexes. X-Ray crystal structure of $[Re(dppn)(CO)_3(py)](OTf)$, *J. Chem. Soc., Chem. Commun.* **1995**, 1191–1193.
35. H. D. Stoeffler, N. B. Thornton, S. L. Temkin, and K. S. Schanze, Unusual photophysics of a rhenium(I) dipyridophenazine complex in homogeneous solution and bound to DNA, *J. Am. Chem. Soc.* **1995**, 117, 7119–7128.
36. V. V. Krishnan and Rupp B., Macromolecular structure determination: comparison of X-ray crystallography and NMR spectroscopy, *Essentials for Life Science*, Wiley, **2012**, 1–13.
37. M. C. Erat and R. K. O. Sigel, Methods to detect and characterize metal ion binding sites in RNA, *Met. Ions Life Sci.*, Royal Society of Chemistry, **2011**, 9, 37–100.

38. C. M. Dupureur and J. K. Barton, Structural studies of Λ- and Δ-[Ru(phen)$_2$dppz]$^{2+}$ bound to d(GTCGAC)$_2$: characterization of enantioselective intercalation, *Inorg. Chem.* **1997**, 36, 33–43.
39. M. Pechlaner and R. K. O. Sigel, Characterization of metal ion-nucleic acid interactions in solution, *Met. Ions Life Sci.*, Springer, **2012**, 10, 1–42.
40. S. Campagne, V. Gervais, and A. Milon, Nuclear magnetic resonance analysis of protein-DNA interactions, *J. R. Soc. Interface* **2011**, 8, 1065–1078.
41. M. Wang, Y. Yu, C. Liang, A. Lu, and G. Zhang, Recent advances in developing small molecules targeting nucleic acid, *Int. J. Mol. Sci.* **2016**, 17, 779.
42. B. P. Hudson and J. K. Barton, Solution structure of a metallointercalator bound site specifically to DNA, *J. Am. Chem. Soc.* **1998**, 120, 6877–6888.
43. J. L. Morgan, C. B. Spillane, J. A. Smith, D. P. Buck, J. G. Collins, and F. R. Keene, Dinuclear ruthenium(II) complexes with flexible bridges as non-duplex DNA binding agents, *Dalton. Trans.* **2007**, 4333–4342.
44. W. Saenger, Principles of nucleic acid structure, Springer New York, New York, **1984**.
45. J. Kendrew and E. Lawrence, The encyclopedia of molecular biology, Blackwell Science, Oxford, **1994**.
46. D. Svozil, J. Kalina, M. Omelka, and B. Schneider, DNA conformations and their sequence preferences, *Nucleic Acids Res.* **2008**, 36, 3690–3706.
47. J. D. Watson and F. H. C. Crick, Molecular structure of nucleic acids: a structure for deoxyribose nucleic acid, *Nature* **1953**, 171, 737–738.
48. M. Kitayner, H. Rozenberg, R. Rohs, O. Suad, D. Rabinovich, B. Honig, and Z. Shakked, Diversity in DNA recognition by p53 revealed by crystal structures with Hoogsteen base pairs, *Nat. Struct. Mol. Biol.* **2010**, 17, 423–429.
49. S. E. Butcher and A. M. Pyle, The molecular interactions that stabilize RNA tertiary structure: RNA motifs, patterns, and networks, *Accounts Chem. Res.* **2011**, 44, 1302–1311.
50. M. D. Disney, I. Yildirim, and J. L. Childs-Disney, Methods to enable the design of bioactive small molecules targeting RNA, *Org. Biomol. Chem.* **2014**, 12, 1029–1039.

51. D. Donghi and R. K. O. Sigel, Metal ion-RNA interactions studied via multinuclear NMR, *Methods Mol. Biol.*, Humana, **2012**, 848.
52. S. P. Velagapudi, A. Pushechnikov, L. P. Labuda, J. M. French, and M. D. Disney, Probing a 2-aminobenzimidazole library for binding to RNA internal loops *via* two-dimensional combinatorial screening, *ACS Chem. Biol.* **2012**, 7, 1902–1909.
53. T. Tran and M. D. Disney, Two-dimensional combinatorial screening of a bacterial rRNA a-site-like motif library: defining privileged asymmetric internal loops that bind aminoglycosides, *Biochemistry* **2010**, 49, 1833–1842.
54. R. K. O. Sigel, Group II Intron ribozymes and metal ions-A delicate relationship, *Eur. J. Inorg. Chem.* **2005**, 2005, 2281–2292.
55. B. B. Konforti, Q. Liu, and A. M. Pyle, A map of the binding site for catalytic domain 5 in the core of a group II intron ribozyme, *EMBO J.* **1998**, 17, 7105–7117.
56. P. Z. Qin and A. M. Pyle, Stopped-flow fluorescence spectroscopy of a group II intron ribozyme reveals that domain 1 is an independent folding unit with a requirement for specific Mg^{2+} ions in the tertiary structure, *Biochemistry* **1997**, 36, 4718–4730.
57. J. H. Davis, M. Tonelli, L. G. Scott, L. Jaeger, J. R. Williamson, and S. E. Butcher, RNA helical packing in solution: NMR structure of a 30 kDa GAAA tetraloop-receptor complex, *J. Mol. Biol.* **2005**, 351, 371–382.
58. J. H. Cate, A. R. Gooding, E. Podell, K. Zhou, B. L. Golden, C. E. Kundrot, T. R. Cech, and J. A. Doudna, Crystal structure of a group I rybozyme domain: principles of RNA packing, *Science* **1996**, 273, 1678–1685.
59. S. E. Butcher, T. Dieckmann, and J. Feigon, Solution structure of a GAAA tetraloop receptor RNA, *EMBO J.* **1997**, 16, 7490–7499.
60. A. M. Pyle, Metal ions in the structure and function of RNA, *J. Biol. Inorg. Chem.* **2002**, 7, 679–690.
61. R. Shiman and D. E. Draper, Stabilization of RNA tertiary structure by monovalent cations, *J. Mol. Biol.* **2000**, 302, 79–91.
62. D. E. Draper, A guide to ions and RNA structure, *RNA* **2004**, 10, 335–343.
63. E. Freisinger and R. K. O. Sigel, From nucleotides to ribozymes-A comparison of their metal ion binding properties, *Coord. Chem. Rev.* **2007**, 251, 1834–1851.

64. R. K. O. Sigel and A. M. Pyle, Alternative roles for metal ions in enzyme catalysis and the implications for ribozyme chemistry, *Chem. Rev.* **2007**, 107, 97–113.

65. A. Zamir, R. Miskin, and D. Elson, Inactivation and reactivation of ribosomal subunits: amino acyl-transfer RNA binding activity of the 30 s subunit of Escherichia coli, *J. Mol. Biol.* **1971**, 60, 347–364.

66. V. K. Misra and D. E. Draper, On the role of magnesium ions in RNA stability, *Biopolymers* **1998**, 48, 113–135.

67. M. R. Stahley and S. A. Strobel, Structural evidence for a two-metal-ion mechanism of group I intron splicing, *Science* **2005**, 309, 1587–1590.

68. R. L. Gonzalez and I. Tinoco, Identification characterization of metal ion binding sites in RNA, *Methods Enzymol.* **2001**, 338, 421–443.

69. Y. Tanaka and A. Ono, Nitrogen-15 NMR spectroscopy of N-metallated nucleic acids: insights into ^{15}N NMR parameters and N-metal bonds, *Dalton. Trans.* **2008**, 4965–4974.

70. Y. Tanaka and K. Taira, Detection of RNA nucleobase metalation by NMR spectroscopy, *Chem. Commun.* **2005**, 2069–2079.

71. J. Feigon, S. E. Butcher, L. David Finger, and N. V. Hud, Solution nuclear magnetic resonance probing of cation binding sites on nucleic acids, *Methods Enzymol.* **2001**, 338, 400–420.

72. D. Donghi, S. Johannsen, R. K. O. Sigel, and E. Freisinger, NMR spectroscopy in bioinorganic chemistry, *CHIMIA* **2012**, 66, 791–797.

73. J. Flinders and T. Dieckmann, NMR spectroscopy of ribonucleic acids, *Prog. Nucl. Magn. Reson. Spectrosc.* **2006**, 48, 137–159.

74. B. Fürtig, C. Richter, J. Wöhnert, and H. Schwalbe, NMR Spectroscopy of RNA, *Chembiochem* **2003**, 4, 936–962.

75. M. P. Latham, D. J. Brown, S. A. McCallum, and A. Pardi, NMR methods for studying the structure and dynamics of RNA, *Chembiochem* **2005**, 6, 1492–1505.

76. K. Wüthrich, NMR of proteins and nucleic acids, Wiley, New York, Chichester, **1986**.

77. C. S. Johnson, Diffusion ordered nuclear magnetic resonance spectroscopy. Principles and applications, *Prog. Nucl. Magn. Reson. Spectrosc.* **1999**, 34, 203–256.

78. Y. Cohen, L. Avram, and L. Frish, Diffusion NMR spectroscopy in supramolecular and combinatorial chemistry: an old parameter-new insights, *Angew. Chem. Int. Ed.* **2005**, 44, 520–554.
79. L. H. Lucas, W. H. Otto, and C. K. Larive, The 2D-J-DOSY experiment: resolving diffusion coefficients in mixtures, *J. Magn. Reson.* **2002**, 156, 138–145.
80. M. Mayer and B. Meyer, Characterization of ligand binding by saturation transfer difference NMR spectroscopy, *Angew. Chem. Int. Ed.* **1999**, 38, 1784–1788.
81. J. Angulo and P. M. Nieto, STD-NMR: application to transient interactions between biomolecules-a quantitative approach, *Eur. Biophys. J.* **2011**, 40, 1357–1369.
82. A. Viegas, J. Manso, F. L. Nobrega, and E. J. Cabrita, Saturation-Transfer Difference (STD) NMR. A simple and fast method for ligand screening and characterization of protein binding, *J. Chem. Educ.* **2011**, 88, 990–994.
83. B. Meyer and T. Peters, NMR spectroscopy techniques for screening and identifying ligand binding to protein receptors, *Angew. Chem. Int. Ed.* **2003**, 42, 864–890.
84. B. Luy and J. P. Marino, Direct evidence for Watson-Crick base pairs in a dynamic region of RNA structure, *J. Am. Chem. Soc.* **2000**, 122, 8095–8096.
85. E. Ennifar, A. Nikulin, S. Tishchenko, A. Serganov, N. Nevskaya, M. Garber, B. Ehresmann, C. Ehresmann, S. Nikonov, and P. Dumas, The crystal structure of UUCG tetraloop, *J. Mol. Biol.* **2000**, 304, 35–42.
86. F. H. Allain and G. Varani, Structure of the P1 helix from group I self-splicing introns, *J. Mol. Biol.* **1995**, 250, 333–353.
87. S. Nozinovic, B. Fürtig, H. R. A. Jonker, C. Richter, and H. Schwalbe, High-resolution NMR structure of an RNA model system: the 14-mer cUUCGg tetraloop hairpin RNA, *Nucleic Acids Res.* **2010**, 38, 683–694.
88. A. C. Pease and D. E. Wemmer, Characterization of the secondary structure and melting of a self-cleaved RNA hammerhead domain by ^{1}H NMR spectroscopy, *Biochemistry* **1990**, 29, 9039–9046.
89. J. K. James and I. Tinoco, The solution structure of a d[C(TTCG)G] DNA hairpin and comparison to the unusually stable RNA analogue, *Nucleic Acids Res.* **1993**, 21, 3287–3293.

90. A. Sigel, H. Sigel, and R. K. O. Sigel, Structural and catalytic roles of metal ions in RNA, Royal Society of Chemistry, Cambridge, **2011**.

91. M. C. Erat, H. Kovacs, and R. K. O. Sigel, Metal ion-N7 coordination in a ribozyme branch domain by NMR, *J. Inorg. Biochem.* **2010**, 104, 611–613.

92. J. Rinnenthal, C. Richter, S. Nozinovic, B. Fürtig, J. J. Lopez, C. Glaubitz, and H. Schwalbe, RNA phosphodiester backbone dynamics of a perdeuterated cUUCGg tetraloop RNA from phosphorus-31 NMR relaxation analysis, *J. Biomol. NMR* **2009**, 45, 143–155.

93. Y. Ma and G. Lu, Differential effects of Mg(II) and N(alpha)-4-tosyl-l-arginine methyl ester hydrochloride on the recognition and catalysis in ATP hydrolysis, *Dalton. Trans.* **2008**, 1081–1086.

94. E. J. Merino, K. A. Wilkinson, J. L. Coughlan, and K. M. Weeks, RNA structure analysis at single nucleotide resolution by selective 2‘-hydroxyl acylation and primer extension (SHAPE), *J. Am. Chem. Soc.* **2005**, 127, 4223–4231.

95. L. H. Lucas and C. K. Larive, Measuring ligand-protein binding using NMR diffusion experiments, *Concepts Magn. Reson.* **2004**, 20A, 24–41.

96. J. S. Gounarides, A. Chen, and M. J. Shapiro, Nuclear magnetic resonance chromatography. Applications of pulse field gradient diffusion NMR to mixture analysis and ligand–receptor interactions, *J. Chromatogr., Biomed. Appl.* **1999**, 725, 79–90.

97. V. Gonzalez-Ruiz, A. I., M. Antonia, P. Ribelles, M. Teresa, and J. Carlos, An overview of analytical techniques employed to evidence drug-DNA interactions. Applications to the design of genosensors, *Biomed. Eng.*, INTECH Open Access Publisher, **2011**.

98. I. Haq, Thermodynamics of drug–DNA interactions, *Arch. Biochem. Biophys.* **2002**, 403, 1–15.

99. M. Sirajuddin, S. Ali, and A. Badshah, Drug-DNA interactions and their study by UV-Visible, fluorescence spectroscopies and cyclic voltametry, *J. Photochem. Photobiol., B* **2013**, 124, 1–19.

100. J. D. McGhee and P. H. von Hippel, Theoretical aspects of DNA-protein interactions: Co-operative and non-co-operative binding of large ligands to a one-dimensional homogeneous lattice, *J. Mol. Biol.* **1974**, 86, 469–489.

101. W. C. Tse and D. L. Boger, A fluorescent intercalator displacement assay for establishing DNA binding selectivity and affinity, *Accounts Chem. Res.* **2004**, 37, 61–69.
102. E. Freire, O. L. Mayorga, and M. Straume, Isothermal titration calorimetry, *Anal. Chem.* **1990**, 62, 950–959.
103. A. L. Feig, Applications of isothermal titration calorimetry in RNA biochemistry and biophysics, *Biopolymers* **2007**, 87, 293–301.
104. K. K.-W. Lo and K. H.-K. Tsang, Bifunctional luminescent Rhenium(I) complexes containing an extended planar diimine ligand and a biotin moiety, *Organometallics* **2004**, 23, 3062–3070.
105. K. Ghosh, P. Kumar, and N. Tyagi, Synthesis, crystal structure and DNA interaction studies on mononuclear zinc complexes, *Inorg. Chim. Acta* **2011**, 375, 77–83.
106. J. E. Ladbury and B. Z. Chowdhry, Sensing the heat. The application of isothermal titration calorimetry to thermodynamic studies of biomolecular interactions, *Chem. Biol.* **1996**, 3, 791–801.
107. M. W. Freyer and E. A. Lewis, Isothermal titration calorimetry: experimental design, data analysis, and probing macromolecule/ligand binding and kinetic interactions, *Methods Cell Biol.*, Elsevier, **2008**, 84, 79–113.
108. C. Y. Huang, Determination of binding stoichiometry by the continuous variation method: the Job plot, Academic Press, New York, London, **1982**.
109. E. J. Olson and P. Buhlmann, Getting more out of a Job plot: determination of reactant to product stoichiometry in cases of displacement reactions and n:n complex formation, *J. Org. Chem.* **2011**, 76, 8406–8412.
110. F. G. Loontiens, P. Regenfuss, A. Zechel, L. Dumortier, and R. M. Clegg, Binding characteristics of Hoechst 33258 with calf thymus DNA, poly[d(A-T)] and d(CCGGAATTCCGG): multiple stoichiometries and determination of tight binding with a wide spectrum of site affinities, *Biochemistry* **1990**, 29, 9029–9039.
111. M. Boccio, A. Sayago, and A. G. Asuero, A bilogarithmic method for the spectrophotometric evaluation of stability constants of 1:1 weak complexes from mole ratio data, *Int. J. Pharm.* **2006**, 318, 70–77.
112. K. S. Klausen, The determination of stability constants from continuous variation data, *Anal. Chim Acta* **1969**, 44, 377–384.

113. K. L. O'Neal, S. Geib, and S. G. Weber, Extraction of pyridines into fluorous solvents based on hydrogen bond complex formation with carboxylic acid receptors, *Anal. Chem.* **2007**, 79, 3117–3125.
114. C. Schmuck and M. Schwegmann, A molecular flytrap for the selective binding of citrate and other tricarboxylates in water, *J. Am. Chem. Soc.* **2005**, 127, 3373–3379.
115. J. Olmsted and D. R. Kearns, Mechanism of ethidium bromide fluorescence enhancement on binding to nucleic acids, *Biochemistry* **2002**, 16, 3647–3654.
116. A. W. McKinley, J. Andersson, P. Lincoln, and E. M. Tuite, DNA sequence and ancillary ligand modulate the biexponential emission decay of intercalated $[Ru(L)_2dppz]^{2+}$ enantiomers, *Chem. - Eur. J.* **2012**, 18, 15142–15150.
117. J. Andersson, L. H. Fornander, M. Abrahamsson, E. Tuite, P. Nordell, and P. Lincoln, Lifetime heterogeneity of DNA-bound dppz complexes originates from distinct intercalation geometries determined by complex-complex interactions, *Inorg. Chem.* **2013**, 52, 1151–1159.
118. A. Spinello, A. Terenzi, and G. Barone, Metal complex-DNA binding: Insights from molecular dynamics and DFT/MM calculations, *J. Inorg. Biochem.* **2013**, 124, 63–69.
119. J. L. Wagstaff, S. L. Taylor, and M. J. Howard, Recent developments and applications of saturation transfer difference nuclear magnetic resonance (STD NMR) spectroscopy, *Mol. BioSyst.* **2013**, 9, 571–577.
120. A. Bhunia, S. Bhattacharjya, and S. Chatterjee, Applications of saturation transfer difference NMR in biological systems, *Drug discovery today* **2012**, 17, 505–513.
121. R. M. Keller and K. Wüthrich, Assignment of the heme c resonances in the 360 MHz ^1H NMR spectra of cytochrome c, *Biochim. Biophys. Acta, Protein Struct.* **1978**, 533, 195–208.
122. M. Mayer and B. Meyer, Group epitope mapping by Saturation Transfer Difference NMR to identify segments of a ligand in direct contact with a protein receptor, *J. Am. Chem. Soc.* **2001**, 123, 6108–6117.
123. J. Klages, M. Coles, and H. Kessler, NMR-based screening: A powerful tool in fragment-based drug discovery, *Analyst* **2007**, 132, 692–705.

124. V. Krishnan, Ligand screening by Saturation-Transfer Difference (STD) NMR spectroscopy, *Curr. Anal. Chem.* **2005**, 1, 307–320.
125. M. Mayer and T. L. James, Detecting ligand binding to a small RNA target via Saturation Transfer Difference NMR experiments in D_2O and H_2O, *J. Am. Chem. Soc.* **2002**, 124, 13376–13377.
126. D. A. Erlanson, J. A. Wells, and A. C. Braisted, Tethering: fragment-based drug discovery, *Annu. Rev. Biophys. Biomol. Struct.* **2004**, 33, 199–223.
127. A. T. Brünger, P. D. Adams, G. M. Clore, W. L. DeLano, P. Gros, R. W. Grosse-Kunstleve, J. S. Jiang, J. Kuszewski, M. Nilges, N. S. Pannu, R. J. Read, L. M. Rice, T. Simonson, and G. L. Warren, Crystallography & NMR System: A new software suite for macromolecular structure determination, *Acta Crystallogr., Sect. D: Biol. Crystallogr.* **1998**, 54, 905–921.
128. C. Schwieters, J. Kuszewski, and G. M. Clore, Using Xplor–NIH for NMR molecular structure determination, *Prog. Nucl. Magn. Reson. Spectrosc.* **2006**, 48, 47–62.
129. C. D. Schwieters, J. J. Kuszewski, N. Tjandra, and G. Marius Clore, The Xplor-NIH NMR molecular structure determination package, *J. Magn. Reson.* **2003**, 160, 65–73.
130. R. K. O. Sigel, D. G. Sashital, D. L. Abramovitz, A. G. Palmer, S. E. Butcher, and A. M. Pyle, Solution structure of domain 5 of a group II intron ribozyme reveals a new RNA motif, *Nat. Struct. Mol. Biol.* **2004**, 11, 187–192.
131. B. Hess, C. Kutzner, D. Van Der Spoel, and E. Lindahl, GROMACS 4: algorithms for highly efficient, load-balanced, and scalable molecular simulation, *J. Chem. Theory Comput.* **2008**, 4, 435–447.
132. D. Van Der Spoel, E. Lindahl, B. Hess, G. Groenhof, A. E. Mark, and H. J. C. Berendsen, GROMACS: Fast, flexible, and free, *J. Comput. Chem.* **2005**, 26, 1701–1718.
133. J. Wang, R. M. Wolf, J. W. Caldwell, P. A. Kollman, and D. A. Case, Development and testing of a general amber force field, *J. Comput. Chem.* **2004**, 25, 1157–1174.
134. A. Pérez, I. Marchan, D. Svozil, J. Sponer, T. E. 3. Cheatham, C. A. Laughton, and M. Orozco, Refinement of the AMBER force field for nucleic acids: improving the description of alpha/gamma conformers, *Biophys. J.* **2007**, 92, 3817–3829.

135. P. Banáš, D. Hollas, M. Zgarbová, P. Jurečka, M. Orozco, T. E. Cheatham, J. Šponer, and M. Otyepka, Performance of molecular mechanics force fields for RNA simulations: stability of UUCG and GNRA hairpins, *J. Chem. Theory Comput.* **2010**, 6, 3836–3849.

136. Y. Zhao and D. G. Truhlar, The M06 suite of density functionals for main group thermochemistry, thermochemical kinetics, noncovalent interactions, excited states, and transition elements. Two new functionals and systematic testing of four M06-class functionals and 12 other functionals, *Theor. Chem. Acc.* **2008**, 120, 215–241.

137. N. Godbout, D. R. Salahub, J. Andzelm, and E. Wimmer, Optimization of Gaussian-type basis sets for local spin density functional calculations. Part I. Boron through neon, optimization technique and validation, *Can. J. Chem.* **1992**, 70, 560–571.

138. A. da Silva and W. F. Vranken, ACPYPE - AnteChamber PYthon Parser interfacE, *BMC Res. Notes* **2012**, 5, 1–8.

139. S. K. Burger, M. Lacasse, T. Verstraelen, J. Drewry, P. Gunning, and P. W. Ayers, Automated parametrization of AMBER force field terms from vibrational analysis with a focus on functionalizing dinuclear Zinc(II) scaffolds, *J. Chem. Theory Comput.* **2012**, 8, 554–562.

140. C. M. Breneman and K. B. Wiberg, Determining atom-centered monopoles from molecular electrostatic potentials. The need for high sampling density in formamide conformational analysis, *J. Comput. Chem.* **1990**, 11, 361–373.

141. G. Bussi, D. Donadio, and M. Parrinello, Canonical sampling through velocity rescaling, *J. Chem. Phys.* **2007**, 126, 14101.

142. T. Darden, D. York, and L. Pedersen, Particle mesh Ewald. An N·log(N) method for Ewald sums in large systems, *J. Chem. Phys.* **1993**, 98, 10089–10092.

143. Z. Molphy, A. Prisecaru, C. Slator, N. Barron, M. McCann, J. Colleran, D. Chandran, N. Gathergood, and A. Kellett, Copper phenanthrene oxidative chemical nucleases, *Inorg. Chem.* **2014**, 53, 5392–5404.

144. A. Greguric, I. D. Greguric, T. W. Hambley, J. R. Aldrich-Wright, and J. G. Collins, Minor groove intercalation of Δ-$[Ru(Me_2phen)_2dppz]^{2+}$ to the hexanucleotide $d(GTCGAC)_2$, *J. Chem. Soc., Dalton Trans.* **2002**, 93, 849.

145. R. Satapathy, H. Padhy, Y.-H. Wu, and H.-C. Lin, Synthesis and characterization of reversible chemosensory polymers: modulation of sensitivity through the attachment of novel imidazole pendants, *Chem. - Eur. J.* **2012**, 18, 16061–16072.
146. P. Kurz, B. Probst, B. Spingler, and R. Alberto, Ligand variations in [ReX(diimine)$(CO)_3$] complexes: effects on photocatalytic CO_2 reduction, *Eur. J. Inorg. Chem.* **2006**, 2006, 2966–2974.
147. P. Ren, R. Wang, S. Pu, G. Liu, and C. Fan, A multi-addressable molecular switch based on a novel diarylethene with an imidazo [4,5- f] [1,10] phenanthroline unit, *J. Phys. Org. Chem.* **2014**, 27, 183–190.
148. P. K. Sahoo, C. Giri, T. S. Haldar, R. Puttreddy, K. Rissanen, and P. Mal, Mechanochemical synthesis, ophotophysical properties, and X-ray structures of N-Heteroacenes, *Eur. J. Org. Chem.* **2016**, 2016, 1283–1291.
149. I. S. Ahuja, R. Singh, and R. Sriramulu, 3- and 4-picolylamine complexes of bivalent metal halides and pseudohalides, *Transition Met. Chem.* **1979**, 4, 65–69.
150. J. Batchelor, J. Feeney, and G. Roberts, Carbon-13 NMR protonation shifts of amines, carboxylic acids and amino acids, *J. Magn. Reson. (1969-1992)* **1975**, 20, 19–38.
151. D. Sarauli, V. Popova, A. Zahl, R. Puchta, and I. Ivanovic-Burmazovic, Seven-coordinate iron complex as a ditopic receptor for lithium salts: Study of host-guest interactions and substitution behavior, *Inorg. Chem.* **2007**, 46, 7848–7860.
152. R.-J. Lin, K.-S. Lin, and I.-J. Chang, Photophysical properties of tricarbonyl(histidine)(diimine)rhenium(I) complexes in aqueous solution, *Inorg. Chim. Acta* **1996**, 242, 179–183.
153. A. W.-T. Choi, M.-W. Louie, S. P.-Y. Li, H.-W. Liu, B. T.-N. Chan, T. C.-Y. Lam, A. C.-C. Lin, S.-H. Cheng, and K. K.-W. Lo, Emissive behavior, cytotoxic activity, cellular uptake, and PEGylation properties of new luminescent rhenium(I) polypyridine poly(ethylene glycol) complexes, *Inorg. Chem.* **2012**, 51, 13289–13302.
154. V. Fernández-Moreira, F. L. Thorp-Greenwood, A. J. Amoroso, J. Cable, J. B. Court, V. Gray, A. J. Hayes, R. L. Jenkins, B. M. Kariuki, D. Lloyd, C. O. Millet, C. F. Williams, and M. P. Coogan, Uptake and localisation of

rhenium fac-tricarbonyl polypyridyls in fluorescent cell imaging experiments, *Org. Biomol. Chem.* **2010**, 8, 3888–3901.

155. C. Kao, S. Rüdisser, and M. Zheng, A Simple and efficient method to transcribe RNAs with reduced 3′ heterogeneity, *Methods* **2001**, 23, 201–205.
156. S. Gallo, M. Furler, and R. K. O. Sigel, *In vitro* transcription and purification of RNAs of different size, *CHIMIA* **2005**, 59, 812–816.
157. J. L. Markley, A. Bax, Y. Arata, C. W. Hilbers, R. Kaptein, B. D. Sykes, P. E. Wright, and K. Wüthrich, Recommendations for the presentation of NMR structures of proteins and nucleic acids, *J. Mol. Biol.* **1998**, 280, 933–952.
158. K. Tarasava, S. Johannsen, and E. Freisinger, Solution structure of the circular g-domain analog from the wheat metallothionein E_c-1, *Molecules* **2013**, 18, 14414–14429.
159. U. Schatzschneider, J. Niesel, I. Ott, R. Gust, H. Alborzinia, and S. Wolfl, Cellular uptake, cytotoxicity, and metabolic profiling of human cancer cells treated with ruthenium(II) polypyridyl complexes $Ru(bpy)_2(N\text{--}N)Cl_2$ with N--N=bpy, phen, dpq, dppz, and dppn, *ChemMedChem* **2008**, 3, 1104–1109.
160. M.-J. Han, Y.-M. Chen, and K.-Z. Wang, Ruthenium(II) complexes of 6-hydroxydipyrido[3,2-a:2′,3′-c]phenazine: self-association, and concentration-dependent acid-base and DNA-binding properties, *New J. Chem.* **2008**, 32, 970.
161. E. Rüba, J. R. Hart, and J. K. Barton, $[Ru(bpy)_2(L)]Cl_2$: luminescent metal complexes that bind DNA base mismatches, *Inorg. Chem.* **2004**, 43, 4570–4578.

List of abbreviations

1D	Mono-dimensional
2D	Two-dimensional
APS	Ammonium persulfate
ATP	Adenosine triphosphate
BB	Bromophenol blue
bpy	2,2’-bipyridine
CIAP	Calf intestinal Alkaline Phosphatase
CT-DNA	Calf Thymus DNA
CTP	Cytidine triphosphate
DMSO	Dimethyl sulfoxide
DNA	Deoxy-ribonucleic acid
DOSY	Diffusion-ordered spectroscopy
dppz	Dipyrido[3,2-a:2',3'-c]phenazine
DSS	4,4-dimethyl-4-silapentane-1-sulfonic acid
DTT	Dithiothreitol
EB	Ethidium bromide
EDTA	Dthylenediaminetetraacetic acid
ESI-MS	Electrospray ionisation mass spectrometry
Equiv	Equivalents
GTP	Guanosine triphosphate
HEPES	4-(2-hydroxyethyl)piperazine-1-ethansulfonic acid
HMBC	Heteronuclear multiple bond correlation
HPLC	High-performance liquid chromatography
HSQC	Heteronuclear single quantum coherence
ITC	Isothermal titration calorimetry
NMR	Nuclear magnetic resonance spectroscopy
NOESY	Nuclear Overhauser spectroscopy
NTP	Nucleoside triphosphate
OT	Original template

PAGE	Polyacrylamide gel electrophoresis
PBS	Phosphate buffer solution
Py	Pyridine
RNA	Ribonucleic acid
RNAse	Ribonuclease
STD	Saturation transfer difference
TBE	Tris/Borate/EDTA
TEMED	N,N,N,N tetramethylendiamine
TOCSY	Total correlation spectroscopy
TRIS	Tris(hydroxymethyl)-aminomethane
TS	Top strand
TXN	Transcription buffer
UTP	Uridine triphosphate
UV-Vis	Ultraviolet/Visible spectrometry
XC	Xylene cyanol

Curriculum Vitae

Personal data

Name	Elena Alberti
Date and place of birth	7th February 1986, Garbagnate Milanese, Italy
Nationality	Italian

Education

1992-1997	Primary school G. Marconi, Limbiate, Italy.
1997-2000	Middle school S. Pertini, Desio, Italy.
2000-2006	High school diploma at Liceo statale classico E. Majorana, Desio, Italy.
2006-2011	Bachelor degree in industrial chemistry at the University of Milan, Milan, Italy. Thesis title: *NMR characterization of peptides mimic of ELAV, proteins involved in the stabilization of mRNA.* Supervisors: Dr. Donatella Potenza, Dr. Francesca Vasile.
2011-2013	Master degree in industrial chemistry and management at the University of Milan, Milan, Italy. Thesis title: *Interaction studies of mRNA and peptides, mimic of ELAV proteins, using Nuclear Magnetic Resonance.* Supervisors: Dr. Donatella Potenza, Dr. Francesca Vasile.
2013-2017	PhD studies at the University of Zurich, Zurich, Switzerland. Thesis title: *Unravelling the interaction of a Re(I)dppz metallo-intercalotor with an RNA internal loop.* Supervisors: Dr. Daniela Donghi, Prof. Dr. Roland. K.O. Sigel.

Teaching experience

Spring semester 2014	Teaching assistant in the inorganic chemistry laboratory course (ACPI) at the department of Chemistry, University of Zurich.
Fall semester 2014	Teaching assistant in the inorganic chemistry laboratory course (ACPII) at the department of Chemistry, University of Zurich.
Spring semester 2015	Teaching assistant in the inorganic chemistry laboratory course (ACPI) at the department of Chemistry, University of Zurich.
Spring semester 2015	Supervisor of a research project (FGP) dealing with the synthesis of a new Re(I)dppz metallo-intercalator at the department of Chemistry, University of Zurich.
Fall semester 2015	Teaching assistant in the inorganic chemistry laboratory course (ACPII) at the department of Chemistry, University of Zurich.

Publications

E. Alberti, M. Zampakou, D. Donghi, *Covalent and non-covalent binding of metal complexes to RNA*, J. Inorg. Biochem. (2016), 163, 278-291.

S. Bartova, E. Alberti, R.K.O. Sigel, D. Donghi, *Metal ion binding to an RNA internal loop*, J. Biol. Inorg. Chem. (2016), 452, 104-110.

E. Alberti, S. Johannsen, J. Palou-Mir, M. Barceló-Oliver, M.P. Coogan, D. Donghi, *Selective interaction of a Re(I)dppz complex with an RNA internal loop*, manuscript to be submitted.

Posters and oral presentations

22-23/08/2014	2nd International Symposium on Functional Metal Complexes that Bind to Biomolecules (COST Action CM1105), Zurich, Switzerland. Elena Alberti, Michael P. Coogan and Daniela Donghi, *Potential RNA Selective Binding Probes: Re(I)-dppz Complexes* (poster).
24-28/08/2014	12th European Biological Inorganic Chemistry Conference, Zurich, Switzerland. Elena Alberti, Michael P. Coogan and Daniela Donghi, *Rhenium(I)-dppz complexes as potential RNA binding agents* (poster (Suppl 2):S824).
01-05/09/2014	Swiss Summer School 2014 in Chemical Biology, Villars sur Ollon, Switzerland. Elena Alberti, Michael P. Coogan and Daniela Donghi, *Re(I)dppz complexes-RNA interaction: studying potential bioimaging agents* (poster).
11/09/2014	Swiss Chemical Society Fall meeting 2014, Zurich, Switzerland. Elena Alberti, Michael P. Coogan and Daniela Donghi, *Unravelling the RNA binding of rhenium(I)-dppz complexes* (poster).
13-16/06/2015	13th International Symposium on Applied Bioinorganic Chemistry (ISABC13), Galway, Ireland. Elena Alberti, Michael P. Coogan and Daniela Donghi, *Insights into the Interaction between RNA and Re(I)dppz Complexes* (poster).

04/09/2015	Swiss Chemical Society Fall meeting 2015, Lausanne, Switzerland. Elena Alberti, Michael P. Coogan and Daniela Donghi, *RNA internal loop: suitable binding site for metallo-intercalators?* (poster).
05/10/2015	Working Group 2 (WG2) Meeting COST Action CM1105, Lisbon, Portugal. Elena Alberti, Michael P. Coogan and Daniela Donghi, *An RNA internal loop as preferential binding site for metallo-intercalators* (poster).
28-29/04/2016	3rd international symposium on functional metal complexes that bind to biomolecules - 4th Whole Action Meeting of the COST Action CM1105, Palma de Mallorca, Balearic Islands, Spain. Elena Alberti, Michael P. Coogan and Daniela Donghi, *Exploiting NMR to assess the interaction between a metallo-intercalator and an RNA internal loop* (oral).
15/09/2016	Swiss Chemical Society Fall meeting 2016, Zurich, Switzerland. Elena Alberti, Michael P. Coogan and Daniela Donghi, *A close look to the interaction of a metallo-intercalator and an RNA internal loop via NMR* (poster).

Awards

August 2015	Forschungskredit grant der Universität Zürich.
October 2016	Poster prize at the 11th edition of the Dorothy Crowfoot Hodgkin Symposium.